



UNIVERSITY  
OF  
JOHANNESBURG

## COPYRIGHT AND CITATION CONSIDERATIONS FOR THIS THESIS/ DISSERTATION



- Attribution — You must give appropriate credit, provide a link to the license, and indicate if changes were made. You may do so in any reasonable manner, but not in any way that suggests the licensor endorses you or your use.
- NonCommercial — You may not use the material for commercial purposes.
- ShareAlike — If you remix, transform, or build upon the material, you must distribute your contributions under the same license as the original.

### How to cite this thesis

Surname, Initial(s). (2012). Title of the thesis or dissertation (Doctoral Thesis / Master's Dissertation). Johannesburg: University of Johannesburg. Available from: <http://hdl.handle.net/102000/0002> (Accessed: 22 August 2017).

**A FREQUENCY DOMAIN WHEELSET-TRACK  
DYNAMICS STUDY ON SHORT PITCH CORRUGATED  
CONCRETE SLEEPERED AND NON-CORRUGATED  
STEEL SLEEPERED RAILWAY TRACKS**



**BINGO MASIZA BALEKWA**

**A thesis submitted in partial fulfilment of the requirements for the degree of**

**DOCTOR OF PHILOSOPHY**

**In the**

**FACULTY OF ENGINEERING AND THE BUILT ENVIRONMENT**

**UNIVERSITY OF JOHANNESBURG**

**June 2021**

# A FREQUENCY DOMAIN WHEELSET-TRACK DYNAMICS STUDY ON SHORT PITCH CORRUGATED CONCRETE SLEEPERED AND NON- CORRUGATED STEEL SLEEPERED RAILWAY TRACKS

Bingo Masiza Balekwa

**Thesis submitted in compliance with the requirements for the qualification: Doctor of  
Philosophy: Engineering: Mechanical in the Department of Mechanical and Industrial  
Engineering Technology at the University of Johannesburg.**



## Publications

**B.M. Balekwa**, D.V.V. Kallon: Correlation of Short Pitch Corrugation with Railway Wheel-track Resonance at Low Frequencies of Excitation. *Vibration*. 2020. Vol 3, Issue 4, Pp 491 – 520.

**B. Balekwa**, D.V.V. Kallon, D. J. Fourie: Vibration Response for class D44 and D39 200 Locomotive Wheelsets due to Dynamic Loads Excitation. *2019 Open Innovations (OI)*. Pp. 397 – 400.

**B. Balekwa**, D.V.V. Kallon, D. J. Fourie: Vertical and Horizontal Vibration Response for Corrugated Track Curves Supported on Steel and PY-Type Concrete Sleepers. *2019 Open Innovations (OI)*. Pp. 474 – 482.

**B. Balekwa**, A. Mashamba, D.V.V. Kallon, P. Dube: Application of Modal Analysis to Establish the Wavelength Fixing Mechanism for Rail Corrugation. *Proceedings of the 11<sup>th</sup> South African Conference of Computational and Applied Mechanics (SACAM)*. 2018. Pp. 212 – 223.



## **Abstract**

Rail corrugation is identified on the running surface around track curves of a twenty seven kilometer long railway line with the smallest and largest curve radii of 140m and 484m respectively. The railway line runs from Belfast to Steelpoort in the Limpopo Province of South Africa. Given that corrugation has not formed on rails for track curves with steel sleepers, the study contributes to the body of knowledge by investigating the difference in dynamic response of rail track with steel and concrete sleepers. This results in significant findings as to why the dynamic response of track with concrete sleepers could be associated with the formation of short pitch rail corrugation in the railway line. In the recent accepted literature researchers are starting to believe frictional self-excited vibration of the wheel-rail system to be an important culprit for short pitch rail corrugation formation. The dynamics of ballasted railway tracks is not studied sufficiently in the recent literature, particularly those installed with steel sleepers, which is key in developing means to prevent short pitch rail corrugation formation.

A corrugation-borne vibration frequency is dependent on wavelengths and train velocities. In the current study these frequencies are matched with natural frequencies of a locomotive traction wheelset, to investigate whether wheels have a resonant influence on the short pitch rail corrugation formation. Experimental modal test is conducted to obtain natural frequencies of a traction wheelset that was used by a locomotive operating in the affected railway line. Finite Element Analysis (FEA) is used to validate dynamic mode shapes at important natural frequencies of the traction wheelset, obtained through experimental modal test. The natural frequencies of the wheelset are correlated with corrugation frequencies for each affected track curve selected for the purpose of the current study. Experimental modal tests are also conducted on tracks with steel and concrete sleepers to obtain natural frequencies of rail tracks with these two types of sleepers. The FEA complex eigenvalue method is used to validate dynamic mode shapes at important natural frequencies of rail tracks with the two types of sleepers. An important traction wheelset axial bending mode is excited at 108Hz when the traction wheelset is free of boundary conditions. This frequency was found to be the short pitch rail corrugation formation frequency for the affected railway line.

This traction wheelset vibration mode was found to reasonably match with corrugation frequencies around each track curve. This axial bending mode of the traction wheelset becomes more damped and shifts to 120Hz when the traction wheelset is coupled to a traction motor and installed in a bogie. Another important resonance mode is also excited at 103Hz in

the circumferential direction when the traction wheelset is installed in a bogie and coupled to a traction motor. These two resonance modes, i.e. axial bending and circumferential, are hence of importance in view of short pitch rail corrugation formation. In light of the dynamic response of rail tracks, an important finding from the complex eigenvalue analysis is that the dynamic response of the rail track with concrete sleepers predominantly presents a second-order rail vertical bending mode at 108Hz. This is essentially consistent with the accepted literature; which is of the view that it is predominantly the vertical dynamics of a rail track that are associated with the formation of short pitch corrugation on rails. It follows that at 108Hz, only a horizontal bending mode occurs from dynamic response of the track with steel sleepers. In light of modal test results for the rails supported on the two types of sleepers, the point Frequency Response Functions (FRFs) obtained from experiments show a more damped response for rails on steel sleepers than for those on concrete sleepers.

In light of the modal test on the two types of sleepers, despite the fact that no resonance mode was excited at 108Hz, a few resonance modes are excited in the frequency range of 0-500Hz corresponding to short pitch rail corrugation. Contrary to expectation, in this frequency range, FRFs for the steel sleeper represent a more damped response, than that from concrete sleeper. This may be explained by the fact that concrete sleepers were notably exposed above the ballast, possibly due to ballast settlement. Steel sleepers were notably more buried into the ballast which may possibly introduce additional damping. The complex eigenvalue and modal analyses are conducted to study the self-excited unsteady vibration of a wheelset-track system and its influence on the formation of short pitch rail corrugation at a frequency range of 0 – 500Hz. The complex eigenvalue model with steel sleepers presents no self-excited unstable vibration in the vertical direction, which is the direction of vibration attributed to the formation of rail corrugation. The same model presents self-excited unstable vibration in the vertical direction when tested on a rail track with concrete sleepers. Hence for the track with concrete sleepers, the current study proposes the wheelset-track self-excited unstable vibration in the vertical direction to be attributed to the formation of short pitch rail corrugation in the railway line of concern.

**Keywords:** Concrete sleeper; FEA; Frequency Response Function; modal analysis; rail corrugation; steel sleeper; vibration.

## Acknowledgements

“Better is the end of a thing than the beginning thereof (Eccl 7: 8)”. Blessed be God who in His divine power has given me everything I need for life and godliness, through the knowledge of my Lord and saviour Jesus Christ, who made His mercies and grace abundantly extended to me throughout the course of this study. I have the greatest pleasure to express my profound gratitude and appreciations to the following persons who have contributed in one way or the other to the success of this study:

**Dr. Daramy Vandi Von Kallon:** thank you for accepting me into your research group under Computational Mechanics. Thank you for taking your time looking into my work, guiding me and reviewing all my work. I enjoyed the close supervision from you for all the time I have spent in my PhD research.

**Dr. Danie Fourie:** for taking your time to assist me with sourcing experimental instruments, being part of experimental setups and being a helping hand during all field work. Thank you for reviewing and advising on my modelling work. I appreciate your consistency and honesty. I value the mentoring that I have been lucky to get from you. Thank you for some motivating words in times I had felt like I was forcing into an impossible path. I have learnt a big deal from your guidance and level of intellect. No word can explain how much I appreciate your time looking into my study and all the advices. God be with you.

**Mr. Gerrit Visser:** thank you for taking your time in inspecting irregularities and obstacles in my FEA simulations. A lot of time was wasted at the initial stage of my simulations, ultimately your advices on my simulations saved me a lot of time.

**Prof. Michele Cali:** for advises on characterisation of damping for the rail pad and ballast.

**The University of Johannesburg:** thank you for some research equipment, material and resources.

**My son Lungelo:** the love for you is what gave me strength and kept me going. Thank you for being my motivation.

*Appreciation is also extended to all who have directly and/or indirectly aided the success of this study.*

## Railway terminology

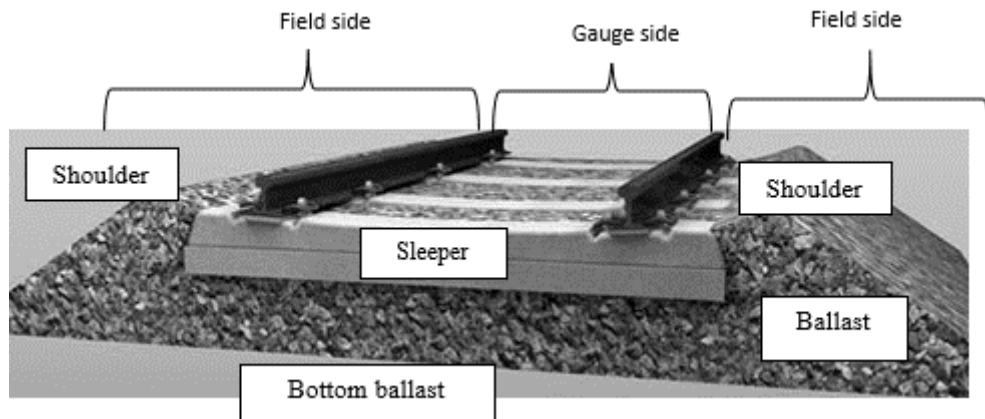


Figure (i). Ballasted track structure

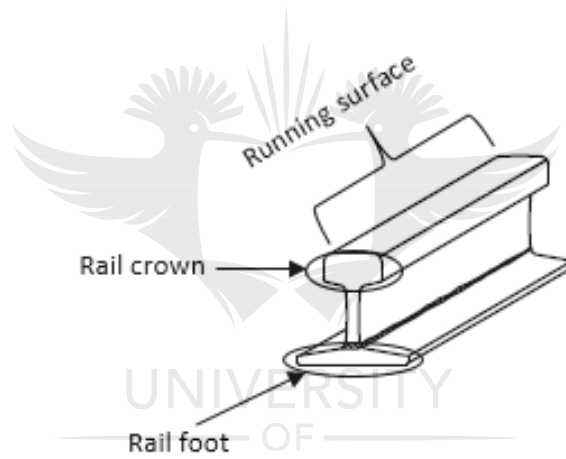


Figure (ii). Running surface, rail crown and rail foot

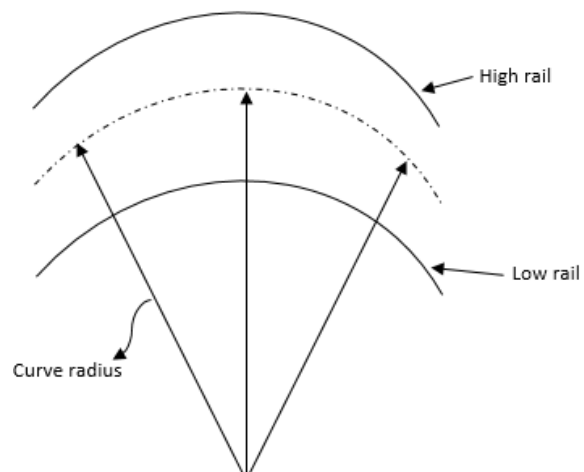
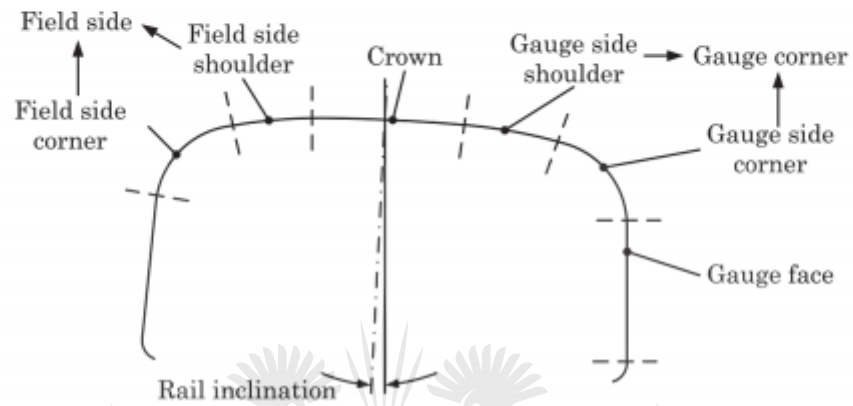
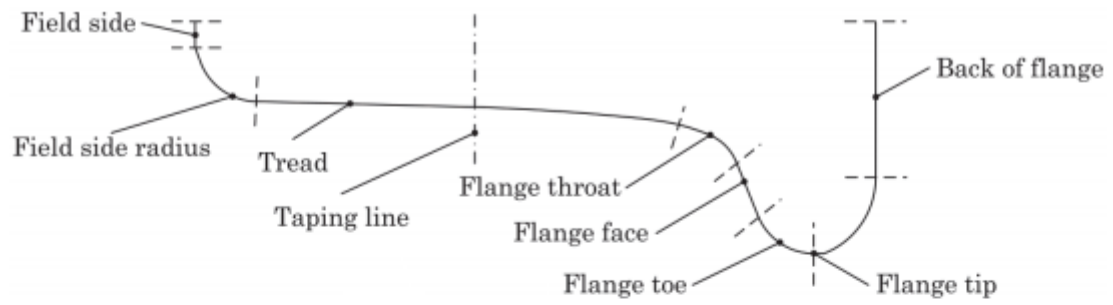


Figure (iii). Low rail, high rail and curve radius





**Figure (iv). Wheel terminology (top) and rail terminology (bottom) [1]**

## Notation

$b_{(\omega)}$	Hysteretic damping coefficient
$C_{AL}$	Connection damping value (lateral)
$C_{AV}$	Connection damping value (vertical)
$c_{eq}$	Equivalent viscous damping coefficient
$K_{AL}$	Connection stiffness (lateral)
$K_{AV}$	Connection stiffness (vertical)
$EI$	Bending stiffness of the rail
$f$	Frequency
$K$	Shear constant of the rail cross section
$k_1$	Rail and sleeper contact stiffness
$k_2$	Sleeper and top ballast layer contact stiffness
$k_3$	Top and middle ballast layer contact stiffness
$k_4$	Middle and bottom ballast layer contact stiffness
$L$	Sleeper bay
$m$	Mass of rail per unit length
$m_r$	Mass of rail
$m_s$	Mass of sleeper
$m_{mbl}$	Mass of middle ballast layer
$m_{bbl}$	Mass of bottom ballast layer
$m_{tbl}$	Mass of top ballast layer
$r_g$	Radius of gyration of the rail
$v$	Train velocity
$\omega$	Excitation frequency
$X_{mbl}$	Displacement of the middle ballast layer
$X_r$	Displacement of rail
$X_s$	Displacement of sleeper
$X_{tbl}$	Displacement of the top ballast layer
$\lambda$	Corrugation wavelength
$-\infty$	Infinite longitudinal direction of the rail in one direction
$+\infty$	Infinite longitudinal direction of the rail, opposite the direction $-\infty$

## Glossary

Description	Meaning
Accelerance	Acceleration of vibration per unit force.
Adhesion	Tendency of two dissimilar materials to cling to each other.
Angle of Attack (AOA)	The angle of attack is the yaw angle of the wheelset from its radial position, as the bogie negotiates the curve. The angle of attack has a positive sense if the wheelset is yawed away from its radial position towards the high rail in the curve.
Contact patch	Wheel-rail system contact point.
Contact point	Wheel-rail system contact patch.
Corrugation wavelength	The distance between successive crests of the waviness on the rail running surface.
Glue	A glue in FEA allows two bodies to be fixed at the contact surface without having the elements of both bodies be the same size and attempting to have the nodes on the two surfaces match.
Frequency Response Function (FRF)	The frequency response function is simply the ratio of the output response of a structure, due to an applied force. The applied force and the response of the structure are simultaneously measured as a result of the applied force. The response can be measured as displacement, velocity or acceleration (accelerance).
Lateral	The direction orthogonal to train movement
Longitudinal	The direction tangential to the railway line in the direction of train movement.

Multi Point Constraints (MPCs)	Elements used in FEA to connect and constrain one or more nodes together to fix two Finite Element Models and ensure that no dislocation occurs in any of the degrees of freedom.
Roughness	Neither the running surface of the wheel or rail is entirely smooth. In the context of railway dynamics, roughness refers to the longer wavelength unevenness found on the rail, and not surface roughness.
Wheelset	An assembly of an axle, wheels and a traction bull gear.



## Table of Contents

1.	Introduction to Rail Corrugation .....	1
1.1.	Problem statement .....	9
1.2.	Research question .....	10
1.3.	Research hypothesis.....	11
1.4.	Research objectives .....	11
1.5.	Research approach .....	13
1.6.	Research scope .....	14
1.7.	Research limitations.....	15
1.8.	Research contribution .....	16
1.9.	Thesis layout.....	17
2.	Literature Review .....	19
2.1.	The Behaviour of Rails.....	19
2.2.	Analytical Models of Rail Corrugations.....	23
2.2.1.	Rail Corrugation Types.....	31
2.2.1.1.	Heavy Haul Corrugation.....	31
2.2.1.2.	Light Rail Corrugation.....	31
2.2.1.3.	Rutting Rail Corrugation .....	32
2.2.1.4.	“Roaring Rails” Rail Corrugation.....	32
2.2.1.5.	Other P2 Resonance Rail Corrugation.....	32
2.3.	Rail Corrugation Categorisation .....	32
2.4.	FEA and Mathematical Modelling of Rail Corrugation .....	35
2.5.	Rail Corrugation Experimental Work.....	40
2.6.	Measures to Identify Rail Corrugation .....	43
2.7.	Vibration Modes and Mode Shapes.....	44
2.8.	Case Study 1: Harmonic Response of a Railway Wheelset.....	45
2.9.	Case Study 2: Wheel-rail Vibrational Analysis and Experimental Modal Analysis on Measures to Suppress Short Pitch Rail Corrugation.....	52
2.10.	Case Study 3: Investigation into Frictional Self-Excited Vibration of a Wheel-Rail System	56
2.11.	Solutions to Rail Corrugation .....	60
	Chapter Two Summary.....	62
3.	Materials and Methods .....	65
3.1.	Railway Track Components .....	65
3.2.	Materials for Experimental Modal Analysis on a Wheelset and Rail Tracks.....	68
3.2.1.	Modal Hammers .....	69
3.2.2.	Accelerometers .....	70
3.2.3.	Dynamic Signal Acquisition System .....	71

3.2.4.	Computer Aided Design (CAD) Softwares .....	71
3.2.5.	FEA Softwares.....	71
3.3.	Methods .....	71
3.3.1.	Experimental Setup for Modal Analysis.....	72
3.3.2.	Mathematics of Dynamic Response Analysis .....	73
3.3.3.	Modelling the Ballast.....	73
3.4.	The Pyramid Model of the Ballast.....	75
3.5.	Flow Diagram for Purpose of Experimental Modal Analysis on a Wheelset Installed in a Bogie	77
3.6.	Flow Diagram for Purpose of FEA Modal Analysis on a Freely Suspended Wheelset .....	77
3.7.	Flow Diagram for Purpose of Complex Eigenvalue Analysis on Railway Track Installed with Steel Sleepers.....	78
3.8.	Flow Diagram for Purpose of Complex Eigenvalue Analysis on Railway Track Installed with Concrete Sleepers .....	78
3.9.	Flow Diagram for Purpose of Linear Static Analysis on a Wheel-Rail System Supported on Steel Sleepers (in Appendix A) .....	79
3.10.	Flow Diagram for Purpose of Linear Static Analysis on a Wheel-Rail System Supported on Concrete Sleepers (in Appendix A).....	80
3.11.	Mass Checking for Finite Element Models (FEMs).....	80
	Chapter Three Summary.....	81
4.	Experimental Modal Analysis on a Wheelset Installed in a Bogie.....	82
4.1.	Experimental Setup for Modal Analysis on a Wheelset installed in a Bogie .....	83
4.1.1.	Environment in which Experimental Modal Analysis Was Conducted on a Wheelset Installed in a Bogie .....	83
4.1.2.	Procedure Followed for Experimental Modal Analysis on a Wheelset Installed in a Bogie	84
4.2.	Results for Experimental Modal Analysis on a Freely Suspended Wheelset and .....	87
	on a Wheelset Installed in a Bogie .....	87
4.2.1.	Results for Experimental Modal Analysis on a Freely Suspended Wheelset .....	88
4.2.2.	Results for Experimental Modal Analysis on a Wheelset Installed in a Bogie .....	90
4.2.3.	Correlation of Results for Experimental Modal Analysis on a Wheelset (Freely Suspended and Installed in a Bogie) with Corrugation Frequencies .....	92
4.3.	Results Discussion .....	94
5.	Experimental Modal Analysis on Rail Tracks Installed with Steel and with Concrete Sleepers	96
5.1.	Experimental Setup for Modal Analysis on Rail Tracks Supported on Steel and Concrete Sleepers.....	96
5.1.1.	Environment in which Experimental Modal Analysis Was Conducted on Rail Tracks with Steel and Concrete Sleepers.....	97
5.1.2.	Procedure Followed for Experimental Modal Analysis on Rail Tracks Supported on Steel and Concrete Sleepers.....	99

5.2.	Results for Experimental Modal Analysis on Railway Tracks Installed with Steel and Concrete Sleepers .....	101
5.2.1.	Results for Experimental Modal Analysis on a Rail Supported on FY-Type Concrete Sleepers .....	101
5.2.2.	Results for Experimental Modal Analysis on a Rail Supported on PY-Type Concrete Sleepers .....	106
5.2.3.	Results for Experimental Modal Analysis on a Rail Supported on Steel Sleepers...	110
5.2.4.	Comparison of Experimental Modal Analysis Results for Rails Supported on FY-type Concrete Sleepers and Steel Sleepers .....	114
5.2.5.	Comparison of Experimental Modal Analysis Results for Rails Supported on PY-type concrete Sleepers and Steel Sleepers .....	119
5.2.6.	Comparison of Experimental Modal Analysis Results for Steel, FY-type and PY-type Concrete Sleepers .....	123
5.3.	Results Discussion .....	125
6.	FEA Modal Analysis on a Freely Suspended Wheelset .....	128
6.1.	Procedure for FEA Modal Analysis on a Freely Suspended Wheelset .....	128
6.2.	Results for FEA Modal Analysis on a Freely Suspended Wheelset .....	130
6.3.	Results Discussion .....	133
6.4.	Recommendations .....	134
7.	Complex Eigenvalue Analysis on Railway Tracks Installed with Steel and Concrete Sleepers .....	136
7.1.	Procedure for Finite Element Complex Eigenvalue Analysis on Rail Tracks Supported on Steel and Concrete Sleepers .....	136
7.2.	Procedure for Modelling of Track Ballast .....	140
7.3.	Results for FEA Complex Eigenvalue Analysis on Rail Tracks Supported on Steel and Concrete Sleepers .....	142
7.4.	Results Discussion .....	145
8.	Implications and Conclusions .....	146
8.1.	Implications .....	146
8.2.	Conclusions .....	147
	References .....	149

## List of Appendices

<b>Appendix A.</b> Wheel-rail contact displacement modelling.....	169
<b>Appendix B.</b> Additional views of results for wheel-rail contact point analysis, for FEM with steel sleepers.....	177
<b>Appendix C.</b> Additional views of results for wheel-rail contact point analysis, for FEM with FY-type concrete sleepers.....	179
<b>Appendix D.</b> Additional views of modal analysis results for the D39 200 wheelset model.....	181
<b>Appendix E.</b> Additional views of results for the complex eigenvalue analysis, for FEM with steel sleepers.....	183
<b>Appendix F.</b> Additional views of results for the complex eigenvalue analysis, for FEM with concrete sleepers.....	185
<b>Appendix G.</b> Images for symptoms of excessive corrugation-born vibration.....	189
<b>Appendix H.</b> Detailed design drawings of CAD models for wheelset and rail track components...	191





## List of Figures

<b>Figure 1.1.</b> (a) Clearly visible rail wear on the running surface of a rail (b) fine chip marks as a result of rail wear on the running surface of a rail. ....	2
<b>Figure 1.2.</b> (a) Thermic welding conducted on a rail to join two pieces of a rail section into one continuous rail (b) final product of a welded rail joint. ....	3
<b>Figure 1.3.</b> (a) Rail material sludge peeling-off, caused by plastic flow on the running surface (b) material build-up on rail running surface due to plastic flow. ....	4
<b>Figure 1.4.</b> Rail running surface ground for removal of railhead irregularities. The rail gauge on top of the rail is used to measure accuracy of the ground surface [19]. ....	5
<b>Figure 1.5.</b> Wear marks as a result of roll-slip oscillation (a) on the rail (b) on the wheel [22]. ....	5
<b>Figure 1.6.</b> Creep force-creepage relationship showing positive, neutral and negative friction characteristics beyond creep saturation [24]. ....	6
<b>Figure 1.7.</b> (a) Short pitch rail corrugation <100mm wavelengths, captured in one of the track curves in the Belfast to Steelpoort railway line (b) long pitch rail corrugation, 100 – 300mm wavelengths captured from one of the high-velocity railway lines in China. ....	8
<b>Figure 2.1.</b> Rail mode shapes under vibrational excitation. Reprinted from [45]. ....	21
<b>Figure 2.2.</b> Displacement of rail in the vertical direction at different train velocities. Measurements taken at Stilton Fen, England, January to May 1993. Reprinted from [47]. ....	22
<b>Figure 2.3.</b> Illustration for rail gauge deviation. ....	23
<b>Figure 2.4.</b> Feedback loop for generation of rail corrugation. ....	30
<b>Figure 2.5.</b> Illustration of the effect of rail pad stiffness on the coupling between rail and sleeper and on the damping of waves in the rail. Reprinted from [106]. ....	42
<b>Figure 2.6.</b> Unstable modal shapes of a railway wheelset at different frequencies of vibration. Reprinted from [173]. ....	45
<b>Figure 2.7.</b> Vertical vibration response of a bi-block track installed with stiff rail pads. Vibration is measured mid-span and above a sleeper. Reprinted from [106]. ....	46
<b>Figure 2.8.</b> Harmonic response of the wheelset. 1N loads applied in the same direction. Reprinted from [174]. ....	49
<b>Figure 2.9.</b> Harmonic response of the wheelset. 1N loads applied in opposite directions. Reprinted from [174]. ....	50
<b>Figure 2.10.</b> Accelerometers installed for vibration test (a) front view of the rail with accelerometers (b) image of accelerometers installed at the base of the rail foot. Reprinted from [34]. ....	53
<b>Figure 2.11.</b> Vibration of the rail in the vertical direction. Cases presented for vibration with and without an absorber. Reprinted from [34]. ....	53
<b>Figure 2.12.</b> Wheel-rail system model with a vibration absorber (a) FE model (b) springs and dampers defined in the rail-absorber contact (c) schematic defining contact between the rail and absorbers. Reprinted from [34]. ....	54
<b>Figure 2.13.</b> Unstable mode of the wheel-rail system (a) at a frequency of 363.9Hz, without the absorber (b) at a frequency of 335.7Hz, with the absorber. Reprinted from [34]. ....	55
<b>Figure 2.14.</b> Wheel-rail contact position for all four wheels in series. Reprinted from [33]. ....	57
<b>Figure 2.15.</b> Wheel-rail model for four wheels in series on the rail (a) overall layout (b) detailed FEM. Reprinted from [33]. ....	58
<b>Figure 2.16.</b> Mode shapes for unstable wheel-rail vibration (a) at a frequency of 331Hz (b) at a frequency of 508.89Hz. Reprinted from [33]. ....	58
<b>Figure 3.1.</b> FY-type concrete sleeper with a FISTclip rail fastening system. (a) exploded view (b) assembled view of the fastening system. ....	66
<b>Figure 3.2.</b> PY-type concrete sleeper with an e-Clip rail fastening system. (a) exploded view (b) assembled view of the fastening system. ....	67

<b>Figure 3.3.</b> Rail on steel sleeper with its fastening system. ....	68
<b>Figure 3.4.</b> Modal hammers: (a) used to excite the traction wheelset (b) used to excite rails and sleepers. ....	69
<b>Figure 3.5.</b> Triaxial accelerometer used for the experiments. Standard units are in inches, converted to millimeters in brackets.....	70
<b>Figure 3.6.</b> Typical experimental modal analysis setup with an impact hammer as the force excitation instrument. Reprinted from [223]. ....	72
<b>Figure 3.7.</b> Railway track model representing inclusion of ballast layers on a track. ....	74
<b>Figure 3.8.</b> Ballasted railway track with a good ballast height.....	75
<b>Figure 3.9.</b> Pyramid models of a ballasted track. Redrawn from [220].....	76
<b>Figure 4.1.</b> D39 200 locomotive class bogie with wheelsets and traction motors. Wheels prepared for experimental modal analysis.....	84
<b>Figure 4.2.</b> Two-nodal-diameter spatially orthogonal axial mode pair. Reprinted from [23]. ....	85
<b>Figure 4.3.</b> Vibration mode shapes of the D39 200 locomotive wheelset (a) at 382Hz (b) at 2463Hz. ....	85
<b>Figure 4.4.</b> Wheel thread locations (A – D) where accelerometer was rigidly mounted and the wheel was excited. ....	86
<b>Figure 4.5.</b> Steel block stuck on traction wheel thread for circumferential excitation. ....	87
<b>Figure 4.6.</b> FRFs for the gear-side wheel of the class D39 200 locomotive wheelset coupled to a traction motor and installed in a bogie. Vibration response for the axial directions (diameter approximately 993.6 mm).....	88
<b>Figure 4.7.</b> FRFs for the gear-side wheel of the class D39 200 locomotive wheelset coupled to a traction motor and installed in a bogie. Vibration response for radial, axial and circumferential directions (diameter approximately 987.2 mm).....	90
<b>Figure 4.8.</b> Fundamental vibration modes of the D39 200 locomotive wheelset matched with corrugation frequencies around each rail track curve.....	93
<b>Figure 5.1.</b> Freight data showing the railway line from Belfast to Steelpoort [230]. ....	97
<b>Figure 5.2.</b> Ecology around the affected railway line (a) trees grown on the sides of the rail track (b) rocks on the sides of the rail track. ....	98
<b>Figure 5.3.</b> Field side rail position for accelerometer and a steel block stuck on the rail running surface for longitudinal excitation.....	99
<b>Figure 5.4.</b> FRF and phase for rail vibration response, vibration measured in the vertical direction from two positions i.e. mid-span and on top of the FY-type concrete sleeper point. ....	102
<b>Figure 5.5.</b> FRF and phase for rail vibration response, vibration measured in the horizontal direction from two positions i.e. mid-span and on top of the FY-type concrete sleeper point. ....	103
<b>Figure 5.6.</b> Comparison of FRFs for rail vibration response, vibration measured in the vertical and horizontal directions on top of sleeper point. Rail is supported on FY-type concrete sleepers.....	104
<b>Figure 5.7.</b> Comparison of FRFs for rail vibration response, vibration measured in the vertical and horizontal directions mid-span. Rail is supported on FY-type concrete sleepers.....	105
<b>Figure 5.8.</b> FRF and phase for rail vibration response, vibration measured in the vertical direction from two positions i.e. mid-span and on top of the PY-type concrete sleeper point. ....	107
<b>Figure 5.9.</b> FRF and face for rail vibration response, vibration measured in the horizontal direction from two positions i.e. mid-span and on top of the PY-type concrete sleeper point. ....	108
<b>Figure 5.10.</b> Comparison of FRFs for rail vibration response, vibration measured in the vertical and horizontal directions mid-span. Rail is supported on PY-type concrete sleepers.....	109
<b>Figure 5.11.</b> Comparison of FRFs for rail vibration response, vibration measured in the vertical and horizontal directions of mid-span. Rail is supported on PY-type concrete sleepers.....	110
<b>Figure 5.12.</b> FRF and phase for rail vibration response, vibration measured in the vertical direction from two positions i.e. mid-span and on top of steel sleeper point. ....	111

<b>Figure 5.13.</b> FRF and phase for rail vibration response, vibration measured in the horizontal direction from two positions i.e. mid-span and on top of steel sleeper point. ....	112
<b>Figure 5.14.</b> Comparison of FRFs for rail vibration response, vibration measured in the vertical and horizontal directions mid-span. Rail is supported on steel sleepers. ....	113
<b>Figure 5.15.</b> Comparison of FRFs for rail vibration response, vibration measured in the vertical and horizontal directions on top of sleeper point. Rail is supported on steel sleepers. ....	114
<b>Figure 5.16.</b> Comparison of FRFs for rail vibration response, rails are supported on FY-Type concrete and on steel sleepers. Vibration measured in the horizontal direction mid-span. ....	115
<b>Figure 5.17.</b> Comparison of FRFs for rail vibration response, rails are supported on FY-Type concrete and on steel sleepers. Vibration measured in the vertical direction mid-span. ....	116
<b>Figure 5.18.</b> Comparison of FRFs for rail vibration response, rails are supported on FY-Type concrete and on steel sleepers. Vibration measured in the vertical direction on top of sleeper point. ....	117
<b>Figure 5.19.</b> Comparison of FRFs for rail vibration response, rails are supported on FY-Type concrete and on steel sleepers. Vibration measured in the horizontal direction on top of sleeper point. ....	118
<b>Figure 5.20.</b> Comparison of FRFs for rail vibration response, rails are supported on PY-Type concrete and on steel sleepers. Vibration measured in the vertical direction mid-span. ....	119
<b>Figure 5.21.</b> Comparison of FRFs for rail vibration response, rails are supported on PY-Type concrete and on steel sleepers. Vibration measured in the horizontal direction mid-span. ....	120
<b>Figure 5.22.</b> Comparison of FRFs for rail vibration response, rails are supported on PY-Type concrete and on steel sleepers. Vibration measured in the vertical direction on top of sleeper point. ....	121
<b>Figure 5.23.</b> Comparison of FRFs for rail vibration response, rails are supported on PY-Type concrete and on steel sleepers. Vibration measured in the horizontal direction on top of sleeper point. ....	122
<b>Figure 5.24.</b> Comparison of FRFs for vibration response of sleepers. Vibration measured in the vertical direction, on the top face of sleeper, by the field side of the rail. ....	123
<b>Figure 5.25.</b> Comparison of FRFs for vibration response of sleepers. Vibration measured in the horizontal direction, on the top face of sleeper, by the field side of the rail. ....	124
<b>Figure 6.1.</b> FEA model for a D39 200 locomotive traction wheelset. ....	129
<b>Figure 6.2.</b> Traction wheelset – mode shape for first-order bending mode. ....	131
<b>Figure 6.3.</b> Traction wheelset – mode shape for second-order bending mode. ....	133
<b>Figure 7.1.</b> Rail track model with steel sleepers. ....	137
<b>Figure 7.2.</b> Concrete sleeper track. (a) rail track model with concrete sleepers (b) rail pad on a concrete sleeper. ....	138
<b>Figure 7.3.</b> FEA model representing ballast underneath concrete sleepers. ....	141
<b>Figure 7.4.</b> Bending mode for rail track with steel sleepers at 108Hz and ballast. ....	143
<b>Figure 7.5.</b> Bending mode for rail track with steel sleepers at 108Hz, no ballast. ....	143
<b>Figure 7.6.</b> Bending mode for rail track with concrete sleepers. ....	144

## List of Tables

<b>Table 2.1.</b> Wavelength fixing mechanisms associated with damage mechanisms [14] .....	33
<b>Table 2.2.</b> Wavelengths and mechanisms associated with rail corrugation types [28] .....	33
<b>Table 2.3.</b> Parameters of the railway coach wheelset modelled for harmonic response investigation [174].....	47
<b>Table 2.4.</b> Resonance frequencies of the harmonic response. 1N load applied in the same direction [174].....	49
<b>Table 2.5.</b> Frequencies of the harmonic response. 1N load applied in opposite directions [174].....	51
<b>Table 3.1.</b> Isotron® accelerometer features .....	70
<b>Table 3.2.</b> FEM mass checking .....	80
<b>Table 4.1.</b> Corrugation frequencies per track curve .....	92
<b>Table 5.1.</b> Track components that are above the ballast and the orientation of the accelerometer during experimental Modal Analysis.....	99
<b>Table 6.1.</b> Mesh details for the traction wheelset.....	129
<b>Table 6.2.</b> Mesh convergence for the traction wheelset model.....	129
<b>Table 6.3.</b> Material properties for FE model of a D39 200 traction wheelset [23] .....	130
<b>Table 6.4.</b> Percentage error between experimental and FEA modal analysis .....	132
<b>Table 7.1.</b> Contacts created for deformable bodies in the steel sleeper model .....	137
<b>Table 7.2.</b> Mesh details for rail track FEM with steel sleepers .....	137
<b>Table 7.3.</b> Material properties for FEMs on rail track model with steel sleepers [23].....	138
<b>Table 7.4.</b> Contacts created for deformable bodies in the concrete sleeper model .....	139
<b>Table 7.5.</b> Mesh details for rail track FEM with concrete sleepers.....	139
<b>Table 7.6.</b> Material properties for FEMs on rail track model with concrete sleepers [23] [224].....	140
<b>Table 7.7.</b> Mesh details for ballast FEM.....	141
<b>Table 7.8.</b> Material properties for ballast FEM [227] .....	142
<b>Table 7.9.</b> Contacts and constraints created for deformable bodies of the ballast .....	142

# Chapter One

## Introduction to Rail Corrugation

### 1. Background

From a young age we always had a common curiosity when watching the entire length of a passenger train with excitement on a train pass. Shortly after that in our teen years some of us had an opportunity to take a short ride in a freight train, which used to bring a cheerful feeling from hearing the unique squealing sound and vibration, until such a time that I progressed in life to an opportunity of being part of those responsible for care of railway trains and infrastructure in the railway industry, where undesired rail track irregularities posing train derailment risks to operations are also encountered.

A train is with no doubt, one of the most efficient and economical modes of transport to move bulk freight and passengers across land. However, noise and vibration from trains are an important source of ecological and environmental annoyances. The current study is concerned with addressing a problem that is significantly linked with vibration borne by wheel-rail interaction; i.e. the short pitch rail corrugation [2].

Transnet is a back bone of the railway industry in South Africa and owns most of the rail network across the land. Operations in the rail network involves transportation of valuable products such as Iron Ore, Manganese, coal, automotive vehicles, liquefied gasses etcetera. It was found that a short pitch rail corrugation formed on the running surface of the rails in the railway track from Belfast to Steelpoort in the Limpopo Province of South Africa. This twenty seven kilometers long railway track has the smallest curve radius of 140m and the largest which is 484m.

Corrugation is referred to as “short pitch” if its wavelengths range between 20 – 100mm, and as “long pitch” if they are greater than 100mm [3]. In metro systems it is common for this phenomenon to also form in wavelengths in a range of 25 – 50mm [4]. The long pitch rail corrugation normally forms with amplitudes in a range of 0.01 – 0.05mm, whilst amplitudes of the short pitch rail corrugation normally fall in the range of 0.1 – 0.9mm [5, 6].

Wavelengths and amplitudes of rail corrugation depend on several factors, such as rail car behaviour, wheel-rail interaction, track configuration, track system and track structure [7]. Nonetheless, from the view of interrelated parameters, rail corrugation wavelengths increase with increased corrugation amplitude depth and a train velocity. However, amplitudes are nonlinearly related to the wavelengths [8]. Wavelengths are generally accepted to be related to the wheelset velocity [9, 10].

Rail corrugation can be categorised in six groups; i.e. (i) Heavy haul, (ii) Light rail, (iii) P2 resonance, (iv) Pinned-pinned resonance, (v) Trackform-specific and (vi) Rutting [11]. This particular rail disease forms due to damage mechanisms (i.e. physical irregularities of wheel and rail) and is sustained by wavelength fixing mechanisms (i.e. wheel-rail natural frequencies) [2].

The damage mechanism occurs from a metallurgical and tribological irregularities such as rail wear, improper rail welding and rail grinding, plastic flow etcetera [10, 12]. Initiation of corrugation on rails is mostly pivoted over rail wear [13]. No matter



(a)

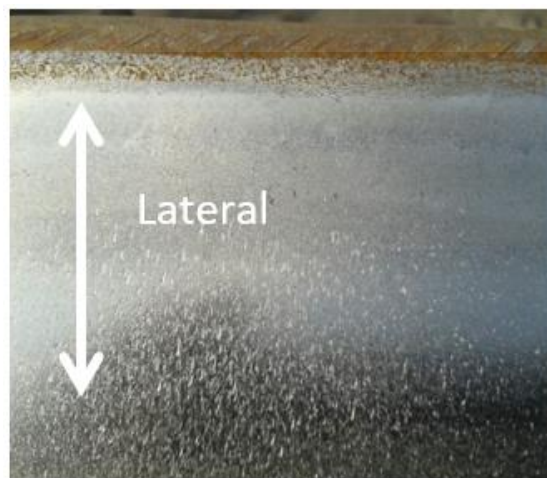


**Figure 1.1.** (a) Clearly visible rail wear on the running surface of a rail (b) fine chip marks as a result of rail wear on the running surface of a rail.



how small a rail wear irregularity is, over time the irregularity may expand and pose sufficient risk for development of corrugation on a rail. Figure 1.1. shows a clearly visible and a fine (not clearly visible) rail wear on the running surface of the rail.

Figure 1.1a. shows a clearly visible rail wear from which unsteady wheel-rail dynamic loads may occur on a train pass. These undesired dynamic loads become severe on a multiple successive wheel passes. Figure 1.1b. shows a minor wear, from which the problem may pose a risk of further enlarged rail wear on a multiple successive train wheel passes. Figure 1.2. shows welding on a rail and a possible damage mechanism on a rail as a result of improper welding.



(a)



(b)

**Figure 1.2.** (a) Thermic welding conducted on a rail to join two pieces of a rail section into one continuous rail (b) final product of a welded rail joint.

Improper (or poor) welding on rails imposes the risk of rail being prone to damage on the (or around the) weld zone. A damage from this kind of irregularity on the running surface gives rise to unsteady dynamic loads during train pass. If all trains pass over a rail at the same velocity, and if vehicles are similar, it is likely that the rails will be worn in the same place by all of the wheels and a corrugation forms [14].

Corrugation forms at first gradually and then more rapidly as the dynamic loads caused by corrugation itself increase [14]. In contrast to using the bolted fish plates, Transnet uses thermic welding to weld-joint two rail pieces together. This is done by heating an external metal to its liquid state and fill it in between the two rails to form a bond. However, the pre-weld and post-weld heat treatment processes are of significant importance in this type of welding, to prevent high residual stress concentrations in the weld zones [15, 16]. If the two processes are not properly followed, irregularities such as a post weld distortion has a risk of occurring and a fatigue crack may develop as a result of excessive dynamic loads experienced by the rail joint on train passes.

Once a crack forms it is easier for it to grow in the rail material, away from the weld joint and towards the rail foot [17]. Although the weld zone itself may be strong enough to take the dynamic loads, the rail material is still exposed to the high risk of crack propagation. Figure 1.3. shows plastic flow on the running surface of the rail. The metallurgy of a rail and thermal dynamics involved during wheel-rail interaction are part of the important functions of plastic flow forming on the running surface of a rail [18]. This ultimately results in a damage mechanism for rail corrugation formation [18]. Plastic flow is mostly clearly visible on the field side shoulder and more towards the field side corner of a rail.



(a)



(b)

**Figure 1.3.** (a) Rail material sludge peeling-off, caused by plastic flow on the running surface (b) material build-up on rail running surface due to plastic flow.



Rail material removal through grinding the running surface is the most commonly used method for removal of wear and plastic flow on rails [1]. Figure 1.4. shows a rail ground (reprofiled) on the running surface, for removal of irregularities on the rail material [19].



**Figure 1.4.** Rail running surface ground for removal of railhead irregularities. The rail gauge on top of the rail is used to measure accuracy of the ground surface [19].

Rail corrugation is removable through rail grinding when it is still not very severe. However, sometimes heavy corrugation cannot be removed through grinding, due to railhead grinding limitations. The other common damage mechanism for which researchers associate result with the formation of rail corrugation is the roll-slip oscillation. Roll-slip oscillation is one of the good examples of sources of irregularities on wheel and rail surfaces [20, 21]. Figure 1.5. shows wear marks on the running surfaces of a wheel and rail, that resulted from the roll-slip oscillation.

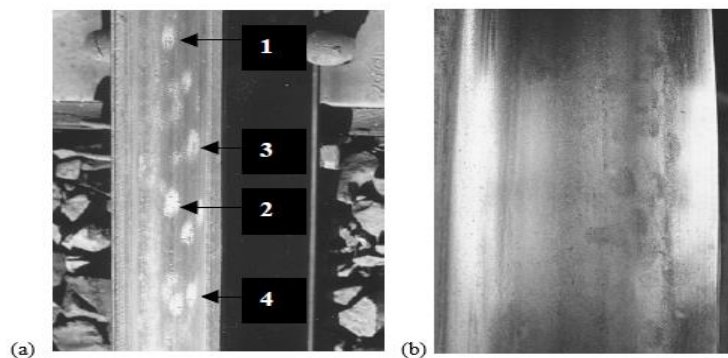


**Figure 1.5.** Wear marks as a result of roll-slip oscillation (a) on the rail (b) on the wheel [22].

The roll-slip oscillation wear marks occur as a result of a periodic, successive, rolling and sliding of a train wheel relative to the running surface of the rail [22]. The marks can also occur on the train wheel tread, posing a risk for unsteady dynamic loads during wheel-rail interaction. The roll-slip oscillation can be explained from the dynamics of the wheel-rail contact patch, resulting from the creep force-creepage relationship [23]. Figure 1.6. shows the creep force-creepage relationship.

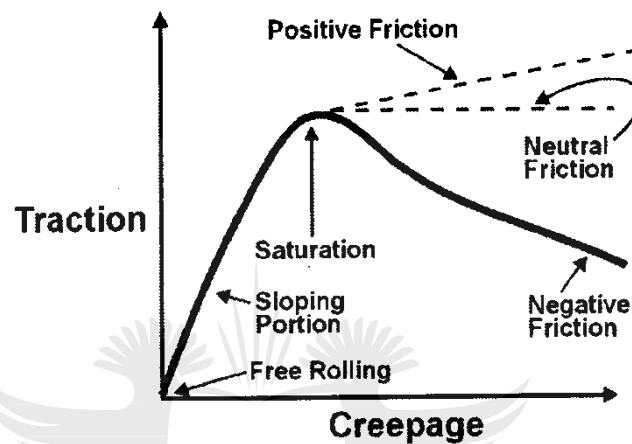


**Figure 1.6.** Creep force-creepage relationship showing positive, neutral and negative friction characteristics beyond creep saturation [24].

Creepage is simply a slide of a wheel relative to the rail, which is normalized by a wheel velocity [23]. When the wheel-rail contact point operates in the vicinity of saturated creepage, the wheel rolls forward whilst the traction force builds up towards the maximum of the traction-creepage curve [25]. Once the maximum is achieved the traction force cannot be increased any further. At this point friction force in the contact point is zero. If the traction force increases further, slip occurs, due to the negative friction characteristic. This cycle of occurrences is referred to as the roll-slip oscillation and it can safely be suggested that it occurs from the oscillation of wheel-rail traction force. Roll-slip marks are mostly observed on surfaces of rails or wheels of slow moving trains.

The wavelength fixing mechanism refers to the resonance of a train wheel, a rail track and any other resonance that may give rise to the development of corrugation at a particular frequency [26]. The wavelength fixing mechanism and its interrelation with

the damage mechanism are further explained in Chapter two. The current study is concerned particularly with the wavelength fixing mechanism of short pitch rail corrugation. The railway line from Belfast to Steelpoort in the Limpopo Province of South Africa experiences a problem of short pitch rail corrugation, with average wavelengths ranging between 59 – 90mm. In the beginning of the current study (January 2018), rail corrugation amplitudes were measured and were found to reach a steady state (highest crests) at 0.8mm.

Measurements were conducted twice in a period of six months (from January to July 2018), in the middle of the test curve located at kilometer point 178/3. In the main line with which the current study is concerned, two types of railway sleepers were installed, i.e. concrete and steel. However, in recent developments, steel sleepers are being replaced by the concrete type in all track curves. Trains in the affected railway line were predominantly hauled by the diesel locomotive class D39 200, before its replacement by the class D44 later in the year 2016. The current study focuses predominantly on work conducted with respect to operations of the class D39 200.

The term rail corrugation refers to a periodic waviness that forms on the running surface of the rail due to dynamics of wheel-rail interaction and tribology. In this particular railway line, the current study focuses on identifying parameters and mechanisms associated with short pitch rail corrugation. The study takes the approach of investigating differences in track dynamics between tracks with concrete and steel sleepers. The short pitch rail corrugation on the affected rail track curves is fixed throughout the entire lengths of each track curve. Despite the fact that the company replaces steel sleepers with concrete sleepers on most of the curves, all rails in track curves with steel sleepers are found without corrugation. The problem of rail corrugation is a crucial concern in the railway industry globally and has a hundred-year-history [27, 28].

Currently there appears to be no permanent cure for rail corrugation. Even though vast literature explains different types of rail corrugation, mechanism that forms the short pitch rail corrugation is still not understood to date [29]. To better understand the key responsible factors causing the short pitch rail corrugation there is a need for reliable models to describe this phenomenon. To date, researchers have proposed different

treatments for rail corrugations, some of which are useful, even though they are uneconomical, such as rail grinding, which can reduce track and ground vibrations by more than 4 dB and 11 dB respectively [30]. Symptoms of short pitch rail corrugation problem in the Belfast to Steelpoort railway line are visible dislocation of track components. These components dislocate due to excessive corrugation-induced vibration. When rail pads displace out of the fastening system, the connection stiffness between the rail and sleeper becomes less, such that, ultimately, rail clips and other components of the fastening system also dislocate. In this way the rail is left to make direct contact with the concrete sleeper.

Images for symptoms of excessive vibration in the Belfast to Steelpoort railway line are found in Appendix G. Parts of the railway line are situated approximately ten meters from erected fences and approximately hundred meters from a human settlement. However, most of the affected rail track curves are situated a few hundred meters from the human settlements. Figure 1.7. shows an image of short pitch rail corrugation measured from one of the track curves in the Belfast to Steelpoort railway line, and one with a long pitch rail corrugation. The long pitch rail corrugation image was captured from one of the high-velocity railway lines in China.



(a)



(b)

**Figure 1.7.** (a) Short pitch rail corrugation  $<100\text{mm}$  wavelengths, captured in one of the track curves in the Belfast to Steelpoort railway line (b) long pitch rail corrugation,  $100 - 300\text{mm}$  wavelengths captured from one of the high-velocity railway lines in China.

For the purpose of empirical tests, the test curve identified for this study is the track curve located at kilometer point 178/3. This track curve is long enough that it has six mass poles erected alongside, i.e. 178/1 to 178/6. Tests and measurements were conducted on the curve length between mass poles 178/3 and 178/4. The design radius of the curve is 147m. This track curve has the latest rails replaced in the year 2016. The curve is one of the sharpest and circular curves that are understood to experience severe forces during train passes. The importance of conducting the current study is linked with the financial benefits that may be realised by the railway company (Transnet) that owns the rail track and operates trains in it. Further benefits of the study include reduction in the frequency of unscheduled train and track components change out.

Train and track components generally experience loose mountings and ultimately dislocate during excessive vibration, thereby requiring frequent unscheduled maintenance. The ecology will also be saved as there will be less vibration by the trees, buildings and fences closer to the rail track. One of the important challenges in implementing the practical solution may be the budget, and that it will be time consuming to capture the problem at its entirety. This is given that a practical solution will only be effective if implemented both on wheels and track components. This makes it difficult to optimise the solution, since time will need to be allocated for trials and monitoring of measures that would be implemented on rail cars and tracks.

This thesis does not assume the reader to be familiar with the field of track engineering and rail corrugation. For such a reader, the word “corrugation” can be replaced by the words “waviness” and “roughness” without any loss of specificity. Similarly, rail, rail tie, sleepers and ballast together may be replaced by the word “track”. In addition, in this work, a corrugated track curve identified for the purpose of tests and measurements can be referred to as a test point “Tp”, a “test curve” or a “test site”.

### **1.1. Problem statement**

Corrugation-induced vibration results in deterioration of the rail track in the Belfast to Steelpoort railway line, in the Limpopo Province of South Africa. This excessive track vibration results in shearing of rubber rail pads and dislocation of rail track fastening

system components. Due to the daily operation of same locomotives in the railway line, there is a significant possibility of loose connections in locomotives, such as traction motor mountings and electronic equipment mountings. Wheel bearings may also deteriorate due to excessive vibration. Currently in this line, rail corrugation is removed from rail profile through grinding, however, sometimes not all corrugation can be entirely removed, due to grinding limitations. Rail corrugation in this railway line only formed on the low rail of track curves with concrete sleepers. There are two categories of concrete sleeper types used in the affected line, i.e. the FY-type and the PY-type. Steel sleepers are the second type used.

Rails on both types of concrete sleepers experience corrugation. This research study establishes the dynamic difference in rail tracks installed with concrete and steel sleepers and establishes how the dynamics influence the formation and sustainment of rail corrugation.

## **1.2. Research question**

### *1.2.1. Why will the short pitch rail corrugation not form on rails supported on steel sleepers?*

From the body of knowledge, it is accepted that corrugation forms on rails due to (and it is sustained by) different mechanisms, as long as there is a wheel running on the rail surface [28, 31]. However, it is not explained (or at least not sufficiently) why the enigma is not found on rail tracks installed with steel sleepers. This significant question requires an extensive effort into studying the dynamics of rail tracks with both types of sleepers (concrete and steel).

### *1.2.2. What resonance modes of the concrete sleepered rail track (not found in the steel sleepered rail track) are found to be associated with the formation of short pitch rail corrugation?*

From the body of knowledge, it is accepted that some resonance modes of a rail track are associated with the formation of rail corrugation [32]. However, a simplified rail track model, with concrete sleepers is required, that will establish the exact resonance modes and a vibration frequency range found to



be associated with the formation of rail corrugation. This model should not predict rail corrugation when used for rail tracks installed with steel sleepers.

- 1.2.3. *What resonance modes of the D39 200 locomotive class wheelset are found to be associated with the formation of short pitch rail corrugation, when the wheels are coupled to a traction motor and installed in a bogie?*

From the body of knowledge, it is accepted that some resonance modes of train wheels are the wavelength fixing mechanism for rail corrugation [14, 26]. A locomotive class wheelset operating in the affected rail line is required to be tested for resonance modes. After which a vibration frequency range found to be closely related to the formation of short pitch rail corrugation in the Belfast to Steelpoort railway line can be identified.

### **1.3. Research hypothesis**

Short-pitch rail corrugation is influenced by friction-induced natural frequencies of a wheel-rail system, with the vertical dynamics of the tracks supported on concrete sleepers favoring the formation of corrugation, at a certain resonant frequency range.

One of the widely accepted theories in the research space for rail corrugations is that the dynamics of braking and traction during train transit may cause a slight railway wheel slip relative to the rail [33, 34]. This slip gives rise to the frictional self-excited vibration in the wheel-rail system, which is the mechanism widely understood to be responsible for the formation of corrugation on rails [33, 34]. However, the difference in dynamics wheelset-tracks with the two types of sleepers in concern is responsible for the reason rail corrugation will not form in steel sleepered track curves [32, 35].

### **1.4. Research objectives**

The primary objectives of the current study are as follows:

- 1.4.1. *To identify rail track curves affected by short pitch rail corrugation in the Belfast to Steelpoort railway.*

This entails driving in the service road alongside the affected railway track and walking to each track curve to inspect the extent of rail corrugation. Some of

the railway track curves have rail corrugation that is light in terms of visibility. This makes things difficult for the researcher to conduct measurements in such track curves. After this inspection the visibility of rail corrugation is categorised as light or heavy in terms of visibility to a naked eye.

1.4.2. *To measure short pitch rail corrugation in the test sites, in the Belfast to Steelpoort railway line.*

This entails measuring rail corrugation amplitudes on a few track curves that are categorised as heavily corrugated. From these measurements the researcher gets to decide on the best track curves to pursue. Given that measurements are conducted manually using a ruler and an angle iron, track curves with clearly visible rail corrugation, with amplitudes that have not reached the steady state yet, are good to pursue corrugation amplitude growth.

On the other hand, track curves with corrugation amplitudes that have reached a steady state are good for investigations of FRF measurements on worn rails. FRFs measured in such track curves will provide accurate measurements for rail material that is worn the most.

1.4.3. *To use experimental and numerical modelling methods to conduct vibration tests for wheels of the D39 200 locomotive traction wheelset.*

The dynamics of train wheels and rail track are attributed to the formation and development of corrugation on rails. It is hence prudent to test such dynamics and analyse how they influence mechanisms responsible for the formation and development of rail corrugation. The resulting outcomes can be used by railway engineers to improve the designs for wheels and tracks.

1.4.4. *To use experimental and numerical modelling methods to conduct vibration tests for rail tracks with two types of sleepers, i.e. steel and concrete.*

Almost all track curves with concrete sleepers are corrugated in the railway line with which the current study is concerned. However, same does not hold



for track curves with steel sleepers. From this, it can only make sense to hypothesise that some mechanism responsible for the existence of short pitch rail corrugation in the railway line rests on the difference in wheel-rail dynamics of the two cases.

1.4.5. *To analyse the difference in track modal dynamics between rail tracks installed with steel and concrete sleepers.*

This entails analysing modelling and experimental results for wheels, wheel-rail and wheelset-track models to better understand factors influencing (and the dynamic difference of) the models with steel and with concrete sleepers.

1.4.6. *To identify parameters, from results of wheels, wheel-rail and wheelset-track models, that can be attributed to the formation of short pitch rail corrugation.*

Not all parameters of vibration response of the wheels or track can be attributed to the formation of rail corrugation in the affected railway line. This is conducted to identify clear parameters of structural response, for instance resonant and anti-resonant natural frequencies, which can be attributed to the formation of rail corrugation. This is done for the frequency range that corresponds to short pitch corrugation. No much emphasis is put on the frequency range beyond the short pitch rail corrugation formation frequency.

## 1.5. Research approach

The current research study adopted an inductive approach, in a sense that it begins with some observation of the nature of the problem and how it manifests. This is followed by generalised theories and hypothesis. Practical and active efforts were put to produce qualitative data and analysis.

- Firstly, the literature was sourced, obtained and continuously reviewed to better understand the problem of short pitch rail corrugations. This literature review material was organised and summarised to better understand the breadth and depth of the problem and the latest developments in attempting to derive a solution. From here the gap was identified in the body of knowledge and the hypothesis was developed,

- Field work was conducted to validate corrugation wavelengths against those measured in the previous study by the author [10]. Rail corrugation amplitudes were measured on a chosen test site and were confirmed twice in a space of six months,
- Experimental work was planned, experimental modal analysis was conducted in the field on a D39 200 locomotive traction wheelset coupled to a traction motor and installed in a bogie. Experimental modal analysis was also conducted on ballasted tracks with the two types of sleepers in concern,
- FRFs were obtained from experimental work, organised and analysed,
- Corrugation frequencies per track curve were matched with natural frequencies of the D39 200 locomotive traction wheelset, on which a modal test was conducted with the wheelset coupled to a traction motor and installed in a bogie,
- Modelling work was planned, the problem was modelled using the D39 200 locomotive traction wheelset and rail tracks installed with the two types of sleepers in concern. Simulation results were obtained, organised and analysed,
- Experimental results were validated against modelling results and conclusions were drawn.

## 1.6. Research scope

This thesis focuses primarily on associating the dynamics of the wheelset-track system with the formation of short pitch rail corrugation. The difference in track dynamics for tracks with concrete and steel sleepers is investigated. Only the vertical excitation is assumed to arise from vertical corrugation, whilst the lateral and longitudinal which are assumed to arise from creep or slip are not studied in this work. The current research study covers the following:

- To observe differences in the terrain and track construction at corrugated curves with concrete and steel sleepers; this entails observing the extent of track damage in terms of rail pads, rail clips, settling of ballast and displacing sleepers due to excessive vibrations,
- To measure corrugation amplitudes in the test curve 178/1 and wavelengths around the rest of the test points with clearly visible corrugation. This was done to validate corrugation wavelengths measured in the previous study by the

author, and to verify the amplitude on which the short pitch rail corrugation reaches the steady state,

- To perform experimental modal analysis on a D39 200 locomotive traction wheelset and on rail tracks with the two types of sleepers in concern. This was conducted to obtain the point FRFs, in order to analyse and better understand the dynamic response of tracks and the D39 200 locomotive traction wheelset,
- To conduct modelling of tracks with the two types of sleepers in concern and for the D39 200 locomotive traction wheelset,
- Matching corrugation-borne frequency per track curve, with the natural frequencies of the D39 200 locomotive traction wheelset, tested whilst coupled to a traction motor and installed in a bogie.

### **1.7. Research limitations**

This current study is limited to the scope outlined in subsection 1.6. and the following further limitations apply:

- The research only focuses on the Belfast to Steelpoort rail track line that runs through Ohrigstad, that is a 223km (two hundred and twenty three kilometer) rail track line,
- In terms of modal tests, the test curves with concrete sleepers located at kilometer points 178/3 and 187/13 installed with the FY-type and PY-type sleepers respectively were used. A track curve 181/6, with steel sleepers, was randomly selected for field work purposes,
- The current study does not look into microstructures, chemical composition and/or metallurgy of the rail and wheel materials,
- Only the D39 200 locomotives class is considered in the current study, given that it is the only class of locomotives that operated at the Belfast to Steelpoort line at the time the problem was first pursued,
- In terms of rolling stock, modal analysis is conducted only on locomotive wheelsets and not on wagons' wheelsets. This is because locomotives are understood to have a greater influence on corrugation formation than wagons – given the fact that locomotives run on rigid frame bogies, and they are also associated with traction. Justification of this limitation is further explained in Balekwa's work [10],

- Natural frequencies of the D39 200 locomotive wheelset are only studied on a traction wheelset suspended away from the ground, even though installed in a bogie for experimental work. This is done to prevent critical damping of the traction wheelset,
- Results obtained and conclusions drawn in the current study are only limited to short pitch rail corrugation that forms only on ballasted tracks.

## **1.8. Research contribution**

The current research study contributes to the body of knowledge with the following efforts:

- Investigating the association of the dynamics of the wheelset-track system with the formation of short pitch rail corrugation on different sleeper materials.
- The wheelset static model on a three-layered ballasted track with monoblock concrete sleepers is novel. Even though most of the railways around the world are constructed with ballasted tracks [36], most conventional dynamic and static models are on floating slab tracks,
- The wheelset static model on a ballasted track with steel sleepers is novel. Most conventional dynamic and static models involve concrete bi-block sleepers,
- The complex eigenvalue method in modelling a three-layered ballasted track is novel. The complex eigenvalue model used as the case study involves bi-block concrete sleepers in series and four wheels arranged in series,
- The method of modelling a three-layered volume to represent a track ballast with different stiffnesses in ballast layers is introduced in the literature by this study,
- Lastly the simplified method to match vibration modes of the traction wheelset to corrugation frequencies per track curve is introduced in the literature.

## **Chapter One Summary**

This chapter comprehensively summarises the background and introduces the problem of short pitch rail corrugation on the affected track curves under investigation. It summarises what the possible causes are and how the problem presents itself. The research problem statement, questions, hypothesis, objectives, scope, limitations,

approach and contribution are outlined. This chapter concludes by presenting a thesis layout.

## 1.9. Thesis layout

Each chapter starts by giving a description of what is addressed, followed by significant results and/or observations thereof where necessary. The details relevant to each chapter are outlined, explained in the body of the chapter and the chapters close by summarising the details in the body of each particular chapter. The thesis chapters are as follows:

- **Chapter two:** This chapter reviews the relevant literature in detail and shows how the problem has been described and studied. The literature containing the detail where short pitch rail corrugation is modelled, is also presented. Three case studies are presented in the chapter. This chapter follows by pointing out the proposed solutions to short pitch rail corrugation and indicates what is being done currently in the short pitch rail corrugation research space. The gap identified in the body of knowledge is pointed out.
- **Chapter three:** This chapter discusses materials used in the current research and different methods adopted in the effort to investigate significant components of the problem.
- **Chapter four:** This chapter outlines experimental modal analysis on railway wheels and summarises the discussion of results thereof.
- **Chapter five:** This chapter outlines experimental modal analysis on railway tracks with steel and concrete sleepers. The chapter further summarises the discussion of results thereof.
- **Chapter six:** This chapter outlines the FEA modal analysis on a railway wheelset and summarises the discussion of results thereof.
- **Chapter seven:** This chapter outlines FEA complex eigenvalue analysis on railway tracks with steel and concrete sleepers. The chapter further summarises the discussion of results thereof.
- **Chapter eight:** This chapter discusses the implications of the current study and draws conclusions based on findings in the current study.

The next chapter outlines the review of related literature and the case studies relevant to the current study.



## Chapter Two

### Literature Review

*How has the short pitch rail corrugation been studied and modelled; and what are the accepted phenomena causing it?*

In this chapter the history of rail corrugation study is reviewed. The chapter focuses on the recent advances in theoretical models to understand the formation mechanism of the short pitch rail corrugation in the recent years. The chapter further discusses some drawbacks of these models, and the measures adopted currently for curing rail corrugation globally. This detailed review first gives a broad overview of the formation of short pitch rail corrugation. It then presents why and how the short pitch corrugation wavelengths are sustained on rails. After which it narrows down by presenting how the short pitch rail corrugation has been modelled through the use of static and dynamic (wheels, wheelsets, rails and track) models. The common causes of the formation and sustaining of corrugation wavelengths on rails are discussed in detail. The existing gap in the accepted literature is pointed out, which the current study addresses. The next subsection outlines information on the behaviour of rails in general.

#### 2.1. The Behaviour of Rails

Two annoyances come to mind when one considers how rails behave in service during train pass, and those are noise and vibration. In some instances, the two annoyances in the wheel-rail system can be interrelated. This is given that apart from the rolling noise caused by vibration in the system, other noise can emanate from the corrugation-borne P2 resonance, rail joints, wheel flats and etcetera. [37 – 39]. The P2 resonance is defined as a resonance of an unsprung mass (i.e. a wheel in this case) bouncing on the contact stiffness of the rail [40].

The smoothness of a railway wheel makes no difference, when a wheel rolls on a rail, vibration will be excited in the system [41]. Vibration waves will occur in different

frequencies and some with wavelengths which can cause rail corrugation [39]. The blame for wheel-rail rail noise and vibration spread equally between the wheel and rail. This is given that a slight roughness on the one can excite resonant vibration on the other, based on the dynamic properties of each one of the two [39]. A typical circumstance is that of train wheels which apply brakes using brake blocks made of cast iron. These types of wheels usually have a large roughness of typical wavelengths of 40 – 80mm [39]. Thompson [39] suggests that such a roughness excites frequencies at which rail track vibration radiates most of the sound. Under this circumstance neither the wheel nor the rail is to blame, but the system at its entirety [39].

Vibration of the rail occurs in all kinds of rail tracks, including tram tracks, railway lines where cargo trains travel, in high velocity trains environment etcetera [42]. The higher the train velocity, the more the vibration excited [42]. Vibration of the rail is varying along its length, hence some parts of the rail have vibration dying out faster than others and this is commonly known as vibration decay rate [39]. A higher vibration decay rate results in a shorter effective radiating length of the rail, hence less noise radiation [43]. Different mode shapes will occur over a different ranges of vibration frequencies. Figure 2.1. shows typical modes shapes of the rail under vibrational excitation

The full track resonance is the lowest possible resonant frequency of a track structure in the vertical direction, with both out-of-phase and in-phase vibrations [44]. As seen in Figure 2.1. the full track resonance vibration is dependent on vibration of the sleepers. For a good quality ballasted railway track that is still in its good condition, the first order full track resonant vibration occurs in the frequency range of 40 – 140Hz [44].



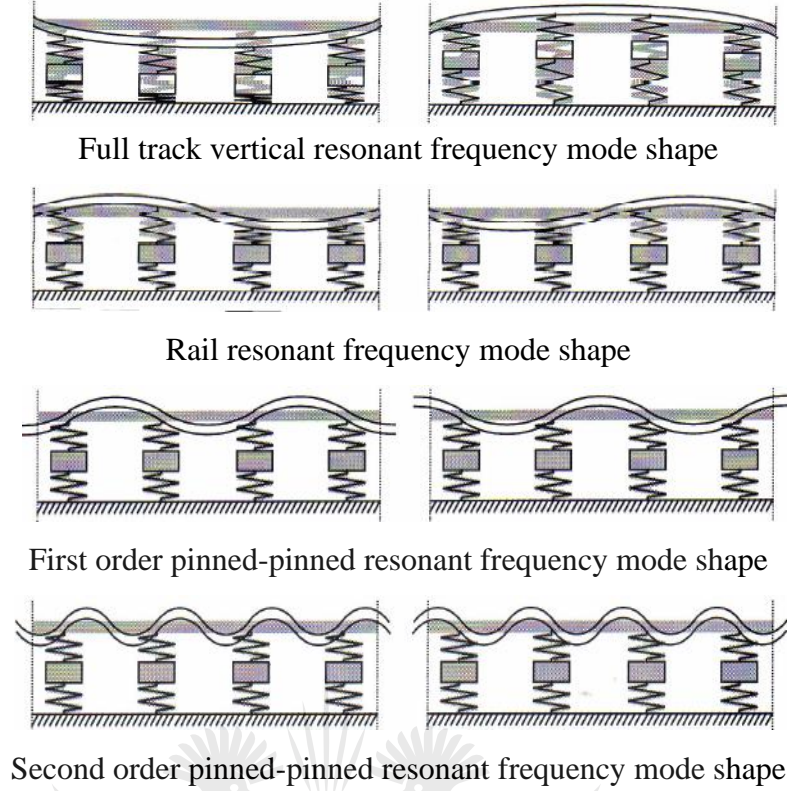


**Figure 2.1.** Rail mode shapes under vibrational excitation.  
Reprinted from [45].

This is followed by the second order resonant vibration in the frequency range of 100 – 400Hz and the third order resonant vibration that occurs in the frequency range of 250 – 1500Hz [44]. As well, the rail resonant frequency exists in the track vibration system. This is a resonance frequency at which the sleepers remain in position, whilst the rail undergoes different vibration mode shapes as seen in Figure 2.1. Here vibration modes of the rail are influenced by properties of the rail pads [45]. This vibration mode is not dependent on properties of the track ballast and sleepers [45].

The pinned-pinned mode is dependent on the sleeper bay (spacing between two sleepers), hence it is likely to occur at higher resonant frequencies. Pinned-pinned resonance mode refers to a sinusoidal bending vibration mode shape of the rail as an infinite body on top of fixed sleepers as seen in Figure 2.1. For the pinned-pinned resonance mode, the wavelength increases as the sleeper bay increases and the frequency of the pinned-pinned resonance mode can be calculated as:

$$f = \frac{\pi}{2L^2} \sqrt{\frac{EI}{m}} \left[ 1 - \frac{1}{2} \left( \frac{\pi r_g}{L} \right)^2 \left( 1 + \frac{2(1+\nu)}{K} \right) \right] \quad (2.1)$$

where  $m$  and  $EI$  are the mass of the rail per unit length and the bending stiffness respectively,  $L$  is the sleeper bay,  $r_g$  is the radius of gyration, and  $K$  ( $\approx 0.34$ ) is the shear constant of the cross section [46]. The frequency of this type of resonance is significantly higher than those of wavelength fixing mechanisms. This is given that it produces shorter wavelengths at a given train velocity [46].

The first pinned-pinned resonant mode occurs at a frequency range of 400 – 1200Hz and the second mode at frequencies slightly four times higher [45]. A slight rail displacement is experienced by the rail on a train pass. This displacement occurs in the horizontal and vertical directions. The horizontal displacement is influenced by the wheel-rail lateral forces and the train velocity [45]. The vertical displacement may also be influenced by a few vehicle-track dynamics. In his doctoral thesis, Suiker [47] points out the influence of a train velocity on the vertical displacement of the rail [47]. Figure 2.2. shows the relationship between a train velocity and rail displacement. Here data is measured and reported for two types of trains.

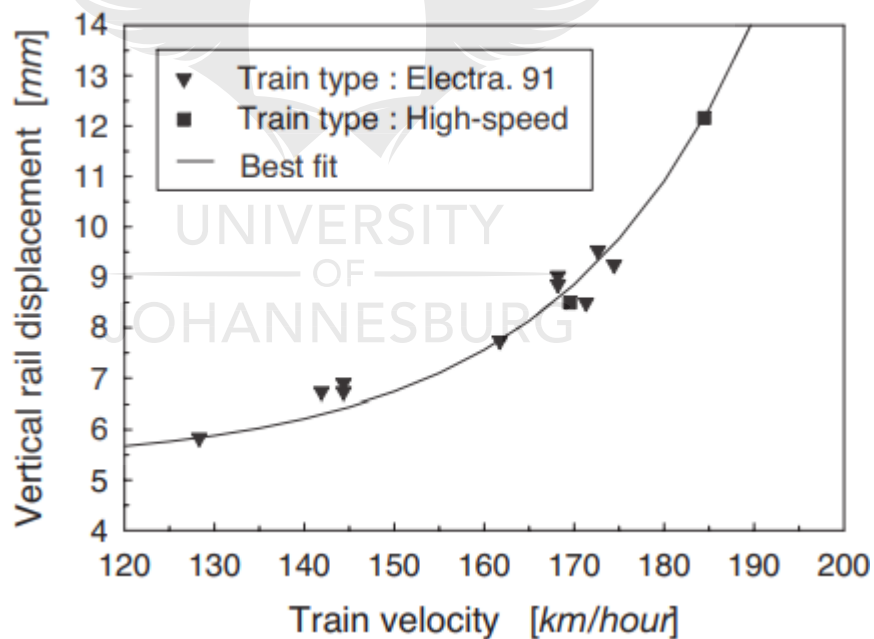


**Figure 2.2.** Displacement of rail in the vertical direction at different train velocities. Measurements taken at Stilton Fen, England, January to May 1993. Reprinted from [47].

It is noted in the quadratic curve in Figure 2.2. that there is a nonlinear increase in the vertical displacement of the rail as the train velocity steadily increases. Apparently, the rail experiences a significantly increased vertical displacement with the increase

in train velocity, such that when the train velocity approaches 180km/h, the rail vertical displacement reaches a magnitude of 12mm [47].

A good quality rail track is a prerequisite for better reliability. In a rail track design, various parameters are determined in order to produce a good quality track, including a rail gauge. A rail gauge is a length from a gauge corner of one rail to the gauge corner of the opposite rail. A rail gauge plays a crucial role in ensuring a better guidance of a train wheelset in transit [10]. However, as a wheel rolls on the rail, the wheel-rail lateral forces ultimately shift the rail away from its vertical plane, forcing the rail gauge to widen, hence the term rail gauge deviation [10]. Smaller radius curves suffer the most from rail gauge deviation, due to severe wheel-rail lateral forces [48]. Figure 2.3. illustrates the rail gauge deviation.

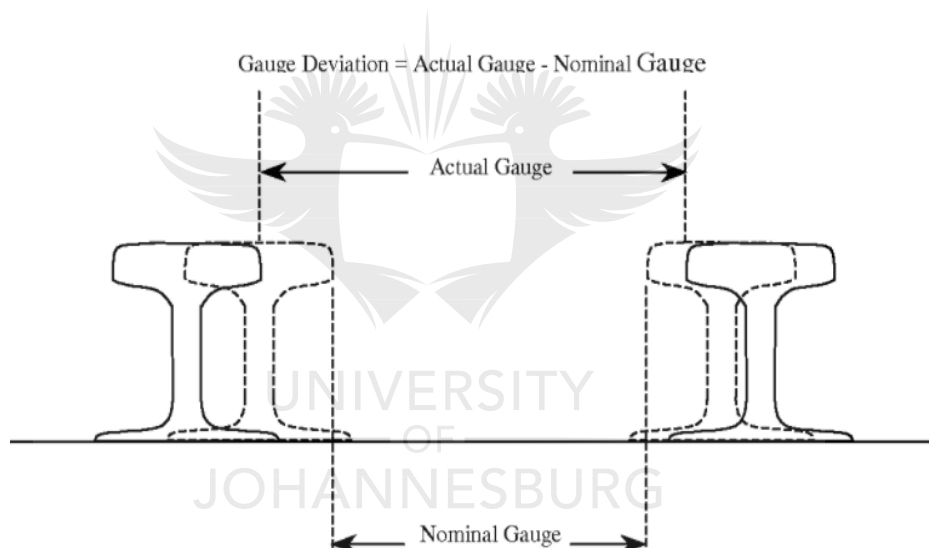


**Figure 2.3.** Illustration for rail gauge deviation.

An increase in train traffic results in inevitable rail gauge deviation. Rail gauge deviation poses a risk of increased train derailments and is also a contributor to the high costs of track maintenance [49]. The next subsection outlines details on the analytical modelling of rail corrugation.

## **2.2. Analytical Models of Rail Corrugations**

Neither the wheel nor rail running surface is entirely smooth when newly manufactured. This leaves a possibility for the dynamic excitation of the vertical wheel

load, hence a change in the initial longitudinal profile of the rail. A dynamic vertical wheel load may be excited whenever an irregularity on the running surface exceeds a depth of 0.01mm, or its wavelength exceeds the contact point dimensions [22].

The dynamics of rail tracks involving concrete material can be significantly linked with the formation and development of rail corrugation [50]. A study by Daniel et al. [50]. investigated corrugation growth rates between a rail track with concrete sleepers and another with wooden sleepers. Here it was found that the growth of rail corrugation is higher on the rail track with concrete sleepers [50].

Gómez and Vadillo [51] pointed out an important observation in their study, that a ballasted rail track which was not corrugated initially, formed short pitch rail corrugation after a spontaneous replacement of the track with the concrete slab type (STEDEF) [51]. It is also important to note that here the sleeper spacing was enlarged from 600mm to 1m. The authors also concluded based on their observations from measurements, that short pitch rail corrugation actually starts forming mid-span first, before spreading to the entire running surface [51].

Rail corrugation also forms on the narrow gauge tracks [52]. Ishida et al. [52] found the lateral force to have a significant influence on the formation of rail corrugation in a narrow gauge track and the effect was reduced with lubrication of the low rail [52]. Afferrante and Ciavarella [53] developed a model based on contact mechanics, which takes into consideration wheel inertia, tangential load, normal load and longitudinal creepage. Here it is found that rail corrugation growth is accelerated as the tractive ratio increases, hence the authors point out the accelerated growth of rail corrugation to be linked with the starting and stopping conditions of a railway car [53].

In another work, Afferrante and Ciavarella [27] introduced a possible mechanism in the longitudinal direction, which has not been explored by other researchers before. This mechanism is not related to wheel-rail resonance, not even the pinned-pinned resonance, but it is rather found to be related to wheel-rail geometrical and loading conditions (i.e. shape of the contact area, creepage ratio, normal and tangential loads, etcetera.) [27]. Wen et al. [54] developed a numerical model to study the effect of scratch on the running surface of the rail during wheel pass. Here the authors showed

that wheel-rail vibration occurs at large amplitudes in the contact point when a wheel runs steadily and repeatedly on the scratched running surface of the rail [54]. This leads to formation and development of rail corrugation induced by plastic deformation [54]. Currently rail corrugation is one of the most serious problems with which railway maintenance engineers and managers are concerned. This is due to the negative impact its results have in the maintenance budget for companies in the railway industry. Results for rail corrugation lead to accelerated degradation of rail car vehicle-track systems and also reduce the lifespan of train and track components [55, 56]. Given that wheels are similar, wavelengths are developed and sustained due to traffic uniformity [14].

A reduction in traffic uniformity reduces the chance of formation (or diversifies the nature) of rail corrugation [14]. In addition, a constant train velocity with consecutive train passes is associated with rail corrugation growth [57]. Theories differ in terms of the relationship between the short pitch rail corrugation wavelengths and amplitudes.

Whilst some researchers, such as Wang et al. [8] find the short pitch rail corrugation amplitudes to increase with an increase in a wavelength, other researchers, such as Jin et al. [58] find the case to be the other way around. Any kind of irregularity on the surface of the wheel and/or rail may initiate corrugation. On a lighter note, the short pitch corrugation does in fact form even on railway wheels. This is referred to as “wheel polygonisation” and researchers are active in developing models to describe and predict the phenomenon [59, 60]. However, polygonised wheels are found to have a negligible influence on the formation of rail corrugation [61]. Due to annual increase in targets to move cargo to the seaports and within the land, in the recent years the railway industry realises a need for increased axle loads for railway wagons and train lengths.

As gradual increases in targets are realised annually, the need for increased train velocities also arise, hence pressure increases on the railway operators to improve their track systems’ capacity. In addition, these changes in railway operations also see railway operators experiencing a rise in railway train and track damages, including rail corrugation [62, 63].

In contrast to the finding that rail corrugation in the Belfast to Steelpoort railway track formed only on curves, particularly on the low rail of track curves, this phenomenon is explained in the recent literature to occasionally form on tangent tracks [64, 65]. This is also seen in the study by Duan [66], where rail corrugation formed on a tangent tram track.

From a layman perspective, it would be expected that corrugation form with a higher rate on tighter rail track curves and should be more visible to a naked eye. Wu et al. [67] explains it to be an extremely common phenomenon that rail corrugation is almost 100% guaranteed to form on the inner rail of track curves with a curve radius less than 350m. The authors explained the phenomenon to barely form on track curves with a radius greater than 650m [67]. Jin and Wen [68] developed an experiment to investigate the effect of lateral displacement and the angle of attack of the wheelset on formation and development of rail corrugation. The investigation is conducted for two cases, i.e. when a lateral displacement is 14mm, whilst the angle of attack is  $0^{\circ}$  and when the lateral displacement is zero, whilst the angle of attack is  $0.43^{\circ}$  [68]. For both cases the test velocity was 50km/h. The results showed that rail corrugation formed from the effect of the angle of attack is more severe than that formed by the lateral displacement of the wheelset [68]. This finding is in better agreement with the proposition from Wu et al. [67] in a sense that the angle of attack in tighter curves will be more severe for smaller radius track curves. In some parts of the world the short pitch rail corrugation has affected almost the entire rail network, such as China and others [69].

In such countries it is common for this short wavelength phenomenon to also form on tangent railway tracks [69]. In some cases the phenomenon affects both the high and low rails of a track curve [70]. In such cases it is normally found on the running surface of the low rail and forms as a uniform wear on the side of the high rail [70]. In the recent study by Cui et al. [71] this enigma is found to have formed early on the high rail and looks more severe than that on the low rail.

When a wheel rolls on a rail, the wheel and rail exchange interaction forces in a wheel-rail contact patch, and the dynamic loads occur, which ultimately initiate rail

corrugation [72]. Dynamic loads occur even from rolling of a new wheel on a new rail, due to rail track configuration, given that sleepers are supporting rails with a specific sleeper spacing [72].

Jin et al. [73] explained discrete sleeper spacing, for sleepers supporting a rail to be an inherent defect that leads to the formation of rail corrugation. Sleeper spacing of the rail track used in the current study is 700mm. According to the study by Ng et al. [74] from which rail corrugation growth is modelled, the sleeper spacing of 700mm leads to higher rail corrugation growth rates. Here the authors proposed a sleeper spacing of 500mm in order to prevent high corrugation growth on rails [74]. The stiffness of each sleeper is also one of the important parameters to consider in aiming to suppress rail corrugation. According to Chen et al. [75] more suppression of the formation of rail corrugation is realised when the sleeper stiffness is reduced.

Wang et al. [76] pointed out the difference between vibration receptance of rail and wheel to be important in attempting to reduce corrugation growth on rails supported on discrete support tracks. Wheelset hunting, angle of attack, lateral creepage and vertical loading form part of several models developed to address the enigma [77 – 79].

When a wheelset negotiates a track curve with the highest angle of attack during vehicle hunting, the wheel-rail lateral creepage oscillates at a frequency of sleeper bay, and hence corrugation forms due to rail wear [77 – 79]. Different types of sleepers are spaced differently on different types of track arrangements. These include short sleeper track, elastic short sleeper track, ladder sleeper track, vibration absorber fastener track, etcetera [80]. However, even in cases where sleepers would represent a uniform base for riding, that would possibly open up another door for an additional problematic mechanism. This is due to the fact that in the recent literature, rail corrugation is also found to form on slab tracks and tram tracks in urban areas [81, 82]. After corrugation forms, a corrugation-induced frequency excited on a train pass is dependent on a train velocity [83]. When this frequency is close enough to the natural frequency of the wheel-rail system, the wheel-rail contact force frequency amplitude rises to maximum [83]. Interestingly, in better agreement with the current study, the bending dynamics of a railway track also have influence in the formation of



rail corrugation. In fact, resonance of a track structure affected is even of great importance in investigating how rail corrugation initiates, its characteristics and how it develops [84].

A resonance phenomenon of a railway track structure forms rail corrugation at a corresponding frequency [85]. In a recent study by Yin and Wei [86], the first and second-order lateral bending of a circular curve of a rail track were found to be associated with the formation of rail corrugation [86]. Resonance vibration of railway track components is one of the important problems linked with rail corrugation, including resonance of rail fasteners [87, 88]. Railway track vibration becomes severe as wheel-rail irregularities such as wheel flats and rail wear occur, which can ultimately promote the formation and development of rail corrugation, from which severe ground-borne vibrations occur [89]. Isolation of rail track vibration is increasingly seen to be important in the railway industry, given that resonance of railway track is increasingly being found to form important part of the wavelength fixing mechanism [32].

Kaewunruen et al. [90] advanced highlights for strategies that can be practicable in isolating railway track vibrations. Although the shock absorber type of rail fasteners is considered as one of the most effective countermeasures in preventing ground-borne vibrations, this measure is found to promote the formation of corrugation on rails [91].

Almost all researchers active in the rail corrugation research space focus on a mechanism for the formation and development of the enigma. In the contrary, Ling et al. [92] developed experimental and numerical investigations to assess the level of damage caused by corrugation-induced vibration on railway bogies. This study focused particularly on the coil springs. Here it is found that short pitch rail corrugation causes a significant reduction in the fatigue life span of the coil spring [92]. The authors further found that an increased damping ratio in the vertical dampers of the primary suspension will significantly reduce the corrugation-induced vibrations to which the railway bogies are subjected [92]. Even though the outcome of the study by Jin et al. [93] is in agreement with this finding, the authors pointed out that the impact of corrugation induced vibration is more significant on the wheelset-track dynamics, than on the bogies and rail car [93].



When rail corrugation already grew to steady state, nothing more can be done to get rid of it, except removing its troughs through rail grinding. However, measures can be effected to alleviate the severity of its impact on rail cars. Zhou et al. [94] developed a model to study the influence of resilient wheels on wheel-rail dynamic interaction during wheel pass on a corrugated section. The results show that resilient wheels installed with a rubber material, in a layer between the wheel rim and web reduce the vertical wheel-rail dynamic loads excited by rail corrugation [94]. The authors point out that this is applicable to a large frequency range [94]. In the contrary, Bionda et al. [95] pointed out in their study that rail corrugation found in one of the subways in Italy may have been associated with interaction of the rail track with a rail car installed with resilient wheels [95].

Wheelset spacing in a bogie has influence in resonance vibration of vehicle-track system, which in turn plays a role in rail corrugation growth [96]. Wang and Wu [97] developed a model involving investigation of the influence of vibration interference between vibrations of two wheels on rail corrugation. The authors found that vibration interference between two wheels can cause radical fluctuation of the wheel-rail contact force, which in turn can form rail corrugation [97]. In addition, the authors [97] found that wavelengths of this rail corrugation are equivalent to unit fractions of the wheelbase. Wheel-rail resonance emanating from train braking also plays a role in the formation of rail corrugation [33]. Wu et al. [98] conducted an investigation on rail corrugation in one of the downhill rail sections in China, where braking is applied by trains. After the rails were ground and braking was not applied by trains, rail corrugation did not form on the rails [98]. From this study the authors found that rail corrugation is associated with wheel-rail vibration of around 430Hz, which emanates from shoe brakes used by trains [98]. Generally, different rails show different characteristics related to rail corrugations [99].

Some researchers such as Grässie and Kalousek [14, 28, 31]. have put much effort into analysing from the theoretical point of view, how the corrugation phenomenon generates and also pointing out the possible treatments. Grässie and Kalousek also conducted much work into categorising rail corrugation by wavelengths and categorising it by different initiators [14, 28, 31]. Six types of rail corrugations were pronounced from the work; i.e. heavy haul, light rail, contact fatigue, booted sleeper,

rutting and roaring rails. The primary difference in the formation of corrugation on rails rests in two mechanisms i.e. the damage and the wavelength fixing mechanisms. The damage mechanism is associated with initiators of corrugation; the commonly considered which is wear [100]. Another possible damage mechanism being plastic deformation [101].

Böhmer and Klimpel [18] considered both plastic deformation and wear in their study, which showed that both wear and plastic deformation will lead to formation of rail corrugation to steady state [18]. The wavelength fixing mechanism is associated with wheel-rail resonances, more in particular the P2 resonance [26, 102]. The damage mechanism and the wavelength fixing mechanism are interrelated and maintain a feedback cycle during the formation and development of corrugation on rails [71]. Figure 2.4. shows the feedback loop for rail corrugation and the wavelength fixing mechanism.

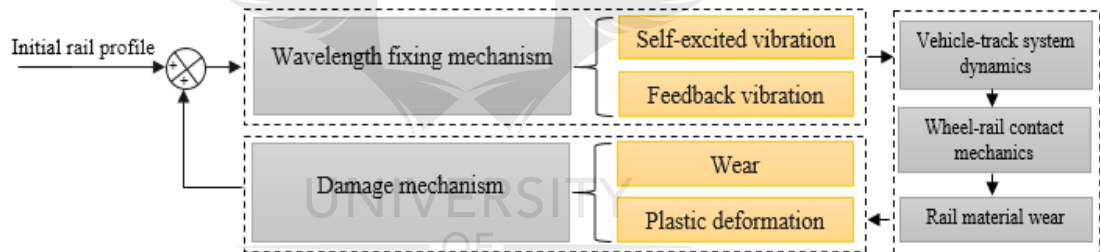


**Figure 2.4.** Feedback loop for generation of rail corrugation.

Figure 2.4. shows a feedback loop for the formation of rail corrugation, whereby a newly manufactured rail is installed with an initial rail profile. Given that the rail is not entirely smooth, a slight vibration will always occur in the wheel-rail contact point, which emanates from frictional self-excited dynamics of the wheel-rail system (self-excited and feedback vibration). From this genesis of dynamics, the vehicle-track system resonance is excited [31]. Given that vertical dynamic loads, lateral creepage, a tighter angle of attack and stick-slip oscillations exist during wheelset motion, the complex wheel-rail contact mechanics ultimately lead to rail material wear and/or plastic deformation [31].

Wear of rails is the commonly understood damage mechanism. Once rail wear or plastic deformation occurs on the running surface of the rail, a new rail profile is initiated [31]. The dynamic loads from the rail damage and the self-excited dynamics begin the process afresh, until the loop is closed once more. The next sub-subsection outlines the types of corrugations forming on rails as reported by Grässie and Kalousek [31].

### **2.2.1. Rail Corrugation Types**

Different types of rail corrugations form on various railway tracks. The dependency lies on several factors influencing its formation, such as train velocity, track geometry parameters, vehicle-track interaction, and etcetera. An outline (according to Grässie [31]) of each corrugation type is provided as follows:

#### **2.2.1.1. Heavy Haul Corrugation**

The term “heavy haul” says it all; this type of corrugation was found on heavy haul railway lines [31]. This type of rail corrugation is mostly found in straight tracks and also on the high rail in track curves [31]. It is also found to form due to the same mechanism on the low rail of tracks with excessive super elevation, where mixed traffic operate with significantly lower axle loads than the heavy haul traffic [31]. This type of corrugation forms due to plastic bending of the rail [31].

#### **2.2.1.2. Light Rail Corrugation**

The light rail corrugation is much similar to the heavy haul type. This type of corrugation propagates from improper welds and fixes wavelengths between 0.5 – 1.5m [31]. One difference between this type of corrugation and the heavy haul is that the light rail corrugation does not form due to plastic bending, as in the case with a heavy haul [31]. One of the important primary treatments for this corrugation type is the straightening of welds and joints; which ultimately reduces the impact of P2 resonance [31].

#### **2.2.1.3. Rutting Rail Corrugation**

This type occurs on the running surface of the low rail of a curve [31]. It has a potential of forming on a tangent track where traction and braking are severe [31]. This type of corrugation forms due to irregularities such as improper welds and joints [31]. It manifests itself with more uniform wavelengths on the rail running surface [31]. Debris of rail wear from this type of rail corrugation is easily visible to a naked eye [31]. It forms due to the torsional vibration of the wheelset mostly at a second torsional vibration frequency range of 250 – 400Hz [31]. A frequency of 250Hz occurs at a typical train velocity of 45km/h and fixes wavelengths of around 50mm. Wear is however the primary damage mechanism [31].

#### **2.2.1.4. “Roaring Rails” Rail Corrugation**

This type of rail corrugation occurs primarily in tangent track and also in long radius curves on which there is minimal wheel-rail flange contact on curving [31]. It mostly forms on the high (than the low) rails for traffic lines with lighter axle loads (of somewhat less than 20ton per axle) [31]. Amplitudes of this type of rail corrugation are easily removable with a grinding trolley at slow moving velocities [31]. This type of rail corrugation is also referred to as a “pinned-pinned” rail corrugation [31].

#### **2.2.1.5. Other P2 Resonance Rail Corrugation**

Other corrugation types fall under the P2 resonance rail corrugation [31]. For these rail corrugations the primary damage mechanism is wear and the wavelength fixing mechanism is the P2 resonance [31]. The next subsection outlines how rail corrugation is categorised per damage and wavelength fixing mechanisms.

### **2.3. Rail Corrugation Categorisation**

Grässie and Kalousek [28] discovered that for any corrugation type, if the damage mechanism proves to be a plastic flow, it is likely that the wavelength fixing mechanism responsible for fixing that particular corrugation will be a P2 resonance

[28]. Table 2.1. shows a list of different wavelength fixing mechanisms associated with the respective damage mechanisms.

**Table 2.1.** Wavelength fixing mechanisms associated with damage mechanisms [14]

<b>Damage mechanism</b>	<b>Wavelength fixing mechanism</b>
Gross plastic flow	P2 resonance
Plastic bending	P2 resonance
Contact fatigue	P2 resonance
Wear	P2 resonance, Axle wind –up, Pinned-pinned resonance, Resiliently booted sleepers, Resonance of concrete sleepers.

In Table 2.1. it is noted that the damage mechanism, wear, is associated with all wavelength fixing mechanisms. This validates the conclusion by the accepted literature that wear is the most common damage mechanism, for all types of rail corrugations [31, 40]. The wavelength fixing mechanisms are associated with different corrugation frequencies, which are influenced by average train velocities on corrugated sections of a rail [10, 103]. It is also noted in Table 2.1. that a P2 resonance is associated with all damage mechanisms. Rail wear has proven to be the only culprit accountable for the formation of rail corrugation in the Belfast to Steelpoort railway track [10]. Table 2.2. shows the most likely wavelengths for different types of rail corrugations. The Table 2.2. also shows the damage and wavelength fixing mechanisms associated with each corrugation type amongst the six [28].

**Table 2.2.** Wavelengths and mechanisms associated with rail corrugation types [28]

<b>Type</b>	<b>Wavelength (mm)</b>	<b>Wavelength Fixing Mechanism</b>	<b>Damage Mechanism</b>
1. Heavy haul	200 – 300	P2 resonance	Plastic flow in troughs
2. Light rail	500 – 1500	P2 resonance	Plastic bending

3. Booted sleeper	45 – 50 51 – 57	Sleeper resonance; flexural resonance of a wheelset	Wear of troughs from lateral oscillation; plastic flow of peaks
4. Contact fatigue	150 – 450	P2 resonance laterally	Rolling Contact Fatigue
5. Rutting	50 200 150 – 450	Torsional resonance of wheelset; Peak vertical dynamic force; for example, P2 resonance	Wear of troughs from longitudinal oscillation
6. Roaring rails	25 – 80	Unknown	Wear of troughs from longitudinal slip

The average typical train velocity on track curves in the Belfast to Steelpoort railway track is 30km/h for both empty and loaded trains [10]. The average corrugation wavelength measured on this line is 80mm [10]. According to the information in Table 2.2. the type of corrugation associated with wavelengths between 25mm – 80mm is referred to as “roaring rails”, which is another word for short pitch rail corrugation [25].

The characteristic frequency excited by a short pitch rail corrugation can be derived from a rail car velocity and corrugation wavelengths [104]. If a train velocity is known, the excitation frequency to the running train (referred here as the “corrugation-borne frequency”) can be calculated as follows:

$$f = v / \lambda \quad (2.2)$$

This is normally a useful method to identify a corrugation source on a railway track [105]. When a train runs at velocity “v”, over a corrugated section with the wavelength “λ”, vibration occurs (hence the radiation of noise, besides the wheel squeal), with the frequency “f”. Corrugation-borne frequency can easily be confused with the wheel-rail natural frequencies. However, every structure has its own natural

frequency at which it vibrates when excited, whilst the corrugation-borne frequency is the frequency experienced by a railway car when running on a corrugated section [10, 106]. A rail track can be modelled as a periodic structure, which makes it easier to calculate its free vibration characteristics, which include resonance frequencies, mode shapes and vibration decay rates [107]. The results from such analysis can be used as significant input parameters to analyze a forced vibration of a track structure, or to better understand the mechanisms involved [107]. In their study on the influence of rail corrugation on rail vehicles, considering safety and ride quality, Skorsetz et al. [108] found that it is not the train velocity that dominates safety, but the factors concerning geometry, that determine the number of wheel-rail contact points [108].

Generally, different modes of vibration are excited at different frequency ranges. For instance, the “pinned-pinned” and torsional modes are excited at very high frequencies above 1000Hz [109]. The pinned-pinned resonance mode of a track occurs when a train passing frequency is close enough to the pinned-pinned frequency of the rail [110]. The author in the current study proposes that in addition to the P2 resonance, the axial bending mode of the locomotive wheelset are associated with corrugation on rails in the Belfast to Steelpoort railway track [32, 111]. Given lower train velocities around corrugated sections, the wavelength fixing mechanism on this railway track was found to be the axial bending of the traction wheelset at the corrugation formation frequency of 108Hz [10, 103].

In the current study this frequency (108Hz) is important and emphasis is put more to it in analysis of the results. Here the frequency range of 0 – 150Hz is of concern in terms of vibration induced by trains [112]. The next subsection outlines the treatment methods widely used to curb formation (and the impact) of rail corrugation.

## **2.4. FEA and Mathematical Modelling of Rail Corrugation**

Just over the past two decades, researchers have steered attention into developing several versatile mathematical models for rail roughness growth, in consideration of the interaction between the wheelset and track [113]. Some of which involve advanced wheel-rail contact approaches [100, 114]. The non-Hertzian models have been considered in some cases [115, 116].

Likewise, there is also a consideration of the contact-induced wear filtering and the effects thereof on developing corrugation [117]. A significant effort came in the year 2009 from Torstensson and Nielsen [118] in studying the irregular wear on the running surface of the rail and the monitoring thereof. Apart from this, the influence of discrete supports is understood to be significant in the formation of rail corrugation [119, 120]. In addition, some of the models considered multiple wheel-rail interactions [121, 122]. Rail corrugation has always been understood to form due to different transient conditions favouring certain wavelengths, however, in the recent work, the self-excited vibration is found as another possible source that may lead to the formation of rail corrugation formation [2, 23, 123, 124].

Grässie et al. [125] developed a simple model of a wheelset resting on rails to investigate the dynamic response of the wheel and rail in excitation on a frequency range of 50 – 1500Hz in a contact point. Here the contact point is excited in the vertical, lateral and longitudinal directions to study the dynamic contact force that results. The vertical excitation is assumed to arise from vertical corrugation, whilst the lateral and longitudinal are assumed to arise from creep or slip [125].

At natural frequencies that involve bending of the wheelset axle, the results show the dynamic contact force caused by corrugation to have same characteristics in all three directions [125]. However, in terms of magnitude the dynamic contact force is low for the vertical, half the magnitude (of the vertical) in the lateral, and at maximum in the contact resonance longitudinally [125], from which it is evident that the dynamic load is the lowest in the lateral direction. This is consistent with the emphasis by Collette and Preumont [102] on rail corrugation forming mostly where the dynamic loads are low. The results from the previous work by the author are also consistent with the observation [10]. Rail corrugation normally forms where large magnitudes of contact forces and sliding of the wheel relative to the rail occurs [33, 126], the severity of which increases on smaller track curves [127].

Most conventional models for rail corrugation are limited to static simulations. In the contrary, Aalami et al. [128] considered a complete rolling of a wheel in showing that plastic strain as a result of rolling contact forces may form corrugation [128]. In addition, Ekberg et al. [129] developed a mathematical model considering the



dynamics of train-track interaction, including train velocities. From that, corrugation on rails is shown to increase the impact of Rolling Contact Fatigue (RCF), more in particular at high-velocity operations [129].

Predictions that are more realistic may be achieved through well-developed, complex three-dimensional mathematical models. These should consider various dynamic behaviours influencing wheel-rail interaction. However, such models can be extremely time consuming and require extremely high computational power [130]. Some researchers such as Morales-Ivorra et al. [131] developed versatile models that can capture several problems arising from different dynamics of the vehicle-track system [131].

Morales-Ivorra et al. [131] developed a model to assess a derailment risk of two rail cars with different characteristics, negotiating two curves with different characteristics. Even though the study was not predominantly conducted for investigation of rail corrugation, the versatility of the model was found to be so high that it was subsequently used for analysis of other development and propagation of irregularities related to vehicle-track interaction [131]. This included the development of rail corrugation [132].

Different types of sleepers produce different corrugation parameters due to dynamics of the transition section [133]. Cui et al. [134] studied a railway curve with a corrugated low rail. The two types of sleepers are used in the track curve, i.e. the Cologne Egg sleeper and the fixed dual short sleepers. In this study the authors found that on a section where the sleeper type changes from Cologne egg sleeper to the fixed dual short sleeper type, unstable vibration occurs on the low rail of the section supported by the Cologne Egg type of sleepers [134]. This vibration occurs at a frequency of 422Hz on the section supported by the Cologne Egg type and at a frequency of 201Hz at a section supported by the fixed dual short sleeper type [134].

The rail section on the Cologne Egg sleepers fixed corrugation with 40-50mm wavelengths, whilst the section on the fixed dual short sleepers fixed it with 90-120mm wavelengths [134]. When only one type of sleepers is used in the track curve, unstable vibration occurs at 420Hz only, for either type of sleepers [134]. In their rail

corrugation investigation model, Gao et al. [135] pointed out 40kN/mm to be the optimal design magnitude for stiffness of the rail-sleeper fastening system.

In a study conducted by Li et al. [136] this magnitude is set even higher, where the authors pointed out that a vertical stiffness of less than 20MN/mm in the rail fasteners can easily produce short pitch rail corrugation with wavelengths of 30 – 63mm [136]. On a similar model, Chen et al. [137] conducted field measurements on three sites and found three different profiles. Here the track configurations are not explained in detail, however, four different sleeper types are used in the line, i.e. (i) a booted short sleeper (ii) short sleeper (iii) a ladder sleeper and (iv) a floating slab. The three sites had three different fasteners, i.e. type DTV12, DTIII2 and the cologne-egg [137].

A Finite Element (FE) method was used to develop three models to predict corrugation frequencies. Here three complete wheelsets are modelled on top of three rail tracks. Measured and predicted corrugation frequencies were found to be in agreement [137]. Chen et al. [137] concludes that the self-excited vibration of the wheel-rail system leads to corrugation on rails. However, according to Chen et al. [137] the accepted literature has not shown why corrugation forms on almost all low rails of tight curves, whilst it is rarely found on the high rails [33, 149]. Although the author is not in full agreement with the opinion, work to this effect is not sufficient in the accepted literature. Oyarzabal et al. [35] modelled corrugation with consideration of track parameters for slab and ballasted tracks.

Two types of slab tracks (STEDEF and AFTRAV) [35] were modelled. Even though the meaning of acronyms are not provided, one of the most noticeable differences in these two types of slab tracks is that the STEDEF track has two layers of elastic slab levels, whilst the AFTRAV has one layer. Each model involved four wheels of a bogie and considered different track radii and train velocities [35]. It is found in this work that the probability of corrugation formation is the greatest for the inner wheel of the leading wheelset of a bogie [35]. Analysis on the rest of the wheels show less probability [35]. In light of corrugation, the AFTRAV slab track works better, followed by the ballasted track [35]. As far as the dynamics of wheelsets are concerned, the leading wheelset of a bogie remains one of the most important culprits linked to the initiation of rail corrugation [138, 139].

Saulot et al. [140] conducted a study that considers metallurgical and tribological effects in studying the corrugation crests. Here micro-chips symbolising corrugation crests wearing in the direction perpendicular to the rolling direction are observed. Saulot et al. [140] are in agreement with Balekwa's study [10] that found similar micro-chips and their direction to be resulting from the effect of longitudinal and transverse action of the wheel on rail.

Saulot et al. [140] found that the leading wheelset is more associated with these longitudinal and transverse effects. Cui et al. [141] also measured vibration on three points of rails on train pass. This was conducted around track curves and it was found that the oscillation amplitude of vibration and the normal contact force on the low rail are larger than those on the high rail. From this, Cui et al. [141] conclude that the rail corrugation caused by the frictional self-excited vibration mainly occurs on the low rail of sharp curved track [141].

Wu et al. [142] developed two FE models to investigate the effect of axlebox positioning in the short pitch rail corrugation. Here an axle box was modelled inside and outside a bogie frame. The results showed that the inner axlebox type is favourable in terms of rail corrugation suppression [142]. El Beshbichi et al. [143] developed a complex eigenvalue analysis model to predict a frictional self-excited vibration of a leading wheelset travelling around a track curve. Here it has been found that the interaction of the wheel cross section and the track gauge influence the self-excited vibration significantly [143]. In predicting the growth rate of rail corrugation, Meehan et al. [144] developed a simplified analytical and numerical feedback model, which takes into account time delay in wheel pass time. From the model the authors developed an expression that can be effectively used to predict rail corrugation and to identify significant parameters, that influence the formation and development of rail corrugation [144].

Bellette et al. [145] modified the same model developed by Meehan et al. [144] to consider variations in vehicle velocities over successive vehicle passes. This enables corrugation amplitude growth rate to be assessed [145]. Fourie et al. [146] developed a model to investigate a short pitch rail corrugation with wavelengths of 70mm. The model takes into account the first and second order torsional modes of the wheelset

and the traction motor pinion-gear dynamics. Here it is found that when the traction motor-axle gear mesh stiffness is increased from zero to maximum traction, the wheelset torsional modes and traction motor pitching become coupled structural modes, leading to the formation of the short pitch rail corrugation [146]. In terms of modelling the enigma, researchers such as Meehan et al. [147] are considering various effects into the models, including environmental effects.

In one of their studies in Australia, the authors [147] discovered that variations in the rainfall have an effect in rail corrugation growth. Their model takes into consideration the average daily rainfall and humidity, together with rail corrugation growth [147]. The next subsection outlines the experimental work conducted in the rail corrugation research space.

## **2.5. Rail Corrugation Experimental Work**

Experiments are one of the most useful ways of studying rail corrugation. Important results can be obtained from experiments, which can later be used as inputs to rail corrugation modelling. Experiments are also widely used by researchers to discover certain dynamics and outcomes of systems. An example of this is an outcome in a study by Hu et al. [148] where a pin-on-disc experiment was conducted to investigate whether corrugation can also form on sliding surfaces. The results of the experiment showed some formation of corrugation on the sliding surface of the disc [148].

Experimental work on rail corrugation rests in the analysis of the dynamic behavior of the railway track and its components and on the railway vehicle wheels [111, 149]. This type of work involves the use of accelerometers to measure the dynamic response of a structure in different directions (vertically, laterally, longitudinally and circumferentially).

In order to achieve measurable excitation of structures in these directions, suitable models of electronically functioning impact hammers are used [150]. The dynamic response is analysed based on point FRFs. In other experimental work, displacement sensors are employed to measure the displacement of rails and sleepers for different frequency ranges [151].

Liu et al. [152] conducted experimental work for a frequency range of 160 – 310Hz. Here the rail vibration dampers are installed to study their effect on rail vibration response. Corrugation growth rate was monitored for a period of about half a year in the railway track with dampers installed. The corrugation growth rate reduced by more than half [152]. The resonance peaks in the frequency range of 160 – 310Hz shifted to a lower frequency range with the dampers installed [152].

On another work the importance of stiffness of rail pads in the vertical direction is pointed out [153, 154]. In the study conducted in China it was established that particularly the rubber rail pads are effective in controlling short pitch rail corrugation growth [155]. Wu et al. [156] studied rail corrugation in one of the metro lines in China and found that increasing the modulus of elasticity and damping coefficient of the rubber rail pads can prevent the formation of rail corrugation. The authors pointed out in particular the damping coefficient and advise that an increase of 0.0001 on this parameter can yield significant results in preventing the formation of rail corrugation [156]. Song et al. [157] investigated the effect of rail pad stiffness on the wheel-rail dynamic loads and on rail corrugation. The authors replaced the rail pads having the stiffness of 50MN/m with the ones having the stiffness of 35MN/m.

After monitoring the performance of the softer rail pads, the results showed that even though the rail experienced more displacement with the softer pads, corrugation formation was significantly eased and a significant reduction in the wheel-rail dynamic loads was realised [157]. Thompson [106], in Chapter three of his book, presents results of experimental modal analysis of a railway track that is studied to understand its behavior. The track had bi-block concrete sleepers with stiffer rail pads. The dynamic response was measured on the point of the rail that is directly on top of a sleeper and on the point between two sleepers [106]. Here the response represents a pinned-pinned mode, in a sense that a peak is noted on the point between two sleepers, and a ditch representing antiresonance on top of sleeper point. This mode occurred on a low frequency of around 500Hz [106].

Given that the rail is one long infinite continuous body, the FRF response is much flatter than that of experiments conducted on wheels [111], where resonance peaks and antiresonance ditches are very much pronounced. Although the damping of the

rail is much more than that of wheels, this damping is not significant in the frequency range of 500 – 1000Hz [106]. The vertical dynamic response of the rail is also investigated for stiffer and softer rail pads and the illustration is found in Figure 2.5.

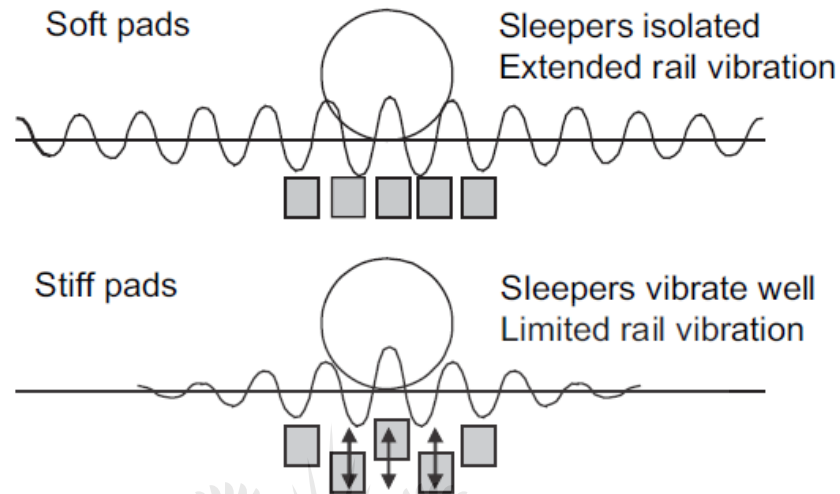


**Figure 2.5.** Illustration of the effect of rail pad stiffness on the coupling between rail and sleeper and on the damping of waves in the rail. Reprinted from [106].

Evident in Figure 2.5. is that the stiffness of a rail pad affects the damping of the rail and the degree of coupling between the sleepers and rail. In addition, the experimental modal analysis for both soft and stiffer rail pads showed a great decay rate in the vertical motion of vibration, and less decay rate in the horizontal [106]. This means that significant noise radiation may occur due to lateral motion of vibration.

The high decay rate of vibration in a system means the system is more damped, hence vibration dies out quicker [106]. On another front, work closely related to rail pads was conducted by Kim et al. [158] where the dynamic behavior of rail clips of the fastening system is studied. Here it is found that the dynamic response of rail clips of the fastening system is associated with rail corrugation [158].

Ilias [159] found that stiffer rail pads promote higher rates of corrugation growth. In a model developed to better understand the wavelength fixing mechanism for rail corrugation, Batten et al. [160] predicted corrugation wavelength growth using experimentally obtained vertical receptance of the rail and typical passing train velocities. The next subsection outlines methods that researchers adopt recently in the research space to detect rail corrugation.

## **2.6. Measures to Identify Rail Corrugation**

The railway industry is realising a gradual transformation into the fast-approaching high technology railway future. Researchers concerned with the formation of corrugation on rails develop measures to identify and assess rail corrugations using high technology computer interventions. However, rail corrugation detection through a human eye is both time-consuming and labour-intensive [161].

Wei et al. [162] developed smart methods of identifying and assessing rail corrugation through a computer vision. Such computerised methods are reliable and accurate. The authors show in the study that such methods are more efficient than traditional methods and can achieve precision and recall rates of over 99.67% and 98.34% respectively [162]. It is normally difficult to get track maintenance schedule to align with train operations schedule, more in particular for underground metro lines.

Often facilities and resources are not available for thorough maintenance of such train operations arrangements. Hence researchers in the rail corrugation space are putting some significant effort in designing rail corrugation monitoring systems that are installed on rail cars [163]. Kaewunruen et al. [164] designed an inspection train, equipped with sensors, which include a gyroscope, accelerometers, ground penetrating radar and etcetera. The train was also installed with high-velocity cameras and produced good results as a supplement to track inspections schedule [164].

A British company by the name of Rail Measurement has developed various tools that are currently used in the industry for measuring of short pitch rail corrugations. These include portable corrugation trolleys which also achieve accurate measurements of corrugation crests amplitudes [165 – 167]. Like in any engineering and operations environment where continuous improvement is of paramount importance, some researchers are working on optimising measuring instruments and tools. Here more focus is put on reducing the number of sensors and accelerometers whilst not compromising the quality of the important function, i.e. accuracy in measuring rail corrugation [168].



Real Herraiz et al. [169] studied the dynamics of a vehicle-track system with a time domain model they developed. Here a numerical FEA model is developed to characterise the track behaviour, whilst the rail car behaviour is characterised by a developed unidirectional model of two masses in the VAMPIRE PRO software. The loads obtained from the dynamic model are used as an input parameter to the numerical FEA model, to obtain the dynamic response of the rail track [169]. From the dynamic model it is deduced that the loads on the low rail of the track curve studied have higher amplitudes than those on the high rail and these amplitudes [169]. In addition, dynamic loads are significantly reduced on the low rail after rail grinding is conducted [169]. This method, consisting of a time domain feedback between a dynamic model of a rail car and the numerical FEA model of the track is one of the interesting tools in studying vehicle-track interaction dynamics [169].

Researchers are also advancing different methods to analyse the short pitch rail corrugation in a frequency domain [162]. Li et al. [170] proposed a new method in a frequency domain for detection of rail corrugation through analysing the background lines of a corrugation captured image [170]. On a similar work a visual inspection system was developed for rail corrugation. The system consists of two parts, i.e. the part that is responsible for capturing an image and the other responsible for identifying corrugation from captured images [171]. Lang et al. [172] developed a method referred to as a Wavelet Packet Energy Entropy (WP-EE) to accurately detect corrugation on rails. The model incorporates a vehicle-track model and a simplified rail corrugation model [172]. The next subsection briefly outlines fundamental details on vibration modes and mode shapes.

## **2.7. Vibration Modes and Mode Shapes**

If it is assumed that the vibration frequency increases with the gradually increased force applied, the mode shapes become more complex as seen in modes 2 and 3 in Figure 2.6. To bring it much closer to the context of mode shapes investigated in the current study, the study by Goo and Kim [173] is considered. In studying the wheel-squeal noise the authors developed a wheelset-track model that resulted in different modes with different mode shapes in various vibration frequencies. Figure 2.6. shows modes obtained in the squeal model by Goo and Kim [173].



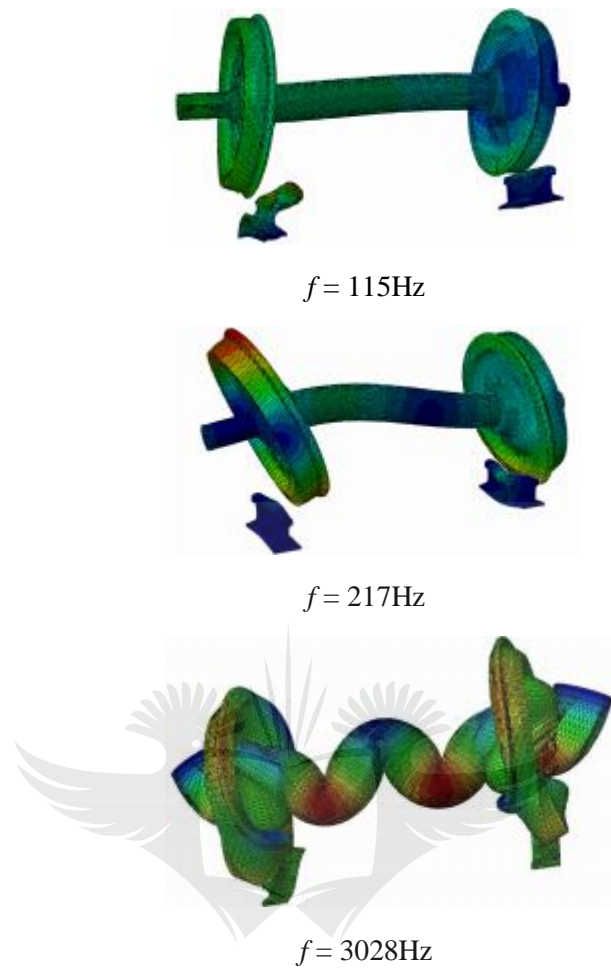


**Figure 2.6.** Unstable modal shapes of a railway wheelset at different frequencies of vibration. Reprinted from [173]

It can be seen in Figure 2.6. that at lower frequencies of vibration mode shapes are not very complex. There is no significant difference in the mode shapes at 115Hz and 217Hz. However, there is a significant difference in the complexity of the mode shapes at the frequency of 217Hz and 3028Hz [173]. This is due to the significant difference in frequencies. The next subsection contains the first case study.

## 2.8. Case Study 1: Harmonic Response of a Railway Wheelset

In the current study the work by Cruceanu and Sorohan [174] on investigation of the harmonic response of a railway vehicle wheelset is reviewed and summarised as the first case study. The FEA method is used for the investigation of the harmonic response of the wheelset. The wheelset investigated is used by a Minden Deutz bogie

of a passenger coach [174]. The aim in analysing the FRFs is to identify how wheel-rail parameters influence vibration levels and the generated rolling noise [174]. The aim of the current study in investigating the vibration response of a locomotive wheelset is only related to identifying resonance modes in the frequency range that corresponds to short pitch rail corrugation.

The FEA method of investigating the harmonic response of a structure is found to be a good approach, given that vibration modes can be excited even at higher frequency ranges, beyond 1500Hz [174]. Even though this proposition by Cruceanu and Sorohan makes better sense for investigation on wheelsets, it is worth noting that vibration modes at high frequency ranges can be excited in other cases as well. The experimental study by Thompson [106] managed to excite vibration modes of a railway track, including in the frequency range of 0 – 5000Hz. Figure 2.7. shows one of the FRFs obtained experimentally in Thompson’s study.

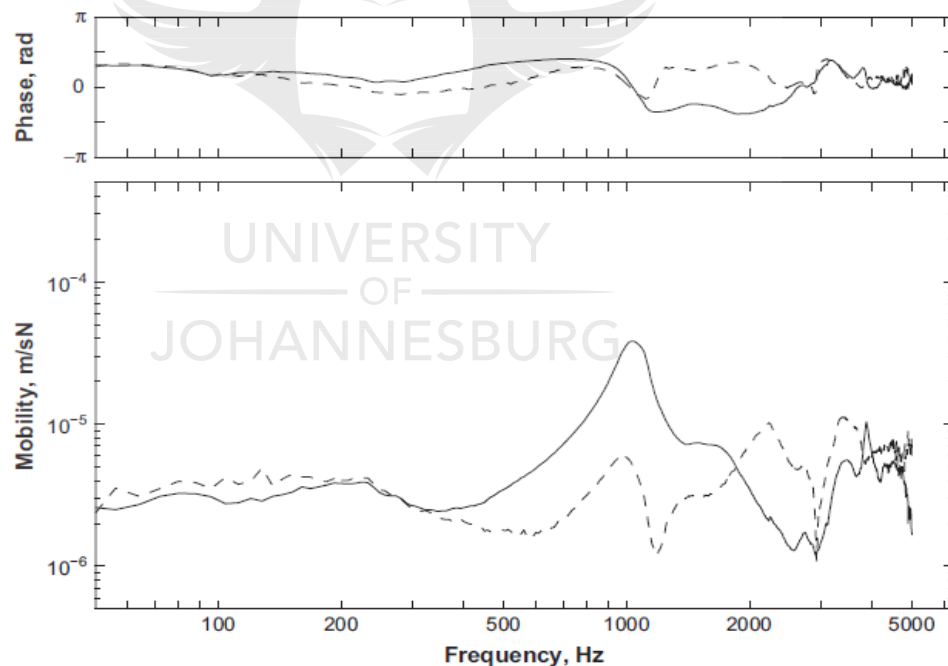


**Figure 2.7.** Vertical vibration response of a bi-block track installed with stiff rail pads. Vibration is measured mid-span and above a sleeper. Reprinted from [106].

As seen in Figure 2.7. the FRFs for vertical mobility of a rail installed in bi-block railway track, some resonance modes are excited in the frequency range of 1000Hz to at least 5000Hz. Studying of wheel-rail vibrations is a better solution towards

mitigating the negative outcomes realised by excessive vibrations in the medium and high frequency range [174].

Kaewunruen [45] also adds the low frequency range of vibration as one of the frequency ranges in which some railway track damage is realised. The low frequency range of vibration is associated with damage of the substructure, which includes the ballast, sub-ballast and subgrade. This occurs particularly in the low frequency range of 0 – 40Hz [45].

In their investigation, Cruceanu and Sorohan [174] modelled a wheelset with new and with used wheels for comparison of FRFs. This is another prudent way of investigating wheelset vibration response in detail, as noted in the current study that resonance modes for the wheelset experimented with used wheels, provides slightly different natural frequencies as that modelled with new wheels [32]. For harmonic response analysis in Cruceanu and Sorohan's study [174], a 1N steady load is applied firstly in the same direction (vertically upwards on the wheel threads) on both wheels. This force (1N) represents a load applied by the rail on the wheel in the wheel-rail contact point. In the second scenario the 1N load is applied in opposite directions (vertically upwards on the threads of one wheel and downwards on the threads of the opposite wheel). The force applied vertically downwards represents the load applied by the wheel on the rail, in the wheel-rail contact point [174].

Table 2.3. shows material properties of the wheelset modelled in the harmonic response investigation by Cruceanu and Sorohan.

**Table 2.3.** Parameters of the railway coach wheelset modelled for harmonic response investigation [174].

<b>Parameter</b>	<b>Value</b>
Density of the material (steel)	7850 kg/m <sup>3</sup>
Young's Modulus of the axle	210 GPa
Shear Modulus	81 GPa
Length of the axle	2.2 m
Diameter of the wheel	0.95 m
Mass of the axle	346 kg
Mass of the new wheel (950 mm)	378 kg
Mass of the worn wheel (890 mm)	288 kg
Mass of the axle box	95 kg

The masses of the wheelsets experimented and modelled in the current study are not measured. The new and used locomotive wheelsets used for modelling and experimental modal analysis respectively in the current study are slightly larger than the railway coach wheelset used in the Cruceanu and Sorohan's investigation [32, 174]. The diameters of the used and new wheels in the current study are 0.985m and 1.016m respectively.

Vibration response in the current study is obtained through a free-free vibration analysis, as opposed to a minor steady load of 1N (102 grams) applied in Cruceanu and Sorohan's investigation [174]. An analytical model is developed by Cruceanu and Sorohan as a base model for FRFs of the railway coach wheelset. Here the wheelset axle is modelled using the Timoshenko beam theories and two rigid bodies attached to represent the wheels [174].

The validation model is developed in FEA thereafter. In the current study the locomotive wheelset FRFs obtained through the experimental modal method are used as the baseline and the FEA response analysis used for validation and to compute resonance mode shapes [32]. The fifty harmonic response modes adopted in the Cruceanu and Sorohan's investigation [174] are too limited for a frequency range of 0 – 1500Hz.

This is due to the fact that similar to brake-disc squeal models, there are repeated root modes in the response system and these are practically one vibration mode, which has a potential to create contradiction in the results [175]. The author's proposition for modal methods (either forced harmonic or free-free responses) is that modes up to at least two times the frequency being investigated, be requested in simulations, preferably three times or more than the highest frequency in the frequency range.

As an example, if a complex mode at 150Hz is of interest, real modes up to at least 300Hz are required. In addition, as an alternative to steer away from that approach, Gao et al. [175] developed a solution to this problem through a curve-fitting technique. The FRF results for the harmonic response of the wheelset modelled with loads in the same direction in Cruceanu and Sorohan's investigation [174] are presented in Figure 2.8. The results are presented for the model with worn wheels.

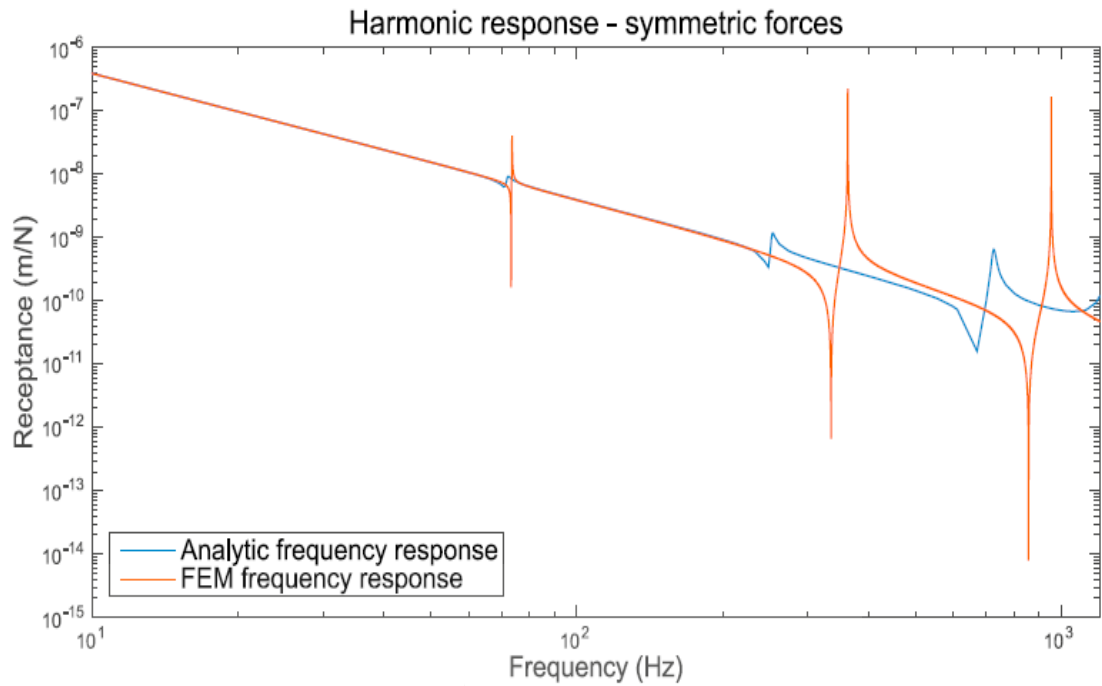


**Figure 2.8.** Harmonic response of the wheelset. 1N loads applied in the same direction. Reprinted from [174].

The harmonic response in Figure 2.8. is presented in form of a receptance, which is represented as the distance per unit force at a certain vibration frequency. FRFs for both analytical and the FEA methods are clear and well pronounced. FRFs are more pronounced if the wheelset is not installed in a bogie and hence a significantly less damping experienced [0, 103]. The peaks on the FRF plots represent a resonant and the ditches represent an antiresonant vibration. Table 2.4. contains frequencies for the response in Figure 2.8.

**Table 2.4.** Resonance frequencies of the harmonic response. 1N load applied in the same direction [174].

Frequency – analytic model (Hz)	Frequency – FEM model (Hz)
73	72
363	254
954	726

The first resonance mode occurs at a frequency of 72Hz. This resonance mode does not differ much with the ones excited through the analytical model. It is seen in Figure 2.8. that there is also an antiresonance that is perhaps slightly below this frequency

(72Hz). The resonance mode excited at the frequency of 72Hz has a very narrow peak, which symbolizes a heavy damping.

The other two resonance modes excited at frequencies of 254Hz and 723Hz respectively represent a more damped response than that occurring at 72Hz. This is noted by broader peaks in these two frequencies. The last two resonance modes (at 254Hz and 723Hz) excited in the FEA are much different from those obtained through the analytical model. It is noted from Table 2.4. that all resonance modes excited through FEA are less than those obtained from an analytical model. This may be due to the difference in assumptions made during FEA modelling, which are not assumed in the analytical mode. As well, the direction in which the loads are applied is specified, however, the direction of the measured response is not specified, which may also contribute to the accuracy of the results. In the current study the response of the wheelset is measured in the direction in which the load is applied [32].

The approach of measuring the response of the structure in the same direction as that of the applied load in the current study proves to lower the percentage error between the experimental and FEA work. Figure 2.9. shows the FRF results for the harmonic response of the wheelset when the 1N loads are applied in opposite directions.

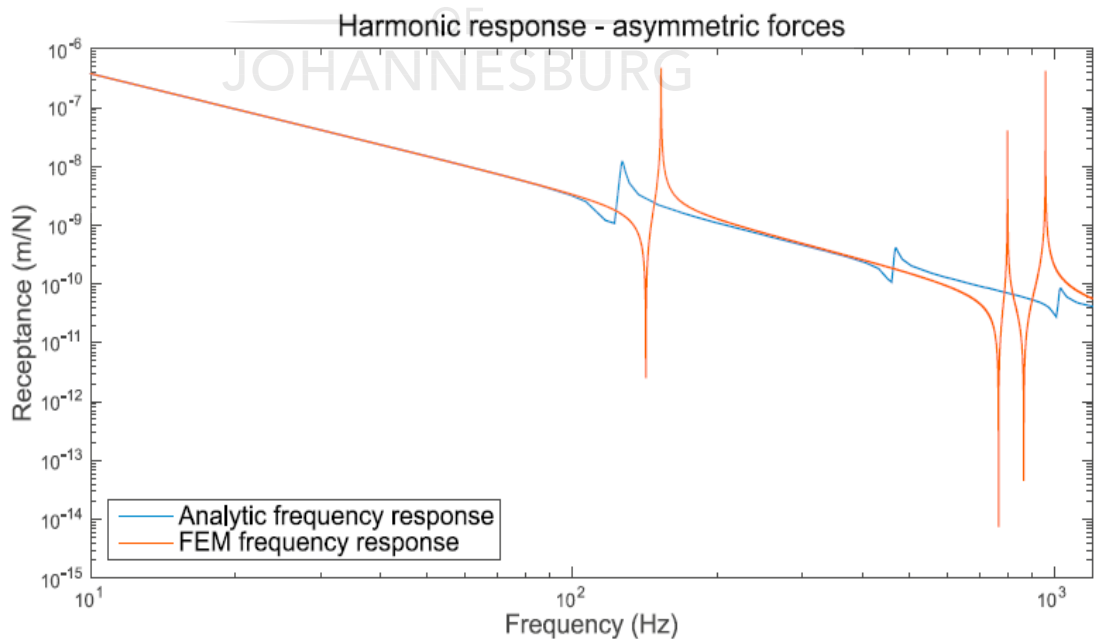


**Figure 2.9.** Harmonic response of the wheelset. 1N loads applied in opposite directions. Reprinted from [174].

It is noted in Figure 2.9. that when the 1N loads are applied in different directions the last two resonance modes are excited at closer frequencies. The response in these resonance modes is also more damped than when the 1N loads are applied in the same direction. The first resonance and antiresonance shifted above 100Hz and looks more damped than when the 1N loads are applied in the same direction. From these facts it can be deduced that the response of the wheelset changes when the direction of the loads applied is not in the same direction, compared to the scenario whereby the loads are in the same direction. Table 2.5. tabulates the frequencies seen in Figure 2.9.

**Table 2.5.** Frequencies of the harmonic response. 1N load applied in opposite directions [174].

Frequency – analytic model (Hz)	Frequency – FEM model (Hz)
153	127
800	469
960	1033

It is noted in Table 2.5. that the frequencies excited through FEA differ significantly with those obtained in the analytical model. For response of the model with worn wheels it is noted that even though the resonance modes excited at lower frequencies look identical, significant changes are experienced in the response as the frequency range increases. Results of the model with new wheels are also slightly different to the ones for worn wheels (presented above) [174]. This is given as the difference in masses of the wheels between the new and worn wheels. This slight difference is also experienced in the wheelset model in the current study, given that the wheelset modelled in FEA has dimensions of new wheels and that used for experimental modal analysis has worn wheels [32]. As well, in the analytical model the axle is modelled as a straight Timoshenko beam, whilst in FEA different geometrical curves are considered.

Lastly, the wheels are modelled as thin discs in the analytical model, as opposed to solids with all profile parameters required for a complete wheelset. Results of the model by Cruceanu and Sorohan [174] differ from those of the wheelset analysis

model in the current study due to minor differences in the wheelset mass and profiles of the geometry [32].

The current study adds to the body of knowledge by investigating the vibration response of a railway wheelset whilst it is coupled to a traction motor and installed in bogie with all its components. The FRFs for a wheelset installed in a complete bogie differ in terms of how pronounced the resonance modes are, given the damping effect from components in a bogie. The next subsection contains the second case study.

## **2.9. Case Study 2: Wheel-rail Vibrational Analysis and Experimental Modal Analysis on Measures to Suppress Short Pitch Rail Corrugation**

The work by Qian et al. [34] on investigating the effect of installation of a rail vibration absorber on short pitch rail corrugation is summarised as the second case study. Here Qian et al. [34] obtained rail FRFs through experimental modal analysis from two rails: one with and one without a vibration absorber, after which two FEA models were developed for validation: one for a rail with and one without a vibration absorber. Both methods used are in better agreement that the installation of a rail damper will damp resonance modes in the frequency range of 20 – 800Hz, which corresponds to short pitch rail corrugation frequency range [34]. Despite the fact that the current study does not deal with the investigation of the effect of the rail vibration absorber itself, the relevance of the study by Qian et al. [34] rests in the methods adopted in both studies.

The rail response measurements in the study by Qian et al. [34] are conducted in a non-ballasted railway track with concrete sleepers. Part of the current study is aimed at addressing the gap that exists in the current literature with respect to analysing responses of ballasted railway tracks. Most analysis are conducted on non-ballasted railway tracks, whereby the dynamics of tracks installed with other types of sleepers, other than concrete sleepers are unthought-of.

Qian et al. [34] used a rail vibration absorber with a mass of ten kilograms, which was applied on the field side of the rail web to suppress rail vibration. Even though Qian et al. [34] managed to develop a damper that suppressed vibration in a frequency range



that includes the 398Hz, it is advisable to first tune the damper [176]. Tuning of a mass damper gives it a special design that is dedicated for suppression of resonance frequencies in specific frequency ranges [176]. Qian et al. [34] used two accelerometers to measure the response of rail in the horizontal and vertical directions. Figure 2.10. shows the arrangement of accelerometers mounted at an angle iron that is attached beneath the rail foot.

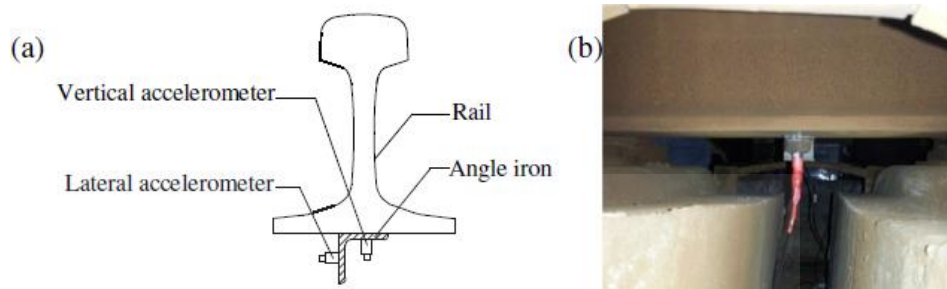


**Figure 2.10.** Accelerometers installed for vibration test (a) front view of the rail with accelerometers (b) image of accelerometers installed at the base of the rail foot. Reprinted from [34].

Rail vibration results for the study by Qian et al. [34] in a time domain are shown in Figure 2.11. The results are presented in form of vibration acceleration in a time period. The results are presented for vibration of the rail with a vibration damper and without the damper.

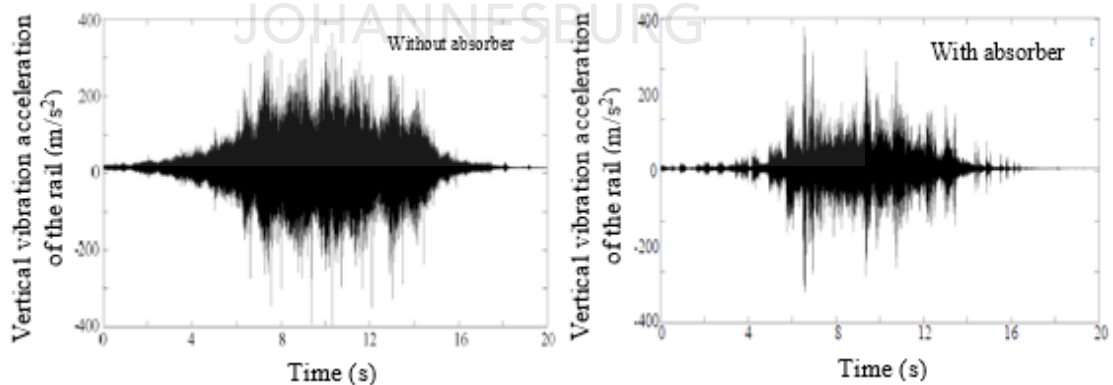


**Figure 2.11.** Vibration of the rail in the vertical direction. Cases presented for vibration with and without an absorber. Reprinted from [34].

It is noted in Figure 2.11. that in both cases (with and without an absorber) the amplitude of rail vibration increases after 4 seconds of vibration. After 12 seconds the vibration amplitude begins to decrease until vibration dies out just before 20 seconds.

The amplitudes for the rail vibration without an absorber seem more than those of rail vibration with an absorber. This is a good indication that a rail vibration absorber is capable of suppressing resonance frequencies of the rail, which are ultimately attributed to the formation of rail corrugation [33]. It is reported by Qian et al. [34] that the absorber suppressed the frequency of 381Hz, which is very much closer to the short pitch corrugation formation frequency of 398Hz.

Further vibrational analysis by Qian et al. [34] are conducted on the wheel-rail model in Figure 2.12.

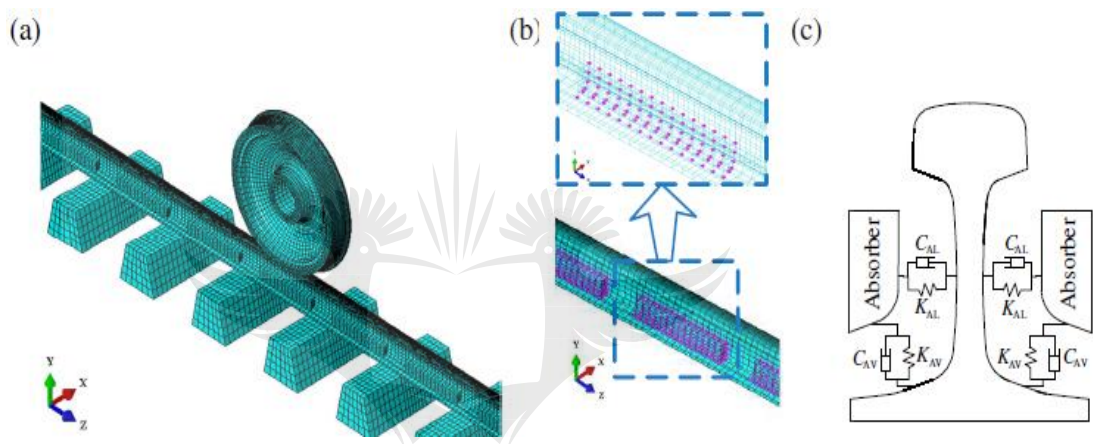


**Figure 2.12.** Wheel-rail system model with a vibration absorber (a) FE model (b) springs and dampers defined in the rail-absorber contact (c) schematic defining contact between the rail and absorbers. Reprinted from [34].

The difference between the “wheel-rail” and the “wheel-rail-absorber” models is the absence of the rail vibration absorber in the wheel-rail model. Similar to the wheelset-track model in the current study, the wheel is modelled in the vicinity of the center of the rail and the creep force is assumed to be saturated [33, 34]. The Abaqus (Standard) solver is used for wheel-rail vibration simulations and contrary to the wheelset-track model in the current study, the analysis are in time domain [34].

The complex eigenvalue analysis method is adopted in studying the stability of wheel-rail vibration in frequency domain [34]. The results show that the wheel-rail vibration frequencies are excited at 363.9Hz (absorber not installed) and 335.7Hz (absorber installed). These frequencies are reasonably close to the short pitch corrugation formation frequency of 389Hz [34].

The formation frequency (389Hz) for short pitch rail corrugation in the study by Qian et al. [34] is quite higher than that of the short pitch rail corrugation with which the current study is concerned. The current study is concerned with the short pitch rail corrugation with the formation frequency of 108Hz [32]. Amongst other wheel-rail parameters, the difference in the short pitch corrugation-borne frequency is influenced by the difference in train velocity [10].

In the study by Qian et al. [34] the train velocity is 70km/h, whilst that of trains operating in the railway line with which the current study is concerned is an average of 30km/h [10]. Figure 2.13. shows the vibration mode excited in the wheel-rail and the wheel-rail-absorber models by Qian et al [34].

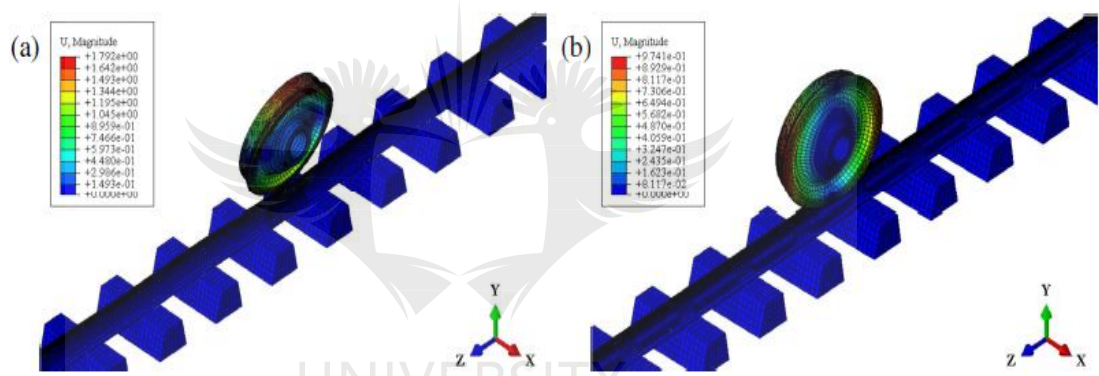


**Figure 2.13.** Unstable mode of the wheel-rail system (a) at a frequency of 363.9Hz, without the absorber (b) at a frequency of 335.7Hz, with the absorber. Reprinted from [34].

In Figure 2.13a. As seen in Figure 2.13a., the unstable mode of vibration occurs along the Z-axis when the rail vibration absorber is not installed. This unstable mode still occurs in the case in Figure 2.13b. where it occurs along the Y-axis, when the rail absorber is installed. It is suggested by Qian et al. [34] that based on analysis from the wheel-rail model simulations, the frictional self-excited vibration in the wheel-rail system can be reduced by a rail vibration absorber. This is apparently true more specifically when the coefficient of friction is 0.4 and above [34]. The frictional self-excited vibration is one of the accepted mechanisms to be the cause for short-pitch rail corrugation [33].

Whilst following on the same hypothesis that the wheel-rail frictional self-excited vibration is the important cause for short pitch rail corrugation, the current study takes a different approach. The current study contributes to the body of knowledge by conducting the wheel-rail vibrational analysis on a railway wheelset modelled on a three-layered ballasted railway track. The analyses are conducted for cases with steel and with concrete sleepers. The next subsection contains the third case study.

#### **2.10. Case Study 3: Investigation into Frictional Self-Excited Vibration of a Wheel-Rail System**

The study by Chen et al. [33] is reviewed and summarised as the third case study. Here Chen et al. [33] investigated the effect of wheel-rail unstable vibration on the formation of rail corrugation. The hypothesis advanced in the study is that a wheel slip relative to the rail generates unstable wheel-rail vibrations that ultimately form rail corrugation [33]. A wheel-rail FEM is developed with four railway wheels in series, one rail and a series of concrete sleepers [33]. It is assumed that the wheel-rail system is operating at a vicinity of a saturated creep [33]. The complex eigenvalue analysis method is adopted. The study by Chen et al. [33] pursued a 1318km high-velocity railway line from Beijing to Shanghai. The line was put into operations in the year 2011 and corrugation formed in some sections of the track after 2 – 3 months of operations [33].

As well, after a period of 1 – 2 years the wheels realised a significant increase in the formation of wheel polygonisation [33]. In this railway line Chen et al. [33] suggested that a more severe rail corrugation occurs in the section of the track where brakes are applied by trains, than in that where brakes are not applied during transit. The contact point position is at the center of the rail as modelled in Figure 2.14.

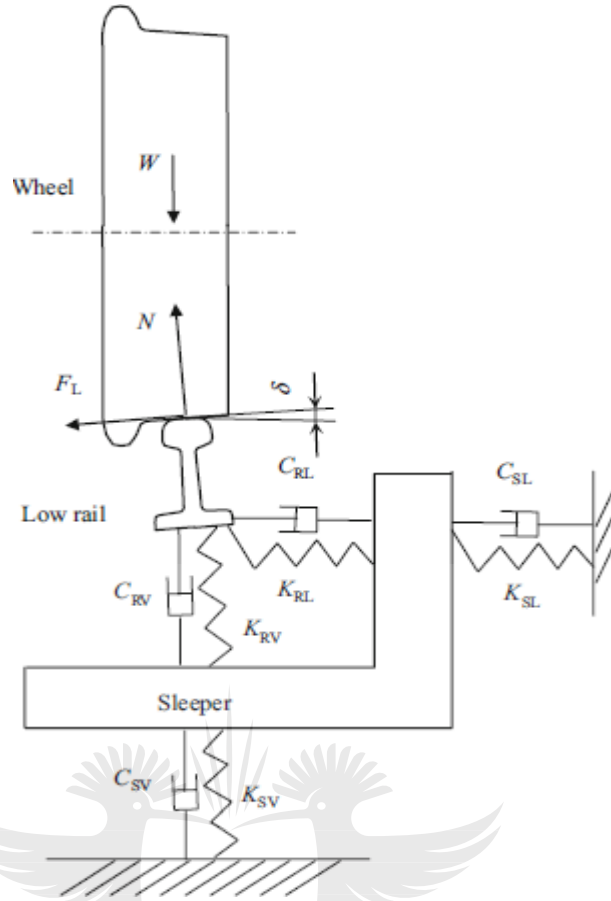


**Figure 2.14.** Wheel-rail contact position for all four wheels in series. Reprinted from [33].

In Figure 2.14. the wheels are modelled in the center of the rail, where  $W$  is the vertical force from the suspension, applied by the axle box,  $N$  is the normal force,  $\delta$  is the wheel-rail contact angle,  $F_L$  is the lateral creep force,  $C_{RL}$  and  $C_{RV}$  are the damping coefficients of the rail fasteners in the lateral and vertical directions respectively.

$K_{RL}$  and  $K_{RV}$  are rail fastener spring stiffnesses in the lateral and vertical directions respectively,  $C_{SL}$  and  $C_{SV}$  are the damping coefficients of the sleeper support dampers in the lateral and vertical directions respectively,  $K_{SL}$  and  $K_{SV}$  are the lateral and vertical stiffnesses of the sleeper support springs respectively [33]. Figure 2.15. shows the wheel-rail FEM.

In Figure 2.15. the railway track is modelled with a series of sleepers on a monolithic track bed. The 8-node hexahedron FEA elements are used on the model. The model is built in the ABAQUS FEA software package. The magnitudes for parameters of the model in Figure 2.15. are detailed in the paper by Chen et al. [33] and are used in the FEA model. The simulation results are limited to a frequency range of 20Hz – 1200Hz.

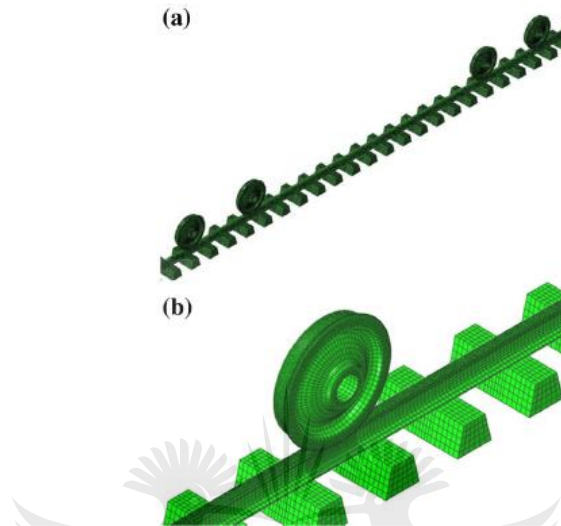


**Figure 2.15.** Wheel-rail model for four wheels in series on the rail (a) overall layout (b) detailed FEM. Reprinted from [33].

This frequency range is accepted to be associated with the formation of rail corrugation [33]. Figure 2.16. shows the results of the simulations.

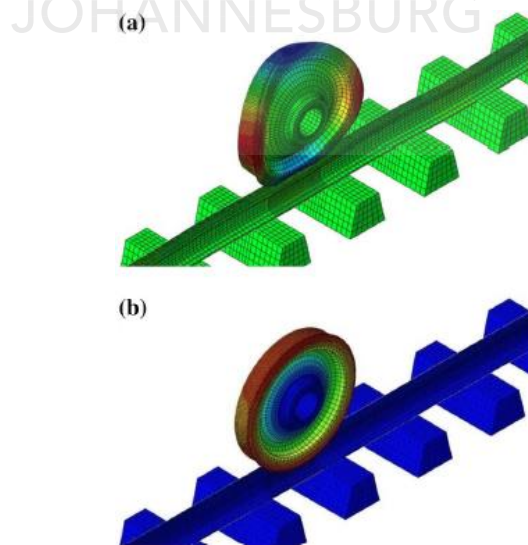


**Figure 2.16.** Mode shapes for unstable wheel-rail vibration (a) at a frequency of 331Hz (b) at a frequency of 508.89Hz. Reprinted from [33].

As seen in the results in Figure 2.16. the vibration mode at a higher frequency (508.89Hz) looks more damped than that at a lower frequency of 331Hz. The damping ratios are reported to be -0.001 for the vibration mode at a frequency of 331Hz, which is less than -0.0094 for the mode that occurs at a frequency of 508.89Hz [33].

The wheel-rail vibration modes in Figure 2.16. are higher than those excited in the wheelset-track model in the current study. This is due to the significant difference in train velocities in the railway lines with which the two studies are concerned. In the study by Chen et al. [33] the average train velocities in the railway line of concern are around 300 – 350km/h, whilst those associated with the current study are around 30km/h [10]. From the simulation results Chen et al. [33] pointed out that when the coefficient of friction is large enough during a wheel-rail creep, unstable vibration that is attributed to the formation of rail corrugation occurs [33]. However, this is contrary to the wheel squeal model by Goo and Kim [173] where it is found that at large creepage, in the lateral direction, when the friction coefficient is less than 0.1 unstable vibration does not occur. The authors further found that in the longitudinal direction, unstable vibration modes occurred when the frequency was high [173]. Both these findings oppose the proposition by Chen et al. [33].

The author's opinion is that this interesting outcome can still be more explored in the case when the adhesion conditions are different from the assumption of a saturated creep. Based on the model results Chen et al. [33] suggested that reducing the slip of a wheel relative to the rail will ultimately reduce the formation of corrugation on the high-velocity railway rails [33].

A slightly similar model is studied in the current study, with a complete railway wheelset modelled on a three-layered ballasted track. Such a model provides a reasonably accurate response of the wheel-rail system with an influence of the ballasted track bed (with its elasticity) on the response of the entire model [32]. The next subsection outlines solutions adopted to prevent or curb corrugation formation in the corrugation research space.



## 2.11. Solutions to Rail Corrugation

Grässie and Kalousek [14] likened rail corrugation to an Influenza; that it probably has infinite diversity; “corrugation is not a phenomenon. It is rather a family of phenomena without a common cause or a single cure” [14]. Efforts from the accepted research work results in proposed preventions for two wavelength fixing mechanisms. The first mechanism involves the vibration borne by wheel-rail interaction [177 – 187]; which may potentially be prevented by widely used rail dampers [34, 176, 188 – 193].

Installation of rail vibration dampers prove beneficial results in different ways. For instance, Qian et al. [194] found that short pitch corrugation wear depths were severe mid-span (position of rail between two sleepers). Here not only did installation of rail vibration damper suppress the short pitch rail corrugation, but uniform wear pattern was first achieved on the running surface of the rail [194].

Rail dampers are increasingly being considered as one of the proposed solutions that produce immediate and long-term positive results with regards to prevention of the short pitch rail corrugation [195]. Chen et al. [196] pointed out that even though there exist several dominant vibration frequencies in a corrugated rail, only vibration of certain specific dominant frequencies will lead to the formation of rail corrugation [196].

The second mechanism involves vibration borne by a stick-slip motion of the wheel relative to the rail [197 – 202]; which may be prevented by application of Positive Friction Modifiers (PFMs). Stick-slip oscillation of a wheel relative to the rail may cause material wear on rails.

PFMs play a significant role in a wheel-rail contact, in preventing such an oscillation [204], effects of which have been included in the modelling of rail corrugation in track curves [205]. In their study to analyse rail corrugation in a rail track curve, Daniel and Meehan [206] found that the leading wheelset of a rail car shows more evident stick-slip irregularities which are associated with both short and long pitch rail corrugations [206].



Eadie et al. [22] have shown that when creep is saturated on the wheel-rail contact point; in the presence of negative friction, a stick-slip oscillation occurs. From this it is further shown that both wheel squeal and short pitch rail corrugation occur, and a high PFM is suggested to alter the friction levels in the contact point [22]. This kind of irregularity is undesired as it increases the residual stress and strain in a rail [207].

In order to reduce excessive positive friction on a wheel-rail contact, lubrication of the wheel tread and running surface of the low rail in sharp track curves is proposed [208]. The water-based lubricants applied in the wheel-rail system prove to produce positive results in light of suppressing rail corrugation and growth. This is given that rail wear and plastic deformation can be effectively suppressed by water-based lubricants in the wheel-rail system [209]. However, solving problems can also lead to bigger ones. Extensive work is required to investigate how such a lubrication method may influence traction ability. It is the author's opinion that wheel-rail contact lubrication may result in different adhesion condition between the two rails, which may lead to first torsional excitation of the wheelset in motion.

In a research conducted in South Africa, Fröhling et al. [210] showed that torsional vibration mode of a wheelset axle may lead to corrugation on wheels i.e. wheel polygonisation [210]. In better agreement, Sebesan et al. [211] conducted a study which resulted in the same finding in Romania. The authors indicate that researchers from the United States had proposed vibration absorbers in 1998, as an important measure to prevent the torsional vibration [211].

Grässie [212] conducted a field trial work to assess the influence of grinding of the rail running surface, on short pitch rail corrugation. Here two new rails were utilised. One of the rails was ground new (before use). On pursuit, the ground new rail showed no signs of corrugation for the first twenty months in service, whilst the newly installed rails without being ground, showed signs at same period of time [212]. The pursuit continued and even after fifty months there was barely a sign of corrugation on the newly ground rails [212]. In the view of designing track structures to remedy the short pitch rail corrugation, it is still expected of researchers to explore different aspects, including assessment of rail corrugation formation on different types of bridges.

Meinke and Stephanides [213] discovered an astonishing finding in a 250m radius rail track curve, referred to as “The Brixentaler” curve in Germany. Part of the track curve is a ballasted track and part is a steel bridge over a small river “Windacher Ache”. The short pitch rail corrugation only formed on the ballasted section of the curve [213]. The authors conducted measurements on a train pass from both parts of the track curve and found that a wheelset rolls freely and quitter on rails installed in the steel bridge section of the curve. However, as expected, the wheelset rolls with noise, bending and torsional vibration modes when rolling on the ballasted track section of the curve. This opens up for a significant question whether steel bridges do prevent the short pitch rail corrugation.

Meinke and Stephanides [213] also confirmed this interesting finding by experience they have with other similar bridges in Germany and in Norway. Here the authors’ assumption is that the railhead vibration of rails installed in a steel bridge railway track reduces the wheel-rail coefficient of friction, hence the smoother rolling of a wheelset [213]. Xiao et al. [214] point out the importance of friction coefficient in self-excited wheel-rail vibration. According to the authors, a reduction of the coefficient of friction to less than or equal to 0.27 will eliminate rail corrugation formation [214]. The next section gives a comprehensive summary of Chapter two.

## **Chapter Two Summary**

In this chapter, the literature related to short pitch corrugation on rails is reviewed. Initiators of the short pitch rail corrugation can be classified in two mechanisms i.e. the damage and the wavelength fixing mechanisms. The primary initiators accepted to form corrugation on rails are discussed. The six types of rail corrugation, their characteristics and causes are outlined.

Existing gaps are identified in the literature, which the current study is concerned with addressing and contributing to the body of knowledge. The short pitch rail corrugation is accepted to be related to a few mechanisms, i.e. transient conditions favouring certain wavelengths, resonance modes of the wheelsets for rail cars, P2 resonance and the recent hypothesis i.e. the self-excited vibration of the wheel-rail system.

Experimental work related to the dynamic behavior of rails (as related to short pitch rail corrugation) has been conducted. Together with some experimental work, much modelling work has been conducted to predict the formation and growth of corrugation on rails. Although more research is still required to this effect; it has been shown through modelling work that the dynamics of the wheels (particularly the inner wheel of the leading wheelset) in a track curve, is more associated with rail corrugation.

Corrugation-borne frequency is mainly related to two components i.e. the wavelength and train velocity. Solutions proposed by the science society are brought forward. Solutions related to the wavelength fixing mechanism add-up to reducing resonance of the wheel-rail system and modifying the wheel-rail contact point friction. Solutions related to the damage mechanism add-up to reducing physical irregularities on rail tracks; such as, improving grinding and welds.

Different treatments are proposed for different types of wavelength fixing mechanisms. Currently the well-known and mostly used treatment for rail corrugation remains reprofiling the rails through grinding. A permanent cure for rail corrugation will only be achieved through having one complex model that will encompass various components of different prediction models. Short pitch rail corrugation is found in almost all curves with rails supported on both the FY-type and PY-type concrete sleepers. Different materials and methods were used for experiments and modeling in the current study.

A summarised critical synthesis of the reviewed literature is as follows:

- The first existing gap observed by the author in the accepted literature is that there must be too little work (if any at all) done to study the difference in dynamics of rails supported on steel and concrete sleepers. In the railway line with which the current study is concerned in South Africa, corrugation is not found on rail track curves supported on steel sleepers.
- The second existing gap is the lack of analyses for three-layered ballasted tracks with their parameters and elasticities. Most of the conventional models include analyses on slab tracks. Three case studies are summarised. One on a railway wheelset vibration analysis and two on wheel-rail vibration analysis.

In terms of novelty, the author undertakes the research work in an attempt to close the gaps existing in the current literature by investigating the difference between the dynamics of ballasted rail tracks with concrete sleepers and those with steel sleepers. This was done through modelling the ballasted track with these two types of sleepers and developing modal analysis experiments for correlation purposes. The next chapter gives an outline of materials and methods used during the course of the study.



## Chapter Three

### Materials and Methods

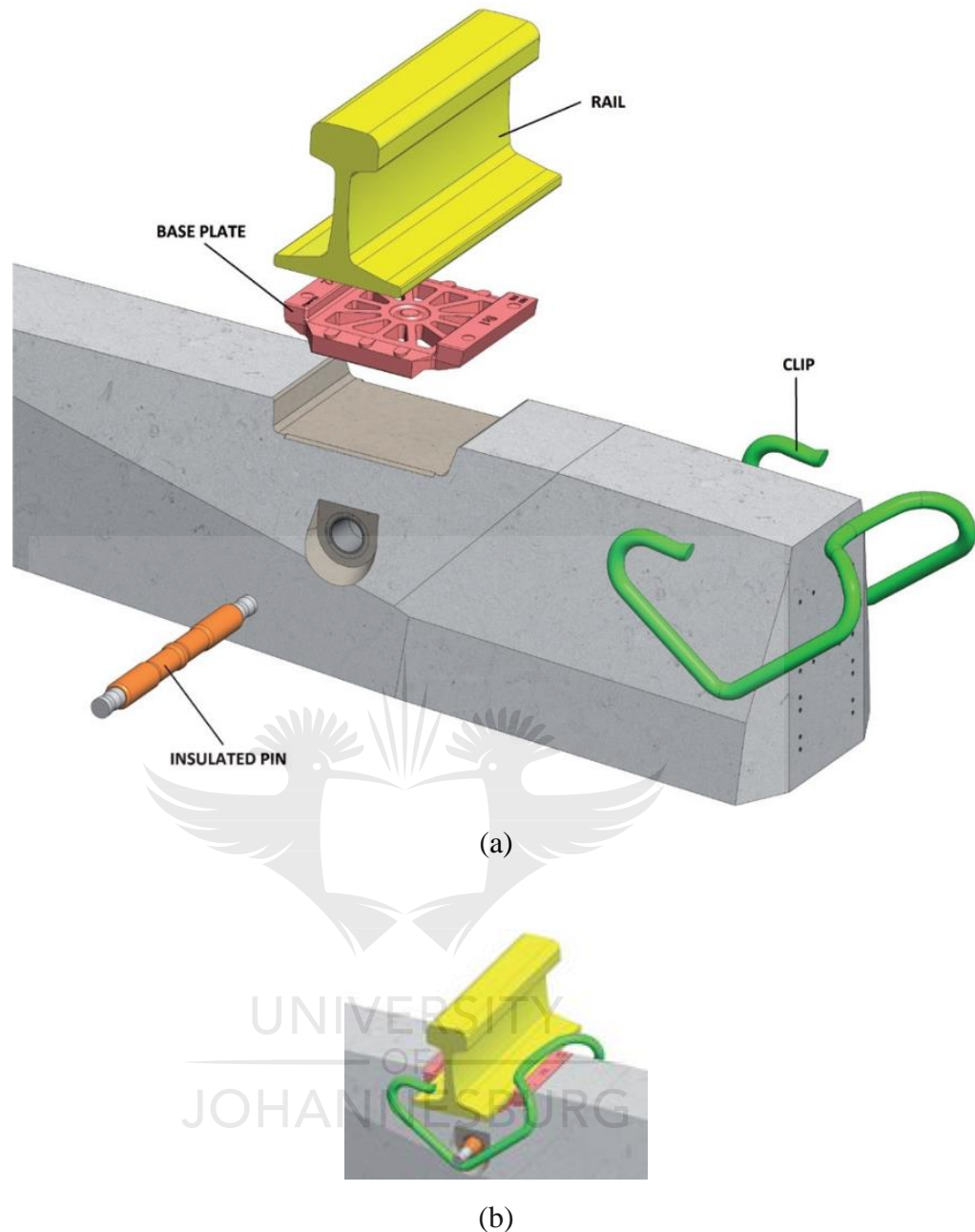
*What materials and methods are used to study wheel-rail track dynamics?*

In order to improve reproducibility of the present work, this chapter presents critical materials used in the experimental and modelling work. The methods are outlined on how these materials were used. With the use of materials, the approach followed was in the chronology of firstly conducting experimental work at a frequency range of 0 – 500Hz. This was followed by developing FEMs to model the dynamic response of wheels and rail tracks; and obtain mode shapes at frequencies of importance. All equipment used for experimental modal analysis was within the calibration cycle.

The corrugation frequency was found to be 108Hz, which falls within a low frequency range less than 1kHz, hence the frequency range of 0 – 500Hz is safe for the analysis. A lower frequency range with which the corrugation frequency falls could have also been chosen. It was in the author's interest to have a view of modes excited beyond the corrugation frequency, until the highest frequency of 500Hz. The next subsection outlines the types of railway track components that were involved in the current study.

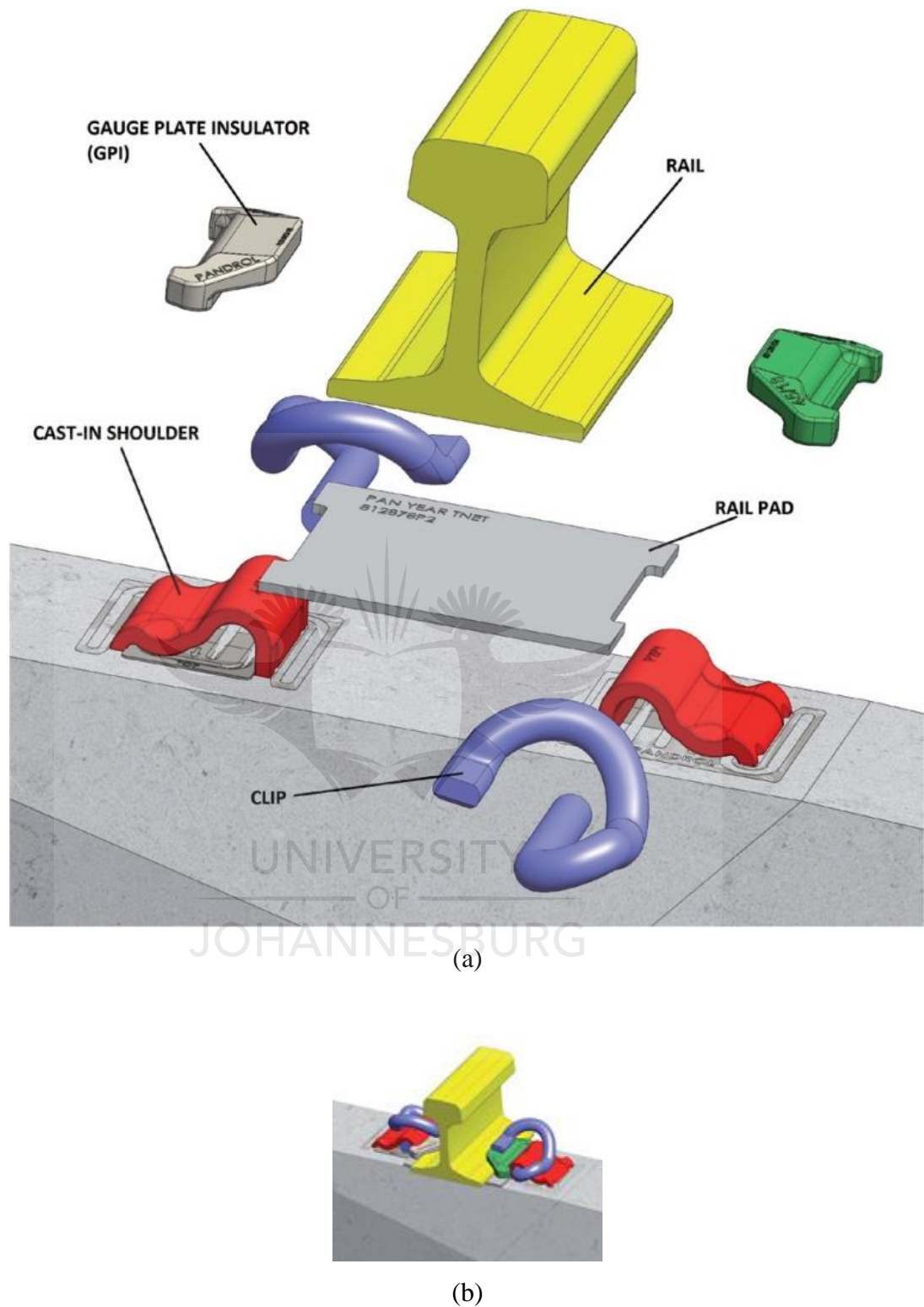
#### 3.1. Railway Track Components

Figure 3.1. shows the exploded and assembled views of the FY-type concrete sleeper and the rail fastening system applicable to it.



**Figure 3.1.** FY-type concrete sleeper with a FISTclip rail fastening system. (a) exploded view (b) assembled view of the fastening system.

As seen in Figure 3.1. the FY-type concrete sleeper has a space designed for the High Density Polyethylene (HDPE) rail pad. The FISTclip fastening system consisting of the clip and insulation pin is used to apply the vertical clamping force between rail, pad and sleeper. The insulation pin and the space designed for the rail pad also constrain lateral displacement of the fastening system components. Figure 3.2. shows the exploded and assembled views of the PY-type concrete sleeper and the rail fastening system applicable to it.



**Figure 3.2.** PY-type concrete sleeper with an e-Clip rail fastening system. (a) exploded view  
 (b) assembled view of the fastening system.

As seen in Figure 3.2. the rail pad sits on top of the PY-type concrete sleeper. The lateral displacement of the fastening system components in this case is constrained by



embedded parts of the fastening system, embedded on the sleeper. These embedded parts are also used to fix the e-Clips. The e-Clips are used to apply the vertical clamping force on the rail, pads and the sleeper. The insulator is used to insulate the contact between the rail and e-Clip. This ultimately prevents rail and/or e-Clip material wear during possible rail displacements relative to the e-Clips or the other way around. Figure 3.3. shows a steel sleeper fastening system.

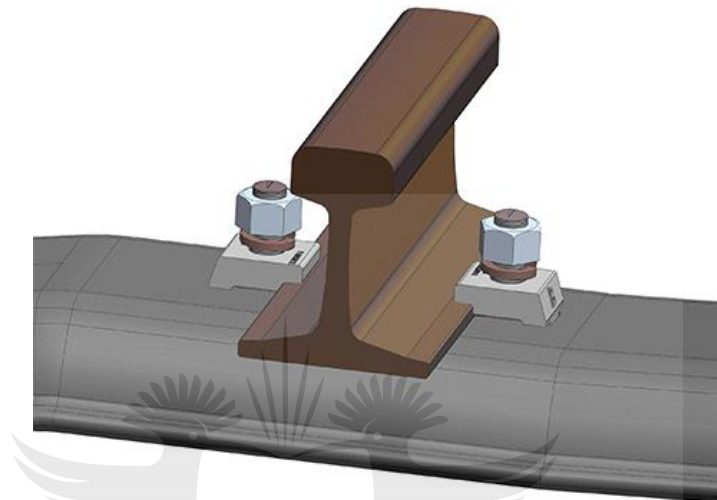


**Figure 3.3.** Rail on steel sleeper with its fastening system.

As seen in Figure 3.3. the steel sleeper fastening system is of a less complex form than that of the concrete sleepers. If the applied torque is adequate on the fastening nuts, the rail-sleeper contact stiffness will be adequate, such that the system can easily respond as a unit to dynamic loads. No rail pad is used in the rail-sleeper contact surface. The next subsection outlines the detail of instruments used to conduct experimental modal analysis.

### **3.2. Materials for Experimental Modal Analysis on a Wheelset and Rail Tracks**

The critical materials used involved the following:

- Isotron® triaxial accelerometer model 65, small size, 10 cubic millimeters, 5g, (Isando, South Africa),
- Modal hammer models 2302 and 2303 manufactured by Endevco®, (New York, USA),



- PXI0-4472 dynamic signal acquisition module for sound and vibration manufactured by Signal Express, (Cary, North Carolina, USA),
- Signal Express® software (2019),
- Uninterrupted Power Supply (UPS). Manufactured by Nashua, (Sunninghill, South Africa),
- Battery bank, manufactured by First National Battery, (Benoni, South Africa).

### 3.2.1. Modal Hammers

Instrumented modal hammers with an integral force transducer were used to excite the traction wheelset, rails and sleepers. Figure 3.4. shows the modal hammers that were used in the experiments.

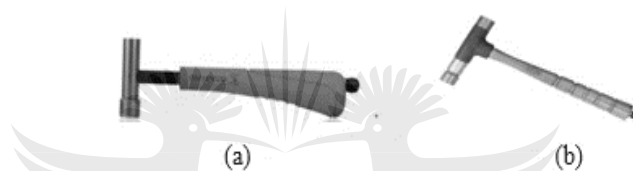


**Figure 3.4.** Modal hammers: (a) used to excite the traction wheelset (b) used to excite rails and sleepers.

The smaller modal hammer in Figure 3.4a. is suitable for experimental work on small structures, whilst the larger one in Figure 3.4b. is suitable for experimental work on medium to large structures such as machinery, shafts, large beams, pipelines, storage tanks, and etcetera. The 12 pounds size is the largest of this model and can excite large structures such as bridges, buildings, decks and floors. For the purpose of this work the smaller hammer was used on wheels and the larger hammer was used on rails and sleepers.

For the model 2302, three interchangeable tips (aluminum, plastic and rubber) that give different widths of an input pulse are available. For experiments in the current study, the aluminum tip was used. The model 2303 is referred to as a “sledge hammer”. The model 2302 hammer used for the purpose of experiments in the current study has two tips (the red and the black). The stiffness of the two tips is notably different when pressed on with a finger. The black tip which produces a better input force signal was used for the purpose of the experiment.

### 3.2.2. Accelerometers

The same model and size of accelerometers were used for experimental work on wheels and track. Figure 3.5. shows an image of the Endevco Isotron® triaxial accelerometer used for experiments.

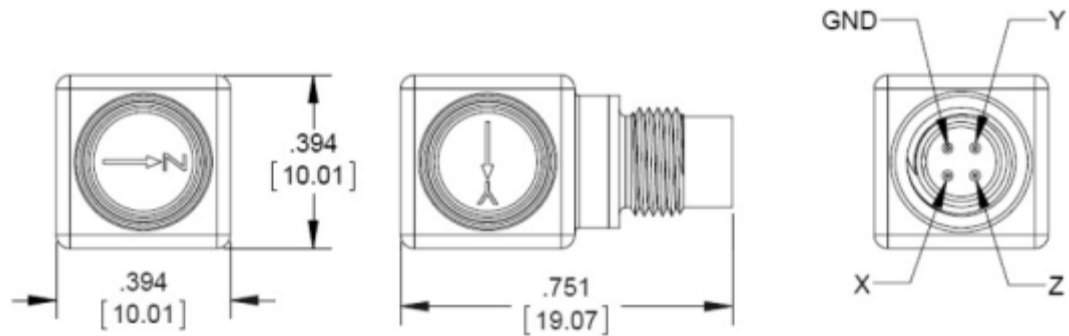


**Figure 3.5.** Triaxial accelerometer used for the experiments. Standard units are in inches, converted to millimeters in brackets.

The accelerometer was rigidly mounted in order to minimize mounting resonances. The side on which the glue was applied was chosen based on the direction of the input force applied and the direction of vibration, which the author was interested in measuring. Table 3.1. tabulates details of the Endevco Isotron® triaxial accelerometer used for experiments.

**Table 3.1.** Isotron® accelerometer features

Model	Dimensions (mm <sup>3</sup> )	Mass (g)	Connector
3202	10	5	4-pin

The 65HT is the lightweight model of an accelerometer that can measure the response of structures in three directions (X, Y and Z) simultaneously. This type of an accelerometer is suitable for use in the environment of automotive, aircraft testing, environmental test chambers, general laboratory testing, and etcetera.

### **3.2.3. Dynamic Signal Acquisition System**

The Signal Express® PXI-4472 model, data acquisition hardware is designed for sound and vibration measurements. It has eight input channels to digitise input signals from the modal hammer and all directions of the accelerometer simultaneously. The Signal Express® signal analysis software was installed in the PXI-4472 hardware. An external monitor and keyboard were used to navigate the software.

### **3.2.4. Computer Aided Design (CAD) Softwares**

CAD models for sleepers and rail pads were developed with the use of Creo Parametric for 3D modelling, version 4.0. Rails, sleepers and the wheelset models were developed with the use of MicroStation for 3D modelling, version 8i. All CAD models were assembled in MicroStation, version 8i. The sources for the CAD models were detailed and approved technical drawings for all geometries.

### **3.2.5. FEA Softwares**

Patran 2019 was used to develop FEMs for analysis and Nastran was used as the post-analysis solver. Patran is widely used in industry for modelling and solving of linear, nonlinear, explicit dynamics, thermal, and other FE problems. Patran is a pre-processing modelling software that supports post-processing solvers such as MSC Nastran, Marc, Abaqus, LS-DYNA, ANSYS, and Pam-Crash. The next subsection outlines details on a typical experimental setup for modal analysis.

## **3.3. Methods**

The important methods adopted in the current study are the experimental modal analysis and the FEA structural response analysis, which includes modal analysis on the locomotive traction wheelset and the complex eigenvalue analysis for wheelset-track modelling.

### 3.3.1. Experimental Setup for Modal Analysis

Figure 3.6. shows a typical experimental setup on a railway wheel.

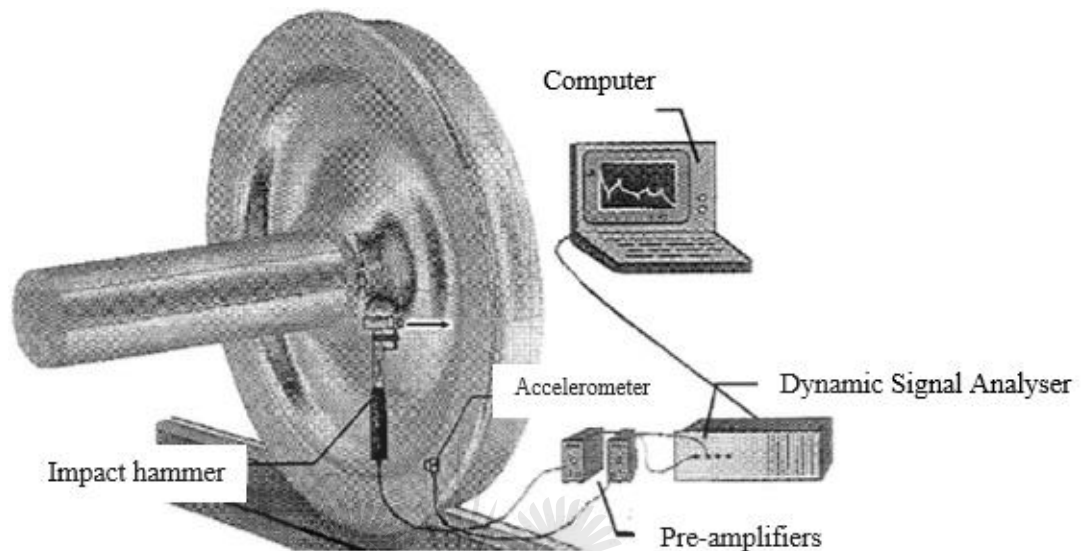


**Figure 3.6.** Typical experimental modal analysis setup with an impact hammer as the force excitation instrument. Reprinted from [223].

Figure 3.6. shows a typical experimental setup of a wheel resting freely on a rail. In the current work a complete wheelset was coupled to a traction motor and installed in a bogie. The same experimental setup for the modal method is adopted in determining the vibrational response of the D39 200 locomotive class wheels and that of rail tracks. Modal analysis is the method of measuring the response of a structure which can be characterised by damping effect, natural frequency, modal mass and mode shape [215].

The response of the structure is measured simultaneously with the unit force [216]. The accurate response of a structure is determined by the system through solving of equations of motion [217]. Modal analysis can be done mathematically and experimentally. The mathematical method involves uncoupling of the equation of motions so that each equation of motion can be separately solved [215].

The numerical approximation methods such as the FE and boundary-element can be used in cases where it is impossible to find the solution [215]. The next sub-subsection outlines details of mathematics behind analysis of a dynamic system.

### 3.3.2. Mathematics of Dynamic Response Analysis

The equation of motion used to solve for mode shapes and natural frequencies is as follows is outlined by Visser [217] as follows:

$$([K] - \omega^2[M])\{U\} = \{0\} \quad (3.1)$$

where  $\omega^2$  is the eigenvalue and  $\{U\}$  is the eigenvector. The eigenvector  $\{U\}$  with the corresponding frequency  $\omega$  is the solution to this equation.

Modal analysis is a commonly used method to study the response of structures in the railway industry [218]. The method can be conducted on a train pass, where the wheels of a train apply unsteady dynamic loads on the rail running surface, thereby exciting the wheel-rail system [106].

A structure can also be manually excited using an impact hammer, where it is not possible to use a shaker or a train pass method. The next sub-subsection outlines modelling of the rail track ballast.

### 3.3.3. Modelling the Ballast

The bottom ballast was modelled as the stiffest of the three layers. Figure 3.7. shows the model representing a ballasted track with three layers.

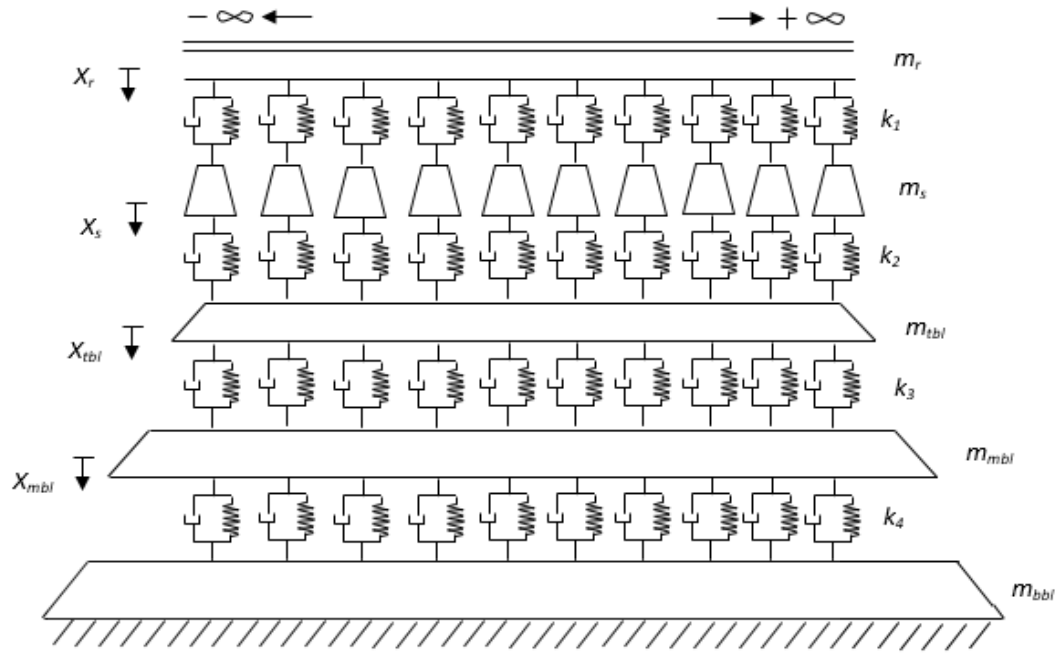


**Figure 3.7.** Railway track model representing inclusion of ballast layers on a track.

In Figure 3.7. a superstructure with rail, rail pad and concrete sleepers is modelled on top of a ballast. Different parameters are represented in the model, where  $m_r$ ,  $m_s$ ,  $m_{tbl}$ ,  $m_{mbl}$  and  $m_{bbl}$  respectively represent the masses of rail, sleeper, top ballast layer, middle ballast layer and the bottom ballast layer. The vertical displacement of the rail, sleepers, top ballast layer, middle ballast layer and bottom ballast layer are represented by  $X_r$ ,  $X_s$ ,  $X_{tbl}$  and  $X_{mbl}$ , respectively.  $k_1$ ,  $k_2$ ,  $k_3$  and  $k_4$  respectively represent the vertical stiffness between the rail and sleepers, the sleeper and top layer ballast, the top and the middle layer ballast, and also, the middle and bottom layer ballast.

In Figure 3.7. the stiffness per unit length,  $k_4$  was taken from the study by Thompson [106] as  $300 \text{ MN/m}^2$  and the degree of stiffness was assumed to reduce by 10% on each layer up to the first layer. This way  $k_3 = 270 \text{ MN/m}^2$ ,  $k_2 = 243 \text{ MN/m}^2$  and  $k_1 = 219 \text{ MN/m}^2$ . The mass of sleepers per unit length,  $m_s$  was taken from Thompson [106] as  $250 \text{ kg/m}$ . The rail mass per unit length,  $m_r = 57 \text{ kg/m}$  for the rail on concrete sleepers and  $48 \text{ kg/m}$  for the rail on steel sleepers. The ballast mass was assumed to constant for the three layers. The bottom ballast mass was calculated from the density of  $2700 \text{ kg/m}^3$  using the volume of one ballast layer, which is  $9.9 \text{ m}^3$ . Hence the ballast mass for the bottom layer was calculated as  $26.73 \text{ ton}$ . The of ballast layer was assumed to reduce by 10% on each layer up to the first layer

### 3.4. The Pyramid Model of the Ballast

A three-layered type of ballast is adopted in the current study. A railway ballast arranged in more than a single layer works better than a single-layered ballast with respect to preventing ballast settlement [219]. In multi-layered ballasted tracks the most bottom layer is designed with the highest vertical stiffness than the other layers above [219, 220]. The stiffness of the most bottom ballast layer usually exceeds that of the top layers by around 20% [231]. Figure 3.8. shows a ballasted track with a good ballast height.



**Figure 3.8.** Ballasted railway track with a good ballast height

When ballast settlement occurs, the ballast rocks are displaced wider than the initial position and the ballast height becomes shorter than prescribed in the design. Parts of track ballast in the current study are adopted from the Ali Zakeri and Ali Mosayebi [220] model, with the use of parameters applicable to the railway track with which the current study is concerned. The method by the authors is pivoted around the pyramid mode.

The model by Ali Zakeri and Ali Mosayebi [220] proposes that in train pass, if the assumed position of the train wheel is between two sleepers, the pyramid shapes occur in the ballast between successive sleepers. The angle at which the stress is distributed increases with an increase in the depth of each ballast layer [220]. This increases the

possibility of overlapping of stresses distributed in the successive layers of the ballast, more in particular in the bottom layers [220]. The authors further derived the theory to determine the stiffness of each ballast layer based on the “pyramid” models seen in Figure 3.9.

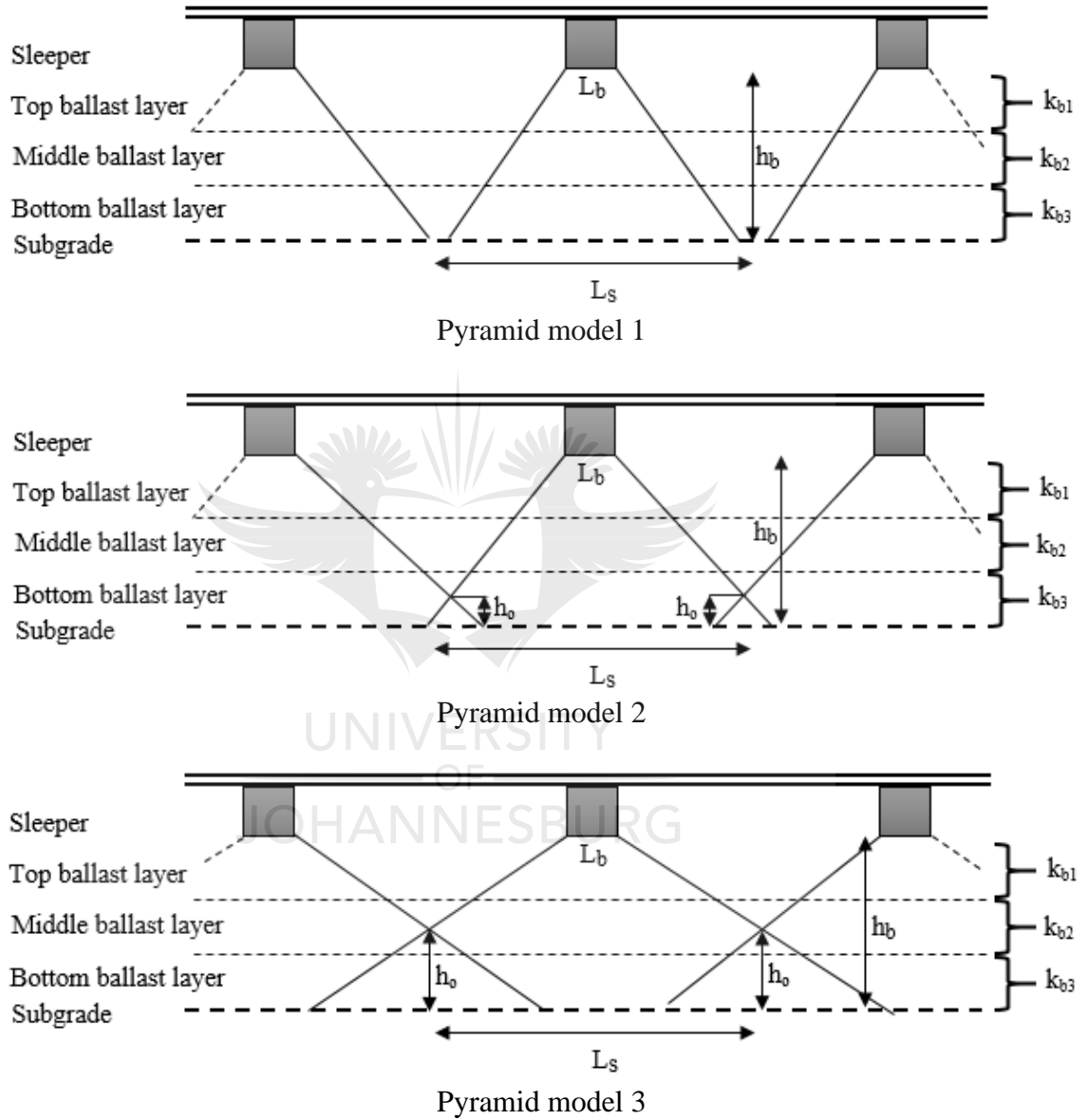


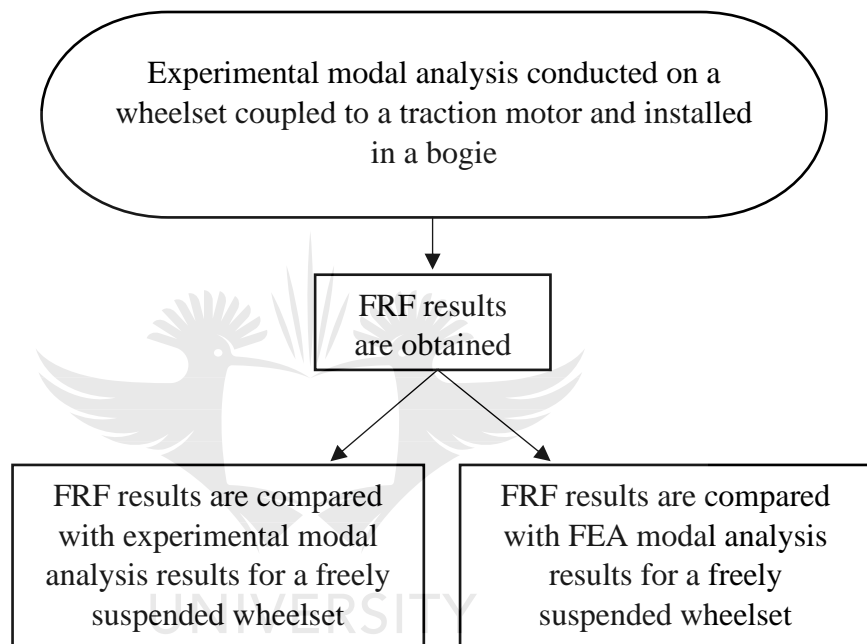
**Figure 3.9.** Pyramid models of a ballasted track. Redrawn from [220]

In the pyramid models in Figure 3.9,  $L_b$ ,  $L_s$  and  $h_b$  are the width of sleepers, length between successive sleepers and the depth of ballast respectively. The depth of ballast in which the overlap occurs is represented by  $h_o$ . The ballast stress is distributed at an angle with reference to the surface of each ballast layer. The stress distribution angles

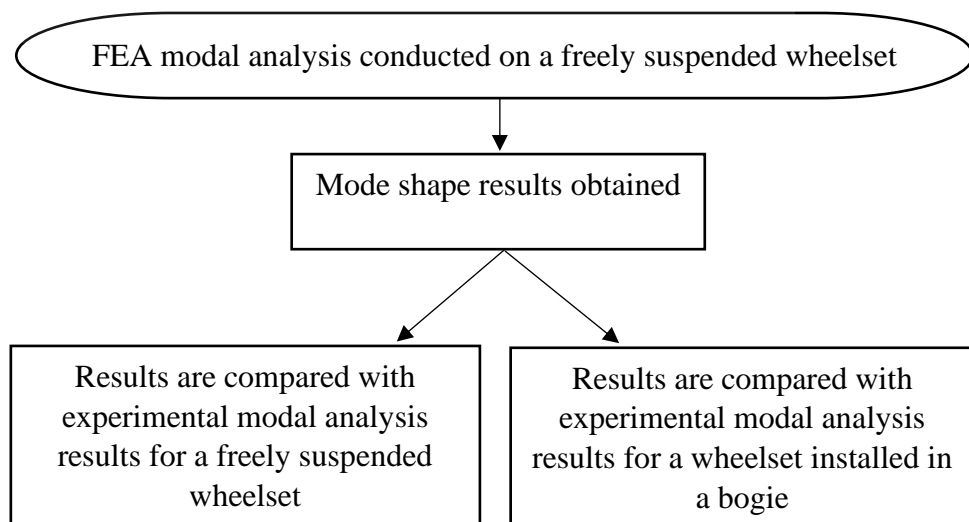


are not shown in Figure 3.9. due to space constraints, however they are clearly visible in [220]. The stress distribution angles are represented by  $\alpha_1$ ,  $\alpha_2$  and  $\alpha_3$  for stress distribution angles in the top, middle and bottom ballast layers respectively [220]. The stiffness of each of the three ballast layers are derived by the authors and represented in the pyramid models by  $k_{b1}$ ,  $k_{b2}$  and  $k_{b3}$  respectively.

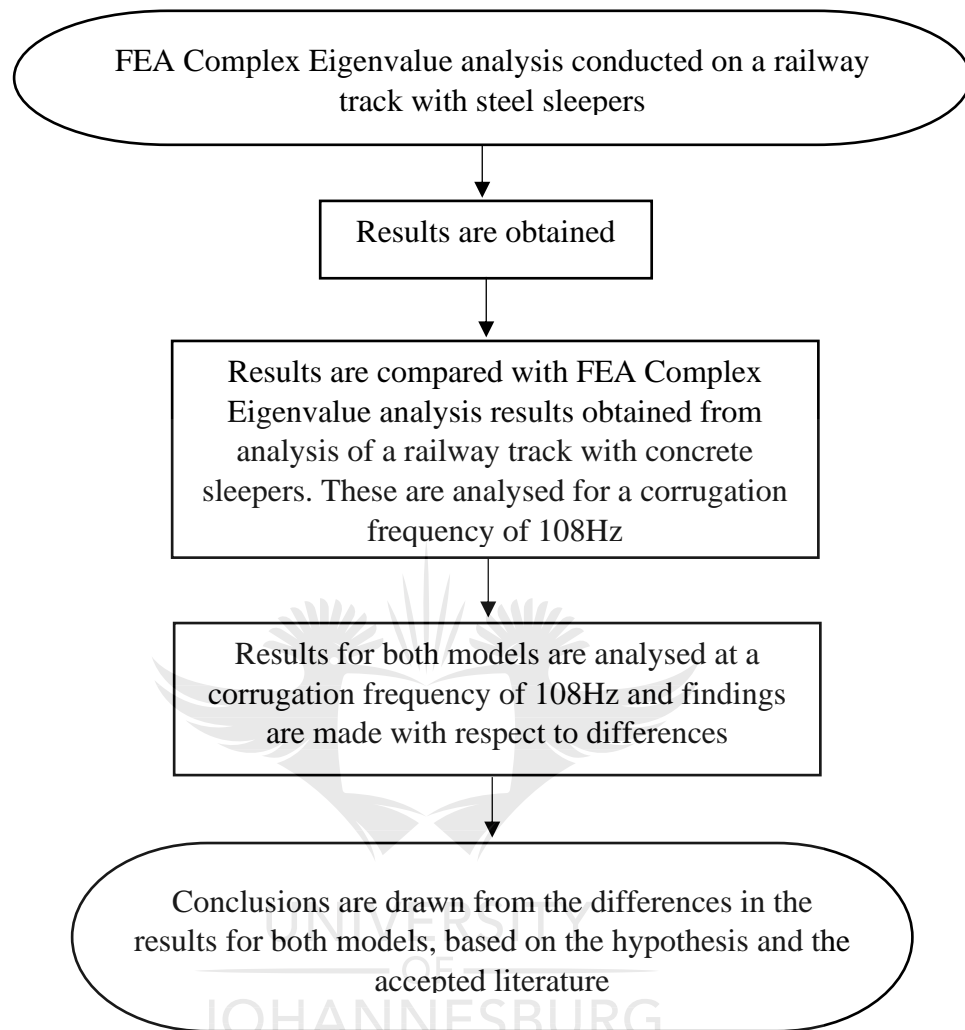
### 3.5. Flow Diagram for Purpose of Experimental Modal Analysis on a Wheelset Installed in a Bogie



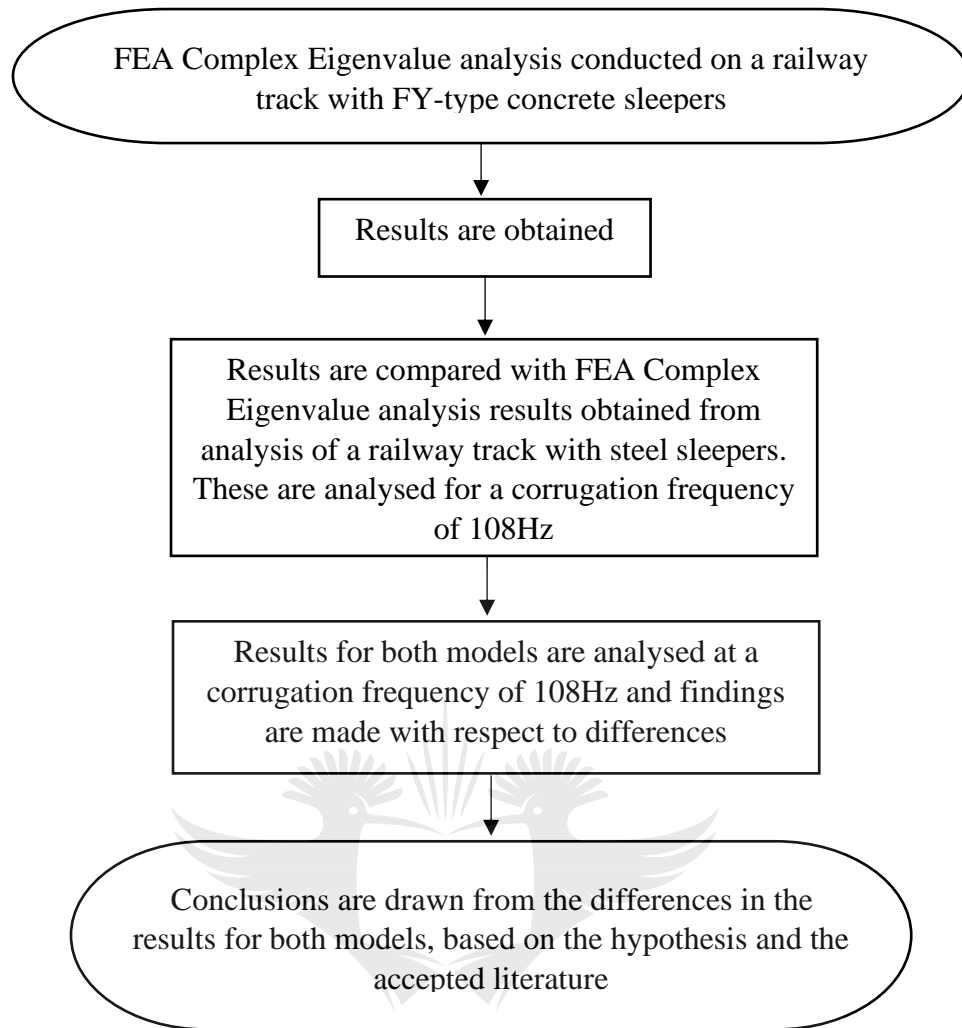
### 3.6. Flow Diagram for Purpose of FEA Modal Analysis on a Freely Suspended Wheelset



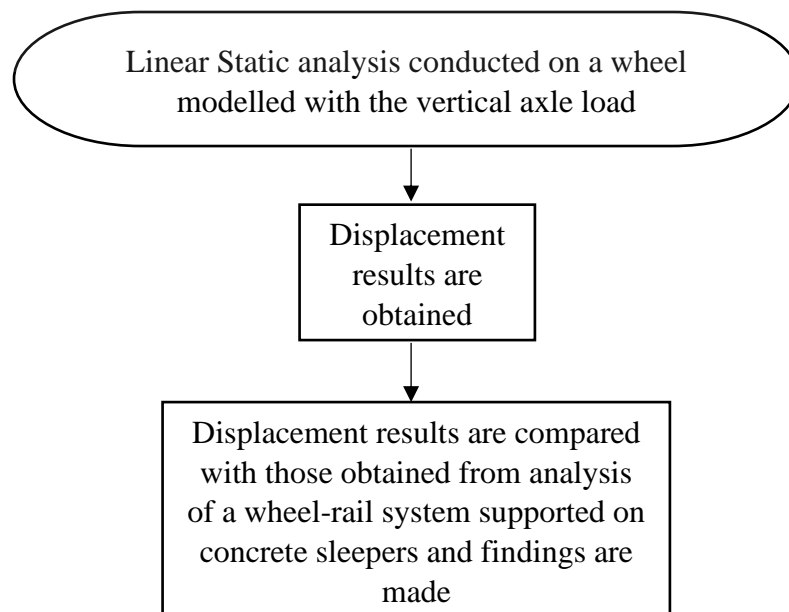
**3.7. Flow Diagram for Purpose of Complex Eigenvalue Analysis on Railway Track Installed with Steel Sleepers**



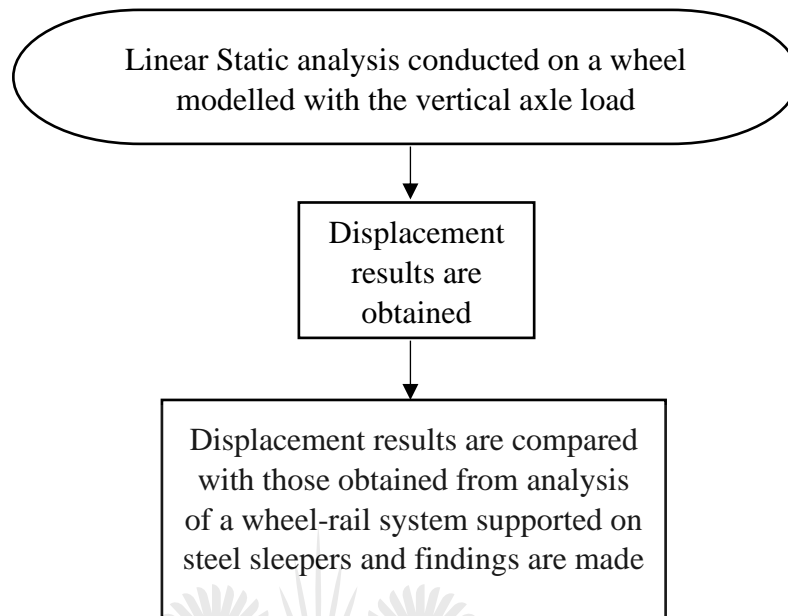
**3.8. Flow Diagram for Purpose of Complex Eigenvalue Analysis on Railway Track Installed with Concrete Sleepers**



### 3.9. Flow Diagram for Purpose of Linear Static Analysis on a Wheel-Rail System Supported on Steel Sleepers (in Appendix A)



### 3.10. Flow Diagram for Purpose of Linear Static Analysis on a Wheel-Rail System Supported on Concrete Sleepers (in Appendix A)



### 3.11. Mass Checking for Finite Element Models (FEMs)

In order to ensure that geometries were modelled accurately, a mass check was conducted manually by comparing the weight of a geometry in the real-world with the mass of the FEM. Table 3.2. shows the comparison between masses of components with their modelled masses.

**Table 3.2.** FEM mass checking

Geometry	Expected Weight (kg)	FEM Weight (kg)
Wheelset	1755.0	1751.91
FY-type concrete sleeper	290.0	287.55
Steel sleeper per meter length	48.4	44.24
Rail (1 meter) for steel sleepers	48.0	48.69
Rail (1 meter) for concrete sleepers	57.0	57.52

The expected weights in Table 3.2. were provided with specifications available for internal use in the Transnet. However, the weight of the steel sleeper was taken from a data sheet from cross section 202 of the British Steel data sheet [221].

### **Chapter Three Summary**

In this chapter, the materials used for the purpose of the research are outlined. Where data was available, particulars of each material are specified. Different materials were used on different experimental and modelling work. The method used for each experiment and modelling is outlined. Parameters used in FEA modelling are outlined for geometry, meshing, properties, loads and boundary conditions (where applicable).

Results for dynamic response of the railway wheel-track were obtained from experimental and modelling work. The results were obtained for analysis of track on concrete and steel sleepers. The next chapter outlines and interprets the results for works conducted in the current study.



## Chapter Four

### Experimental Modal Analysis on a Wheelset Installed in a Bogie

*What results were obtained from experimental work conducted to study wheelset dynamics, and how are they interpreted?*

The purpose of this chapter is to investigate the wheelset resonance modes when the wheelset is installed in a bogie in order to account for possible bogie elastic modes. The primary aim of the experiment was to establish whether there are possible wheelset vibration modes that may be associated with rail corrugation at a corrugation frequency of 108Hz. The secondary aim of the experiment was to compare the FRF results with those obtained in the previous study [10], in which the wheelset was freely suspended. Experimental work on wheels was conducted on one wheelset of the D39 200 locomotive class. This section gives details and results on experimental modal analysis conducted. Given that rail corrugation fixed on rails in the current study is of short pitch wavelengths, with average train velocities of around 30km/h, the results are reported for a low frequency range of vibration. The frequency range of importance in the current study is 0 – 120Hz and the results are reported for the frequency range of 0 – 500Hz.

The previous research study [10] by the author on the same railway line found corrugation wavelengths to be fixed by the axial bending of the locomotive wheelsets at a frequency of 108Hz. This finding was more evident for wheels used by loaded trains, hence in terms of the wheelset dynamics, the current study investigates dynamics of the wheels at the short pitch corrugation formation frequency of 108Hz, when the wheelset is installed in a bogie [10].

The next subsection outlines the environment in which the experimental modal analysis was conducted on wheels.

#### **4.1. Experimental Setup for Modal Analysis on a Wheelset installed in a Bogie**

The experimental setup for modal analysis on freely suspended wheelset are detailed in the previous study [10] by the author. In order to account for interaction of a bogie with the wheelset on corrugated rails, the experimental modal analysis in the current study also involves a wheelset installed in a bogie.

A bogie already used by one of the D39 200 class locomotives was used for the experiment. The procedure followed in the experimental work for modal analysis on wheels is first outlined, followed by the presentation of the results obtained. The next sub-subsection outlines the environment in which the experimental modal analysis on a wheelset installed in a bogie was conducted.

##### **4.1.1. Environment in which Experimental Modal Analysis Was Conducted on a Wheelset Installed in a Bogie**

The experiment was setup in the Minor Overhaul Program (MOP) workshop for locomotives at the Transnet Engineering (TE) facility situated in the East of Pretoria, in South Africa. A complete bogie with wheelsets coupled to traction motors was removed from one of the class D39 200 locomotives and put aside for testing. In the previous study by the author [10] experimental modal analysis was conducted on a freely suspended wheelset, the experimental procedure for which is well detailed in the same study [10].

In the current study the wheelset is installed in a bogie to account for elastic modes from the bogie structure. The results are presented for both cases. An overhead crane was used for lifting the bogie frames slightly clear from the ground, to prevent critical damping of the wheels. Figure 4.1. shows how the bogie was suspended.



**Figure 4.1.** D39 200 locomotive class bogie with wheelsets and traction motors. Wheels prepared for experimental modal analysis

The PXI, computer monitor and keyboard were put on the bogie frame, further away from the wheels, such that they would not interfere with the measured response of the wheelset. No vibrating equipment and machinery was put closer to the testing area and some of the locomotive equipment was moved away from the bogie to create a clear and better environment for testing.

The next sub-subsection outlines the procedure followed in conducting the experimental modal analysis on a wheelset installed in a bogie.

#### **4.1.2. Procedure Followed for Experimental Modal Analysis on a Wheelset Installed in a Bogie**

The first step in experimental modal analysis on the traction wheelset was to locate the best part of the wheel on which the excitation force would be applied. This is done following Fourie's [23] explanation of the dynamic behavior of a railway wheel. This fundamental step is also important in order to ensure that the excitation force and the accelerometer are not applied at a node.

Fourie explains a railway wheel behavior and likens it with a flat surface disc when under vibration. The primary difference being that the cross section of the railway



wheel is not symmetrical. During vibration a disc forms different mode shapes. These mode shapes form such that, if a disc is perfectly symmetrical, two points of a disc can vibrate orthogonally relative to one another as seen in Figure 4.2. [23].

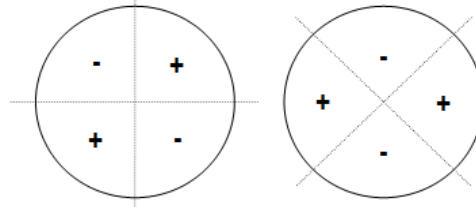


**Figure 4.2.** Two-nodal-diameter spatially orthogonal axial mode pair. Reprinted from [23].

The vibration phase of one part of the disc relative to the other is denoted by positive and negative. Vibration of two orthogonal parts of the disc may be in phase or out of phase relative to one another. This theory was validated with the use of a Finite Element model of the D39 200 locomotive wheel, on a different study in which the author was involved, which was yet to be published. Figure 4.3. shows the mode shapes of the D39 200 wheel at two frequencies.

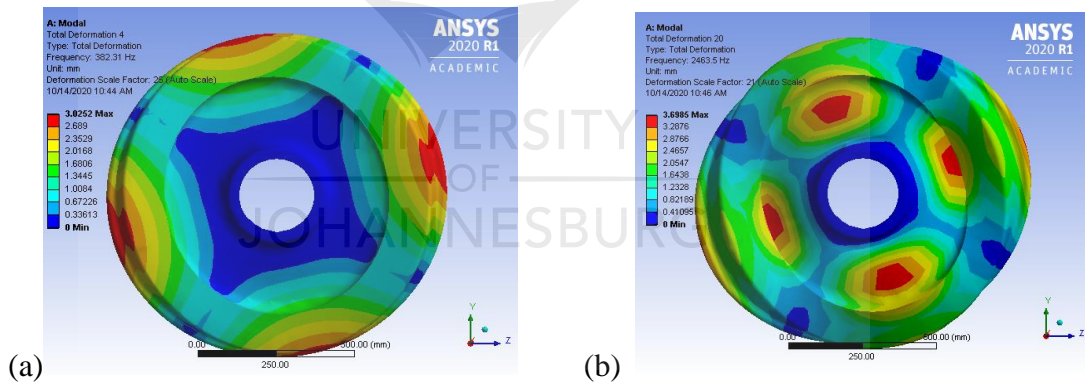


**Figure 4.3.** Vibration mode shapes of the D39 200 locomotive wheelset (a) at 382Hz (b) at 2463Hz.

Fourie [23] further explains that there are three modes during vibration of the flat surface disc i.e. axial, radial and circumferential. The axial mode occurs when vibration is normal to the disc surface. The radial mode occurs when vibration is normal to the circumference. Lastly, the circumferential mode occurs when vibration is tangential to the circumference of the disc [23].

Figure 4.4. shows the measurement points on the wheel profile, on which the accelerometer was placed. Impacts were applied as close as possible (approximately 5mm) to each accelerometer placement point (from A to D) on the wheel thread. In order to ensure that the points A – D in Figure 4.4. were not nodal points the manual verification was conducted, where two impacts were applied and the response was assessed in the response window. About 30 averages were used to better define a single FRF. The repeatability was ensured by repeating averages twice at the same location. The system was given sufficient time to stabilise after each impact. Each impact was delivered as normal to the surface as possible.

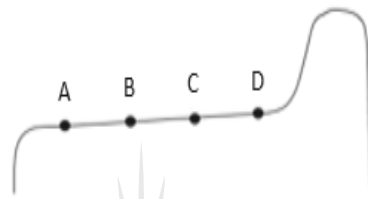


**Figure 4.4.** Wheel thread locations (A – D) where accelerometer was rigidly mounted and the wheel was excited.

A wheelset already used by a locomotive was utilised for the experiments. The used wheelset had a diameter of approximately 987.2mm. The minimum and condemning diameters for the wheelset are 927 and 1016mm respectively. The wheel profile was cleaned using a die grinder and was wiped. The wheel circumference was measured and accurately divided into four quarters using a tape measure and a marker.

The wheelset was coupled to a traction motor and installed in a bogie. The entire bogie structure was freely suspended from the ground. The FRFs were measured from response of both the gear and non-gear side wheels. The distance between each point from points A to D in Figure 4.4. is 30mm. Excitation was applied in the radial (normal to the wheel thread), axial (normal to the wheel rim) and circumferential (tangential to the wheel thread) directions.

A steel block was rigidly mounted on the wheel thread as seen in Figure 4.5. in-between the excitation points B and C, leaving approximately 5mm away from each point. Circumferential impacts were applied on the steel block.



**Figure 4.5.** Steel block stuck on traction wheel thread for circumferential excitation.

The circumferential impacts were applied using a smaller model (2302) hammer in the direction of the red arrow in Figure 4.5. A steel block in Figure 4.5. has a negligibly small mass (approximate dimensions: 20mm x 20mm x 20mm) when compared to the mass of the wheel. In order to ensure that enough data is obtained for analysis the Nyquist theorem [222] was applied, which states that the sample rate used should be twice or greater than the highest signal frequency analysed. The experiment was hence sampled at 2kHz.

In order to obtain a point FRF from axle coupling, one wheel was excited whilst the response was measured from an opposite wheel of the same wheelset. In this way vibration energy in the excited wheel is transferred to the opposite wheel through the axle. The next subsection reports on the results obtained from experimental modal analysis on a freely suspended wheelset.

#### **4.2. Results for Experimental Modal Analysis on a Freely Suspended Wheelset and on a Wheelset Installed in a Bogie**

The results for experimental modal analysis are presented for two cases: firstly, for the traction wheelset freely suspended and secondly for the case in which the wheelset was coupled to a traction motor and installed in a bogie, in order to account for wheelset-bogie integration. The results for the freely suspended wheelset were reprinted from the previous study [10] by the author and those for the wheelset installed in a bogie are obtained in the current study.

Given that vibration modes of the circumferential response were not found to be clearly pronounced in the previous study [10] by the author, FRFs for dynamic response of wheels were presented for the radial and axial (lateral) directions, whilst

in the current study they were also found to be well pronounced in the circumferential direction. The traction wheelset used for the experiment and modelling belongs to the class D39 200 diesel locomotive. The wheelset was suspended from the ground to avoid critical damping of vibration of the wheelset.

In FEA modal analysis to investigate mode shapes of the traction wheelset, only the freely suspended wheelset was modelled. The exact bogie could not be modelled due to copyright restrictions from the supplier. The next sub-subsection reports on results for experimental modal analysis on the freely suspended wheelset.

#### 4.2.1. Results for Experimental Modal Analysis on a Freely Suspended Wheelset

Figure 4.6. shows FRFs representing vibration response for the freely suspended class D39 200 locomotive wheelset in the radial and axial directions. Only the FRFs for the lateral vibration response were found to be well pronounced for the freely suspended wheelset. The FRFs for both wheels of the wheelset were found to be well pronounced and hence were presented for both wheels (gear and non-gear side).

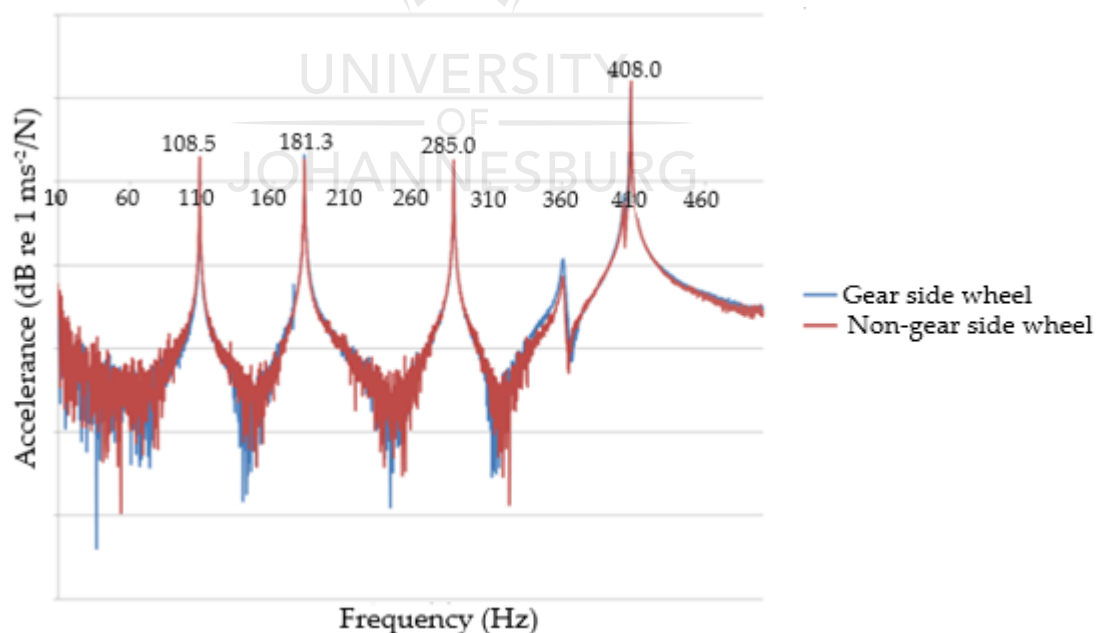


**Figure 4.6.** FRFs for the gear-side wheel of the class D39 200 locomotive wheelset coupled to a traction motor and installed in a bogie. Vibration response for the axial directions (diameter approximately 993.6 mm).

In Figure 4.6. the accelerance on the Y-axis represents the acceleration per unit force and the X-axis represents the frequency at which the accelerance occurs. The narrow peaks of the FRF represent resonance vibration of the wheel at a given frequency. The ditches represent the anti-resonance of the wheel vibration. At anti-resonance the wheel does not vibrate with the highest vibration amplitude, and the case is otherwise with vibration at resonance.

The vibration frequency window captured is at a frequency range of 0–500Hz; interesting resonance modes and anti-resonance vibration are noted in a frequency range of 10–460Hz. This frequency range corresponds to a short pitch corrugation frequency. In Figure 4.6. it is noted that during vibration of the wheels in the lateral direction, the second bending vibration mode of the wheels occurs at 108.5Hz and the first torsional mode at 181.3Hz. The second torsional mode occurs at 285Hz and the second torsion at 408Hz.

In Figure 4.6, the resonance mode occurring at a frequency of 360Hz is heavily damped, and hence not considered in the investigation. The damping of the FRF is noted by a broader peak, which is not very narrow on the tip. There also proves not to be much activity on the vibration mode at 360Hz given a slow acceleration of the response per the unit force applied, whilst the wheel is noted to vibrate at antiresonance around same frequency.

#### 4.2.2. Results for Experimental Modal Analysis on a Wheelset Installed in a Bogie

Figure 4.7. shows FRFs representing vibration response for the class D39 200 locomotive wheelset in the radial, axial and circumferential directions.

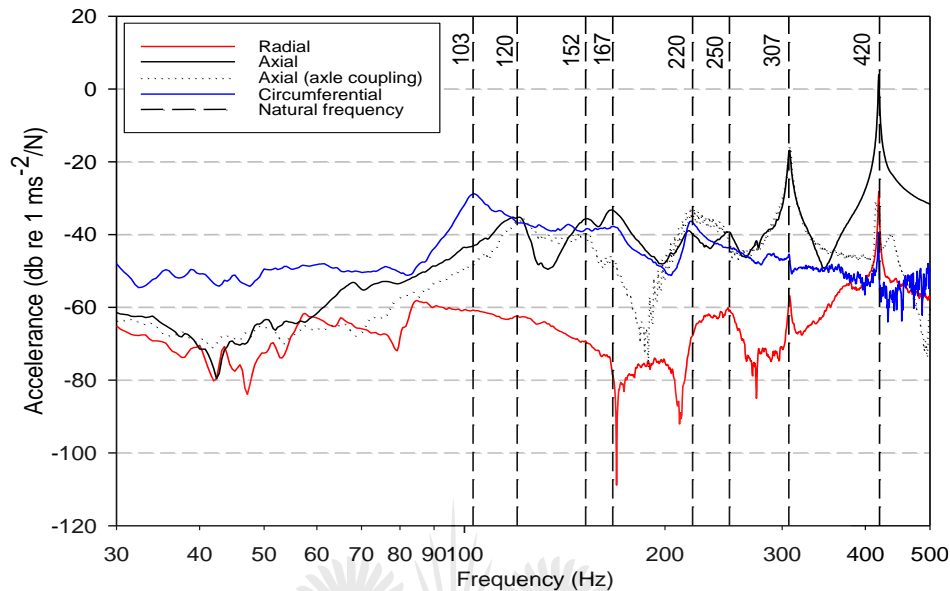


**Figure 4.7.** FRFs for the gear-side wheel of the class D39 200 locomotive wheelset coupled to a traction motor and installed in a bogie. Vibration response for radial, axial and circumferential directions (diameter approximately 987.2 mm).

In Figure 4.7. experimental modal analysis was conducted on a used wheelset with a diameter of approximately 987.2mm, installed in a bogie. Due to similarity in the results obtained from modal testing of both wheels of the traction wheelset, the FRF results presented are for the gear-side wheel only. The minimum and condemning diameters for the wheelset are 927mm and 1016mm respectively.

The FRFs data was obtained for different directions of response as an output from the Fast Fourier Transform (FFT) analyzer and the data points were manually categorized by the author, according to the direction of vibration response. The first resonance mode occurs at 103Hz in the circumferential direction. The first resonance mode in the axial direction occurs at 120Hz. From the FRF for response of the wheel in the axial direction; the resonance modes show some resonance damping in the frequency range of 0 – 250Hz, where resonance peaks are broader than those in the frequency range of 250 – 500Hz.

In addition, resonance modes occur with less accelerance (acceleration per unit force) as compared to those in the frequency range beyond 250Hz. Vibration response of the wheelset is lightly damped for resonance modes that occur at a frequency of 307Hz and 420Hz, where resonance peaks are sharp and narrower. For the axle coupling response in the axial direction, the response is also damped in the frequency range of 0 – 250Hz, where resonance modes have broad peaks.

Considering the FRF for response of the wheel in the circumferential direction; most of the response is heavily damped, given that most of the FRF is flatter. In this direction, two damped resonance modes occur at 103Hz and 220Hz. A lightly damped cross-coupling resonance mode occur at 420Hz in three directions i.e. axial, radial and circumferential. Considering all four FRFs; the response in the axial direction is the most pronounced at frequencies of 307Hz and 420Hz, with easily identifiable resonance peaks.

In terms of accelerance, the FRF representing the radial response has the lowest accelerance. Response is damped in all directions in the frequencies below 103Hz. A resonance mode excited at a frequency of 103Hz in the circumferential direction is the closest to the corrugation formation frequency (108Hz). Two axial vibration modes, which include the wheelset axle cross-coupling mode, that occur at 120Hz are reasonably closer the corrugation formation frequency.

The axle-coupling mode was excited from measuring vibration response of one wheel of the wheelset, whilst the dynamic loads are applied on the opposite wheel. This mode is excited at 120Hz. This is in better agreement with the previous study [10] by the author that found the axial vibration of the wheelset for the same locomotive class, to be associated with corrugation formation frequency.

The next sub-subsection correlates the resonance modes obtained from experimental modal analysis on wheelsets freely suspended and installed in a bogie, with corrugation frequencies in the affected railway line.



#### 4.2.3. Correlation of Results for Experimental Modal Analysis on a Wheelset (Freely Suspended and Installed in a Bogie) with Corrugation Frequencies

In the previous study [10] by the author corrugation frequencies in track curves were determined with the use of train velocities and corrugation wavelengths measured from each track curve. Table 4.1. contains corrugation frequencies calculated using velocities associated with loaded trains.

**Table 4.1.** Corrugation frequencies per track curve

Test Point	Track Kilometer Point	Average Wavelength (m)	Average Loaded Trains' Velocities (m/s)	Average Empty Trains' Velocities (m/s)	Corrugation Frequency Associated with Loaded Trains (Hz)
4	165/8	0.09	10.83	13.33	120.37
5	169/3	0.082	7.5	10	91.46
6	172/14	0.086	8.89	10.56	103.36
7	178/3	0.084	8.33	10.83	99.21
7	178/3	0.082	8.33	10.83	101.63
8	181/13	0.068	7.78	11.39	114.38
9	183/3	0.074	8.61	10.28	116.37
10	183/7	0.082	8.89	7.78	108.4
11	184/4	0.068	8.06	9.17	118.46
12	184/13	0.082	8.61	8.06	105.01
18	215/15	0.058	8.61	9.17	148.47
20	216/18	0.077	8.61	9.17	111.83

In Table 4.1. the track curves from which wavelengths were measured are referred to as “Test Points”. The average wavelengths were measured at the beginning and in the middle of the curve for test point 7, to validate repeatability of the results. The train velocities used were for loaded and empty trains, hence the results were distinguished between corrugation frequencies associated with loaded and empty trains. It was found that only corrugation frequencies associated with loaded trains (presented in the current study) are reasonably closely related to resonance modes of the D39 200 locomotive wheels. Figure 4.8. shows natural frequencies of the D39 200 locomotive wheelsets freely suspended and installed in a bogie. These natural frequencies are matched with corrugation frequencies per track curve.

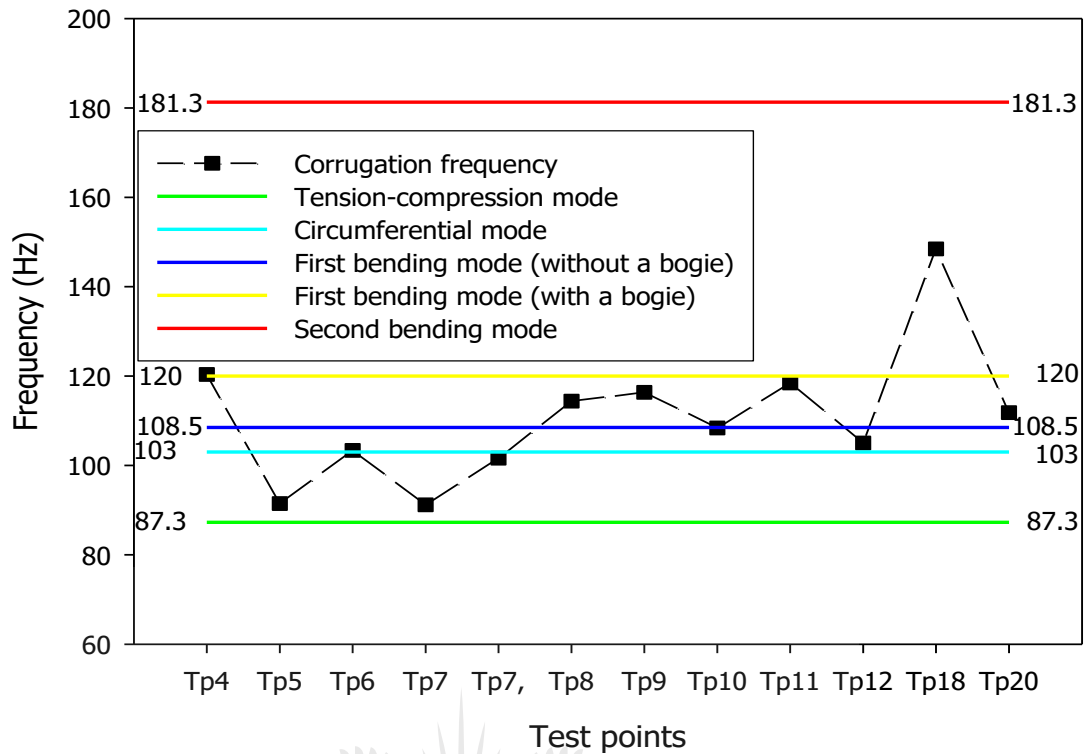


**Figure 4.8.** Fundamental vibration modes of the D39 200 locomotive wheelset matched with corrugation frequencies around each rail track curve.

Evident in Figure 4.8. is that corrugation frequencies around each track curve investigated are more associated with the first axial bending and circumferential modes of the D39 200 locomotive wheelset. The circumferential mode occurs at 103Hz when a wheelset is coupled to a traction motor and installed in a bogie, whilst the first axial bending mode occurred at 108Hz when only the wheelset was freely suspended.

This first axial bending mode at 108Hz shifts to a frequency of 120Hz when the wheelset is installed in a bogie. The second axial bending mode of the wheelset (at 181.3Hz) is not closely associated with corrugation frequencies. The tension-compression mode of the wheelset that occurs in the longitudinal direction is barely closely associated with corrugation frequencies around track curves.

Corrugation wavelengths were measured with a 300mm long ruler. The running surface of the rail was first cleaned and wiped for clear visibility of corrugation peaks. Corrugation peaks were marked at the center of each peak. Complete wavelengths were measured on a peak-alley-peak sequence to complete a wavelength. An average

wavelength was calculated from the data. Together with train velocities, average wavelengths per track curve were used to calculate a corrugation-borne frequency.

With respect to the number of samples used to estimate the average wavelengths; eleven track curves were selected amongst a total of twenty seven track curves. Only the heavily corrugated track curves were included. The light and heavily corrugated curves were differentiated based on visual inspection. Fifteen corrugation wavelengths were measured on each track curve, after which the average wavelength was calculated for each track curve.

The average wavelength for a track curve was calculated by summing up the wavelengths, divided by the number of complete waves. With respect to the number of samples used to estimate the average train velocities, the velocities data were downloaded from each of the thirteen locomotives for a trip when it was running loaded and empty on each track curve.

Velocities were measured for thirteen locomotives on each track curve. However, fifteen data points were obtained, given that two of the thirteen locomotives were measured twice for the trips when they were running loaded and empty. The average velocity around each track curve was ultimately calculated by summing up train velocities from fifteen trips, divided by fifteen [10].

The next subsection discusses critical findings on results for experimental modal analysis on wheelsets freely suspended and installed in a bogie. In addition, it discusses how resonance modes obtained relate to corrugation frequencies in corrugated track curves.

### **4.3. Results Discussion**

In addition to the axial mode at 108Hz that was obtained from a freely suspended wheelset, this study found an additional mode in the circumferential direction, which is associated with corrugation frequencies on track curves. From the wheelset modal analysis results it is concluded that two resonance modes of the D39 200 locomotive

wheelset are associated with the formation of corrugation on rails in the Belfast to Steelpoort railway line.

This is found when the dynamic response of the traction wheelset is investigated in the frequency range corresponding to short pitch rail corrugation. These resonance modes are found to match (reasonably), the average corrugation-borne frequency calculated for each rail track curve using average train velocities and wavelengths in the previous study by the authors.

The average corrugation frequencies used in the current study were calculated using average train velocities for loaded trains. The first resonance mode of the traction wheelset occurs at 103Hz in the circumferential direction, when the wheelset is coupled to a traction motor and installed in a bogie.

The other resonance mode when the traction wheelset is installed in a bogie occurs at 120Hz in the axial direction, this mode shifts to 108Hz when the wheelset is removed from the bogie and freely suspended. The first-order axial bending mode at 120Hz is also excited from a cross-coupling of resonance vibration through a wheelset axle.

Resonance modes look more damped from the FRFs when the traction wheelset is installed in a bogie. From the traction wheelset modal analysis, the first axial bending mode shape can be used to identify parts of the traction wheelset on which wheelset dampers can be applied. This will prevent the traction wheelset from responding erratically to dynamic loads during train movement, more in particular at 103Hz, 108Hz and 120Hz. The next chapter outlines details of the experimental modal analysis on railway tracks.

## Chapter Five

### **Experimental Modal Analysis on Rail Tracks Installed with Steel and with Concrete Sleepers**

*What results were obtained from experimental work conducted to study track dynamics, and how are they interpreted?*

The purpose of this chapter is to investigate the rail tracks' resonance modes for tracks installed with steel and with concrete sleepers. The primary aim of the experiment was to establish whether there are possible rail track vibration modes that may be associated with rail corrugation at a corrugation frequency of 108Hz. The secondary aim of the experiment was to compare the FRF results of the rail tracks supported on steel and concrete sleepers, with those obtained using the Finite Element method for the railway tracks supported on steel and concrete sleepers. The experimental work was conducted on two types of railway tracks: two with concrete sleepers and one with steel sleepers. One of the two tracks was installed with the FY-type concrete sleepers and the other with the PY-type concrete sleepers. This chapter gives details and results on experimental modal analysis conducted on tracks installed with steel and concrete sleepers. The frequency range of importance in the current study is the same as that of experimental work on wheels (which is 0 – 120Hz) even though the results are reported for the frequency range of 0 – 500Hz. This frequency range includes the short pitch rail corrugation formation frequency of 108Hz, which is of importance in the current study. The next subsection deals with how the experiment was set up on rail tracks supported on steel and concrete sleepers.

#### **5.1. Experimental Setup for Modal Analysis on Rail Tracks Supported on Steel and Concrete Sleepers**

One procedure was used to conduct experimental modal analysis on rail tracks with steel and with concrete sleepers. The procedure followed in the experimental work for modal analysis on rail track is first outlined, followed by the presentation of the results obtained. The next sub-subsection discusses the environment in which experimental modal analysis on rail tracks was conducted.

### 5.1.1. Environment in which Experimental Modal Analysis Was Conducted on Rail Tracks with Steel and Concrete Sleepers

The railway line from Belfast to Steelpoort goes through other two towns: Ohrigstad and Lydenburg. The railway line is 223 kilometers long. Research work in this thesis focuses mainly on the part of the railway line between Ohrigstad and Steelpoort, which is a 27 kilometers railway line. This part of the railway line is situated between the rail track kilometer points 163 and 223, which is the part of the rail track that has more severe corrugation. Figure 5.1. shows the freight data that has the railway line from Belfast to Steelpoort, through Lydenburg.

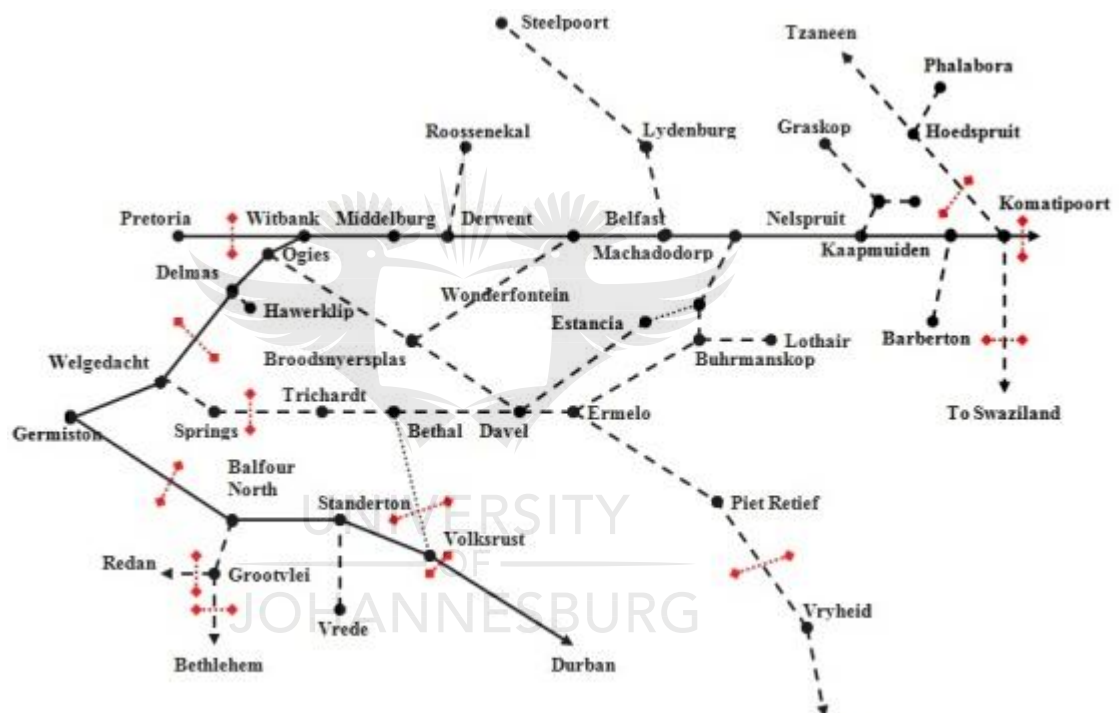


Figure 5.1. Freight data showing the railway line from Belfast to Steelpoort [230].

In terms of altitude, Belfast is higher (2025m above sea level) than Steelpoort (which is 755m above sea level). This means trains are braking for most of the journey when transiting empty from Belfast to Steelpoort to load Ferrochrome. The trains will be in traction for most of the journey when loaded with the product going back from Steelpoort to Belfast. Even though the small town of Steelpoort is missing in the freight data in Figure 5.1. it is situated between Lydenburg and Steelpoort. The ecology around the affected railway line involves houses and shacks, which are a bit far from the railway curves for most of the railway line. However, some are closer



(about 100 meters) to a few affected railway curves. Most part of the affected railway line has trees and large rocks grown on the sides of the railway track. A few parts of the line have a fence closer to the track, to protect animals from crossing into the rail track. Figure 5.2. shows part of the ecology around the corrugated railway track.



(a)



(b)

**Figure 5.2.** Ecology around the affected railway line (a) trees grown on the sides of the rail track (b) rocks on the sides of the rail track.

In some railway track curves the trees have grown much closer to the track. It is only a few track curves that are situated between the hills as seen in Figure 5.2. Some of the track curves are situated on steeper gradients than others and some have smaller radii than others [10]. The inspections and experimental work were always conducted around the summer season for the current study. The climate around the rail track section between Steelpoort and Ohrigstad is usually mostly sunny with somewhat warm temperatures in summer. The next sub-subsection outlines the procedure followed in conducting experimental modal analysis on the railway tracks.



### 5.1.2. Procedure Followed for Experimental Modal Analysis on Rail Tracks Supported on Steel and Concrete Sleepers

The description of the equipment used for the experiment is same as that detailed in Chapter 3 and also shown in Chapter 4, except the fact that sledge hammer, details of which are provided in Chapter 3 was used for experimental work on rail tracks. On all three track curves the procedure followed for the experiment was cleaning of the running surface of the rail using a wheel grinder, measuring and marking the center point of rail between two sleepers and the point of the rail that is resting on top of the sleeper. Figure 5.3. shows the accelerometer position and a steel block used to apply excitations in the longitudinal direction of the rail.



**Figure 5.3.** Field side rail position for accelerometer and a steel block stuck on the rail running surface for longitudinal excitation.

In Figure 5.3. the accelerometer is stuck on the field side of the rail and a steel block for longitudinal excitation on the running surface of the rail. A steel block in Figure 5.3. has a negligibly small mass (approximate dimensions: 30mm x 10mm x 30mm) when compared to the mass of the rail. The longitudinal impacts were applied in the direction of the yellow arrows in Figure 5.3. The accelerometer orientation applicable to each track curve is tabulated in Table 5.1. Details of other track components are also contained in the Table (5.1).

**Table 5.1.** Track components that are above the ballast and the orientation of the accelerometer during experimental Modal Analysis

Accelerometer orientation and track components	
Track kilometer point	178/3
Sleeper type	FY-type concrete sleeper
Fastening system	FISTclip

Rail pad	HDPE
Rail mass	57 kg/m
Accelerometer orientation	<ul style="list-style-type: none"> <li>• X-side of the accelerometer facing vertically down towards the ground to capture the vertical response of the rail,</li> <li>• Y-side facing along the rail in the direction towards the loading site (Steelpoort) to capture the longitudinal response of the rail,</li> <li>• Z-side facing towards the field in the direction orthogonal to the rail to capture horizontal response of the rail.</li> </ul>
Track kilometer point	181/6
Sleeper type	Steel sleeper
Fastening system	Bolt
Rail pad	Not applicable
Rail mass	48 kg/m
Accelerometer orientation	<ul style="list-style-type: none"> <li>• X-side of the accelerometer facing vertically down towards the ground to capture the vertical response of the rail,</li> <li>• Y-side facing along the rail in the direction towards the offloading site (Belfast) to capture the longitudinal response of the rail,</li> <li>• Z-side facing towards the field in the direction orthogonal to the rail to capture horizontal response of the rail.</li> </ul>
Track kilometer point	187/13
Sleeper type	PY-type concrete sleeper
Fastening system	e-Clip
Rail pad	Hytrel/6358
Rail mass	57 kg/m
Accelerometer orientation	<ul style="list-style-type: none"> <li>• X-side of the accelerometer facing vertically down towards the ground to capture the vertical response of the rail,</li> <li>• Y-side facing along the rail in the direction in the direction towards the loading site (Steelpoort) to capture the longitudinal response of the rail,</li> <li>• Z-side facing towards the field in the direction orthogonal to the rail to capture horizontal response of the rail.</li> </ul>

As seen in Table 5.1. the rails supported on both types of concrete sleepers weight 57 kilograms per meter length, whilst the one on steel sleepers weighs 48 kilograms per

meter. Track kilometer points are used to locate the railway track curves. The experiment was conducted on the high rail of the test curve (178/1), on the low rail in track curve 181/6 and on the low rail in track curve 187/13. The types of sleepers installed in the track curves are the FY-type concrete, steel and the PY-type concrete sleepers for track curves 178/1, 181/6 and 187/13 respectively. The next subsection reports on the results for experimental modal analysis on railway tracks supported on steel and concrete sleepers.

## **5.2. Results for Experimental Modal Analysis on Railway Tracks Installed with Steel and Concrete Sleepers**

FRFs on rail tracks are obtained for dynamic response of rails in the vertical, horizontal and longitudinal directions. FRFs are also obtained for vibration response of railway sleepers. The FRF results are reported for track models with concrete (both the FY- and PY-types), and with steel sleepers. FRFs for tracks with concrete sleepers are also compared with those of the track with steel sleepers.

The results are first outlined for rails supported on the FY-type concrete sleepers, followed by the PY-type concrete sleepers, thirdly for the rails supported on steel sleepers and lastly for vibrational response of the two types of sleepers (steel and concrete). The next sub-subsection reports on results for the response of a rail supported on FY-type concrete sleepers.

### **5.2.1. Results for Experimental Modal Analysis on a Rail Supported on FY-Type Concrete Sleepers**

Figure 5.4. shows FRFs and face representing vibration response of rail supported on top of the FY-type concrete sleepers. Here the results are reported for vibration measured in the vertical direction. The results are measured mid-span and on top of sleeper point. In all FRF figures for all experimental modal analyses conducted, the natural frequencies are depicted by the dash lines which were manually identified through a peak-picking method and plotted by the author.

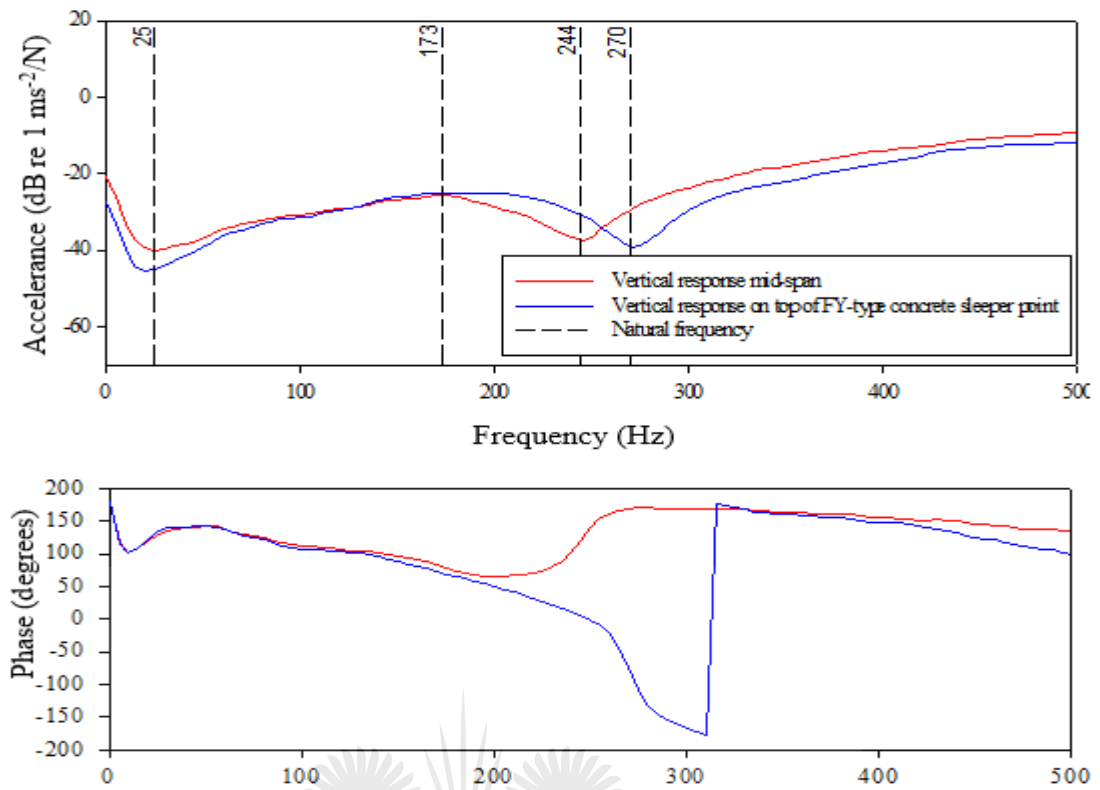


**Figure 5.4.** FRF and phase for rail vibration response, vibration measured in the vertical direction from two positions i.e. mid-span and on top of the FY-type concrete sleeper point.

Evident in Figure 5.4. is that FRFs for vibration response of rail are not as pronounced as those of wheels. The reason for this is explained to be the fact that the wheel is a finite and lightly damped structure [106]. On the other hand, the rail is an infinite continuous body which as a result, easily works as a waveguide, allowing one or more waves to spread away and sideways (along the rail length) from the point of excitation. Thus, the rail presents one or two resonance modes, after which it works as a waveguide.

In addition, a rail is much more damped as compared to a wheel [106]. As seen in Figure 5.4. in the vertical direction, vibration response of the rail mid-span is in phase with that measured on top of sleeper point, at least for the frequency range of 0 – 173Hz. The vibration response of rail is at antiresonance at a frequency of 25Hz. Accelerance of vibration increases from this antiresonance until at the critically damped resonance mode occurring at 173Hz. Accelerance is the frequency-dependent acceleration of a point divided by the force excitation. Given that it is acceleration, it is measured in meters per squared second, after it is measured, it is expressed in

decibels using a reference of one. This makes the graphical representation of data easier, given that FRFs represent response of vibration, and a decibel is a concept of measure that is central to noise and vibration. At a frequency range beyond 173Hz, two antiresonance troughs are identified at 244Hz and 270Hz. At antiresonance the rail vibrates at the lowest amplitude or displacement. Evident in Figure 5.4. is that in the vertical direction, the response of rail to vibration is mostly not at resonance, with one critically damped resonance mode identified.

For the rest of vibration response, the rail acts as a waveguide, hence no more resonance modes are identified. From the FRF results in Figure 5.4. it is understood that, mid-span and on top of sleeper point, no resonance mode is excited in the vertical direction, to exactly match the corrugation formation frequency of 108Hz in the line. Figure 5.5. shows FRFs and face representing vibration response of rail supported on top of the FY-type concrete sleepers.

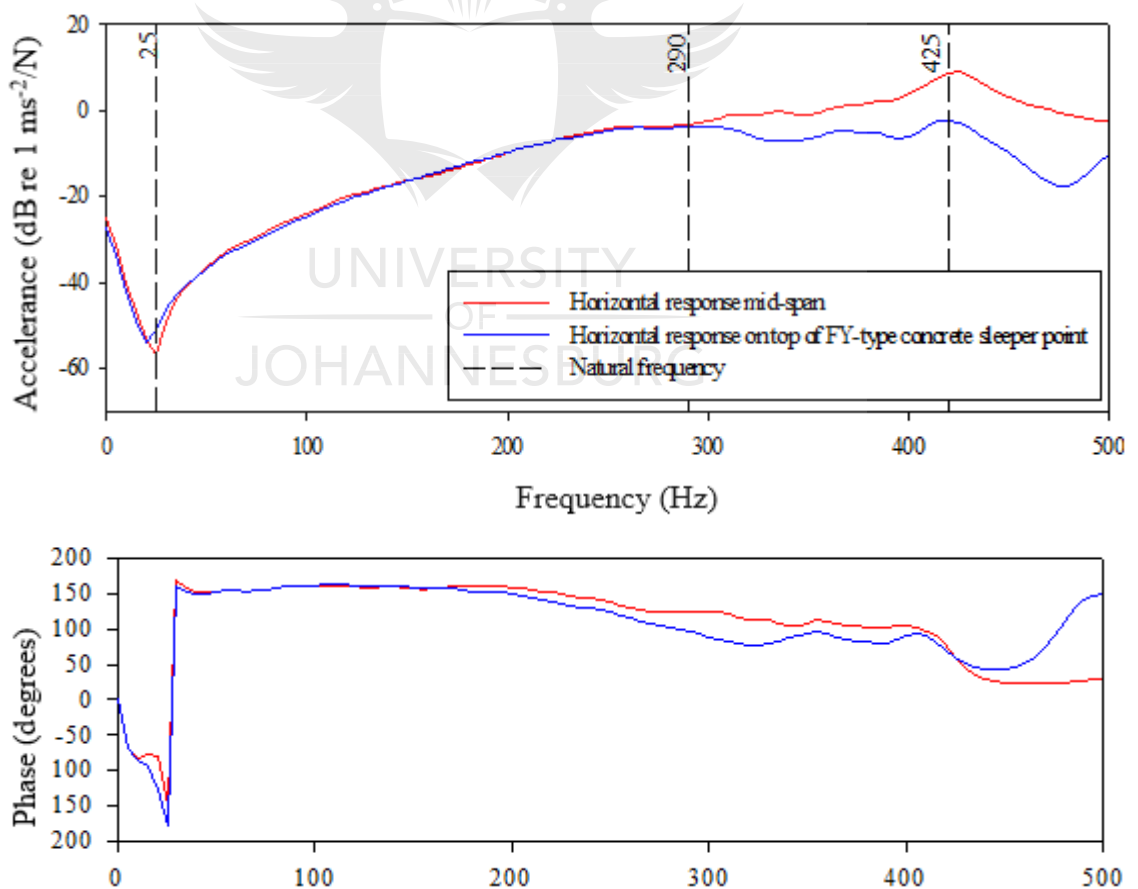


**Figure 5.5.** FRF and phase for rail vibration response, vibration measured in the horizontal direction from two positions i.e. mid-span and on top of the FY-type concrete sleeper point.

In Figure 5.5. the results are reported for vibration measured in the horizontal direction. The results are measured mid-span and on top of sleeper point. Evident in Figure 5.5. is that the in the horizontal direction, the rail starts vibrating at antiresonance at a frequency of 25Hz. In the horizontal direction, the rail responds with the same accelerance and in phase for the mid-frequency range of 0 – 290Hz at both excitation points.

Rail vibration accelerance starts to isolate from the frequency of 290Hz, where the mid-span horizontal vibration occurs with a higher accelerance than that on top of sleeper point. A resonance mode is excited at 425Hz at both positions of the rail and the rail responds in phase on these two positions. Given the FRF results in Figure 5.5. it is understood that the horizontal dynamic response of rail supported on FY-type concrete sleepers, mid-span position and on top of sleeper point, excites no resonance mode to exactly match the corrugation formation frequency at 108Hz.

Figure 5.6. shows comparison of FRFs between the vertical and horizontal vibration response measured mid-span. The response is measured from rail supported on FY-type concrete sleepers.

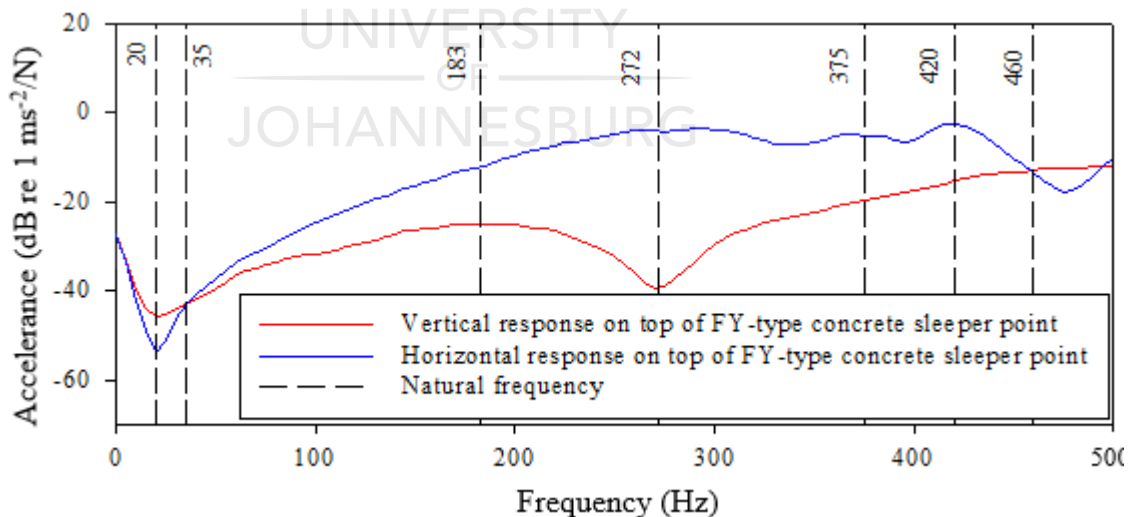


**Figure 5.6.** Comparison of FRFs for rail vibration response, vibration measured in the vertical and horizontal directions on top of sleeper point. Rail is supported on FY-type

Natural frequencies are heavily damped in Figure 5.6. making it not easy to identify resonance peaks. Evident in Figure 5.6. is that mid-span, in the frequency range of 0 – 500Hz, one resonance mode is excited in each direction of vibration. In the vertical

direction the resonance mode occurs at a frequency of 173Hz. In terms of the mid-span response of the rail on the FY-type concrete sleeper, this resonance mode is the closest to the corrugation formation frequency of 108Hz. In the horizontal direction the resonance mode occurs at 425Hz, which is the frequency much higher than the corrugation formation frequency in the Belfast to Steelpoort railway line.

The resonance mode in the vertical direction is more damped than that of vibration in the horizontal. At mid-span the acceleration of vibration is more in the horizontal direction than in the vertical. Two antiresonance modes are identified. i.e. one at a frequency of 25Hz, which occurs in both directions of vibration, and the other at a frequency of 244Hz in the vertical direction.

At mid-span the acceleration of vibration is higher in the vertical direction only at start of excitation in the frequency range of 0 – 50Hz. Beyond this frequency range, acceleration of vibration becomes significantly higher in the horizontal direction for the entire frequency range of 50 – 500Hz. Figure 5.7. shows comparison of FRFs between the vertical and horizontal vibration response measured on top of the FY-type concrete sleeper point. From the mid-span response of rail supported on the FY-type concrete sleepers, no resonance mode is excited to exactly match the corrugation formation frequency at 108Hz.

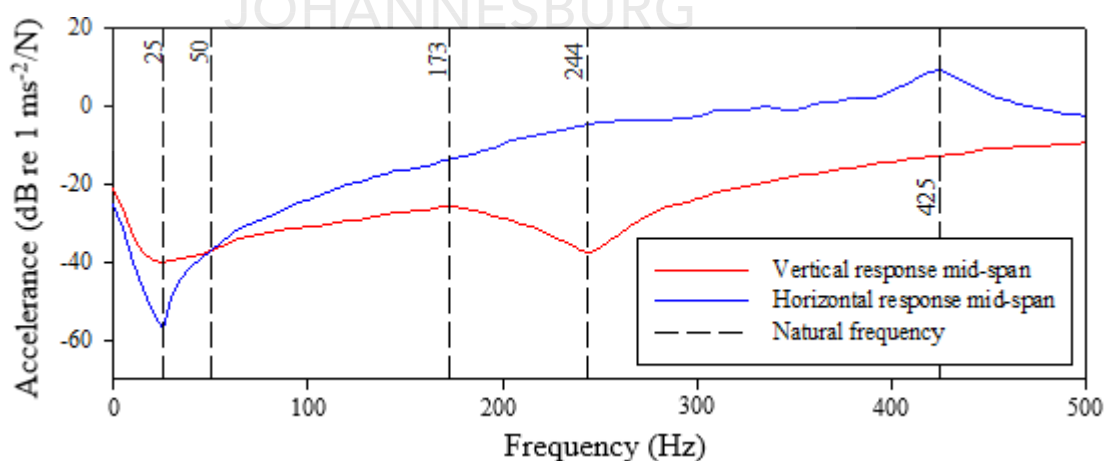


**Figure 5.7.** Comparison of FRFs for rail vibration response, vibration measured in the vertical and horizontal directions mid-span. Rail is supported on FY-type concrete sleepers.



Evident in Figure 5.7. on top of the FY-type concrete sleeper point, the two resonance modes in the horizontal direction occur at 375 and 420Hz. One mode excited in the vertical direction occurs at 183Hz. In terms of vibration response from the position on top of sleeper point, this is the closest resonance mode to the corrugation formation frequency of 108Hz. This mode looks more damped with a broader peak than the two modes in the horizontal direction. Similar to the response measured mid-span position, on top of FY-type concrete sleeper point the rail responds with higher acceleration in the horizontal direction. Anti-resonance occurs at 20Hz in the vertical and horizontal directions, and also at a frequency of 272Hz in the vertical direction.

The response of rail has more pronounced resonance modes in the horizontal direction in the frequency range of 272 – 420Hz than in the vertical direction. On top of sleeper point the rail responds with more acceleration in the horizontal direction than in the vertical, for almost the entire response period. No resonance mode is excited at 108Hz on top of sleeper point.

Similar to the response from the mid-span position, the closest resonance mode to the corrugation formation frequency occurs in the vertical direction. The next subsection reports on results for the response of rail supported on the PY-type concrete sleepers.

#### **5.2.2. Results for Experimental Modal Analysis on a Rail Supported on PY-Type Concrete Sleepers**

Figure 5.8. shows FRFs and phase representing vibration response of rail supported on top of the PY-type concrete sleepers. Here the results are reported for vibration measured in the vertical direction. The results are measured mid-span and on top of sleeper point

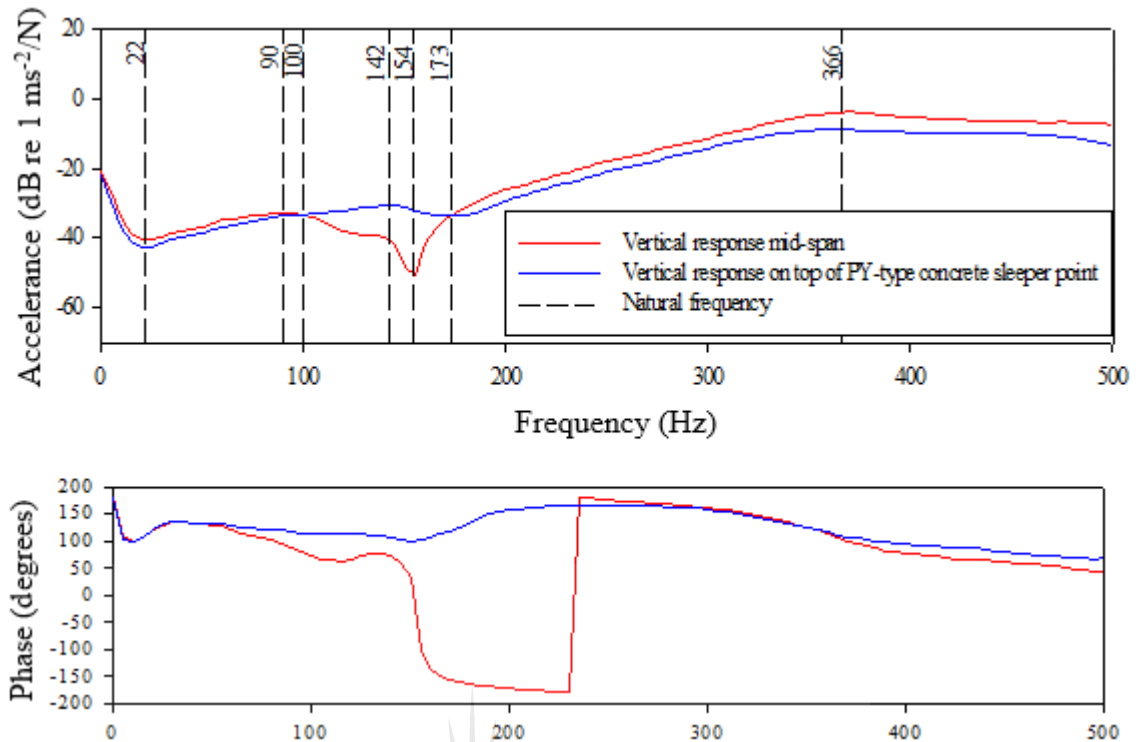


**Figure 5.8.** FRF and phase for rail vibration response, vibration measured in the vertical direction from two positions i.e. mid-span and on top of the PY-type concrete sleeper point.

Evident in Figure 5.8. is that in the vertical direction, there is more activity from response of rail supported on PY-type concrete sleepers, than that supported on the FY-type in Figure 5.8. A few resonance and antiresonance modes are identified from the response of rail supported on the PY-type concrete sleepers. From the response the vertical direction, two resonance modes are identified mid-span and two on top of sleeper point.

At mid-span the resonance modes occur at 90Hz and 366Hz. On top of sleeper point they occur at 142Hz and 366Hz. An antiresonance occur at 22Hz at both positions of the rail. Other two antiresonance occur at a frequency of 154Hz and 173Hz mid-span and on top of sleeper point respectively. The rail responds with a higher accelerance mid-span for most of the response period, except at the frequency range of 100 to 173Hz.

In terms of the vertical response of rail supported on the PY-type concrete sleeper, the closest resonance mode to 108Hz occurs in the vertical direction at a frequency of 90Hz. No resonance mode is identified to exactly match the corrugation formation

frequency at 108Hz. The closest resonance mode to the corrugation formation frequency in the Belfast to Steelpoort railway line occurs at a frequency of 90Hz. This resonance mode occurs mid-span of the rail. Figure 5.9. shows FRFs and phase representing vibration response of rail supported on top of the PY-type concrete sleepers. Here the results are reported for vibration measured in the horizontal direction. The results are measured mid-span and on top of sleeper point.

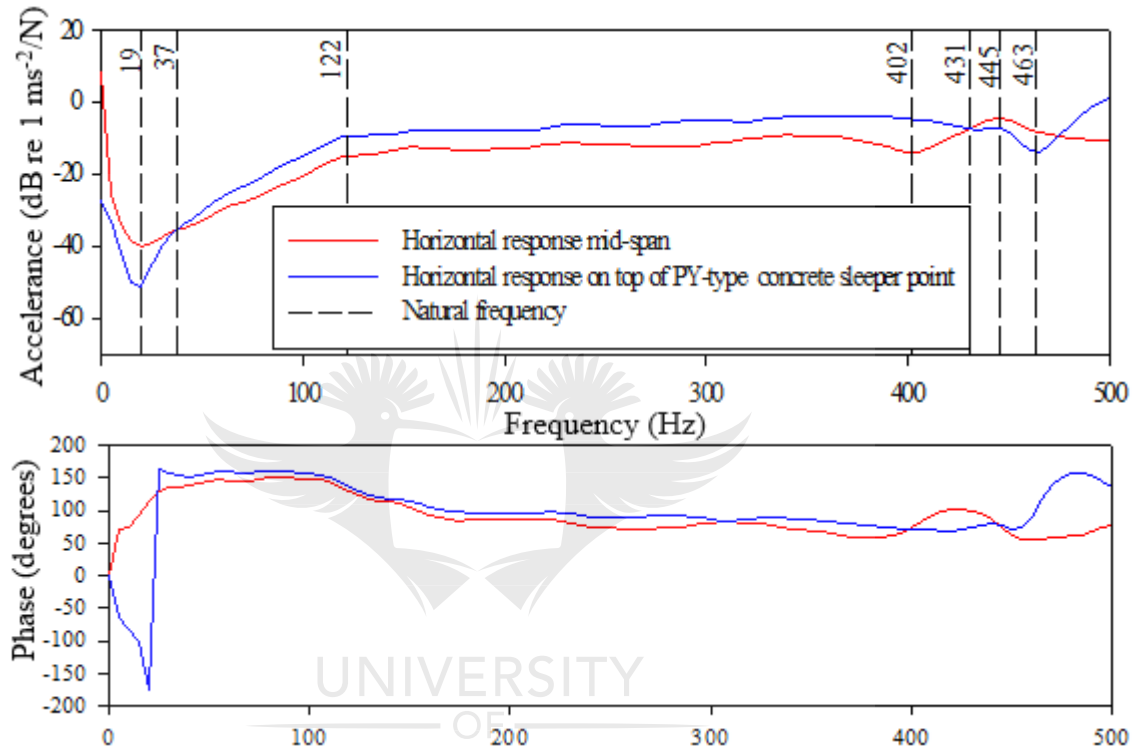


**Figure 5.9.** FRF and phase for rail vibration response, vibration measured in the horizontal direction from two positions i.e. mid-span and on top of the PY-type concrete sleeper point.

Evident in Figure 5.9. is that for response of rail on PY-type concrete sleepers, in the horizontal direction, there are no resonance modes of vibration closely associated with the corrugation formation frequency in the Belfast to Steelpoort railway line. This is more evident in particular in the frequency range of 0 – 431Hz. The FRFs are flat in the frequency range of 122 – 402Hz which indicates no much activity occurring at both rail positions.

One resonance mode at 445Hz is identified in the horizontal direction mid-span. Anti-resonance occurs at a frequency of 463Hz on top of sleeper point. In the horizontal direction the rail responds with a higher acceleration on top of sleeper point than mid-span. This applies on a frequency range of 37Hz to 431Hz. Figure 5.10. shows

comparison of FRFs between the vertical and horizontal vibration response measured mid-span. The response is measured from rail supported on PY-type concrete sleepers.

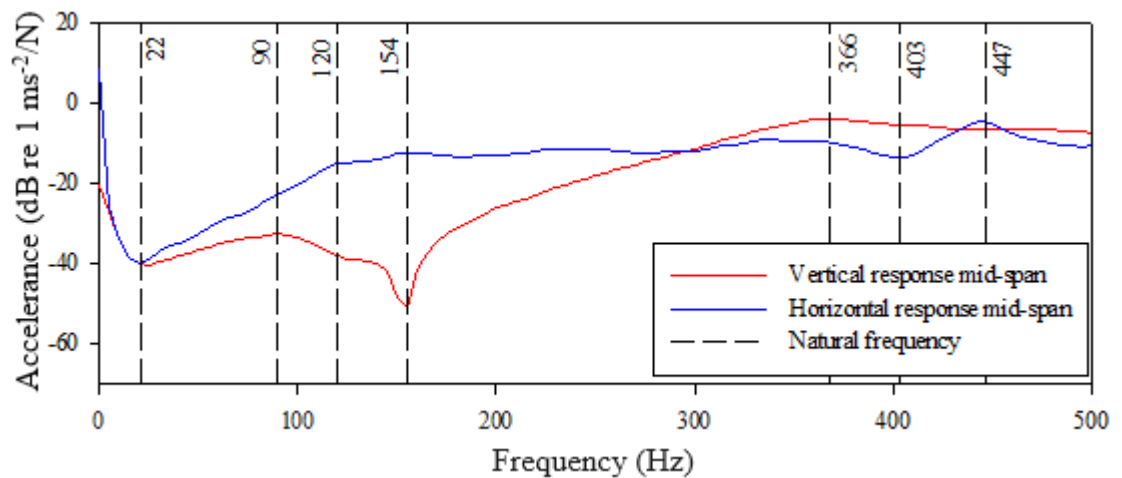


**Figure 5.10.** Comparison of FRFs for rail vibration response, vibration measured in the vertical and horizontal directions mid-span. Rail is supported on PY-type concrete sleepers.

Evident in Figure 5.10. is that response of rail shows a flatter FRF in the horizontal direction mid-span, than in the vertical direction. No resonance modes are identified in the frequency range of 0 – 403Hz in the horizontal direction. In contrast, two damped resonance modes are identified mid-span in the vertical direction. These occur at frequencies of 90Hz and 366Hz.

The one resonance mode identified from the mid-span response in the horizontal direction occurs at a frequency of 447Hz. At mid-span the closest resonance mode to the corrugation formation frequency in the Belfast to Steelpoort railway line occurs in the vertical direction at 90Hz. From the response of rail at both directions of mid-span, no resonance mode precisely matches the corrugation formation frequency in the Belfast to Steelpoort railway line.

Figure 5.11. shows comparison of FRFs between the vertical and horizontal vibration response measured on top of sleeper point. The response is measured from rail supported on PY-type concrete sleepers.

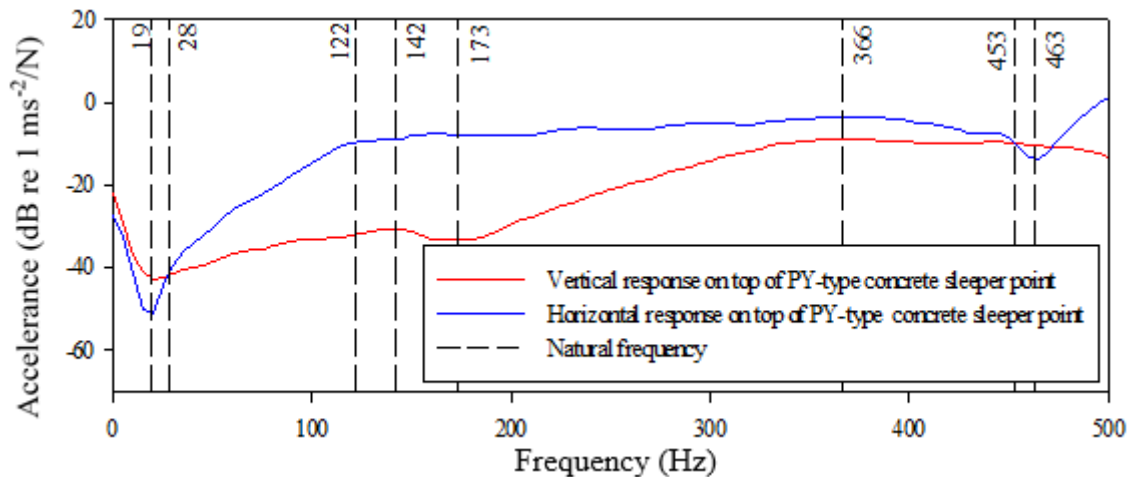


**Figure 5.11.** Comparison of FRFs for rail vibration response, vibration measured in the vertical and horizontal directions of mid-span. Rail is supported on PY-type concrete

Evident in Figure 5.11. is that similar to the mid-span response, the response of rail shows a flatter FRF in the horizontal direction on top of sleeper point, than in the vertical direction. This is evident particularly for the frequency range of 122 – 453Hz. No resonance modes are identified in the frequency range of 0 – 403Hz in the horizontal direction. In the contrary, two damped resonance modes are identified on top of sleeper point in the vertical direction.

These occur at frequencies of 142Hz and 366Hz. On top of sleeper point the rail responds with a higher accelerance in the horizontal direction than in the vertical. This is evident particularly in the frequency range of 28 – 453Hz. The next sub-subsection reports on the results for response of rail supported on steel sleepers.

### 5.2.3. Results for Experimental Modal Analysis on a Rail Supported on Steel Sleepers

Vibration response of rail on steel sleepers was measured for comparison to that of rails supported on both types of concrete sleepers. Results for vibration response of rail on steel sleepers are first reported for the vertical direction at both positions of the rail. After which the results are reported for the horizontal direction for both positions.

Lastly the results of vibration response of the rail on steel sleepers were compared with those of the rails supported on concrete sleeper types. Figure 5.12. shows FRFs and phase representing vibration response of rail supported on top of FY-type concrete

sleepers. Here the results are reported for vibration measured in the vertical direction. The results are measured mid-span and on top of sleeper point.

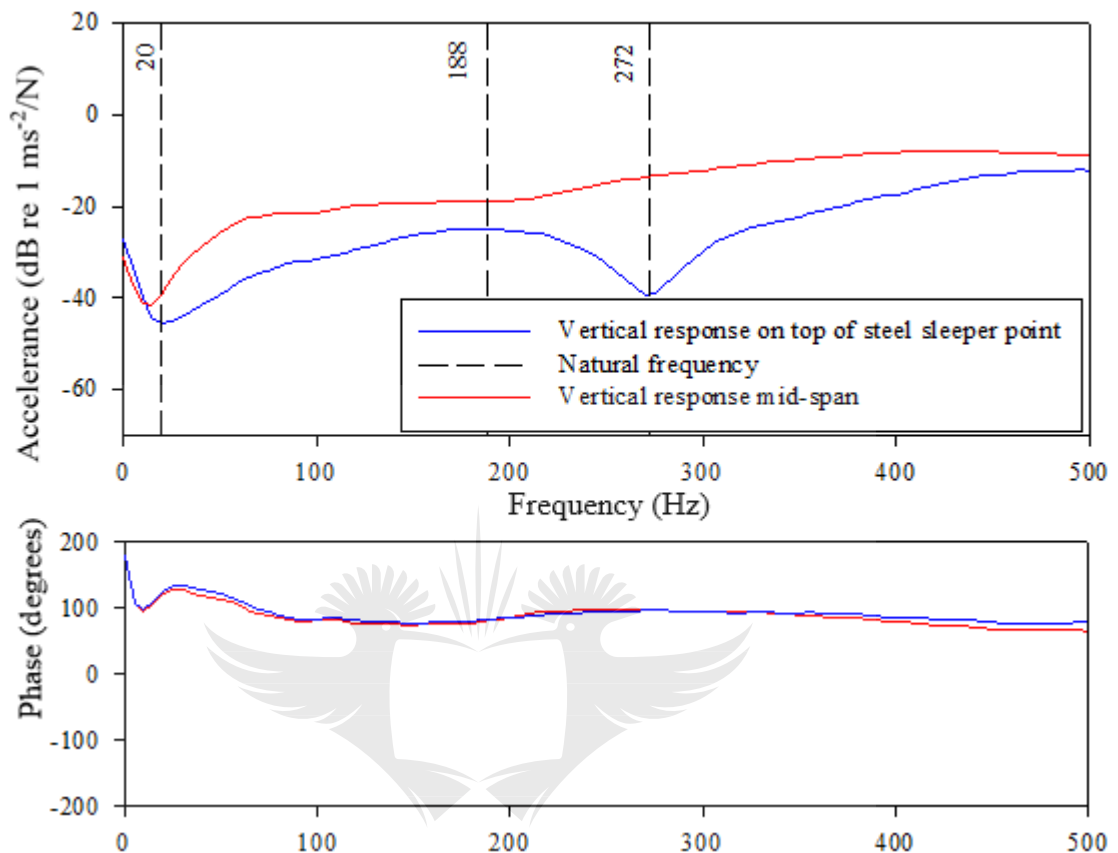


**Figure 5.12.** FRF and phase for rail vibration response, vibration measured in the vertical direction from two positions i.e. mid-span and on top of steel sleeper point.

Evident in Figure 5.12. is that there is no much activity from vibration response of the rail in the vertical direction mid-span. A damped resonance mode is identified at 188Hz on top of sleeper point. No other resonance modes are excited in the frequency range of 0 – 500Hz at both positions of the rail. The mid-span response in the vertical direction is more damped than in the horizontal, the FRF for mid-span response is almost entirely flat with no identified resonances.

An anti-resonance occurs at 272Hz in the vertical direction on top of steel sleeper point. In the vertical direction, vibration occurs with a higher accelerance mid-span than on top of sleeper point. In terms of vibration response in the vertical direction, no resonance mode is excited to match the corrugation formation frequency in the Belfast to Steelpoort railway line.

Figure 5.13. shows FRFs and phase representing vibration response of rail supported on top of steel sleepers. Here the results are reported for vibration measured in the horizontal direction. The results are measured mid-span and on top of sleeper point.

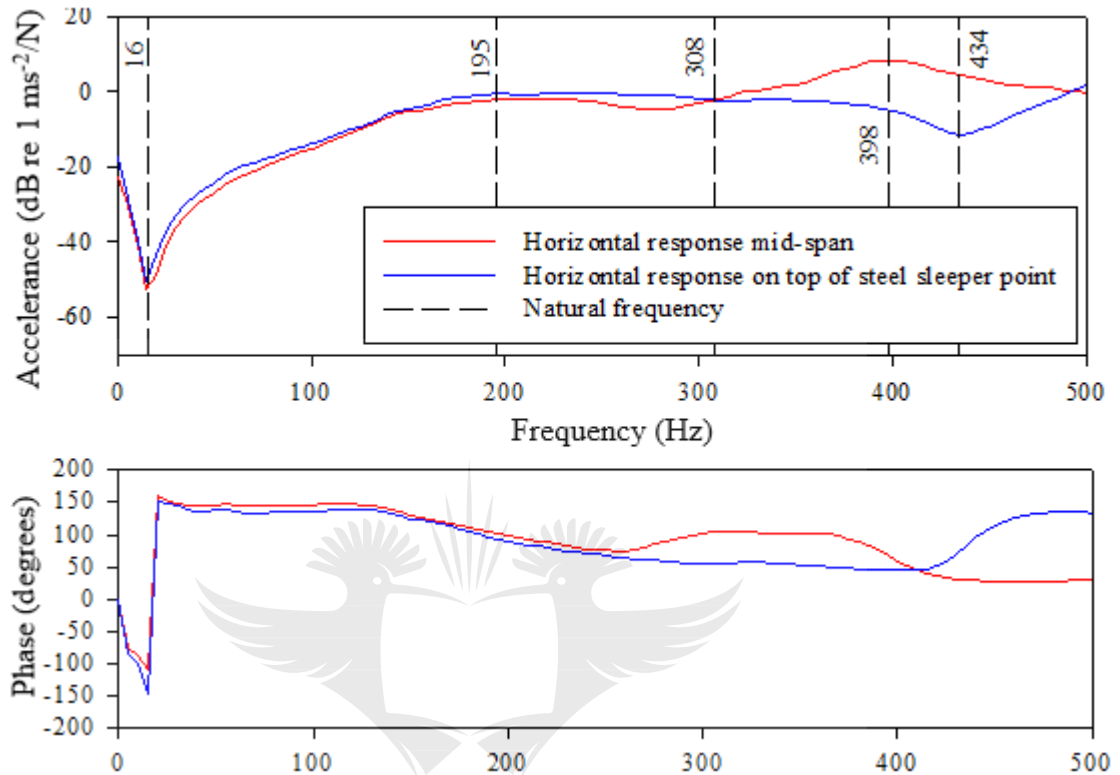


**Figure 5.13.** FRF and phase for rail vibration response, vibration measured in the horizontal direction from two positions i.e. mid-span and on top of steel sleeper point.

Evident in Figure 5.13. is that in the horizontal direction the response of rail mid-span is in phase with that on top of steel sleeper point. This is evident in particular for most of the frequency range of 0 – 308Hz. Two resonance modes are excited i.e. at 398Hz in the horizontal direction mid-span and at 195Hz at both positions of the rail.

The resonance mode at 195Hz is damped and occurs at both positions of the rail. Anti-resonance occurs at a frequency of 434Hz in the horizontal direction, on top of steel sleeper point. In the horizontal direction, for most of the response window, the rail responds with a higher accelerance on top of sleeper point, than mid-span. This is evident in particular for the frequency range of 0 – 308Hz.

No resonance mode excited exactly matches the corrugation formation frequency in the Belfast to Steelpoort railway line. Figure 5.14. shows comparison of FRFs between the vertical and horizontal vibration response measured mid-span. The response is measured from rail supported on steel sleepers.

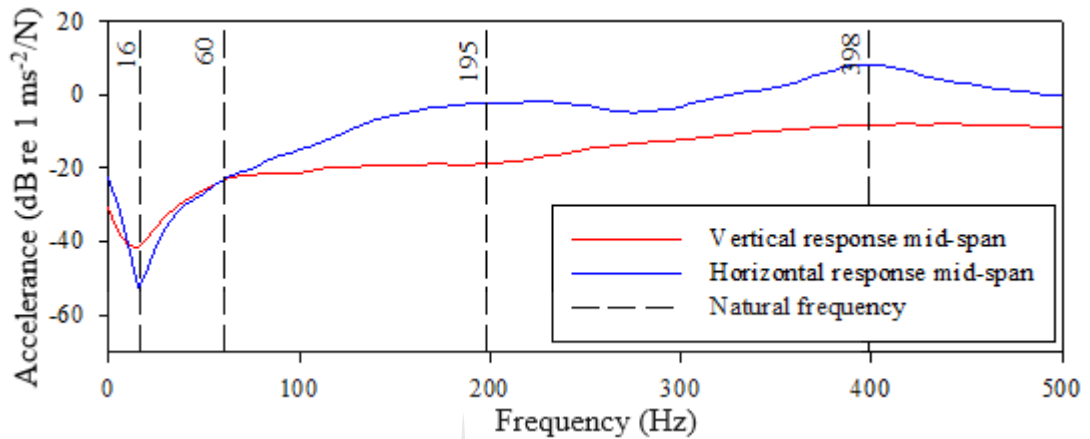


**Figure 5.14.** Comparison of FRFs for rail vibration response, vibration measured in the vertical and horizontal directions mid-span. Rail is supported on steel sleepers.

Evident in Figure 5.14. is that the response in the vertical direction mid-span is more damped than that in the horizontal direction. The vertical FRF looks flatter than the horizontal and shows more damping at resonances more in particular for the frequency range of 60 – 500Hz. There are no identified resonance modes in the vertical direction.

Two resonance modes are excited mid-span in the horizontal direction at 195Hz and 398Hz. Mid-span the rail responds with more acceleration in the horizontal direction than in the vertical, particularly for the frequency range of 60 – 500Hz. Figure 5.15. shows comparison of FRFs between the vertical and horizontal vibration response measured on top of sleeper point.

The response is measured from rail supported on steel sleepers. From the response or rail on steel sleeper, mid-span, it is deduced that more activity and resonance occurs in the horizontal direction than in the vertical.



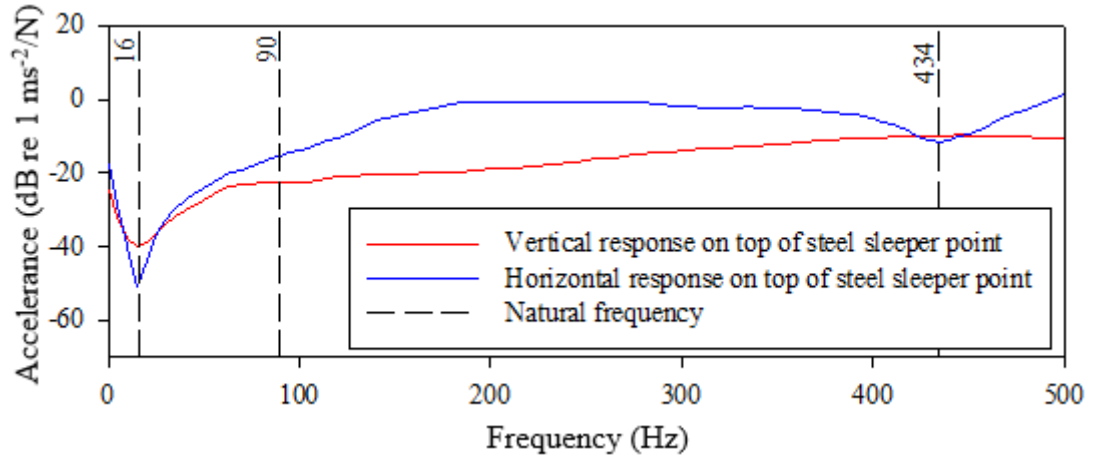


**Figure 5.15.** Comparison of FRFs for rail vibration response, vibration measured in the vertical and horizontal directions on top of sleeper point. Rail is supported on steel

Evident in Figure 5.15. is that there is no much vibration response activity in both directions on top of sleeper point. The rail responds with higher accelerance in the horizontal direction for most of the response period. An anti-resonance occurs at 16Hz in both directions and at 434Hz in the horizontal direction. The vertical FRF is flatter than the horizontal for the entire response period beyond 90Hz.

No resonance mode is identified in both directions for the entire response period. The next sub-subsection compares the response of rail supported the FY-type concrete sleepers and on steel sleepers.

#### **5.2.4. Comparison of Experimental Modal Analysis Results for Rails Supported on FY-type Concrete Sleepers and Steel Sleepers**

One of the most critical objectives of the current study is to establish the difference between the dynamic response of the two types of tracks i.e. one with concrete and one with steel sleepers. The results are compared for two positions of the rail i.e. mid-span and on top of sleeper points. The results are compared for response in the same direction, and on the same position for both types of tracks.

Figure 5.16. shows comparison of FRFs for the vertical vibration response measured mid-span. The response is measured from rails supported on FY-type concrete and on steel sleepers.

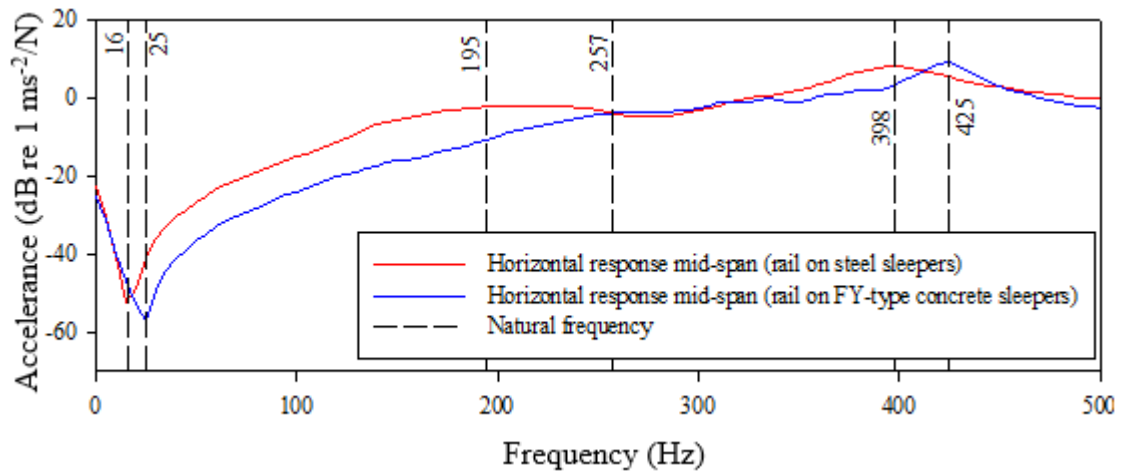


**Figure 5.16.** Comparison of FRFs for rail vibration response, rails are supported on FY-Type concrete and on steel sleepers. Vibration measured in the horizontal direction mid-

Evident in Figure 5.16. is that mid-span the vertical horizontal of the rail on steel sleepers is more damped than that of rail supported on the FY-type concrete sleepers. No resonance mode is identified from the mid-span response of rail supported on steel sleepers. One resonance mode occurs at a frequency of 425Hz, from the response of rail supported on FY-type concrete sleepers.

At mid-span the rail supported on concrete sleepers vibrates with more accelerance (vertically) than that supported on steel sleepers, for most of the vibration response window. It is only in the frequency range of 25 – 122Hz that the accelerance is less for the rail supported on FY-type concrete sleepers. No activity of interest occurs from the vertical mid-span vibration of the rail supported on steel sleepers.

In the vertical direction, no resonance mode was found to match the corrugation formation frequency in the Belfast to Steelpoort railway line, for both rails supported on concrete and steel sleepers. Figure 5.17. shows comparison of FRFs for the horizontal vibration response measured mid-span. The response is measured from rails supported on FY-type concrete and on steel sleepers.

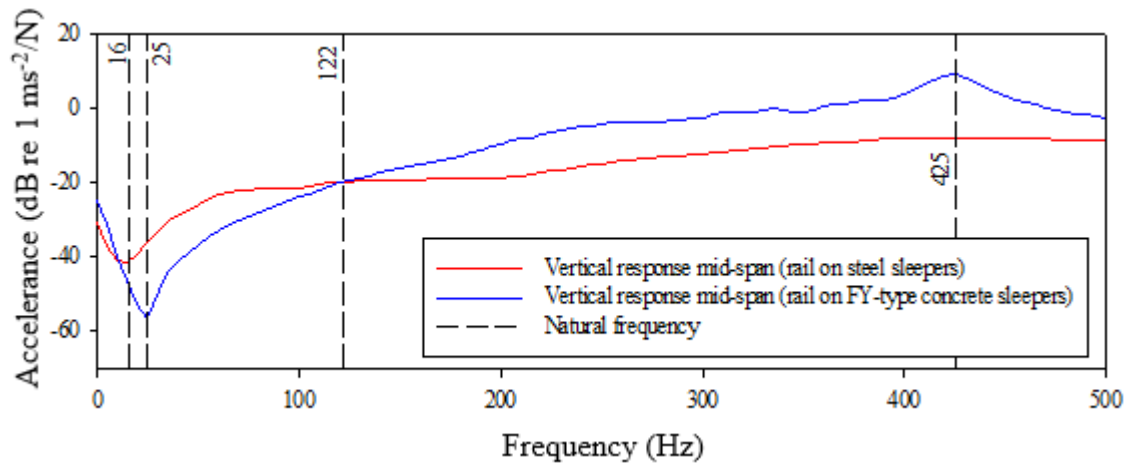


**Figure 5.17.** Comparison of FRFs for rail vibration response, rails are supported on FY-Type concrete and on steel sleepers. Vibration measured in the vertical direction mid-span.

Evident in Figure 5.17. is that in the horizontal direction, mid-span, the rails on FY-type concrete and on steel sleepers respond in somewhat a similar manner. Two resonance modes are identified in the horizontal direction from a mid-span vibration of the rail supported on steel sleepers. Two resonance modes occur at a frequency of 195Hz and 398Hz, with the mode at 195Hz being the more than that at 398Hz.

One resonance mode is identified in the horizontal direction, mid-span, from response of rail supported on the FY-type concrete sleepers. This resonance mode occurs at 425Hz. In the horizontal direction, mid-span, the rail on steel sleepers vibrates with more accelerance in the low frequency range of 16 – 257Hz. No resonance mode is found to exactly match the corrugation formation frequency in the Belfast to Steelpoort railway line.

The FRFs in Figure 5.17. look critically damped. With the FRF for rail on steel sleepers looking more damped. One of the explanations to this may be difference in the fastening for the two types of rails on sleepers. The steel sleeper-rail system responds to excitation as a unit, given the bolting method of the fastening system, which should possibly account for some degree of damping in the vertical direction. The difference in damping Figure 5.18. shows comparison of FRFs for the vertical vibration response measured on top of sleeper point. The response is measured from rails supported on FY-type concrete and on steel sleepers.

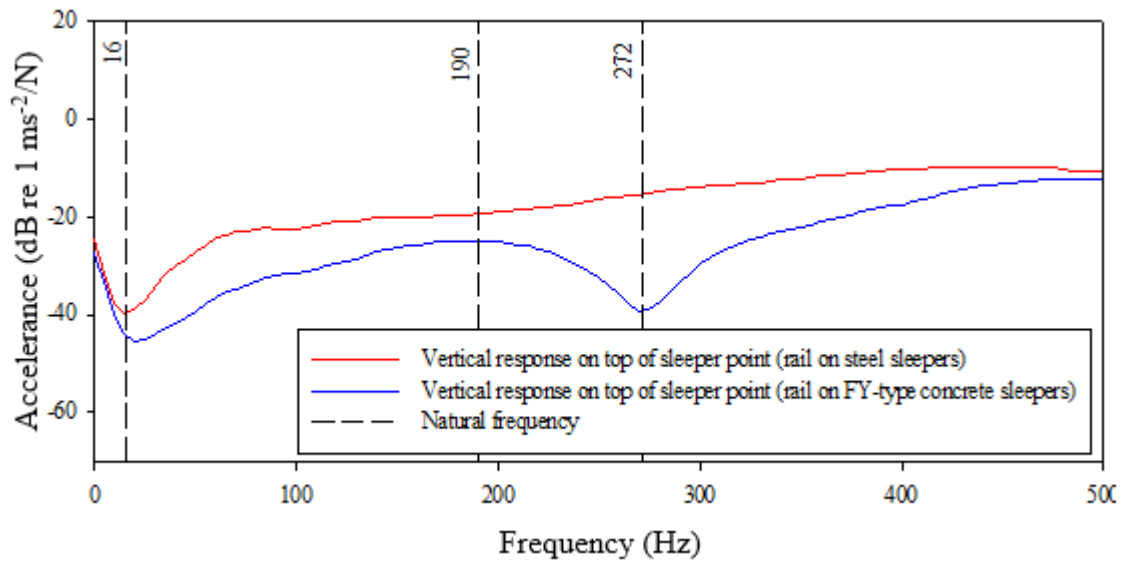


**Figure 5.18.** Comparison of FRFs for rail vibration response, rails are supported on FY-Type concrete and on steel sleepers. Vibration measured in the vertical direction on top of sleeper point.

Evident in Figure 5.18. is that similar to the response measured mid-span, in the vertical direction, on top of sleeper point, there is no much activity from the response of rail supported on steel sleepers. The FRF for vertical response of rail on steel sleepers, on top of sleeper point, is much flatter than that of rail supported on the FY-type concrete sleepers.

One resonance mode occurs at 190Hz in the vertical direction, from response of rail supported on FY-type concrete sleeper point. An antiresonance occurs from response of rail supported on FY-type concrete sleepers at a frequency of 272Hz. On top of sleeper point, the rail supported on steel sleepers responds with more accelerance than that supported on the FY-type concrete sleepers, for the entire response period of 0 – 500Hz.

No resonance mode is found to match the corrugation formation frequency in the Belfast to Steelpoort railway line. The closest resonance mode to the corrugation formation frequency in the Belfast to Steelpoort railway line occurs at 190Hz in the vertical direction, from rail supported on top of FY-type concrete sleepers. Figure 5.19. shows comparison of FRFs for the horizontal vibration response measured on

top of sleeper point. The response is measured from rails supported on FY-type concrete and on steel sleepers.

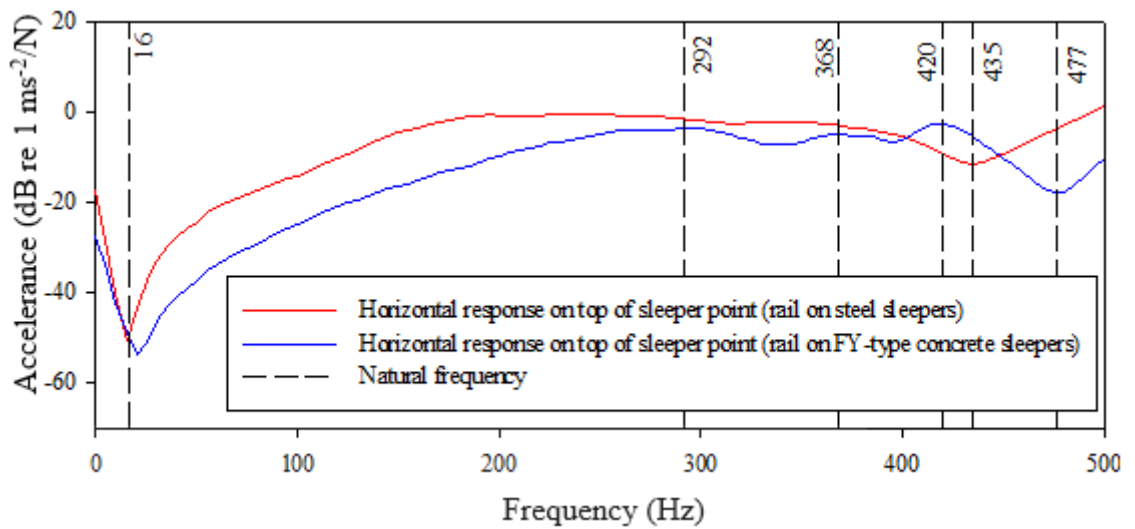


**Figure 5.19.** Comparison of FRFs for rail vibration response, rails are supported on FY-Type concrete and on steel sleepers. Vibration measured in the horizontal direction on top of sleeper point.

Evident in Figure 5.19. is that on top of sleeper point, in the horizontal direction, more activity occurs from response of rail supported on FY-type concrete sleepers. No resonance mode is identified in the horizontal direction on top of steel sleeper point, instead, one antiresonance mode is identified at 435Hz. In the contrary, three resonance modes are identified from rail response in the horizontal direction on top of FY-type concrete sleepers.

The three resonance modes occur at 292Hz, 368Hz and 420Hz. One antiresonance occurs from response of rail supported on FY-type concrete sleepers in the horizontal direction, on top of sleeper point at 477Hz. No resonance mode is found to match the corrugation formation frequency in the Belfast to Steelpoort railway line. In the horizontal direction, the rails start to go on a resonance vibration beyond 200Hz.

The first vibration mode occurs at 292Hz from response of rail supported on top of FY-type concrete sleepers. Similar to the vertical response, the rail supported on steel sleepers responds with higher accelerance for most of the response period. The next

sub-subsection compares the response of rail supported the PY-type concrete sleepers and on steel sleepers.

#### 5.2.5. Comparison of Experimental Modal Analysis Results for Rails Supported on PY-type concrete Sleepers and Steel Sleepers

The results for comparison of response of rails on PY-type concrete sleepers and on steel sleepers is reported in a similar chronology to that of comparison for rails on FY-type concrete sleepers and on steel sleepers. The results are compared for two positions of the rail i.e. mid-span and on top of sleeper points. The results are compared for response in the same direction, and at the same position, for both types of tracks.

Figure 5.20. shows comparison of FRFs for the vertical vibration response measured mid-span. The response is measured from rails supported on PY-type concrete and on steel sleepers.

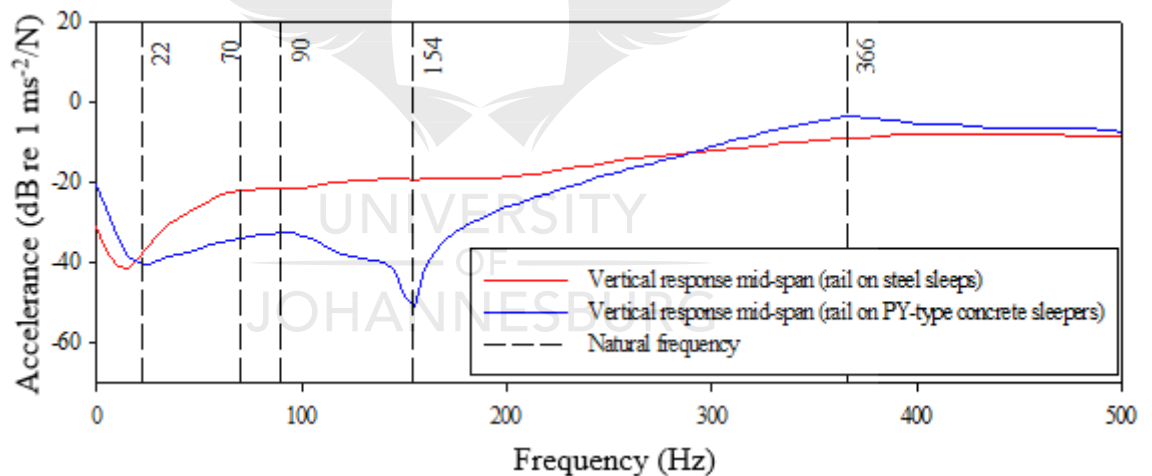


**Figure 5.20.** Comparison of FRFs for rail vibration response, rails are supported on PY-Type concrete and on steel sleepers. Vibration measured in the vertical direction mid-span.

Evident in Figure 5.20. is that in the vertical direction, mid-span, vibration response of the rail supported on top of the PY-type concrete sleepers has more activity than that of the rail supported on steel sleepers. No resonance mode is identified from response of rail supported on steel sleepers. Two resonance modes are identified from response of rail supported on PY-type concrete sleepers.

The resonance modes occur at frequencies of 90Hz and 366Hz respectively. Vibration response from rail supported on steel sleepers is more damped than that from rail supported on the PY-type concrete sleepers, with a much flatter FRF in the frequency range of 70 – 500Hz. An antiresonance occurs at a frequency of 154Hz on response of rail supported on PY-type concrete sleepers.

No resonance mode is found to exactly match the corrugation formation frequency in the Belfast to Steelpoort railway line. The closest resonance mode to the corrugation formation frequency occurs at 90Hz, from response of rail supported on PY-type concrete sleepers. Figure 5.21. shows comparison of FRFs for the horizontal vibration response measured mid-span. The response is measured from rails supported on PY-type concrete and on steel sleepers.

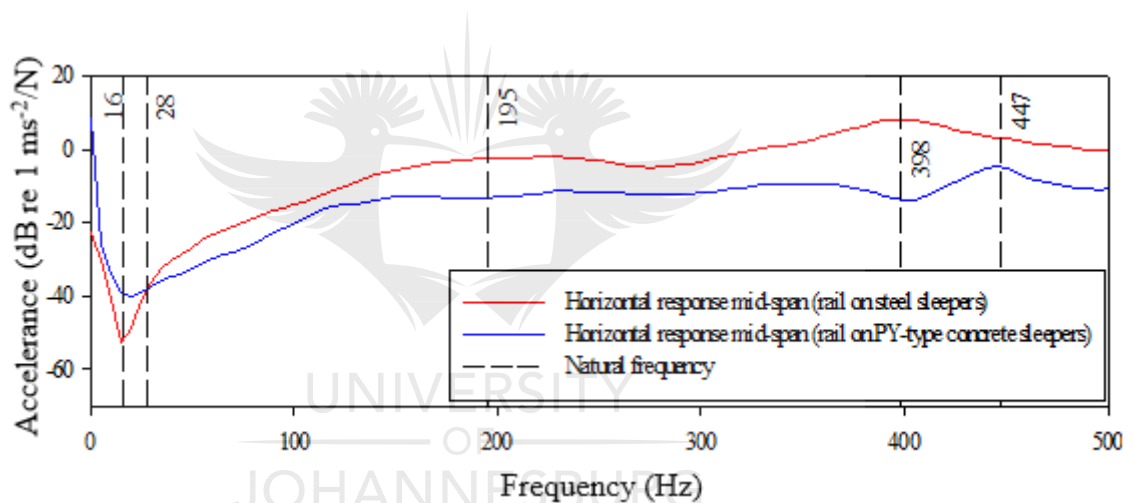


**Figure 5.21.** Comparison of FRFs for rail vibration response, rails are supported on PY-Type concrete and on steel sleepers. Vibration measured in the horizontal direction mid-

Evident in Figure 5.21. is that in the horizontal direction, mid-span, the rail on steel sleepers responds with two resonance modes, whilst that on PY-type concrete sleepers responds with one. The two resonance modes from response of rail on steel sleepers occur at frequencies of 195Hz and 396Hz, whilst that from the rail supported on PY-type concrete sleepers occurs at 477Hz.

Antiresonance occurs from response of rail supported on PY-type concrete sleepers at 398Hz; at this frequency the rail on steel sleepers responds with resonance vibration. The rail on steel sleepers responds with higher accelerance than the rail on PY-type



concrete sleepers for almost the entire response period, starting from the frequency of 28Hz.

No resonance mode is found to match the corrugation formation frequency in the Belfast to Steelpoort railway line. Figure 5.22. shows comparison of FRFs for the vertical vibration response measured on top of sleeper point. The response is measured from rails supported on PY-type concrete and on steel sleepers.

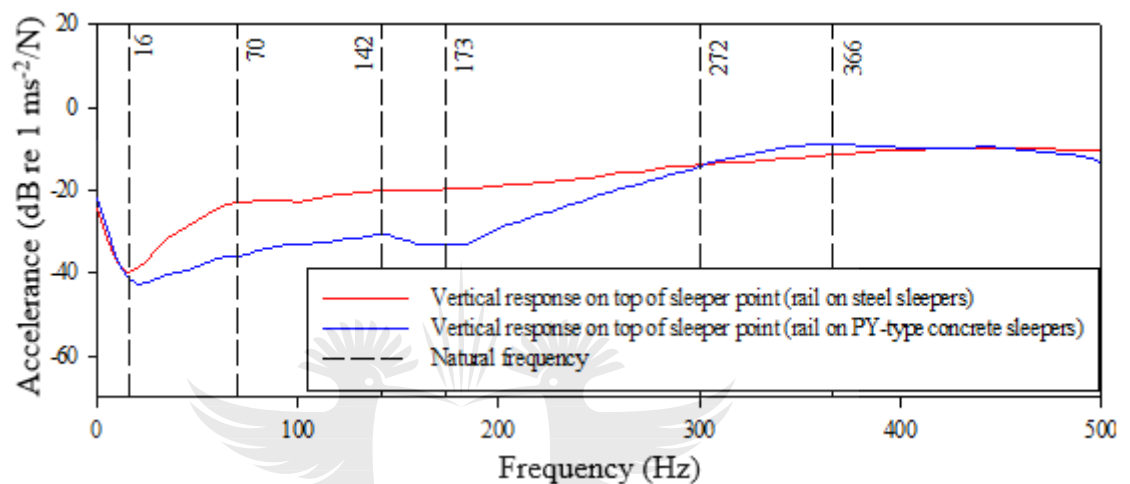


**Figure 5.22.** Comparison of FRFs for rail vibration response, rails are supported on PY-Type concrete and on steel sleepers. Vibration measured in the vertical direction on top of sleeper point.

Evident in Figure 5.22. is that on top of sleeper point, in the vertical direction, the rail on steel sleepers has a more damped response than that supported on PY-type concrete sleepers. The FRF for response of rail on steel sleepers is much flatter than that of rail supported on PY-type concrete sleepers in the frequency range of 70 – 500Hz. No much activity occurs from response of rail supported on steel sleepers.

Two damped resonance modes occurring at frequencies of 142Hz and 366Hz are identified from response of rail supported on PY-type concrete sleepers. Antiresonance occurs at a frequency of 173Hz from response of rail supported on PY-type concrete sleepers. The rail on steel sleepers responds with higher accelerance than that on PY-type concrete sleepers in the low frequency range of 16 – 272Hz.

No resonance mode is found to match the corrugation formation frequency in the Belfast to Steelpoort railway line. The closest resonance mode to the corrugation formation frequency in the Belfast to Steelpoort railway line occurs at a frequency of 142Hz. Figure 5.23. shows comparison of FRFs for the horizontal vibration response measured on top of sleeper point. The response is measured from rails supported on PY-type concrete and on steel sleepers.

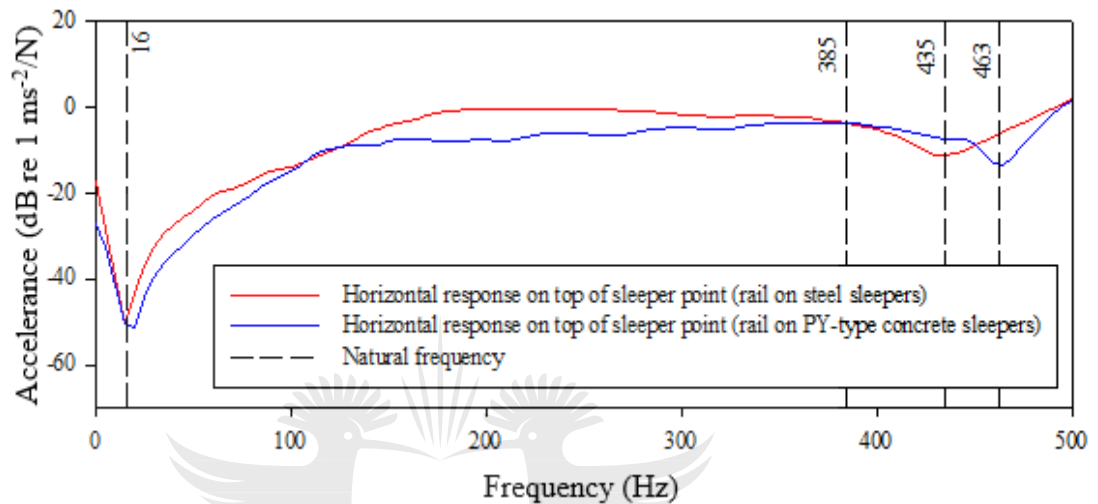


**Figure 5.23.** Comparison of FRFs for rail vibration response, rails are supported on PY-Type concrete and on steel sleepers. Vibration measured in the horizontal direction on top of sleeper point.

Evident in Figure 5.23. is that in the horizontal direction, on top of sleeper point, there is no much activity occurring, from rails supported on both steel and PY-type concrete sleepers. No resonance modes are identified from response of rails supported on both sleeper types, instead, rails supported on both sleeper types vibrate at antiresonance. The antiresonance occurs at frequencies of 435Hz and 463Hz for rails supported on steel and on PY-type concrete sleepers respectively.

The rail on steel sleepers responds with higher acceleration than that on PY-type concrete sleepers, for most of the response in the frequency range of 16 – 385Hz. No resonance mode is found to match the corrugation formation frequency in the Belfast to Steelpoort railway line. The next sub-subsection reports on results for vibrational response of the three types of sleepers whilst installed in the tracks.

### 5.2.6. Comparison of Experimental Modal Analysis Results for Steel, FY-type and PY-type Concrete Sleepers

Excitations were applied on the rail crown, whilst the response was measured directly on the sleepers. Vertical excitations were applied on the running surface of the rail, directly on top of sleeper point. Horizontal excitations were applied on the field side of the rail crown, directly on top of sleeper point. Figure 5.24. shows comparison of FRFs for the vertical vibration response measured on sleepers. The response is measured from steel, FY-type and PY-type concrete sleepers.

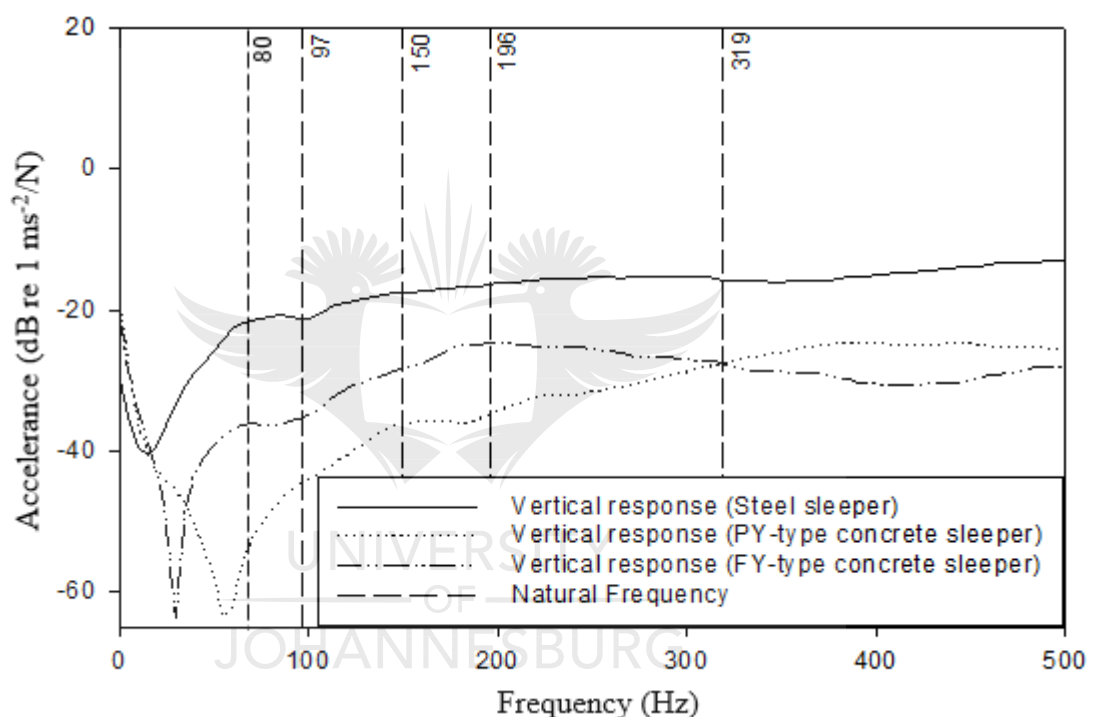


**Figure 5.24.** Comparison of FRFs for vibration response of sleepers. Vibration measured in the vertical direction, on the top face of sleeper, by the field side of the rail.

Evident in Figure 5.24. is that the response of sleepers is less pronounced than that of wheels in the frequency range of 0 – 500Hz. In the vertical direction, sleepers respond in a similar manner as compared to the rail. At the beginning of vibration, one or two resonance modes occur, whereafter the sleepers vibrate at no resonance. The steel sleeper has a more damped response in the vertical direction, than the concrete sleepers.

This is evident in particular for the response in the frequency range of 97 – 500Hz. In this frequency range the response of a steel sleeper is much flatter than that of the concrete sleepers, with no identified resonance modes. The steel sleeper responds with a higher acceleration than concrete sleepers, for the entire response period. The first resonance mode occurs at a frequency of 80Hz for steel and FY-type concrete sleepers, whilst it occurs at 150Hz for the PY-type concrete sleeper. The second resonance mode for the FY-type sleeper occurs at 196Hz. The FY-type concrete sleeper vibrates with a higher acceleration than the PY-type from the beginning of vibration to 319Hz. The PY-type concrete sleeper only vibrates at higher acceleration than the FY-type in the frequency range of 319 – 500Hz. No resonance mode is found to match the corrugation formation frequency in Belfast to Steelpoort railway line.

The closest resonance mode to corrugation formation frequency occurs at 80Hz from response of steel and FY-type concrete sleepers. Figure 5.25. shows comparison of FRFs for the vertical horizontal response measured on sleepers. The response is measured from steel, FY-type and PY-type concrete sleepers.

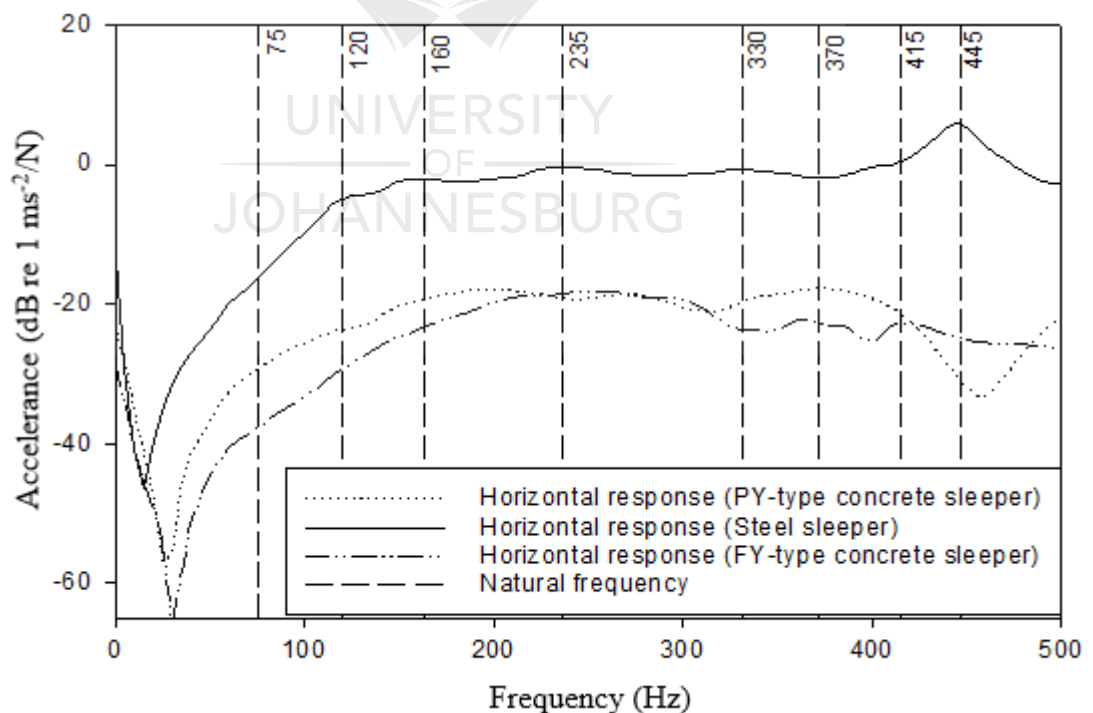


**Figure 5.25.** Comparison of FRFs for vibration response of sleepers. Vibration measured in the horizontal direction, on the top face of sleeper, by the field side of the rail.

Evident in Figure 5.25. is that in the horizontal direction more activity occurs from response of steel sleepers than the other two types of concrete sleepers. Similar to the vertical direction, vibration of sleepers in the horizontal direction reaches peak time at different frequencies. This is the time from the beginning of vibration to the first highest peak, whereafter the FRF starts to take a different response.

The peak time for response of concrete sleepers occurs around 75Hz, whilst that of steel sleepers occurs at 120Hz. In the frequency range of 120 – 500Hz, more resonance modes are identified from response of steel sleepers than from that of concrete sleepers. The steel sleeper resonance modes are identified at frequencies of 160Hz, 235Hz, 330Hz and 445Hz. These resonance modes are damped, with broad and flat FRF peaks.

One damped resonance mode is identified at 370Hz from response of the PY-type concrete sleeper. The FY-type concrete sleeper also vibrates with a damped resonance mode at this frequency (370Hz), whilst the steel sleeper vibrates with antiresonance. The second resonance mode for the FY-type concrete sleeper occurs at 415Hz. In the horizontal direction, the steel sleeper vibrates with a higher acceleration than the concrete sleepers for the entire response period of 0 – 500Hz.

The PY-type concrete sleeper vibrates with a higher acceleration than the FY-type in the frequency range of 0 – 235Hz. No resonance mode is found to occur at a corrugation formation frequency in the Belfast to Steelpoort railway line. The next subsection summarises the discussion of results for experimental modal analysis on railway tracks supported on steel and concrete sleepers.

### **5.3. Results Discussion**

In light of comparison between the dynamic response of rail on steel and FY-type concrete sleepers, a few differences are noted. On top of the FY-type sleeper point the horizontal response of the rail is more pronounced than the vertical, more in particular for a frequency range of 272 – 460Hz. The rail responds with higher acceleration in

the horizontal direction at both positions of the rail on FY-type concrete sleepers, for most of the response window.

At both positions the rail on steel sleepers, the rail responds with higher acceleration in the horizontal direction than in the vertical direction for the entire mid-frequency response window. A few differences are also noted in comparing the dynamic response of rail on steel and PY-type concrete sleepers. For response of rail on PY-type concrete sleepers, mid-span, the vertical response is more pronounced than the horizontal.

The horizontal response mid-span is flatter than the vertical response. Two resonance modes occur in the vertical direction mid-span at frequencies 90Hz and 366Hz, whilst one resonance mode is excited in the horizontal direction mid-span at a frequency of 477Hz. On top of the PY-type concrete sleeper point, no resonance mode is excited in the horizontal direction and the horizontal response FRF is flatter than the vertical, particularly for the mid-frequency range of 122 – 453Hz.

For steel sleepers no resonance modes are excited in the vertical direction for response at both positions of the rail. Two resonance modes are excited in the horizontal direction at frequencies 195Hz and 398Hz. The FRFs representing the response at both positions of the rail on steel sleeper is flat for the entire response window, particularly from 70Hz.

In terms of vibration response of rails on steel and concrete sleepers, it is established that mid-span and on top of sleepers point, the rail on steel sleepers has a more damped response than that on concrete sleepers. This is evident from flatter FRFs for response of rail on steel sleepers, whilst more resonance modes are identified from the response of rail on concrete sleepers. However, the opposite is established in terms of acceleration. The rail on steel sleepers responds with a higher acceleration than that on concrete sleepers for most of the response window in the frequency range corresponding to short pitch rail corrugation. This can be explained by the difference in mass for the two rails. The rail on the steel sleepers is at 48kg/m while that on the

concrete sleepers is at 57kg/m. It is commonly understood that a lower mass and a stiffer beam results in an increased frequency.

With respect to vibration response of sleepers, vibration of steel sleepers is more damped in the vertical (but not as damped in the horizontal) direction than that of concrete sleepers. This can be seen in Figure 5.12. where the FRF is flat for steel sleepers in the vertical direction, and Figure 5.13. where a few resonance modes are identified for the same sleepers in the horizontal. Similar to the response of rails, accelerance is higher for steel sleepers than that of concrete sleepers.

In terms of response of concrete sleepers, a few resonance modes are identified vertically and horizontally. Experimentally, no resonance mode was excited on rails and sleepers at 108Hz. From the current study, a few opportunities exist, which may ultimately reduce the impact of the current problem in the railway tracks and the ecology surrounding it. The next chapter outlines details of FEA modal analysis on wheels.



## Chapter Six

### FEA Modal Analysis on a Freely Suspended Wheelset

*What results were obtained from FEA modelling work conducted to study wheelset dynamics, and how are they interpreted?*

The purpose of this chapter is to investigate vibration modes of a freely suspended wheelset of a D39 200 locomotive through the normal modes eigen-solver. The primary aim of the analysis was to establish whether there are any vibration response modes that may be associated with the rail corrugation with which the current study is concerned. The secondary aim of the analysis was to compare the vibration response results of a freely suspended wheelset with those obtained experimentally for two cases: (i) for a freely suspended wheelset, (ii) for a wheelset installed in a bogie. A complete wheelset is modelled for vibrational response. Here the wheelset is subjected to a free-free vibration.

The next subsection outlines details of the FEA procedure adopted in modelling vibrational response of the D39 200 locomotive class wheelset. Modal analysis results in this Chapter are subsequently compared with experimental modal analysis results for a freely suspended wheelset for the D39 200 locomotive class. The FEA modal analysis was conducted after the experimental part, given that no output parameters were required from the FEA modal analysis to be used as input parameters to the experiment.

#### 6.1. Procedure for FEA Modal Analysis on a Freely Suspended Wheelset

A 3D FE model of the D39 200 locomotive traction wheelset was developed as shown in Figure 6.1.

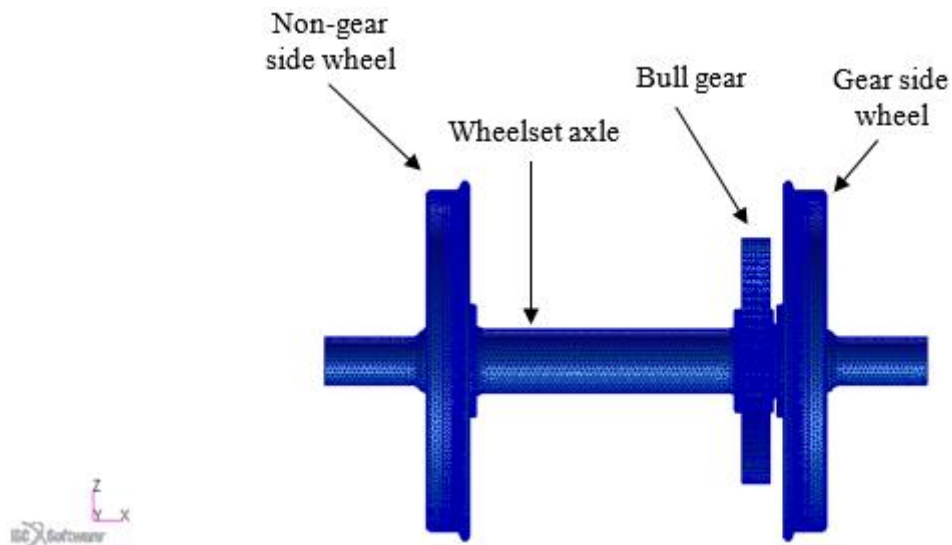


**Figure 6.1.** FEA model for a D39 200 locomotive traction wheelset.

The traction wheelset model in Figure 6.1. includes a bull gear mounted on a wheelset axle. The bull gear was modelled to accurate dimensions with teeth profile. The coupling between the bull gear and traction motor pinion is not modelled. The gear case is also not modelled. This is for accurate comparison of experimental modal analysis results with those of a freely suspended wheelset FEA model.

The mesh details for the FEM are tabulated in Table 6.1. Tet10 solid elements were used on all solids of the wheelset model to ensure better contact definition.

**Table 6.1.** Mesh details for the traction wheelset

Mesh Item	Mesh Details
Mesh type	Solid
Element type	Tetrahedron
Mesher	TetMesh
Topology	Tet 10

The element nodes were equivalenced to 0.1 mm to ensure better alignment of the nodes on created contacts, and also to get rid of unnecessary nodes in the model. Table 6.2. tabulates mesh convergence for the wheelset model. Mesh convergence was measured on the first bending mode only, for all mesh sizes.

**Table 6.2.** Mesh convergence for the traction wheelset model

Element Global Edge Length (mm)	Number of Nodes	Maximum Displacement (mm)
250	48,188	42.3

50	182,346	43.8
10	763,491	54.7
5	823,157	57.3
4	834,568	57.7
3.5	869,498	58.1
3	905,567	58.1

Evident in Table 6.2. is that the mesh used in the traction wheelset FEM converges at a global edge length of 3.5mm. Materials are understood to be isotropic and the material properties of steel used in the FEA model are tabulated in Table 6.3. The material of steel used in modelling the D39 200 wheelset is used in practice.

**Table 6.3.** Material properties for FE model of a D39 200 traction wheelset [23]

<b>Material</b>	<b>Young's Modulus (GPa)</b>	<b>Density (kg/m<sup>3</sup>)</b>	<b>Poisson's ration</b>
Steel	210	7850	0.3

Constraints and loads were not applied in the model in all six DOF. Vibration frequency is set to a range of 0 – 500Hz to capture the vibration modes that correspond to a short pitch corrugation on rails. Vibration modes requested are 16, which include the first six rigid body modes. Hence the vibration mode number seven is in principle the first mode. A rigid mode occurs at the beginning of the vibration process of a structure, where its translation and or rotation does not result in a significant internal deformation. This typically occurs at in the first six vibration modes of the structure [217].

The bull gear material properties used are the same as those of the entire wheelset. The next subsection reports on the results for the FEA modal analysis on a freely suspended wheelset.

## 6.2. Results for FEA Modal Analysis on a Freely Suspended Wheelset

To validate experimental results of modal analysis conducted on a freely suspended wheelset and on a wheelset installed in a bogie, an FEA model of a freely suspended wheelset model is developed. Figure 6.2. shows the axle bending mode of the traction

wheelset at a frequency 100Hz. This is the first wheelset axle bending mode after the six rigid body modes. In order to better resolve bending stresses, the FEM was meshed significantly finer, with the global edge length of 3.5mm. This resulted in over 1.3 million nodes for the entire FEM.

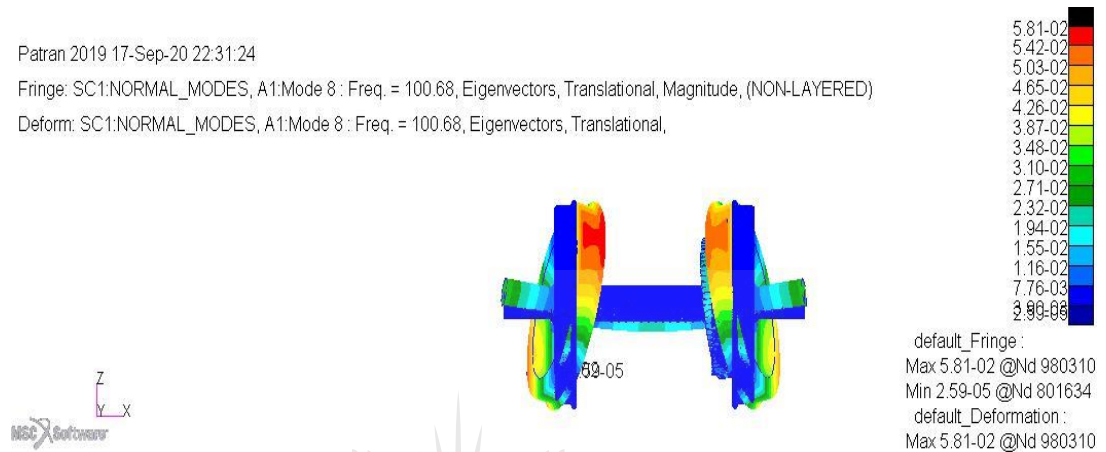


**Figure 6.2.** Traction wheelset – mode shape for first-order bending mode.

Evident in Figure 6.2. is that at 100Hz the axle bends along the horizontal plain, such that it shall ultimately form an arc. This mode forces the wheels to tilt sideways along the vertical plain as though they are pivoted on the points where they couple to the axle. The bending of the axle to sort of form an arc shape naturally forces one wheel to tilt in the opposite direction to the next wheel in the vertical plane.

This mode shape is the most closely associated with the resonance that occurs at the short pitch corrugation formation frequency of 108Hz and that at 120Hz of the axial FRF in Figure 4.8. given that the mode shape presents an axial bending of the wheels due to axle bending. Even though it would have made more sense for this mode to occur exactly at 108Hz, a percentage error played a role in the slight deviation in frequency between experimental and modelling.

A percentage error makes for the difference in the frequency at 108Hz and 100Hz obtained experimentally from a freely suspended wheelset and through FEA modal analysis respectively. Table 6.4. shows the percentage errors for two cases: (i) when results of the modelled freely suspended wheelset are compared to those of experimental modal analysis on a freely suspended wheelset (ii) when results of the

modelled freely suspended wheelset are compared to those of experimental modal analysis a wheelset installed in a bogie.

**Table 6.4.** Percentage error between experimental and FEA modal analysis

	<b>Frequency (Hz) for First Bending Mode (Experimental Modal Analysis)</b>	<b>Frequency (Hz) For First Bending Mode (FEA Modal Analysis)</b>	<b>% Error</b>
Freely suspended wheelset	108	100	7.4
Wheelset installed in a bogie	120	100	16.6

A percentage error exists between experimental and modelling work, typically due to the assumptions made (and also those not made) by the FEA and the accuracy of the modelled geometry [174]. Some of the assumptions not made by the FEA in a freely suspended wheelset in the current study are slinging effects of the wheelset using a steel chain, thermal and corrugation effects, friction, gravity and bolt loading were not considered. In the case of the wheelset installed in a bogie, some elastic modes of the bogie structure may interfere with the response of the wheelset.

In addition, outcomes of experimental work may also be influenced by environmental factors during time of conducting the experiment. From the mode shape in Figure 6.2. it is safely deduced that in order to reduce the association of the first bending resonance mode of the wheelset, with rail corrugation formation frequency, efforts shall be made to firstly prevent excessive bending of the axle along the horizontal plane.

The second part of the solution is to damp resonance of the wheels in the axial direction, particularly on the wheel web, towards the wheel profile. It is understood from the accepted literature that the flexibility of railway wheels has a significant influence on the flexibility of the entire wheelset [223]. This is the first-order wheelset axle bending mode after the six rigid body modes as shown in Figure 6.2.

The second-order wheelset bending mode occurs at a frequency of 158Hz as seen in Figure 6.3.

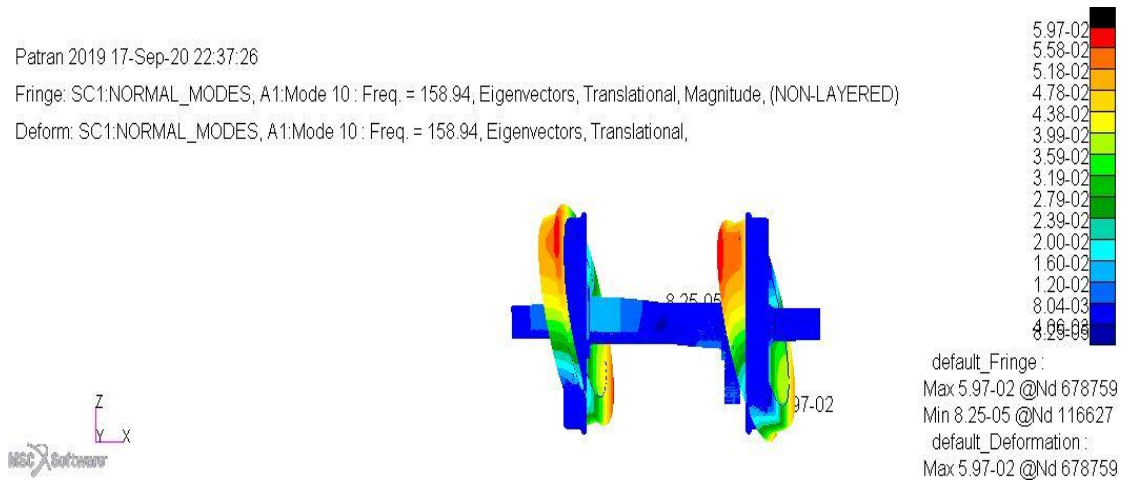


**Figure 6.3.** Traction wheelset – mode shape for second-order bending mode.

Evident in Figure 6.3. is that the wheelset still experiences an axle bending mode at 158Hz. This is the second bending mode, where the axle bends along the horizontal plain, such that it will ultimately form a sine wave. This mode forces the wheels to tilt sideways along the vertical plain as though they are pivoted on the points where they couple to the axle. The next subsection summarises the discussion of the results for FEA modal analysis on a freely suspended wheelset.

### 6.3. Results Discussion

Evident from the FEA modal analysis results is that the first-order axle bending mode of the D39 200 wheelset is excited at a frequency of 100Hz. This vibration mode is reasonably close to that excited experimentally at 108Hz on a freely suspended wheelset. This bending mode at 100Hz excited on FEA modal analysis was also compared with the first axial bending mode excited experimentally when the wheelset was installed in a bogie and the results were still reasonably close. However, the percentage error is larger for the case in which the FEA modal analysis bending mode is compared with that of a wheelset installed in a bogie. This can be explained by the effects of elastic modes of a bogie, as these may have effects in the response of the wheelset.

The wheelset presents a second-order axle bending mode shape at 158Hz. The bending of the axle to sort of form a sine wave naturally forces both wheels to tilt in the same direction in the vertical plane. From the mode shape in Figure 6.3. it is safely deduced

that in order to reduce association of resonance of the second bending mode of the wheelset, with rail corrugation formation frequency, it would be safer to apply a damping mechanism along the entire length of the axle, and not only in the middle.

A smaller size damper applied in the middle of the axle may sit directly at the node of the second-order bending mode. In terms of the FEA modal analysis some modes are not excited. None of the wheel vibration modes presented circumferential binding in the frequency range of 0 – 500Hz. The rest of the mode shapes at different frequencies are found in Appendix D.

These mode shapes occur at frequencies higher than 150Hz, making them not to be closely associated with the rail corrugation formation frequency in the Belfast to Steelpoort railway line.

The next chapter outlines details of the FEA complex eigenvalue analysis on railway tracks installed with steel and concrete sleepers.

#### **6.4. Recommendations**

Short pitch rail corrugation is a complex problem that will require different pieces of well-established models describing and predicting elements of the problem. Ultimately these will form a complex model that may be used to solve short pitch rail corrugation problem in different rail track environments. These models may be developed with the use of other well-known models in the rail corrugation space.

From the current study, the following recommendations that could be useful are outlined:

- Development of a numerical and analytical models to assess the effect of damping of wheel resonance modes, on short pitch rail corrugation.
- Development of numerical and analytical models to assess the effect of damping of rail resonance modes, on short pitch rail corrugation,
- Development of numerical and analytical models to assess the effect of altering the damping and stiffness of rail pads, on short pitch rail corrugation,



- Development of numerical and analytical models to assess the effect of damping of the concrete sleepers (possibly with installation of booted sleepers), on short pitch rail corrugation,
- Development of numerical and analytical models to assess the effect of increasing the vertical fastening stiffness of the FISTclip and e-Clip rail fasteners, on short pitch rail corrugation,
- In the Belfast to Steelpoort railway line; to study the effect of altering the rail foot angle, on short pitch rail corrugation,
- In the interim, whilst researchers make efforts to develop a permanent cure, reinstallation of steel sleepers is recommended on all track curves in the line. Design of steel sleepers shall be improved in line with latest axle loads and considering the future product movement targets for the line.



## Chapter Seven

### Complex Eigenvalue Analysis on Railway Tracks Installed with Steel and Concrete Sleepers

*What results were obtained from the complex eigenvalue analysis for modelling work conducted to study tracks' dynamics, and how are they interpreted?*

The purpose of this chapter is to use a Finite Element method to investigate the rail tracks' resonance modes for tracks supported on steel and with concrete sleepers. The primary aim of the experiment was to establish whether there are possible rail track vibration modes that may be associated with rail corrugation at a corrugation frequency of 108Hz. The secondary aim of the experiment was to compare the vibration response results of the rail tracks supported on steel and concrete sleepers, with those obtained from experimental modal analyses of the two railway tracks supported on steel and concrete sleepers.

The Complex Eigenvalue analyses were adopted to identify the possible unstable modes in terms of the coupling phenomena. The complex eigenvalue analysis models for rail tracks include a traction wheelset for the class D39 200 diesel locomotive on top of rails. In these track models the wheelset is modelled without a bogie and traction motor. The next subsection outlines the procedure adopted in conducting the complex eigenvalue analysis on railway tracks.

#### **7.1. Procedure for Finite Element Complex Eigenvalue Analysis on Rail Tracks Supported on Steel and Concrete Sleepers**

For the complex eigenvalue analysis, two rail track models were developed for investigation of mode shapes, i.e. the steel and concrete sleeper track models. The primary difference between the models is the sleeper types, rail mass and the fact that there are no rail pads in the steel sleeper track model. Figure 7.1. shows a side view of the steel sleeper model.

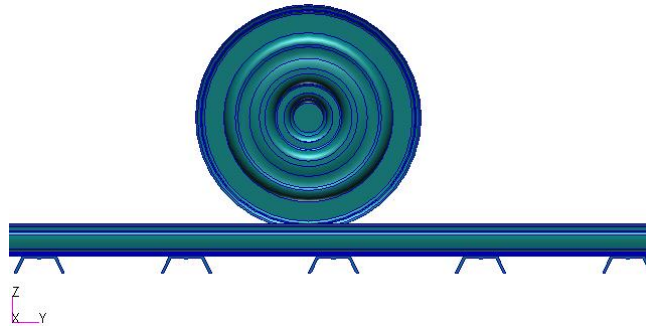


**Figure 7.1.** Rail track model with steel sleepers.

The model in Figure 7.1. has 30m long rails and a sleeper bay of 700mm in the Y-direction, which makes fourty three steel sleepers. The D39 200 locomotive traction wheelset is modelled at a center distance from rail ends. Contacts created for deformable bodies are tabulated in Table 7.1.

**Table 7.1.** Contacts created for deformable bodies in the steel sleeper model

Geometry (in contact)	Geometry (in contact with)	Contact
Wheelset axle	Wheels	Glue
Wheels	Rails	Glue
Rails	Sleepers	MPC
Sleepers	Ballast	MPC

Glued contacts were created for connections between the wheelset axle and wheels. The same was done for the connection of wheels to rails. The MPCs were used for connection between the bottom face of rail foot and the sleepers. Similar to the wheel-rail contact model with steel sleepers; the rail foot does not make contact with the entire top face of the sleeper, only a few points of the geometries make contact.

The same method of the MPCs was used for connection of the bottom face of sleeper legs and the top face of the top ballast layer. Table 7.2. tabulates details of the mesh used in the FEM for rail track with steel sleepers.

**Table 7.2.** Mesh details for rail track FEM with steel sleepers

Mesh item	Mesh details
Mesh type	Solid
Element type	Tetrahedron
Mesher	TetMesh
Topology	Tet 10

The element nodes were equivalenced to the tolerance of 0.1mm. Materials are understood to be isotropic and the material properties allocated to each FEM solid are tabulated in Table 7.3. Given that steel sleepers are not sufficiently studied, material properties of the steel sleeper were provided by the Track Technology department at Transnet.

**Table 7.3.** Material properties for FEMs on rail track model with steel sleepers [23]

FEM Solid	Material	Density (kg/m <sup>3</sup> )	Young's Modulus (GPa)	Poisson's Ratio	Shear Modulus (GPa)
Axle	Steel	7850	210	0.30	
Wheel	Steel	7850	210	0.30	
Rail	Steel	7800	210	0.30	
Sleeper	Steel	7870	205	0.29	80

Figure 7.2. shows the concrete sleeper model. Only the rail track with FY-type concrete sleepers is modelled. Similar to the model with steel sleepers; the model in Figure 7.2. has 30m long rails and a sleeper bay of 700mm in the Y-direction; which makes fourty three concrete sleepers. The D39 200 locomotive wheelset is modelled at a center distance from rail ends.

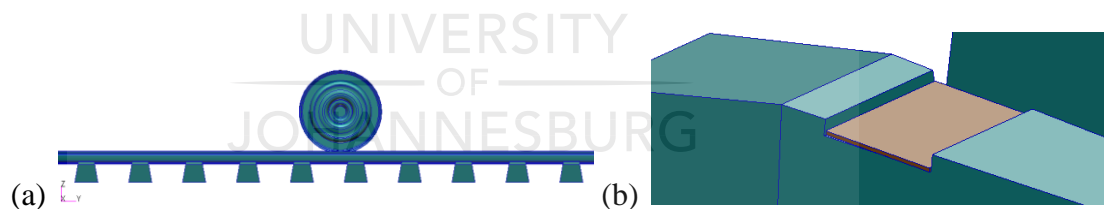


**Figure 7.2.** Concrete sleeper track. (a) rail track model with concrete sleepers (b) rail pad on a concrete sleeper.

More contacts were created for the concrete sleeper model, given that it includes rubber rail pads. Two contacts were created for rails' pads, i.e. contact for rail with the rubber pads and for pads with the sleepers. Contacts created for deformable bodies are tabulated in Table 7.4.

**Table 7.4.** Contacts created for deformable bodies in the concrete sleeper model

<b>Geometry (in contact)</b>	<b>Geometry (in contact with)</b>	<b>Contact</b>
Wheelset axle	Wheels	Glue
Wheels	Rails	Glue
Rails	Pads	MPC
Pads	Sleepers	Nodes equivalenced
Sleepers	Ballast	Glue

In order to prevent FEMs from dislocating from touching connections in the track model with concrete sleepers, glued contacts were created for connections between the wheelset axle and wheels. The same was done for the connection of wheels to rails. In order to save simulation time, MPCs were used for connection between the bottom face of the rail foot and pads.

Nodes were created in the rail foot to align to those of the rail pads. This made it easier for MPCs to connect. Edges of rail pads were perfectly aligned with those of the top surface of the sleepers, hence the nodes were only equivalenced for the pad and sleeper. This achieved a significant saving in computation time. A glued contact was used for connection of the bottom face of sleepers and the top face of the top ballast layer. Table 7.5. tabulates details of the mesh used in the FEM for rail track with concrete sleepers.

**Table 7.5.** Mesh details for rail track FEM with concrete sleepers

<b>Mesh item</b>	<b>Mesh details</b>
Mesh type	Solid
Element type	Tetrahedron
Mesher	TetMesh
Topology	Tet 10

The element nodes were equivalenced to the tolerance of 0.1mm. Materials are understood to be isotropic and the material properties allocated to each FEM solid are tabulated in Table 7.6. Given that the rail pads are not sufficiently studied, material properties of the rubber rail pad were provided by the Track Technology department at Transnet.

**Table 7.6.** Material properties for FEMs on rail track model with concrete sleepers [23] [224]

FEM Solid	Material	Density (kg/m <sup>3</sup> )	Young's Modulus (GPa)	Poisson's Ratio	Damping Coefficient
Axle	Steel	7850	210.000	0.30	
Wheel	Steel	7850	210.000	0.30	
Rail	Steel	7800	210.000	0.30	
Pad	Rubber	1300	0.080	0.45	0.34
Sleeper	Concrete	2400	36.406	0.20	

The rail pad material properties used were found from Chen et al [137]. The damping for the rail pad was characterized following the procedure for rail pads material models [225]. From the models in Heunis [225], the Hysteretic damping coefficient was used, which is represented by equation (7.1).

$$b(\omega) = \frac{\pi \omega c_{eq}}{2} \quad (7.1)$$

In equation 7.1  $\omega$  is the excitation frequency and  $c_{eq}$  is the equivalent viscous damping coefficient. The corrugation frequency (108Hz) was used as the excitation frequency and the equivalent viscous damping coefficient of 0.002 Ns/m was taken Grässie's [226] analysis of the dynamic behaviour for rail pads. In order to represent the gravitational force, the inertial load of -9.81 was created along the z-direction. The inertial load was created for both models of rail tracks with steel and concrete sleepers. The next subsection outlines the procedure adopted for modelling of the three-layered track ballast.

## 7.2. Procedure for Modelling of Track Ballast

A track ballast is understood to have a possible effect in response of a railway track structure to dynamic loads. Both tracks with concrete and steel sleepers were modelled with ballast. Effects from the subgrade (native soil layer underneath the ballast) are not considered in the current study. As well, it is assumed that the contact surface between the soil (ground) and the bottom ballast is uniform in the longitudinal direction, likewise with the contact surface between ballast layers. The ballast was divided into three layers i.e. top, middle and bottom. The top layer ballast was modelled as less stiffer than the middle.

Figure 7.3. shows the ballast as modelled underneath the sleepers in the FEA model.

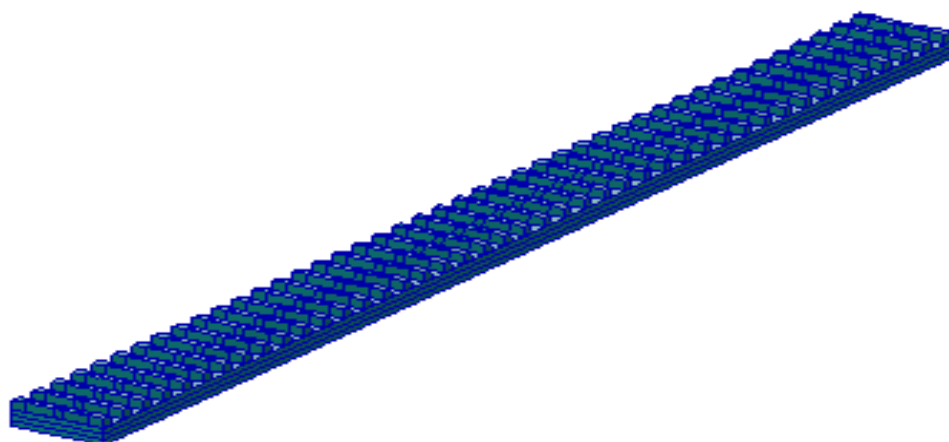


**Figure 7.3.** FEA model representing ballast underneath concrete sleepers.

The same size of ballast was used for FEA models of both tracks with steel and concrete sleepers. To model the ballast, a volume of 30m x 2.2m x 0.45m was developed. The volume was divided into three layers of same thickness i.e. 0.15m, which yields the total height of 0.45m for the entire ballast. Table 7.7. tabulates details of the mesh used in the ballast FEM.

**Table 7.7.** Mesh details for ballast FEM

Mesh item	Mesh details
Mesh type	Solid
Element type	Tetrahedron
Mesher	TetMesh
Topology	Tet 10

The same mesh type and size was used for both ballast FEMs of steel and concrete sleepered tracks. The same mesh element size and nodes were used for all three ballast layers, which provided for ease of mesh optimisation. The element nodes were equivalenced to the tolerance of 0.1mm between all layers. The ballast material was treated as isotropic. The assumption was that tamping of the ballast was sufficiently done such that no ballast settlement would occur, causing the stiffness to be the same along and across the length of the ballast. The material properties allocated to the ballast FEM are tabulated in Table 7.8.

**Table 7.8.** Material properties for ballast FEM [227]

<b>FEM Solid</b>	<b>Material</b>	<b>Density (kg/m<sup>3</sup>)</b>	<b>Young's Modulus (MPa)</b>	<b>Poisson's Ratio</b>	<b>Structural Damping</b>
Top layer ballast	Stones	2500	256	0.2	0.01
Middle layer ballast	Stones	2600	276	0.2	0.01
Bottom layer ballast	Stones	2700	300	0.2	0.01

The ballast material properties used were found from Aikawa [227], and different parameters of ballast properties were established following the Zakeri and Mosayebi method that achieves different stiffnesses between layers [220]. Two contacts were created for ballast layers; contact for bottom face of the top ballast in contact with the top face of the middle ballast; and the bottom face of the middle ballast in contact with the top face of the bottom ballast.

Contacts created for deformable bodies are tabulated in Table 7.9. For complex eigenvalue analysis the ballast is the only FEM on which constraints were applied. Table 7.9. also tabulates the loads and boundary conditions applied on the ballast.

**Table 7.9.** Contacts and constraints created for deformable bodies of the ballast

<b>Geometry (in contact)</b>	<b>Geometry (in contact with)</b>	<b>Contact</b>	<b>Fix translation</b>	<b>Fix rotation</b>
Top layer ballast	Middle layer ballast	Glue		
Middle layer ballast	Bottom layer ballast	Glue		
Bottom layer ballast			<0,0,0>	<0,0,0>

Only the nodes on the bottom face of the bottom ballast were fixed for translation and rotation in all six DOFs. The ballast was treated as a structure erected above ground (not partially buried), hence the nodes on the side faces of the ballast were not constrained. The next subsection reports on the results for complex eigenvalue analysis on railway tracks supported on steel and concrete sleepers.

### **7.3. Results for FEA Complex Eigenvalue Analysis on Rail Tracks Supported on Steel and Concrete Sleepers**

Figure 7.4. shows complex eigenvalue analysis results for the railway track model with steel sleepers at 108Hz.



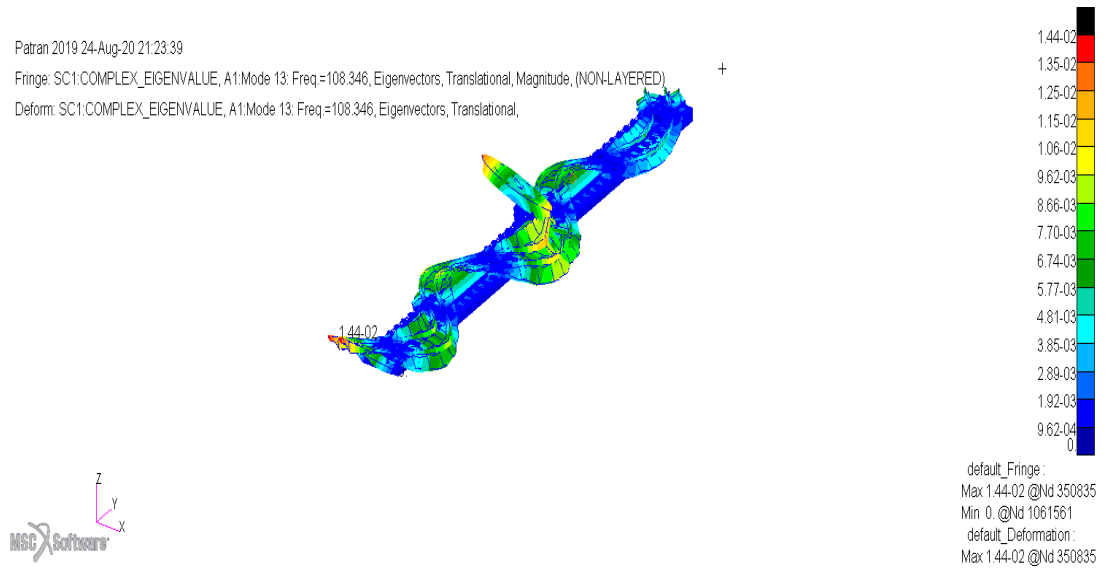


**Figure 7.4.** Bending mode for rail track with steel sleepers at 108Hz and ballast.

The rail track model results in Figure 7.4. show the deformed and undeformed shapes. For normalization, a generalized modal mass is equal to unity. The color coding in the legend correspond to the colors in the deformed shape of the model results. It is seen in Figure 7.4. that at 108Hz the rail on steel sleepers vibrates with a bending mode in the horizontal direction. At this mode the ballast remains at its original position, whilst the sleepers are taking shape of the rail as they are joined together. The wheelset at this mode also presents a complicated shape as it is glued to the rails to avoid dislocation during vibration. Figure 7.5. shows a clearer view of this vibration mode for sleepers and rail.

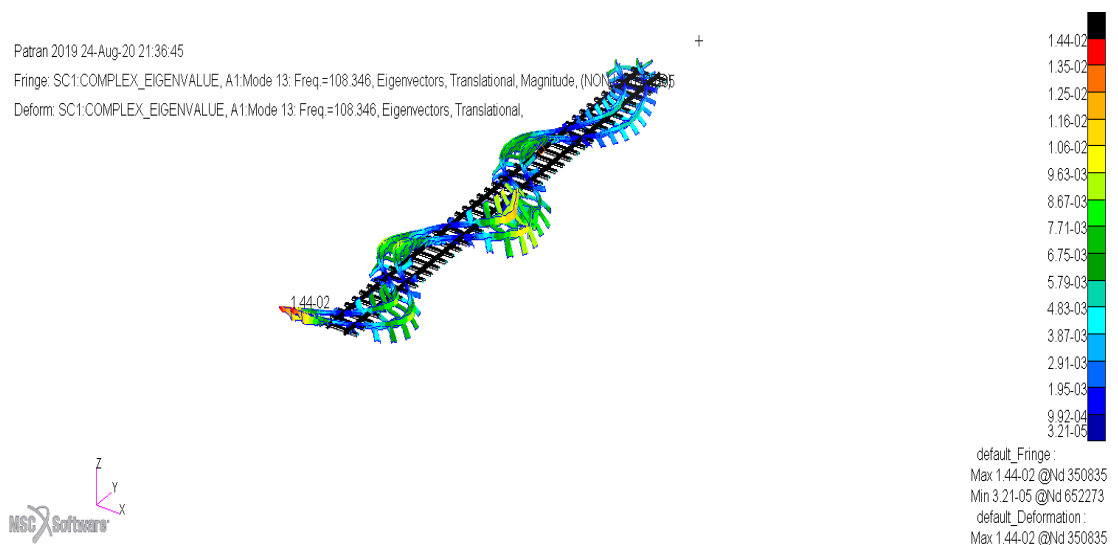


**Figure 7.5.** Bending mode for rail track with steel sleepers at 108Hz, no ballast.

It is clear from this Figure (7.5.) that at 108Hz the rail merely bends horizontally without any vertical bending and/or attempting to twist the track. This complex eigenvalue model does not present the self-excited unstable vibration in the vertical direction, which is the direction of vibration that is associated with the formation of rail corrugation [34]. The rest of the mode shapes at different frequencies are found in Appendix E. Figure 7.6. shows complex eigenvalue analysis results for the railway track model with concrete sleepers at 108Hz.

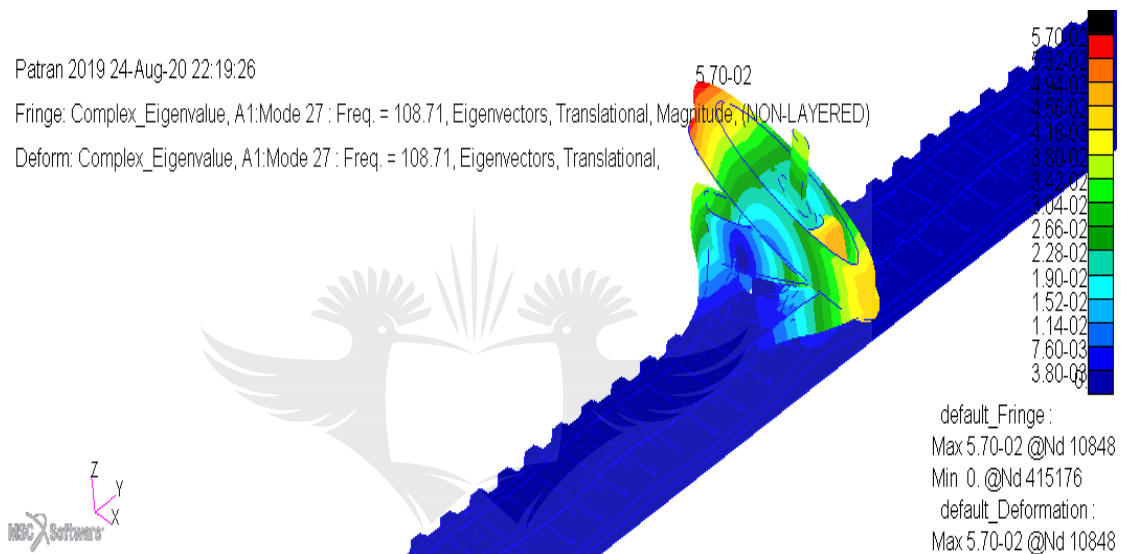


**Figure 7.6.** Bending mode for rail track with concrete sleepers.

As seen in Figure 7.6. contrary to the rail track model with steel sleepers, the rail track with concrete sleepers shows no vibration modes in the horizontal direction. The rail track with concrete sleepers shows a vertical bending mode at 108Hz. This complex eigenvalue model presents the self-excited unstable vibration in the vertical direction, which is the direction of vibration that is associated with the formation of rail corrugation [34].

In the middle of the track the wheelset-rail system shows a complex vibration mode. This is due to the fact that the wheelset is glued to the rails, hence the rails follow the wheelset bending. More resonance modes that showed some clear activity occur in frequencies lower than 108Hz are found in Appendix F.

#### 7.4. Results Discussion

Given that the first important resonance mode of the traction wheelset was identified to reasonably match the average corrugation frequencies at 108Hz, rail track models were developed to investigate the dynamic response at the same frequency. From the complex eigenvalue analysis, it is established that at 108Hz the rail track with concrete sleepers responds with a vertical bending mode.

This is noted by the bending mode of rails in the vertical direction with complete waves, giving a mode that Garcia [151] refers to as a “rail vibration” mode. This (rail track with concrete sleepers) is the rail track on which corrugation formed. It is generally accepted that formation of corrugation on rails is linked with vertical vibration [151, 228], and increasing the vertical clamping force of rail fasteners reduces corrugation formation [33].

No vertical mode is excited at 108Hz for the rail track with steel sleepers. This finding is in line with the modal analysis results for track with steel sleepers in Figures 5.14. where no resonance mode is excited in the vertical direction for the track with steel sleepers. In the same Figure (5.14.) two resonance modes are excited in the horizontal direction, even though these occur at higher frequencies than the short pitch corrugation formation frequency.

For rail track curves with concrete sleepers in the Belfast to Steelpoort railway line, increasing the vertical fastening stiffness has to be taken as one of the critical measures in an attempt to reduce corrugation formation. Only a horizontal bending is identified at 108Hz for rail track with steel sleepers. At frequencies beyond 108Hz the rail tracks respond with complex vibration modes, where twisting of the tracks occurs.

At these modes it is not easy to identify the shape that the track takes, since the track twists many times in a short span. The next chapter discusses the implications of the current study and concludes on the findings thereof.

## Chapter Eight

### Implications and Conclusions

*What impact will the current study have on future research, what major conclusions are drawn from the research study and what direction should be considered next?*

#### 8.1. Implications

It was of importance to conduct the current study in an attempt to reduce corrugation formation on the running surface of rails in the Belfast to Steelpoort railway track curves. The experiment conducted on the traction wheelset adds to the current body of knowledge with introduction of the method of coupling a wheelset to a traction motor and installing it in a bogie. This method is beneficial in aiming to yield more reasonably accurate FRF results where wireless accelerometers are not available.

The FEA conducted on modelling the traction wheelset on a reasonably long track structure adds to the current body of knowledge with introduction of excitation of the entire track structure and the wheelset simultaneously. The common methodology in the field of rail corrugation investigations often has wheels analysed separately from the rails. In this way the results may prove not to be as accurate where FRFs of the wheels are correlated to those of the rail track.

This model of the ballasted railway track with steel sleepers is novel. Most conventional models are developed for slab tracks with monoblock and bi-block concrete sleepers. If any literature exists, it is not sufficient and advanced enough to explore the dynamics of ballasted railway tracks installed with steel sleepers. On a lighter note, concrete sleepers are arguably the most common type used on modelling corrugation on rails, both in high and low velocity operations [33, 35].

The pyramid model adopted in modelling the track ballast will assist researchers in the rail corrugation space to achieve more accurate modelling results. This is given that parameters of each ballast layer are accurately defined in the pyramid model. The model allows different ballast layer stiffnesses to be defined in an attempt to achieve more accurate results [220]. Given that experimental modal analysis of FRFs in the

current study are obtained from a three-layered ballasted track, it makes more sense, hence, that modelling is conducted on same arrangement of the ballast.

The current study will impact the latest research work by adding the complex eigenvalue FEA procedure in modelling ballasted tracks. The experimental modal analysis procedure will also be effectively used to obtain point FRFs for rails of ballasted rail tracks and sleepers installed in ballasted railway tracks. The easier basic method to match vibration modes of the traction wheelset to corrugation frequencies per track curve will add to the latest body of knowledge.

A need still exists to develop further analytical and numerical models, to be used together with models in the current study, to prevent a short pitch corrugation from forming in the future. This will ultimately produce a complex model that will be used in solving the short pitch corrugation problem in the railway space.

## **8.2. Conclusions**

In the frequency range that corresponds to short pitch rail corrugation, there exists important differences in dynamic responses of ballasted rail tracks with steel and concrete sleepers. The vertical bending mode of the ballasted rail track with concrete sleepers could be attributed to existence of corrugation on rails. This is concluded given the dynamic behaviour of the ballasted rail track at a frequency of 108Hz, which can be strongly associated with the short pitch corrugation formation.

It is well known that the vertical vibration of rails has an effect of significance on corrugations on rails [151, 228]. The rail supported on concrete sleepers responds reasonably with more resonance modes that are supported on steel sleepers. This is generally found mid-span and on top of sleeper point, in the vertical and horizontal directions. Damping of the first axial bending resonance mode remains critical in an attempt to prevent the wavelength fixing mechanism for short pitch rail corrugation.

The first axial bending mode of the D39 200 locomotive traction wheelset is excited on vibration response, when the traction wheelset is uncoupled from the traction motor and is freely suspended. This mode is also excited when the traction wheelset is coupled to a traction motor and installed in a bogie. This traction wheelset mode reasonably matches corrugation frequencies for nearly all corrugated track curves.

More damping of this resonance mode is noted from the FRFs when the wheelset is coupled to a traction motor and installed in a bogie. This first axial bending mode is also excited by cross-coupling of vibration response by the axle. From these three scenarios the importance of this mode is validated and given emphases. In the frequency range that corresponds to short pitch rail corrugation, the dynamic response of concrete sleepers shows a few undesired resonance modes in the vertical direction, which could contribute in the rail track structure responding erratically to vibration during train pass. It is of importance to reduce resonance of all components closely connected to the rails, such as rail pads and sleepers.



## References

- [1] U. Spangenberg, Doctoral Thesis: Reduction of Rolling Contact Fatigue Through the Control of the Wheel Wear Shape, Pretoria: UPSpace, <http://hdl.handle.net/2263/62796>, 2016.
- [2] S. L. Grässie, Rail Corrugation: Chapter 11, in *Wheel/Rail Interface Handbook*; Lewis, R, Olofsson, U., Boca Raton, Florida, USA: CRC Press, 2009, pp. 349 - 376.
- [3] C. Zhao, P. Wang , X. Sheng and D. Meng, “Theoretical Simulation and Experimental Investigation of a Rail Damper to Minimize Short-Pitch Rail Corrugation,” *Mathematical Problems in Engineering*, vol. 2017, no. Article ID 2359404, p. <https://doi.org/10.1155/2017/2359404>, 2017.
- [4] J. Han, X. Xiao, Y. Wu, Z. Wen and G. Zhao, “Effect of Rail Corrugation on Metro Interior Noise and its Control,” *Applied Acoustics*, vol. 130, no. <https://doi.org/10.1016/j.apacoust.2017.09.007>, pp. 63 - 70, 2018.
- [5] X. Cui, Z. Cheng, Z. Yang, B. Huang and Z. Du, “Study on the Phenomenon of Rail Corrugation on High-Speed Rail Based on the Friction-Induced Vibration and Feedback Vibration,” *International Journal of Vehicle Mechanics and Mobility*, vol. DOI: 10.1080/00423114.2020.1817507, 2020.
- [6] Y.-C. Chen and S.-Y. Lee, “Elastic-Plastic Wheel-Rail Thermal Contact on Corrugated Rails During Wheel Braking,” *Journal of Tribology*, vol. 131, no. 011401-1, 2009.
- [7] S. Kaewunruen, “Monitoring of Rail Corrugation Growth on Sharp Curves For Track Maintenance Prioritisation,” *International Journal of Acoustics and Vibration*, vol. 23, no. 1, pp. 35 - 43, 2018.
- [8] K. Wang, P. Liu, W. Zhai, C. Huang, Z. Chen and J. Gao, “Wheel/Rail Dynamic Interaction Due to Excitation of Rail Corrugation in High-Speed Railway,” *Science China Technological Sciences*, vol. 58, no. 2015, p. 226–235, 2015.
- [9] X. Jin, Z. Wen, W. Zhang and Z. Shen, “Numerical Simulation of Rail Corrugation on a Curved Track,” *Computers & Structures*, vol. 83, no. 25 - 26, pp. 2052 - 2065, 2005.
- [10] B. M. Balekwa, Master's Dissertation: Corrugation Wavelength Fixing Mechanism and its Relation to Train and Track Geometry Parameters, Johannesburg: University of Johannesburg, 2017.
- [11] Y. Q. Sun and S. Simson, “Vehicle-Track Modelling for Rail Corrugation Initiation Investigation,” *Proceeding of Joint Rail Conference*, pp. 65 - 71, 16 - 18 March 2005.

- [12] A. Saulot and S. Descartes, "A Tribological Characterization of the "Damage Mechanism" of Low Rail Corrugation on Sharp Curved Track," *Wear*, vol. 260, no. 9 - 10, pp. 984 - 995, 2006.
- [13] C. Ma, L. Gao, T. Xin, X. Cai, M. M. Nadakatti and P. Wang, "The Dynamic Resonance Under Multiple Flexible Wheelset-Rail Interactions and Its Influence on Rail Corrugation for High-Speed Railway," *Journal of Sound and Vibration*, vol. 498, no. <https://doi.org/10.1016/j.jsv.2021.115968>, 2021.
- [14] S. Grässie and J. Kalousek, "Rail Corrugation: Causes and Cures," *IRJ. Wheel-Rail Technology*, pp. 24-26, July 2000.
- [15] Y. Chen, F. V. Lawrence and C. P. L. Barkan, "Weld Defect Formation in Rail Thermite EWlds," *Proceedings of the Institution of Mechanical Engineers Part F Journal of Rail and Rapid Transit*, vol. 220, no. 4, DOI: 10.1243/0954409JRRT44, pp. 373 - 384, December 2006.
- [16] O. Popovic and R. Prokic-Cvetkovic, "Surface Welding as a Way of Railway Maintenance," in *Mechanical Engineering, Dr. Murat Gokcek (Ed.), ISBN: 978-953-51-0505-3*, Rijeka, Croatia, InTech, April 2012, p. 252.
- [17] Y. Liu, K. S. Tsang, E. T. Zhi'En, N. A. Subramaniam and J. H. L. Pang, "Investigation on Material Characteristics and Fatigue Crack Behavior of Thermite Welded Rail Joint," *Construction of building materials*, vol. 276, no. <https://doi.org/10.1016/j.conbuildmat.2021.122249>, 2021.
- [18] A. Böhmer and T. Klimpel, "Plastic Deformation of Corrugated Rails — A Numerical Approach Using Material Data of Rail Steel," *Wear*, vol. 253, no. 1 - 2, pp. 150 - 161, 2002.
- [19] AGICO GROUP, "How Much Do You Know About Rail Grinding?," [Online]. Available: <http://www.railway-fasteners.com/news/rail-grinding.html>. [Accessed 8 11 2020].
- [20] M. Ishida, "History of Mitigating Rolling Contact Fatigue and Corrugation of Railway Rails in Japan - Review," *EPI International Journal of Engineering*, vol. 1, no. 2, pp. 13 - 24, 2018.
- [21] X. Zhao, P. Zhang and Z. Wen, "On the Coupling of the Vertical, Lateral and Longitudinal Wheel-Rail Interactions at High Frequencies and the Resulting Irregular Wear," *Wear*, Vols. 430 - 431, no. <https://doi.org/10.1016/j.wear.2019.05.017>, pp. 317 - 326, 2019.
- [22] D. T. Eadie, J. Kalousek and K. C. Chiddick, "The Role of High Positive Friction Modifier in the Control of Short Pitch Corrugations and Related Phenomena," *Contact Mechanics 2000*, July 2000.
- [23] D. J. Fourie, Doctoral Thesis: Railway Wheel Squeal as a Result of Unsteady Longitudinal and Spin Creepage, Pretoria: University of Pretoria, 2018.



- [24] S. Zakhrov, Part 3: Wheel and Rail Performance. In: Guidelines to Best Practices for Heavy Haul Railway Operations: Wheel and Rail Interface Issues, Virginia: International Heavy Haul Association, 2001.
- [25] M. Ciavarella and J. Barber, "Influence of Longitudinal Creepage and Wheel Inertia on Short-Pitch Corrugation: A resonance-Free Mechanism to Explain the Roaring Rail Phenomenon," *Part J: Journal of Engineering Tribology*, pp. 171 - 181, 2008.
- [26] International Heavy Haul Association, in *Guidelines To Best Practices For Heavy Haul Railway Operations Handbook: Wheel and Rail Interface Issues*, Virginia, 2001.
- [27] L. Afferrante and M. Ciavarella, "Short-pitch Rail Corrugation: A Possible Resonance-Free Regime a Step Forward to Explain the "Enigma"," *Wear*, vol. 266, no. 2009, pp. 934 - 944, 2008.
- [28] S. L. Grässie and J. Kalousek, "Rail Corrugation: Characteristics, Causes and Treatments," *Part F: Journal of Rail and Rapid Transit*, vol. 207, pp. 57-68, 1993.
- [29] S. Müller and K. Knothe, "Numerical simulation of the formation of short pitch corrugation," *Journal of Applied Mathematics and Mechanics*, vol. 80, no. S1, pp. 53 - 56, 2011.
- [30] T. Xin , S. Wang, L. Gao, H. Huo, Y. Ding, P. wang, P. Chen and P. Liu, "Field Measurement of Rail Corrugation Influence on Environmental Noise and Vibration: A Case Study in China," *Measurement*, vol. 164, no. ISSN 0263-2241, p. <https://doi.org/10.1016/j.measurement.2020.108084>, 2020.
- [31] S. L. Grässie, "Rail Corrugation: Characteristics, Causes and Treatments," *Part F: Rail and rapid Transit* 264, vol. 223, pp. 1-16, 2009.
- [32] B. Balekwa and D. V. V. Kallon, "Correlation of Short Pitch Rail Corrugation with Railway Wheel-Track Resonance at Low Frequencies of Excitation," *Vibration*, vol. 3, no. 4, pp. 491 - 520, 2020.
- [33] G. X. Chen, X. L. Cui and W. J. Qian, "Investigation into Rail Corrugation in High Speed Railway Tracks from the Viewpoint of the Frictional Self-Excited Vibration of a Wheel-Rail System," *Journal of Modern Transportation*, vol. 24, pp. 124 - 131, 2016.
- [34] W. J. Qian, Y. F. Wu, G. X. Chen and H. Ouyang, "Experimental and Numerical Studies of the Effects of a Rail Vibration Absorber on Suppressing Short-Pitch Rail Corrugation," *Journal of Vibroengineering*, vol. 18, no. 2, pp. 1133 - 1144, July 2016.
- [35] O. Oyarzabal, N. Correa, E. G. Vadillo, J. Santamaria and J. Gomez, "Modelling Rail Corrugation with Specific-Track Parameters Focusing on Ballasted Track and Slab Track," *Vehycle System Dynamics*, vol. 49, no. 11, pp. 1733 - 1748, November 2011.

- [36] T. Abadi, L. L. Pen, A. Zervos and W. Powrie, "A Review and Evaluation of Ballast Settlement Models using Results from the Southampton Railway Testing Facility (SRTF)," *Procedia Engineering*, vol. 143, no. 2016, pp. 999 - 1006, 2016.
- [37] Q. Guan, Y. Zhou, W. Li and Z. f. Wen, "Study on the P2 Resonance Frequency of Vehicle Track System," *Journal of Mechanical Engineering*, vol. 55, no. 8, pp. 118 - 127, April 2019.
- [38] D. J. Fourie, Master's thesis: Mechanism Influencing Railway Wheel Squeal in Large Radius Curves, Johannesburg: UJContent, 2011.
- [39] D. J. Thompson, In Chapter 1: Railway Noise and Vibration Handbook: Mechanisms, Modelling and Means of Control, Southampton: Elsevier, 2009.
- [40] P. T. Torstensson, Doctoral Thesis: Rail Corrugation Growth on Curves, Goteborg, Sweden: Chalmers Reproservice, 2012.
- [41] Z. Li, "Squats on Railway Rails," in *Wheel–Rail Interface Handbook*, Cambridge, England, Woodhead Publishing Limited, 2009, pp. 819 - 842.
- [42] G. Kouroussis, D. P. Connolly and O. Verlinden, "Railway-induced ground vibrations – a review of vehicle effects," *International Journal of Rail Transportation*, vol. 2, no. 2, pp. 69 - 110, 2014.
- [43] W. Li, J. Jiang, R. Dwight and C. Schulten, "An investigation of a Method for Track Decay Rate Measurement Using Train Pass-bys," in *Proceedings of ACOUSTICS 2011*, Gold Coast, Australia, 2 - 4 November 2011.
- [44] S. Kaewunruen and A. M. Remennikov, "Field Trials for Dynamic Characteristics of Railway Track and Its Components Using Impact Excitation Technique," *NDT&E International*, vol. 40, no. 7, pp. 510 - 519, 2007.
- [45] S. Kaewunruen and A. Remennikov, Dynamic Properties of Railway Track and Its Components : a State-of-the-Art Review, Wollongong, Australia: DOI: <https://ro.uow.edu.au/engpapers/493>, 2008.
- [46] A. P. de Man, "Pin-Pin Resonance as a Reference in Determining Ballasted Railway Track Vibration Behaviour," *HERON*, vol. 45, no. 1, 2000.
- [47] A. S. J. Suiker, Doctoral Thesis: The Mechanical Behaviour of Ballasted Railway Tracks, Delft, Netherlands: DUP Science: an imprint of Delft University Press, June 2002.
- [48] S. Offenbacher, J. Neuhold, P. Veit and M. Landgraf, "Analyzing Major Track Quality Indices and Introducing a Universally Applicable TQI," *Applied Sciences (MDPI)*, vol. 10, no. 8490, ; doi:10.3390/app10238490, p. 16, November 2020.
- [49] A. Falamarzi, S. Moridpour, N. Majidreza and S. Cheraghi, "Prediction of Tram Track Gauge Deviation Using Artificial Neural Network and Support Vector

- Regression,” *Australian Journal of Civil Engineering*, vol. 17, no. 1, pp. 63 - 71, 2019.
- [50] W. J. T. Daniel, R. J. Horwood, P. A. Meehan and N. Wheatley, “Wear-Type Rail Corrugation Prediction: Field Study,” in *Conference on Railway Engineering*, Melbourne. 30 April - 03 May , 2006.
- [51] I. Gómez and E. G. Vadillo, “An analytical Approach to Study a Special Case of Booted Sleeper Track Rail Corrugation,” *Wear*, vol. 251, no. 1, pp. 916 - 924, 2001.
- [52] M. Ishida , T. Moto and M. Takikawa, “The Effect of Lateral Creepage Force on Rail Corrugation on Low Rail at Sharp Curves,” *Wear*, vol. 253, no. 1 - 2, pp. 172 - 177, 2002.
- [53] L. Afferrante and M. Ciavarella, “CORRUGATION MODELS AND THE ROARING RAILS ENIGMA: A SIMPLE ANALYTICAL CONTACT MECHANICS MODEL BASED ON A PERTURBATION OF CARTER’S SOLUTION,” *Journal of Mechanics of Materials and Structures*, vol. 4, no. 2, pp. DOI: <https://msp.org/jomms/2009/4-2/jomms-v4-n2-p02-p.pdf>, 2009.
- [54] Z. Wen, X. Jin, X. Xiao and Z. Zhou, “Effect of a Scratch on Curved Rail on Initiation and Evolution of Plastic Deformation Induced rail Corrugation,” *International Journal of Solids and Structures*, vol. 45, no. 2008, p. 2077 – 2096, 2007.
- [55] K. Giannakos, “Modeling the Influence of Short Wavelength Defects in a Railway Track on the Dynamic Behavior of the Non-Suspended Masses,” *Mechanical Systems and Signal Processing*, Vols. 68 - 69, pp. 68 - 83, 2016.
- [56] Z. Wei, A. Nunez, Z. Li and R. Dollevoet, “Evaluating Degradation at Railway Crossings Using Axle Box Acceleration Measurements,” *Special Issue: Sensors for Transportation* , vol. 17, no. 10, p. <https://doi.org/10.3390/s17102236>, 2017.
- [57] P. A. Meehan, R. D. Batten and P. A. Bellette, “The Effect of Non-Uniform Train Speed Distribution on Rail Corrugation Growth in Curves/Corners,” *Wear*, vol. 366 – 367, no. <https://doi.org/10.1016/j.wear.2016.05.009>, pp. 27-37, 2016.
- [58] X. S. Jin, Z. F. Wen and K. Y. Wang, “Effect of Track Irregularities on Initiation and Evolution of Rail Corrugation,” *Journal of Sound and Vibration*, vol. 285, no. 2005, pp. 121 - 148, 2005.
- [59] R. Pan, X. Zhao, P. Liu and R. Ren, “Micro-mechanism of Polygonization Wear on Railroad Wheels,” *Wear*, Vols. 392 - 393, pp. 213 - 220, 2017.
- [60] W. Cai, M. Chi, P. Shackleton , D. Crosbee and Y. Zhao, “Experimental and Numerical Investigation into Formation of Metro Wheel Polygonalization,” *Shock and Vibration* , vol. 2019, no. Article ID 1538273, p. <https://doi.org/10.1155/2019/1538273>, 2019.

- [61] A. Johansson, Doctoral Thesis: Out-of-Round Railway Wheels - Causes and Consequences an Investigation Including Field Tests, Out-of-Roundness Measurements and Numerical Simulations, Chalmers, Sweden, 2005.
- [62] Y. Q. Sun, M. Spiryagin, Q. Wu, C. Cole and W. H. Ma, "Feasibility in Assessing the Dipped Rail Joint Defects Through Dynamic Response of Heavyhaul Locomotive," *Journal of Modern Transportation*, vol. 26, no. 2018, pp. 96 - 106, 2018.
- [63] Y. K. Al-Douri, P. Tretten and R. Karim, "Improvement of Railway Performance: A Study of Swedish Railway Infrastructure," *Journal of Modern Transportation*, vol. 24, no. 2016, pp. 22 - 37, 2016.
- [64] NeTIRail, "Needs Tailored Interoperable Railway Infrastructure (NeTIRail) Project," 16 May 2018. [Online]. Available: [http://netirail.eu/IMG/pdf/netirail\\_d26\\_tailoring\\_track\\_to\\_avoid\\_corrugations.pdf](http://netirail.eu/IMG/pdf/netirail_d26_tailoring_track_to_avoid_corrugations.pdf). [Accessed 14 October 2019].
- [65] I. Arai, Y. Kawano, S. Watanabe, N. Kemmotsu and N. Kubo, "Observation of Inner Rail Characteristics in Terms of Corrugation Focused on rail Fastening Device of the Track Structure," *11th International Conference on Contact Mechanics and Wear of Rail/Wheel Systems*, pp. 50 - 55, 24 - 27 September 2018.
- [66] F. Duan, Doctoral Thesis, Numerical Tribology of the Wheel-Rail Contact: Application to Corrugation Defect, Lyon, France: <http://theses.insa-lyon.fr/publication/2015ISAL0019/these.pdf>, 2015.
- [67] B. W. Wu, G. X. Chen, J. Z. Lv, Q. Zhu and X. Kang, "Generation Mechanism and Remedy Method of Rail Corrugation at a Sharp Curved Metro Track with Vanguard Fasteners," *Journal of Low Frequency Noise, Vibration and Active Control*, vol. 39, no. 2, pp. 368 - 381, 2019.
- [68] X. Jin and Z. Wen, "Rail Corrugation Formation Studied With a Full-Scale Test Facility and Numerical Analysis," *Part J: Engineering Tribology*, vol. 221, pp. 675 - 698, 2007.
- [69] G. Fang, Y. Wang, Z. Peng and T. Wu, "Theoretical Investigation Into the Formation Mechanism and Mitigation Measures of Short Pitch Rail Corrugation in Resilient Tracks of Metros," *Part F: Journal of Rail and Rapid Transit*, vol. 232, no. 9, p. <https://doi.org/10.1177/0954409718769750>, 2018.
- [70] Z. Wang, Z. Lei, Y. Zhao and Y. Xu, "Rail Corrugation Characteristics of Cologne Egg Fastener Section in Small Radius Curve," *Shock and Vibration*, vol. 2020, no. <https://doi.org/10.1155/2020/1827053>, p. Article ID 1827053, 2020.
- [71] X. Cui, B. Huang, Z. Du, H. Yang and G. Jiang, "Study on the Mechanism of the Abnormal Phenomenon of Rail Corrugation in the Curve Interval of a Mountain City Metro," *Tribology Transactions*, vol. 63, no. 6, pp. 996-1007, 2020.

- [72] L. Chiacchiari and G. Loprencipe, "Measurement Methods and Analysis Tools for Rail Irregularities: A Case Study for Urban Tram Track," *Journal of Modern Transportation*, vol. 23, no. https://doi.org/10.1007/s40534-015-0070-6, pp. 137 - 147, 2015.
- [73] X. Jin, Z. Wen, K. Wang and X. Xiao, "Effect of Passenger Car Curving on Rail Corrugation at a Curved Track," *Wear*, vol. 260, no. 6, pp. 619 - 633, 2006.
- [74] A. K. Ng, L. Martua and G. Sun, "Influence of Sleeper Distance on Rail Corrugation Growth," *International Conference on Intelligent Rail Transportation (ICIRT)*, pp. 1 - 5, 12 - 14 December 2018.
- [75] G. X. Chen, W. J. Qian, J. L. Mo and M. H. Zhu, "Effect of the Rail Support Stiffness on the Occurrence Propensity of Rail Corrugation Based on the Self-excited Vibration of a Wheel-Rail System," *Vibration Engineering and Technology of Machinery*, vol. 23, no. DOI: https://0-doi-org.ujlink.uj.ac.za/10.1007/978-3-319-09918-7\_96, pp. 1083 - 1090, 2015.
- [76] A. Wang, Z. Wang, Z. Zhang, N. Xu, X. Qiao and M. Du, "Effects of Rail Lateral Dynamic Deflection and Vibration Level on Rail Corrugation Development," *Noise and Vibration Mitigation for Rail Transportation Systems*, vol. 139, no. https://0-doi-org.ujlink.uj.ac.za/10.1007/978-3-319-73411-8\_26, pp. 355 - 366, 2018.
- [77] X. Jin, X. Xiao, Z. Wen and Z. Zhou, "Effect of Sleeper Pitch on Rail Corrugation at a Tangent Track in Vehicle Hunting," *Wear*, vol. 265, no. 2008, p. 1163 - 1175, 2008.
- [78] Y. Q. Sun and S. Simson, "Nonlinear Three-Dimensional Wagon-Track Model For the Investigation of Rail Corrugation Initiation on Curved Track," *Vehicle System Dynamics*, vol. 45, no. 2, pp. 113 - 132, 2007.
- [79] Y. Q. Sun and M. Dhanasekar, "A Three-Dimensional Model for the Lateral and Vertical Dynamics of Wagon-Track Systems," *Part F: Journal of Rail and Rapid Transit*, vol. 217, no. 1, pp. 31 - 45, 2003.
- [80] H. Xiao, S. Yang, H. Wang and S. X. Wu, "Initiation and Development of Rail Corrugation Based on Track Vibration in Metro Systems," *Part F: Journal of Rail and Rapid Transit*, vol. 232, no. 9, pp. 2228 - 2243, 2018.
- [81] L. Zheng, J. Yang, Y. Sun and S. Zhu, "Analysis on Limiting Value of Rail Corrugation of Floating-Slab Track Based on Wheel/Rail Multi-Point Contact," *Chinese Science Bulletin*, vol. 64, no. 25, pp. 2590 - 2599, 2019.
- [82] J. I. Real-Herraiz, S. Morales-Ivorra, C. Z. Martin and S. B. Vicente, "Analysis of Vibrations Generated by the Presence of Corrugation in a Modeled Tram Track," *Mathematical Problems in Engineering*, vol. 2015, no. https://doi.org/10.1155/2015/290164, p. Article ID 290164, 2018.



- [83] X. Jia, G. Li, X. Liu and P. Chen, "Research on the Relationship Between the Rail Corrugation and the Vibration Response of the Wheel-Rail System," *2019 8th International Conference on Transportation and Traffic Engineering (ICTTE 2019)*, vol. 02002, no. 308, p. <https://doi.org/10.1051/mateconf/202030802002>, 2020.
- [84] W. Li, H. Wang, Z. Wen, X. Du, L. Wu, X. Li and X. Jin, "An Investigation Into the Mechanism of Metro Rail Corrugation Using Experimental and Theoretical Methods," *Part F: Journal of Rail and Rapid Transit*, vol. 230, pp. 1025 - 1039, 2015.
- [85] Z. Lei and Z. Wang , "Generation Mechanism and Development Characteristics of Rail Corrugation of Cologne Egg Fastener Track in Metro," *KSCE Journal of Civil Engineering* , vol. 24, no. 2020, p. 1763–1774, 2020.
- [86] X. Yin and X. Wei, "Development Characteristics of Inner Rail Corrugation in Small Radius Curve of Metro," *IOP Conference Series: Earth and Environmental Science*, vol. 587, no. 012077, pp. doi:10.1088/1755-1315/587/1/012077, 2020.
- [87] H. Zhang, W. Liu and J. Chen, "Track Dynamic Dehaviour at High Frequencies: Mechanism of Rail Corrugation at Egg Fastening System Sections on Beijing Metro," in *10th International Conference on Contact Mechanics of Wheel / Rail Systems*, heyenne Mountain Resort ,Colorado, Springs, United States, 2015.
- [88] H. Zhang, W. Liu, W. Liu and Z. Wu, "Study on the cause and treatment of rail corrugation for Beijing metro," *Wear*, vol. 317, no. 1 - 2, pp. 120 - 128, 2014.
- [89] J. I. Real, A. Galisteo, T. Asensio and L. Montalbán, "Study of Railway Ground Vibrations Caused by Rail Corrugation and Wheel Flat," *Journal of Vibroengineering*, vol. 14, no. 4, pp. 1724 - 1733, 2012.
- [90] S. Kaewunruen and A. M. Remennikov, "Current State of Practice in Railway Track Vibration Isolation: an Australian Overview," *Australian Journal of Civil Engineering*, vol. 14, no. 1, pp. 63 - 71, 2016.
- [91] C. Zhao, P. Wang and M. Xing, "Research on the Matching of Fastener Stiffness Based on Wheel-Rail Contact Mechanism for Prevention of Rail Corrugation," *Mathematical Problems in Engineering*, vol. 2017, no. Article ID 6748160, p. <https://doi.org/10.1155/2017/6748160>, 2017.
- [92] L. Liang, L. Wei, F. Elbert, W. Lei, W. Zefeng and J. Xuesong, "Investigation into the Vibration of Metro Bogies Induced by Rail Corrugation," *Chinese Journal of Mechanical Engineering*, vol. 30, no. 1, pp. 93 - 102, 2017.
- [93] X. S. Jin, Z. F. Wen, K. Y. Wang, Z. R. Zhou, Q. Y. Liu and C. H. Li, "Three-Dimensional Train-Track Model of Study of Rail Corrugation," *Journal of Sound and Vibration* , vol. 293, no. 2006, pp. 830 - 855, 2006.
- [94] X. Zhou, X. Zhao, B. Wu, Y. Zhao and X. Jin, "Influence of Resilient Wheel on Dynamic Characteristics of Metro Wheel/Rail System Under Rail Corrugation

- Excitation,” *Proceedings of the 11th International Conference on Contact Mechanics and Wear of Rail/wheel Systems*, pp. 1206 - 1212, 24 - 27 September 2018.
- [95] S. Bionda, M. Bocciolone, A. Collina, R. Corradi, E. Di Gialleonardo and G. Diana, “Numerical and Experimental Analysis on the Corrugation Caused by a Vehicle Equipped with Resilient Wheels,” *25th Symposium of the International Association of Vehicle System Dynamics (IAVSD)*, pp. 1135 - 1140, 14 - 18 August 2018.
- [96] C. Andersson and A. Johansson, “Prediction of Rail Corrugation Generated by Three-Dimensional Wheel–Rail Interaction,” *Wear*, vol. 257, no. 3 - 4, pp. 423 - 434, 2004.
- [97] Y. Wang and T. X. Wu, “The Growth and Mitigation of Rail Corrugation due to Vibrational Interference Between Moving Wheels and Resilient Track,” *Vehicle System Dynamics*, vol. 58, no. 8, pp. 1257 - 1284, 2020.
- [98] B. W. Wu, G. X. Chen, X. Kang and Q. Zhu, “Study on the Origin of Rail Corrugation at a Long Downhill Braking Section Based on Friction-Excited Oscillation,” *Journal of Tribology Transactions*, vol. 63, no. 3, pp. 439 - 452, 2020.
- [99] W. Wang, J. Bai, S. Wu, J. Zheng and P. Zhou, “Experimental Investigations on the Effects of Fatigue Crack in Urban Metro Welded Bogie Frame,” *Applied Sciences*, vol. 10, no. 1537, pp. DOI: <https://www.mdpi.com/2076-3417/10/4/1537/pdf>, 2020.
- [100] L. Baeza, P. Vila, A. Roda and J. Fayos , “Prediction of Corrugation in Rails using a Non-stationary Wheel-Rail Contact Model,” *Wear*, pp. 1156 - 1162, 2008.
- [101] S. Li, Z. Li, A. Nunez and R. Dollevoet, “New Insights into the Short Pitch Corrugation Enigma Based on 3D-FE Coupled Dynamic Vehicle-Track Modeling of Frictional Rolling Contact,” *Applied Sciences*, vol. doi:10.3390/app7080807, no. 807, 2017.
- [102] C. Collette and A. Preumont, “Laser Measurement of Torsional Vibrations/Longitudinal Creepage of a Railway Wheelset on a Scaled Test Bench,” *Optics and Laser in Engineering*, vol. 47, no. 3 - 4, pp. 385 - 389, 2009.
- [103] B. Balekwa, D. Kallon, A. Mashamba and P. Dube, “Application of Modal Analysis to Establish the Wavelength Fixing Mechanism for Rail Corrugation,” *Proceedings of the 11th South African Conference of Computational and Applied Mechanics (SACAM)*, pp. 212 - 223, 2018.
- [104] J. Zeng, L. Wei and P. Wu, “Safety Evaluation for Railway Vehicles Using an Improved Indirect Measurement Method of Wheel–Rail Forces,” *Journal of Modern Transportation*, vol. 24, no. 2016, pp. 114 - 123, 2016.
- [105] A. Wang, Z. Wang, Z. Zhao, Y. Zhang, Y. Duan , T. Lei and M. Du, “Effects of Track Stiffness and Tuned Rail Damper on Rail Roughness Growth and Rail Vibration Levels on Metro System.,” *Noise and Vibration Mitigation for Rail Transportation Systems*, pp. 667 - 674, 2015.

- [106] D. J. Thompson, In Chapter 3: Railway Noise and Vibration Handbook: Mechanisms, Modelling and Means of Control, Southampton: Elsevier, 2009.
- [107] X. Sheng, "Generalization of the Fourier Transform-Based Method for Calculating the Response of a Periodic Railway Track Subject to a Moving Harmonic Load," *Journal of Modern Transportation*, vol. 23, no. 2015, pp. 12 - 29, 2015.
- [108] S. Skorsetz, T. Strobel, D. C. Alcocer and C. Salander, "Influence of Rail cCorrugation on Light Rail Vehicles in Terms of Ride Quality and Safety," *11th International Conference on Contact Mechanics and Wear of Rail/Wheel Systems*, pp. 896 - 901, 24 - 27 September 2018.
- [109] A. P. de Man, "Pin-pin Resonance as a Referrence in Determining Ballasted Railway Track Vibration Behaviour," *HERON*, vol. 45, no. 1, 2000.
- [110] M. Yu, W.-d. Wang, J.-z. Liu and S.-c. Sun, "The Transient Response of high-Speed Wheel/Rail Rolling Contact on "Roaring Rails" Corrugation," *Part F: Journal of Rail and Rapid Transit*, vol. 233, no. 10, p. <https://doi.org/10.1177/0954409719825682>, 2019.
- [111] B. Balekwa, D. V. V. Kallon and D. J. Fourie, "Vibration Response for class D44 and D39 200 Locomotive Wheelsets due to Dynamic Loads Excitation," *Proceedings of OIC 2019*, pp. 418 - 421, 2 - 4 October 2019.
- [112] L. Auersch, "The Excitation of Ground Vibration by Rail Traffic: Theory of Vehicle–Track–Soil Interaction and Measurements on High-Speed Lines," *Sound and Vibration*, vol. 284, no. 1 - 2, pp. 103 - 132, 2005.
- [113] N. Correa, E. Vadillo, J. Santamaria and J. Herreros, "A Versatile Method in the Space Domain to Study Short-Wave Rail Undulatory Wear Caused by Rail Surface Defects," *Wear*, Vols. 352 - 353, no. <https://doi.org/10.1016/j.wear.2016.02.012>, pp. 196 - 208, 2016.
- [114] G. Xie and S. D. Iwnicki, "Calculation of Wear on a Corrugated Rail using a Threedimensional Contact Model," *Wear* 265, no. 9 - 10, pp. 1238 - 1248, 2008.
- [115] G. Xie and S. D. Iwnicki, "A Rail Roughness Growth Model for a Wheelset with Nonsteady non-Hertzian Contact," *Vehicle System Dynamics*. DOI: [10.1080/00423110903410518](https://doi.org/10.1080/00423110903410518), 2010.
- [116] J. Piotrowski and W. Kik, "A Simplified Model of Wheel/Rail Contact Mechanics for non-Hertzian Problems and Its Application in Rail Vehicle Dynamics Simulations," *Vehicle System Dynamics*, vol. 46, no. 1, pp. 27 - 48, 2008.
- [117] P. A. Bellette, P. A. Meehan and W. J. T. Daniel, "Contact Induced Wear Filtering and Its Influence on Corrugation Growth," *Wear* 268, no. 11 - 12, pp. 1320 - 1328, 2010.



- [118] P. T. Torstensson and J. C. O. Nielsen, "Monitoring of Rail Corrugation Growth due to Irregular Wear on a Railway Metro Curve," *Wear* 267, no. 1 - 4, pp. 556 - 561, 2009.
- [119] X. S. Jin and Z. F. Wen, "Effect of Discrete Track Support by Sleepers on Rail Corrugation at a Curved Track," *Sound and Vibration*, no. 1 - 2, pp. 279 - 300, 2008.
- [120] E. G. Vadillo, J. A. Tarrago, G. Garate and C. Angulo, "Effect of Sleeper distance on Rail Corrugation," *Wear* 217, pp. 140 - 146, 1998.
- [121] T. X. Wu and D. J. Thompson, "An Investigation into Rail Corrugation due to Microslip under Multiple Wheel-Rail Interactions," *Wear* 258, no. 7 - 8, pp. 1115 - 1125, 2005.
- [122] T. X. Wu and D. J. Thompson, "Behaviour of the Normal Contact Force under Multiple Wheel-Rail Interaction," *Veh. Sys. Dyn. International Journal of Vehicle Mechanics and Mobility*, vol. 37, no. 3, pp. 157 - 174, 2002.
- [123] K. H. Oostermeijer, "Review on Short Pitch Rail Corrugation Studies," *Wear* 265, vol. 265, no. 9 - 10, pp. 1231 - 1237, 2008.
- [124] Y. Sato, A. Matsumoto and K. Knothe, "Review on Rail Corrugation Studies," *Wear*, vol. 253, no. 1 - 2, pp. 130 - 139, July 2002.
- [125] S. L. Grässie, R. W. Gregory and J. L. Johnson, "The Behaviour of Railway Wheelsets and Track at High Frequencies of Excitation," *Mechanical Engineering Science*, vol. 24, no. 2, pp. 103-111, 1982.
- [126] P. T. Torstensson and J. C. O. Nielsen, "Rail Corrugation Growth on Curves - Measurements, Modelling and Mitigation," *Noise and Vibration Mitigation for Rail Transportation Systems*, pp. 659 - 666, 2015.
- [127] X. L. Cui, G. X. Chen, B. W. Wu, W. Y. Yan and H. Ouyang, "Effects of Track Radius on Rail Corrugation," in *Dynamics of Vehicles on Roads and Tracks, Vol 2*, London, Taylor and Francis Group, 2017.
- [128] M. R. Aalami, A. Anari, T. Shafighfard and S. Talatahari, "A Robust Finite Element Analysis of the Rail-Wheel Rolling Contact," *Advances in Mechanical Engineering*, p. DOI: 10.1155/2013/272350, 2013.
- [129] A. Ekberg, E. Kabo, J. C. Nielsen and R. Lunder, "Subsurface Initiated Rolling Contact Fatigue of Railway Wheels as Generated by Rail Corrugation," *Journal of Solids and Structures*, vol. 44, pp. 7975-7987, 2007.
- [130] A. Bohmer and T. Klimpel, "Plastic Deformation of Corrugated – a Numerical Approach Using Material Data of Rail Steel," *Wear*, no. 253, pp. 150 - 161, 2002.
- [131] X. Li, X. Zhang, J. Zhang, J. Zhang, Z. Wen and X. Jin, "A Theoretical Model of Rail Corrugation on a Slab Track," *The Fifth International Conference on*

*Transportation Engineering*, p. DOI:  
<https://ascelibrary.org/doi/abs/10.1061/9780784479384.150>, 2015.

- [132] S. Morales-Ivorra, J. I. Real, C. Hernandez and L. Montalban, "Derailment Risk and Dynamics of Railway Vehicles in Curved Tracks: Analysis of the Effect of Failed Fasteners," *Journal of Modern Transportation*, vol. 24, no. 2016, pp. 38 - 47, 2016.
- [133] X. L. Cui, G. X. Chen, H. G. Yang, H. Ouyang, J. L. Mo and M. H. Zhu, "Study on Rail Corrugation on a Sharp Curved Track Supported by Different Types of Sleepers," in *10th International Conference on Contact Mechanics of Wheel / Rail Systems*, Cheyenne Mountain Resort, Colorado, Springs, United States, 2015.
- [134] X. Cui, G. Chen, H. Yang, H. Ouyang and W. Yan, "A Case Study of Rail Corrugation Phenomenon Based on the Viewpoint of Friction-Induced Oscillation of a Wheelset-Track System," *Journal of Vibroengineering*, vol. 19, no. 6, pp. 4516 - 4530, 2017.
- [135] . X. Gao, A. Wang, X. Gu and . W. Li, "Impact of Dynamic Characteristics of Wheel-Rail Coupling on Rail Corrugation," *SAE International Journal of Vehicle Dynamics, Stability, and NVH*, vol. 3, no. 2, pp. 131 - 141, 2019.
- [136] W. Li, Q. Zhu, Z. Wen and X. Jin, "Study on Short-Pitch Rail Corrugation in Metro Tracks with a Resilient Fastener," *Proceedings of the 11th International Conference on Contact Mechanics and Wear of Rail/wheel Systems*, pp. 550 - 558, 24 - 27 September 2018.
- [137] G. X. Chen, X. Zhang, B. W. Wu, X. N. Zhao, Z. F. Wen, H. Ouyang and M. H. Zhu, "Field Measurement and Model Prediction of Rail Corrugation," *Proceedings of the Institution of Mechanical Engineers*, p. <https://doi.org/10.1177/0954409719877318>, October 2019.
- [138] A. Carlberger, P. T. Torstensson, J. C. Nielsen and A. Frid, "An Iterative methodology for the prediction of Dynamic Vehicle–Track Interaction and Long-Term Periodic Rail Wear," *Part F: Journal of Rail and Rapid Transit*, vol. 232, no. 6, p. <https://doi.org/10.1177/0954409717747127>, 2018.
- [139] P. T. Torstensson and J. C. O. Nielsen, "Rail Corrugation Growth on Curves – Measurements, Modelling and Mitigation," *Noise and Vibration Mitigation for Rail Transportation Systems*, vol. 126, no. DOI: [https://doi.org/10.1007/978-3-662-44832-8\\_78](https://doi.org/10.1007/978-3-662-44832-8_78), pp. 659 - 666, 2015.
- [140] A. Saulot, S. Descartes, D. Desmyter, D. Levyc and Y. Berthier, "A Tribological Characterization of the "Damage Mechanism" of Low Rail Corrugation on Sharp Curved Track," *Wear*, vol. 260, no. 2006, pp. 984 - 995, 2006.
- [141] X. L. Cui, G. X. Chen, J. W. Zhao, W. Y. Yan, H. Ouyang and M. H. Zhu, "Field Investigation and Numerical Study of the Rail Corrugation Caused by Frictional Self-Excited Vibration," *Wear*, pp. 1919 - 1929, 2017.

- [142] B. W. Wu, G. X. Chen, J. Z. Lv, Q. Zhu, X. N. Zhao and X. Kang, "Effect of the Axlebox Arrangement of the Bogie and the Primary Suspension Parameters on the Rail Corrugation at the Sharp Curve Metro Track," *Wear*, Vols. 426 - 427, no. Part B, pp. 1828 - 1836, 2019.
- [143] O. El Beshbichi, C. Wan, S. Bruni and E. Kassa, "Complex Eigenvalue Analysis and Parameters Analysis to Investigate the Formation of Railhead Corrugation in Sharp Curves," *Wear*, Vols. 450 - 451, no. <https://doi.org/10.1016/j.wear.2019.203150>, 2020.
- [144] P. A. Meehan, W. J. T. Daniel and T. Campey, "Prediction of the Growth of Wear-Type Rail Type Rail Corrugation," *Wear*, vol. 258, no. 7 - 8, pp. 1001-1013, 2005.
- [145] P. A. Bellette, P. A. Meehan and W. J. T. Daniel, "Effects of Variable Pass Speed on Wear-Type Corrugation Growth," *Journal of Sound and Vibration*, vol. 314, no. 3 - 5, pp. 616 - 634, 2008.
- [146] D. Fourie, R. Fröhling and S. Heyns, "Railhead Corrugation Resulting from Mode-Coupling Instability in the Presence of Veering Modes," *Tribology International*, vol. 152, no. 106499, p. DOI: <https://doi.org/10.1016/j.triboint.2020.106499>, 2020.
- [147] P. A. Meehan, P. A. Bellette and R. J. Horwood, "'Does God Play Dice With Corrugations?': Environmental Effects on Growth," *Wear*, vol. 314, no. 1 - 2, pp. 254 - 260, 2014.
- [148] W. P. Hu, P. Wang, G. X. Chen, Y. Hu, X. L. Cui, J. F. Peng and M. H. Zhu, "Experimental Study on Corrugation of a Sliding Surface Caused by Frictional Self-Excited Vibration," *Tribology Transactions*, vol. 59, no. 1, pp. 8 - 16, 2016.
- [149] B. Balekwa, D. V. V. Kallon and D. J. Fourie, "Vertical and Horizontal Vibration Response for Corrugated Track Curves Supported on Steel and PY-Type Concrete Sleepers," *Proceedings of OIC 2019*, pp. 474 - 482, 2-4 October 2019.
- [150] A. P. de Man and C. Esveld, "Recording, Estimating and Managing the Dynamic Behaviour of Railway Structures," *International Conference on Modal Analysis Noise and Vibration*, pp. 1 - 6, Sep 2000.
- [151] O. A. Garcia, Masters Dissertation: Numerical and Experimental Analysis of the Vertical Dynamic Behaviour of a Railway Track, Delft, Netherlands: Delft University of Technology, 24 April, 2014.
- [152] W. Liu, H. Zhang, W. Liu and J. Thompson, "Experimental Study of the Treatment Measures for Rail Corrugation on Tracks with Egg Fasteners in the Beijing Metro," *Proceedings of the Institution of Mechanical Engineers, Part F: Journal of Rail and Rapid Transit*, p. DOI: [10.1177/0954409717721635](https://doi.org/10.1177/0954409717721635), 2017.
- [153] Z. Wei, Z. Li, Z. Qian, R. Chen and R. Dollevoet, "An Investigation Into the Vertical Dynamics of Tracks With Monoblock Sleepers With a 3D Finite-Element Model," *Part F: Journal of Rail and Rapid Transit*, vol. 4, pp. 20 - 36, 2015.

- [154] M. Oregui, A. Nunez, R. Dollevoet and Z. Li, "Sensitivity Analysis of Railpad Parameters on Vertical Railway Track Dynamics," *Journal of Engineering Mechanics*, vol. 143, no. 5, p. 04017011, 2017.
- [155] L. Weifeng, L. Weining, W. Zongzhen and Z. Hougui, "Test Study on Treating Rail Corrugation for Egg Fastener in Beijing Metro," *Journal of Mechanical Engineering*, vol. 2015, no. 21, pp. DOI: [http://en.cnki.com.cn/Article\\_en/CJFDTotal-JXXB201521010.htm](http://en.cnki.com.cn/Article_en/CJFDTotal-JXXB201521010.htm), 2015.
- [156] B. W. Wu, G. X. Chen, X. N. Zhao, J. Z. Lv, Q. Zhu, X. Kang and H. Ouyang, "Formation Mechanism and Countermeasures of Rail Corrugation at a Tight Curved Metro Track with Vanguard Fasteners," *Proceedings of the 11th International Conference on Contact Mechanics and Wear of Rail/wheel Systems*, pp. 1107 - 1113, 24 - 27 September 2018.
- [157] X. Song, Y. Qian, K. Wang and P. Liu, "Effect of Rail Pad Stiffness on Vehicle–Track Dynamic Interaction Excited by Rail Corrugation in Metro," *Journal of the Transportation Research Board*, vol. 2674, no. 6, pp. 225 - 243, 2020.
- [158] M.-C. Kim, W.-H. You and H.-B. Sim, "Rail Corrugation Effects on the Dynamic Behavior of Clips of Rail Fastening System in Operation Environment of Urban Railway," *Journal of the Korean society for railway*, vol. 4, no. 19, pp. 489 - 497, 2016.
- [159] H. Ilias, "THE INFLUENCE OF RAILPAD STIFFNESS ON WHEELSET/TRACK INTERACTION AND CORRUGATION GROWTH," *Journal of Sound and Vibration*, vol. 227, no. 5, pp. 935 - 948, 1999.
- [160] R. D. Batten, P. A. Bellette, P. A. Mehaan, R. J. Horwood and W. J. T. Daniel, "Field and Theoretical Investigation of the Mechanism of Corrugation Wavelength Fixation Under Speed Variation," *Wear* 271, no. 1 - 2, p. DOI: 10.1016/j.wear.2010.10.027, May 2011.
- [161] A. K. Ng, Z. Bin Alias, J. -F. Chassin and J. H. Yebra, "Managing Rail Corrugation Through Modelling, Simulation, and Instrumentation Technologies," *2016 IEEE International Conference on Intelligent Rail Transportation (ICIRT)*, pp. 307 - 314, 23 - 25 August 2016.
- [162] D. Wei, X. Wei, Y. Liu, L. Jia and W. Zhang, "The Identification and Assessment of Rail Corrugation Based on Computer Vision," *Applied Sciences*, vol. 9, no. 18, p. <https://doi.org/10.3390/app9183913>, 2019.
- [163] K. Alten and A. Fuchs, "Detecting and Classifying Rail Corrugation Based on Axle Bearing Vibration," *International Conference on Acoustics, Speech and Signal Processing (ICASSP)*, vol. DOI: 10.1109/ICASSP.2019.8683317, 12 - 17 May 2019.
- [164] S. Kaewunruen and M. Stephen, "Severity and Growth Evaluation of Rail Corrugations on Sharp Curves Using Wheel/Rail Interaction," *Paper presented at*

2015 National Convention in Civil Engineering, Pattaya, Thailand, pp. 1 - 10, 8 - 10  
July 2015.

- [165] S. L. Grässie, M. J. Saxon and J. D. Smith, "MEASUREMENT OF LONGITUDINAL RAIL IRREGULARITIES AND CRITERIA FOR ACCEPTABLE GRINDING," *Journal of Sound and Vibration*, vol. 227, no. 5, pp. 949 - 964, 1999.
- [166] C. Dong, Q. Mao, X. Ren, D. Kou, J. Qin and W. Hu, "Algorithms and Instrument for Rapid Detection of Rail Surface Defects and Vertical Short-Wave Irregularities Based on FOG and Odometer," *IEEE Access*, vol. 7, no. doi: 10.1109/ACCESS.2019.2903488, pp. 31558 - 31572, 2019.
- [167] H. Tanaka and A. Shimizu, "Practical Application of Portable Trolley for the Continuous Measurement of Rail Surface Roughness for Rail Corrugation Maintenance," *Quarterly Report of RTRI*, vol. 57, no. 2, pp. 118 - 124, 2016.
- [168] W. Jeong and D. Jeong, "Acoustic Roughness Measurement of Railhead Surface Using an Optimal Sensor Batch Algorithm," *Applied Sciences*, vol. 10, no. 2110, p. <http://dx.doi.org/10.3390/app10062110>, 2020.
- [169] J. I. Real, C. Zamorano, J. L. Velarte and A. E. Blanco, "Development of a Vehicle–Track Interaction Model Topredict the Vibratory Benefits of Rail Grinding In the Time Domain," *Journal of Modern Transportation*, vol. 23, no. 2015, pp. 189 - 201, 2015.
- [170] Q. Li, H. Zhang, S. Ren, P. Dai and W. Li, "Detection Method for Rail Corrugation Based on Rail Image Feature in Frequency Domain," *China Railway Science*, Vols. DOI: 10.3969/j.issn.1001-4632.2016.01.04, pp. 24 - 30, 2016.
- [171] Q. Li, Z. Shi, H. Zhang, Y. Tan, S. Ren, P. Dai and W. Li, "A Cyber-Enabled Visual Inspection System for Rail Corrugation," *Future Generation Computer Systems*, vol. 79, no. 1, pp. 374 - 382, 2018.
- [172] K. Lang, Z. Xing, W. Dong and X. Gao, "A Rail Corrugation Detection Method Based on Wavelet Packet Energy Entropy," *Proceedings of the 3rd International Conference on Electrical and Information Technologies for Rail Transportation (EITRT)*, pp. 205 - 214, doi-org.ujlink.uj.ac.za/10.1007/978-981-10-7989-4\_21 2018.
- [173] B. C. Goo and J. C. Kim, "Complex Eigenvalue Analysis of Railway Wheel/Rail Squeal," *International Journal of Engineering, Science and Technology*, vol. 8, no. 1, pp. 1 - 12, 2016.
- [174] I. C. Cruceanu and S. Soroohan, "Determination of the Harmonic Response of a Railway Wheelset using the Finite Element Analysis Method," *Procedia Manufacturing*, vol. 46, no. 2020, pp. 173 - 179, 2020.



- [175] P. Gao, Y. C. Du, Y. Wang and Y. Lv, "Study on Repeated-Root Modes in Substructure Modal Composition Analysis," *SAE International Journal of Passenger Cars - Mechanical Systems*, vol. 9, no. 1, pp. 160 - 166, 2016.
- [176] A. Wang, Y. Li, Z. Zhang, Z. Wang, G. Dong and J. Liu, "Effects of Tuned Slab Damper on Low Frequency Ground Vibration Levels on Metro Systems," *Noise and Vibration Mitigation for Rail Transportation Systems*, pp. 533 - 545, 2018.
- [177] A. R. Valdivia, "A Linear Dynamic Wear Model to Explain the Initiating Mechanism for Corrugation," *Vehicle System Dynamics*, no. 17, pp. 493 - 496, 1998.
- [178] E. Tassilly and N. Vincent , "A Linear Model for the Corrugation of Rails," *Journal of Sound and Vibration*, no. 150, pp. 25 - 45, 1991.
- [179] S. A. Muller, "A Linear Wheel-Rail Model to Investigate Stability and Corrugation on Straight Track," *Wear*, no. 243, pp. 122 - 132, 2000.
- [180] A. Igeland and H. Ilias, "Rail Head Corrugation Growth Predictions Based on Non-Linear High Frequency Vehicle/Track Interaction," *Wear*, no. 213, pp. 90 - 97, 1997.
- [181] P. T. Torstensson and J. C. O. Nielsen, "Simulation of Dynamic Vehicle Track Interaction on Small Radius Curves," *Vehicle System Dynamics*, no. 49, pp. 1711 - 1732, 2011.
- [182] X. Sheng, D. J. Thompson, C. J. C. Jones and G. Xie, "Simulations of Roughness Initiated and Growth on Railway Rails," *Journal of Sound and Vibration*, no. 293, pp. 819 - 829, 2006.
- [183] M. Hiensch, J. C. O. Nielson and E. Verheijen, "Rail Corrugation in the Netherlands - Measurements and Simulations," *Wear*, no. 253, pp. 140 - 149, 2002.
- [184] E. Tassilly and N. Vincent , "Rail Corrugations: Analytical Model and Field Tests," *Wear*, no. 144, pp. 163 - 178, 1991.
- [185] P. Vila, J. Fayos and L. Baeza, "Simulation of the Evolution of Rail Corrugation Using a Rotating Flexible Wheelset Model," *Vehicle System Dynamics*, no. 49, pp. 1749 - 1769, 2011.
- [186] L. Baeza, P. Vila, G. Xie and S. D. Iwnicki, "Prediction of Rail Corrugation Using a Rotating Flexible Wheelset Coupled with a Flexible Track Model and a Non-Hertzian/Non-Steady Contact Model," *Journal of Sound and Vibration*, no. 330, pp. 4493 - 4507, 2011.
- [187] S. Q. Liu, "Study on Rail Corrugation on Metro Tracks and Its Suppression," *Railway Signal Communication*, no. 5, pp. 18 - 19, 2014.
- [188] T. X. Wu and Y. R. Wang, "Modeling of Wheel-Track Interaction with Rail Vibration Damper and Its Application for Suppressing Short Pitch Rail Corrugation," *Noise and Vibration Mitigation for Rail Transportation Systems*, pp. 361 - 368, 2015.

- [189] J. Chen, W. Liu and X. Sun, "Effects of Tuned Rail Damper on Track Dynamic Characteristics Optimization," *International Conference on Structural Dynamics*, no. 199, pp. 1616-1622, 2017.
- [190] B. E. Croft, C. J. C. Jones and D. J. Thompson, "Modelling the Effect of Rail Dampers on Wheel-Rail Interaction Forces and Rail Roughness Growth Rates," *Sound and Vibration*, vol. 323, no. 1 - 2, pp. 17 - 32, 2009.
- [191] B. E. Croft, The Development of Rail-Head Acoustic Roughness, Doctoral Thesis: University of Southampton: ePrints Soton, October, 2009.
- [192] L. Liu and W. Shao, "Design and Dynamic Response Analysis of Rail with Constrained Damped Dynamic Vibration Absorber," *Procedia Engineering*, no. 15, pp. 4983-4987, 2011.
- [193] M. Torward and D. Thompson, "Laboratory Methods for Testing the Performance of Acoustic Rail Dampers," *Proceedings of the Acoustics 2012*, <https://hal.archives-ouvertes.fr/hal-00810837>, April 2012.
- [194] W. J. Qian, Z. Q. Huang, H. Ouyang, G. X. Chen and H. J. Yang, "Numerical Investigation of the Effects of Rail Vibration Absorbers on Wear Behaviour of Rail Surface," *Part J: Journal of Engineering Tribology*, vol. 233, no. 3, p. <https://doi.org/10.1177/1350650118785061>, 2019.
- [195] T. X. Wu, "Effects on Short Pitch Rail Corrugation Growth of a Rail Vibration Absorber/Damper," *Wear*, vol. 271, no. 1 - 2, pp. 339 - 348, 2011.
- [196] G. X. Chen, Y. F. Wu, X. L. Cui and H. Ouyang, "Study on the Vibration Causing Rail Corrugation," *25th Symposium of the International Association of Vehicle System Dynamics, IAVSD 2017*, pp. 971 - 976, 14 - 17 August 2018.
- [197] C. A. Brockley and P. L. Ko, "An Investigation of Rail Corrugation Using Friction-Induced Vibration Theory," *Wear*, no. 128, pp. 99 - 105, 1988.
- [198] Y. Suda, M. Hanawa, M. Okumura and T. Iwasa, "Study on Rail Corrugation in Sharp Curves of Commuter Line," *Wear*, no. 253, pp. 193 - 198, 2002.
- [199] Y. Q. Sun and S. Simson, "Wagon-Track Modelling and Parametric Study on Rail Corrugation Initiation due to Wheel Stick-Slip Process on Curved Track," *Wear*, no. 265, pp. 1193 - 1201, 2008.
- [200] A. Saulot and L. Baillet, "Dynamic Finite Element Simulations for Understanding Wheel-Rail Contact Oscillatory States Occurring Under Sliding Conditions," *Journal of Tribology*, no. 128, pp. 761 - 770, 2006.
- [201] G. X. Chen, Z. R. Zhou, H. Ouyang, X. S. Jin, M. H. Zhu and Q. Y. Liu, "A Finite Element Study on Rail Corrugation Based on Saturated Creep Force-Induced Self-Excited Vibration," *Journal of Sound and Vibration*, no. 329, pp. 4643 - 4655, 2010.

- [202] X. L. Cui, G. X. Chen, H. G. Yang, Q. Zhang, H. Ouyang and M. H. Zhu, "Effect of the Wheel/Rail Contact Angle and the Direction of the Saturated Creep Force on Rail Corrugation," *Wear*, no. 330, pp. 554 - 562, 2015.
- [203] A. Matsumoto, Y. Sato, H. Ono, M. Tanimoto, Y. Oka and E. Miyauchi, "Formation Mechanism and Countermeasures of Rail Corrugation on Curved Track," *Wear*, vol. 253, no. 1 - 2, pp. 178 -184, 2002.
- [204] O. Arias-Cuevas, Z. Li, R. Lewis and E. A. Gallardo-Hernandez, "Rolling-Sliding Laboratory Test of Friction Modifiers In Dry and Wet Wheel-Rail Contacts," *Wear* 268, no. 3 - 4, pp. 543 - 551, 2010.
- [205] W. J. T. Daniel, C. -Y. Cheng and P. A. Meehan, "Medelling the Effect of Friction Modifiers on Rail Corrugation in Cornering," *Vehicle System Dynamics*, vol. 46, no. 9, pp. 845 - 866, 2008.
- [206] W. J. T. Daniel and P. A. Meehan, "Analysis of Rail Corrugation in Cornering," *Wear*, vol. 265, no. 9 - 10, pp. 1183 - 1192, 2008.
- [207] Z. Wen, X. Jin and Y. Jiang, "Elastic-Plastic Finite Element Analysis of Nonsteady State Partial Slip Wheel-Rail Rolling Contact," *Journal of Tribology*, vol. 127, no. 4, pp. 713 - 721, 2005.
- [208] M. Ishida, B. Takumi , K. Iida, H. Ishida and F. Auki, "Effect of Moderating Friction of Wheel/Rail Interface on Vehicle/Track Dynamic Behaviour," *Wear* 265, no. 9-10, pp. 1497 - 1503, 2008.
- [209] M. Beck, R. Stock and B. Temple, "Rail Corrugation Growth in Curves – Friction Management as a Sustainable Solution," *24th Symposium of the International Association for Vehicle System Dynamics (IAVSD)*, pp. 1265 - 1276, 17 - 21 August 2016.
- [210] R. Frohling , U. Spangenberg and E. Reitmann, "Root Cause Analysis of Locomotive Wheel Tread Polygonisation," *Wear* , no. DOI: 10.1016/j.wear.2019.05.026, pp. 432 - 433, May 2019.
- [211] I. SEBEŞAN, C.-N. BADEA, L.-V. PĂDURARU, A. BADEA and G. POPA, "UNDULATING WEAR OF A RAILROAD TRACKS," *Sinteze de Mecanica Teoretica si Aplicata*, vol. 7, no. 1, pp. 33 - 50, 2016.
- [212] S. L. Grässie, "Short Wavelength Rail Corrugation: Field Trials and Measuring Technology," *Wear*, vol. 191, no. 1 - 2, pp. 149 - 160, January 1996.
- [213] P. Meinke and J. Stephanides, "Do Steel Bridges Prevent Rail Corrugations?," *THE ARCHIVES OF TRANSPORT*, vol. XXII, no. 1, pp. 110 - 118, 2010.
- [214] X. L. Xiao, G. X. Chen, J. L. Mo and M. H. Zhu, "Mechanism for Friction to Suppress a Wear-Type Rail Corrugation," *Journal of Vibration and Shock*, vol. 32, no. 8, pp. 166 - 170, 2013.



- [215] T. Rossing , “Modal Analysis,” in *Springer Handbook of Acoustics*, New York, Springer, New York, NY; [https://doi.org/10.1007/978-0-387-30425-0\\_28](https://doi.org/10.1007/978-0-387-30425-0_28), 2007, pp. 1127 - 1138.
- [216] P. Avitabile, “Modal Analysis: A Simple Non-Mathematical Presentation,” in *In book: Modal Testing: A Practitioner's Guide*, Lowell, Massachusetts, DOI: 10.1002/9781119222989.ch1, 2001, pp. 1 - 35.
- [217] G. Visser, “Modal Analysis: What It Is and Is Not,” 25 Jovember 2014. [Online]. Available: <https://simteq.co.za/blog/modal-analysis/>. [Accessed 18 October 2019].
- [218] X. Jin, “Experimental and Numerical Modal Analyses of High-Speed Train Wheelsets,” *Proceedings of the Institution of Mechanical Engineers, Part F: Journal of Rail and Rapid Transit*, vol. 230, no. 3, 2016.
- [219] L. Huiqi and M. Glenn , “Discrete element modelling of two-layered ballast in a box test,” *Granular Matter*, vol. 76, no. 22, pp. <https://doi.org/10.1007/s10035-020-01046-6>, 2020.
- [220] J. Ali Zakeri and S. Ali Mosayebi, “Study of Ballast Layer Stiffness in Railway Tracks,” *Gradevinar*. DOI: 10.14256/JCE.1232.2015, vol. 4, no. 68, pp. 311 - 318, 2016.
- [221] B. Steel, “Profile Selection - Sleepers,” [Online]. Available: <https://britishsteel.co.uk/what-we-do/rail/steel-sleepers/profile-selection-steel-sleepers/>. [Accessed 12 May 2020].
- [222] P. Colarusso, H. L. Kidder, I. W. Levin and E. Neil Lewis, “Raman and Infrared Microspectroscopy,” *Encyclopedia of Spectroscopy and Spectrometry*, vol. <https://doi.org/10.1006/rwsp.2000.0402>, pp. 1945 - 1954, 1999.
- [223] N. Chaar, Doctoral Thesis: Wheelset Structural Flexibility and Track Flexibility in Vehicle-Track Dynamic Interaction, Stockholm: KTH Engineering Sciences, 2007.
- [224] S. Kaewunruen, E. k. Gamage and A. M. Remennikov, “Modelling Railway Prestressed Concrete Sleepers (Crossties) With Holes and Web Openings (WMCAUS 2016),” *Worl Multidisciplinary Civil Engineering-Architecture-Urban Planning Symposium*, vol. 161, no. 2016, pp. 1240 - 1246, 2016.
- [225] J. J. Heunis, PhD Thesis: Material Models for Rail Pads, Stellenbosch: Stellenbosch University SUNScholar Repository, 2011.
- [226] S. L. Grässie, “Resilient Railpads: Their Dynamic Behaviour in the Laboratory and on Track,” *Proceedings of Institution for Mechanical Engineers*, vol. 203, pp. 25 - 32 , 1988.
- [227] A. Aikawa, “Determination of Dynamic Ballast Characteristics Under Transient Impact Loading,” *Special issue: Electronic Journal of Structural Engineering*, vol. 1, no. 13, pp. 17 - 34, 2013.

- [228] I. Gómez and E. G. Vadillo, “A Linear Model to Explain Short Pitch Corrugation on Rails,” *Wear*, vol. 255, no. 7 - 12, pp. 1127 - 1142, 2003.
- [229] T. Shafighfard and S. Talatahari, “A Robust Finite Element Analysis of the Rail-Wheel Rolling Contact,” *Advances in Mechanical Engineering*, pp. DOI: 10.1155/2013/272350. 1 - 9, October 2013.
- [230] MPUMALANGA PROVINCE GOVERNMENT: Public Works Roads and Transport, “Mpumalanga Province Freight Data Bank,” [Online]. Available: <http://www.safiri.co.za/mpfdb/rail-overview.html>. [Accessed 6 July 2019].



## Appendix A. Wheel-rail contact displacement modelling.

### (i) *Procedure for Finite Element Wheel-Rail Contact Analysis:*

A single wheel was modelled on top of a rail to find the wheel-rail contact and analyse displacements around the contact point. Here two models are considered, i.e. one model is for rail on steel sleepers and the other is for rail on concrete sleepers. The difference between the two models is pertaining the sleepers and rail size. The size of rail on steel sleepers is at 48kg/m, whilst that on concrete sleepers is at 57kg/m. Figure A1. shows the CAD models used in the contact point analysis.

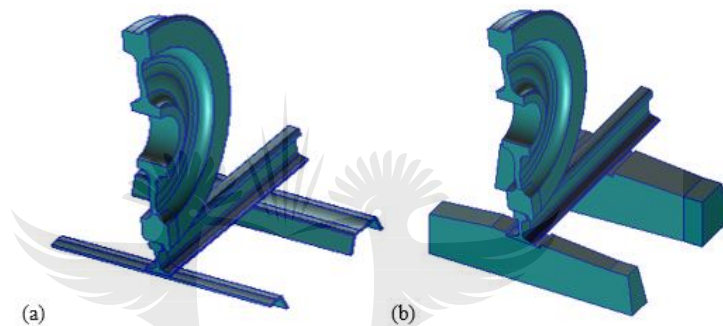


**Figure A1** – CAD model used in the wheel-rail contact point FEA. (a) wheel-rail model on steel sleepers (b) wheel-rail model on concrete sleepers.

In order to save on computational time by exploiting the symmetry of the wheel, the wheel-rail model is cut into a half model, such that the contact point is cut in the middle as seen in Figure A2.

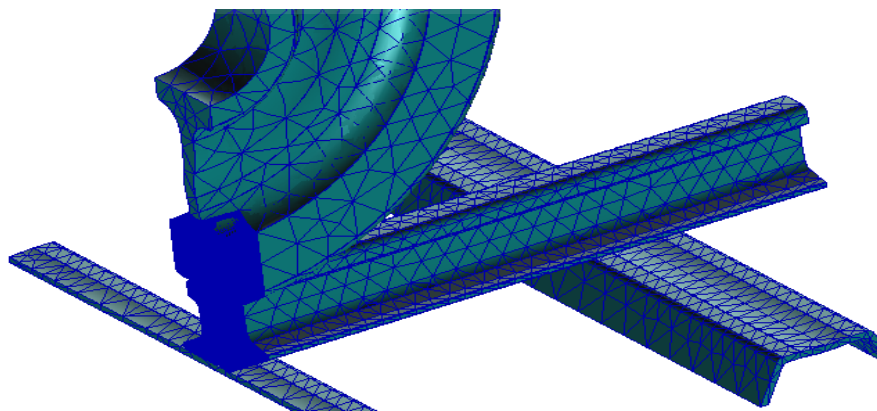


**Figure A2** – Finer mesh around the wheel-rail contact point.

Four deformable body contacts were created for the FEM in Figure A2. Given that the model is cut in the middle and also due to the fact that the smaller wheel and rail pieces are cut from the main wheel and rail, the model in Figure A2. ultimately comprised of five FEM pieces. The wheel has a smaller piece cut out, referred to as the “wheel piece”, the rail also has a smaller piece cut out, referred to as the “rail piece”.

The wheel is also referred to as a “half wheel”. Table A1. tabulates the contacts created for deformable bodies.

**Table A1.** Contacts created for deformable bodies for the wheel-rail contact FEMs

<b>Geometry (in contact)</b>	<b>Geometry (in contact with)</b>	<b>Contact</b>
Wheel piece	Half wheel	Glue
Wheel piece	Rail piece	Touching
Rail piece	Rail	Glue
48kg/m rail	Steel sleepers	MPC
57kg/m rail	Concrete sleepers	Glue

In order to prevent FEMs from dislocating from the touching connections, glued contacts were created for connections between the wheel piece and half wheel; also for rail piece and rail. A touching contact was created for the wheel-rail contact point. In order to save on simulation time, the Multi Point Constrains (MPCs) were used for the connection between the bottom face of rail foot (and rail piece foot); to the steel sleepers.

As seen in Table A1. a glued contact was created for rail on concrete sleepers. MPCs were easy to apply on a few points of the steel sleeper, that make contact with the rail foot. The mesh details for mesh used on the FEMs in Figure A2. are tabulated in Table 6.2.

**Table A2.** Mesh details for wheel-rail contact analysis FEMs

<b>Mesh item</b>	<b>Mesh details</b>
Mesh type	Solid
Element type	Tetrahedron
Meshing	TetMesh
Topology	Tet 10

The element nodes were equivalenced to a tolerance of 0.1mm. Mesh optimisation was conducted on both the wheel piece and rail piece. Mesh optimisation was conducted manually by the author, by running the model and keeping record of the results at completion of each run. Figure A2. shows a finer mesh around the wheel-rail contact point. It was critical to create a denser mesh around the contact point, in order to better define displacements. The mesh is left coarser on the rest of the FEM groups. Table A3. tabulates details of mesh optimisation for the wheel-rail contact analysis model with steel sleepers.

**Table A3.** Mesh convergence for wheel-rail contact model with steel sleepers

<b>Element Global Edge Length (mm)</b>	<b>Number of Nodes for 48kg/m rail piece</b>	<b>Number of Nodes for the wheel piece</b>	<b>Maximum Displacement (mm)</b>
20	47,426	61,323	0.082
15	60,189	94,277	0.088
10	84,633	191,727	0.177
5	151,751	262,912	0.198
4	184,865	291,115	0.224
2.5	252,486	451,485	0.224

The mesh converges at an element global edge length of 4mm as is in the wheel-rail contact analysis model for rail on steel sleepers. Mesh optimisation details for the wheel-rail contact analysis model with concrete sleepers is tabulated in Table A4.

**Table A4.** Mesh convergence for wheel-rail contact model with concrete sleepers

<b>Element Global Edge Length (mm)</b>	<b>Number of Nodes for 57kg/m rail piece</b>	<b>Number of Nodes for the wheel piece</b>	<b>Maximum Displacement (mm)</b>
20	57,826	61,323	0.063
15	78,965	94,277	0.079
10	99,153	191,727	0.091
5	178,427	262,912	0.102
3.5	249,736	291,115	0.104
2.5	316,223	451,485	0.104

The mesh converges at an element global edge length of 3.5mm as is in the wheel-rail contact analysis model for rail on steel sleepers. Materials are understood to be isotropic and material properties allocated to each FEM of the wheel-rail contact

models are tabulated in Table A5. Material properties in Table 6.5. are for FEMs utilised on both models with steel and concrete sleepers.

**Table A5.** Material properties of FEMs for wheel-rail contact analysis models [23] [224]

FEM Solid	Material	Density (kg/m <sup>3</sup> )	Young's Modulus (GPa)	Poisson's Ratio
Half wheel	Steel	7850	210.000	0.30
Wheel piece	Steel	7850	210.000	0.30
Rail	Steel	7800	210.000	0.30
Rail piece	Steel	7800	210.000	0.30
Steel sleeper	Steel	7870	205.000	0.29
Concrete sleeper	Concrete	2400	36.406	0.20

The axle load was applied in the axle bore, on the part of the surface where the wheelset axle sits. Figure A3. shows the surface of the axle box on which the load was applied. The nodes selected for load application are circled in the red line seen in Figure A3. The red arrows illustrate the direction of the load.

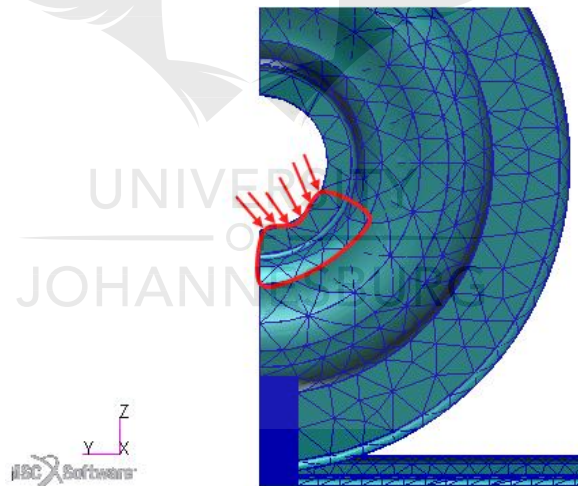


**Figure A3** – Axle load application area.

The total axle load per wheelset is 20tons, which is equivalent to 196.2kN. It is assumed that each wheel carries a load of 98.1kN. In addition, given that the wheel is cut in the middle, a load of 49.05kN is applied in the axle bore. In order to represent the gravitational force, the inertial load of -9.81 was created along the z-direction. The inertial load was created for both wheel-rail models with steel and concrete sleepers. Table A6. tabulates details of the loads and boundary conditions for the wheel-rail

analysis models. The loads and boundary conditions in Table A6. are applicable to wheel-rail contact analysis with both steel and concrete sleepers.

**Table A6.** Loads and boundary conditions for both wheel-rail contact analysis FEMs

<b>Geometry (in contact)</b>	<b>Load (&lt;x,y,z&gt;)</b>	<b>Fix translation (&lt;x,y,z&gt;)</b>	<b>Fix rotation (&lt;x,y,z&gt;)</b>
Axle bore	<0,0,-891.82>		
Wheel rim		<0,0, >	<0,0, >
Rail piece face		<0,0,0>	<0,0,0>
Rail face		<0,0,0>	<0,0,0>
Bottom of sleepers		<0,0,0>	<0,0,0>

A load of 891.82N was applied on 55 nodes in the axle bore, to yield a total load of 49.050kN, which is equivalent to a mass of 5tons. The load is applied downwards in the direction “z” (or in “-z”). One node in the wheel rim was fixed in all six DF. The face of one end of the wheel piece and one end of the rail were fixed in all six Degrees of Freedom (DOF). All nodes at the base face of sleepers were fixed in all six DOF.

(ii) *Results for FEA Wheel-Rail Contact Analysis for Rail on Steel and Concrete Sleepers:*

The first part of modelling is concerned with finding the wheel-rail contact displacements for both wheel-rail models with steel and concrete sleepers. Here only a short piece of track without ballast is considered to analyse displacements around the wheel-rail contact point. Figure A4. shows the displacement distribution around the wheel-rail contact point for the wheel-rail FEM with steel sleepers. More views of this Figure (A4.) are found in Appendix B.



Patran 2019 28-Oct-20 22:10:57

Fringe: SC1:LINEAR\_STATIC\_ANALYSIS, A1:Static subcase, Displacements, Translational, Magnitude, (NON-LAYERED)

Deform: SC1:LINEAR\_STATIC\_ANALYSIS, A1:Static subcase, Displacements, Translational,

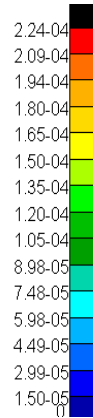
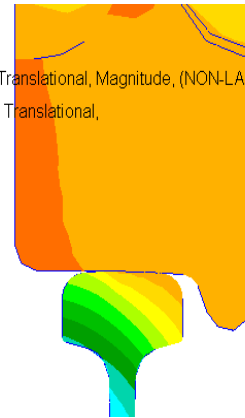
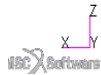


**Figure A4** – Displacement distribution around wheel-rail contact point, for wheel-rail FEM with steel sleepers.

In Figure A4. the analysis of displacements taking into account the plastic and elastic strains in the wheel and rail is performed. The wheel-rail contact model results in Figure A4. show the displacements distribution around the wheel-rail contact point. The legend in the Figure (A4.) presents displacements with the units in meters. For normalization, a generalised modal mass is equal to unity.

The color coding in the legend correspond to the colors in the deformed shape of the model results. It is noted in Figure A4. that the nodes of the wheelset situated around the light blue color of the deformed shape displace the least, with the smallest displacement being 0.015mm. The nodes situated around the green and yellow color experience average displacement, whilst the modes around the orange, red, and black colors experience the largest displacement.

The largest displacement experienced is 0.224mm. It is seen in Figure A4. that the contact displacements is average around the wheel-rail contact point. The contact displacement is more on the part of the wheel that is towards the field side. The rail web takes the least displacement during contact. Overall, the displacements are very minimal (less than a millimeter) and no severe displacements are experienced around the wheel-rail contact point.

Figure A5. shows the displacement distribution around the wheel-rail contact point for the wheel-rail FEM with concrete sleepers. More views of this Figure are found in Appendix C.

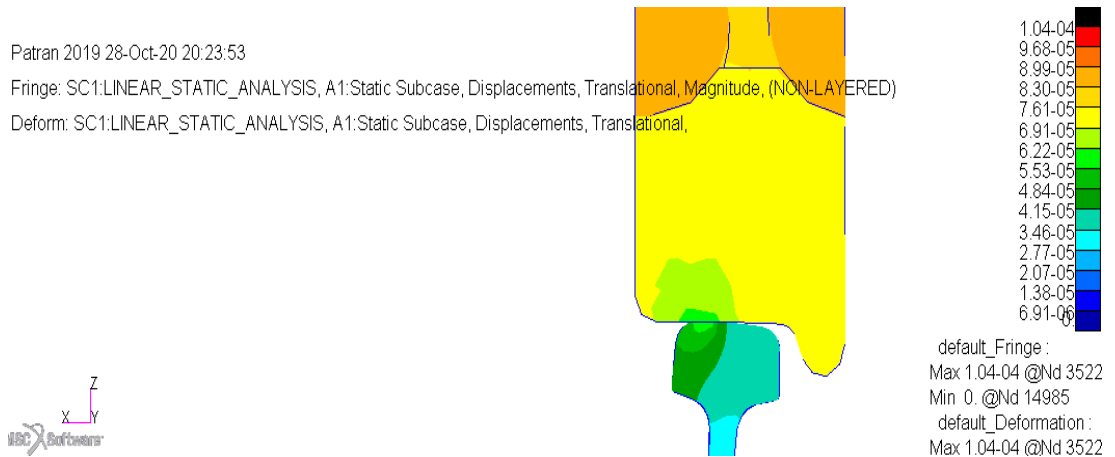


**Figure A5** – Displacement distribution around wheel-rail contact point, for wheel-rail FEM with concrete sleepers.

Evident in Figure A5. is that the displacements of the wheel-rail contact model are slightly less than those seen on the wheel-rail contact model with steel sleepers in Figure A4. Displacement distribution in Figure A5. is more concentrated towards the field face of the rail crown. This is given that, contrary to the wheel-rail model with steel sleepers, in the model with concrete sleepers the wheel-rail contact is not situated exactly at the center of the wheel and rail widths.

From the assembly drawings in the Appendix H it can be seen that the shape of the concrete sleeper is not entirely flat on the top face, which forces the rail pad and rail to slightly lean inwards. Contrary to that, horizontally the top face of the steel sleeper is completely flat, which allows the rail to seat straight along the vertical plane. The displacements concentration in Figure A5. is more on the rail than on the wheel.

From a closer view it can be seen that the displacements is more severe in the material closer to the contact point, than further from the contact point. It is common for displacements to be more concentrated on the rail when a load is applied vertically in a wheel-rail contact analysis and these displacements can be beyond the yield point of the rail [173] [229].

(iii) *Results Discussion:*

From the FEA models developed to find the wheel-rail contact point when the wheel-rail system is modelled with steel and concrete sleepers, a difference in the wheel-rail

contact point location is noted. The wheel-rail contact point for wheel-rail system on concrete sleepers is not located exactly in the middle of the wheel-rail system.

This is caused by the fact that the rail is not positioned exactly upright along the vertical plane, due to the slightly banked top surface of the concrete sleepers. This ultimately causes displacement concentration towards the field side of the wheel-rail system, which may ultimately wear the rails and wheels one point on train passes.

It can be seen in the wheel-rail contact analysis in the wheel squeal model by Goo and Kim [173] that when a load is applied in the vertical direction, the wheel-rail displacement distribution can occur evenly around wheel-rail contact point region. However, the wheel has to be modelled accurately in the vicinity of the center of the rail.

El Beshbichi et al. [143] showed how significant the interaction of a wheel cross section and the track gauge influence the self-excited vibration, which favours the development of the short pitch rail corrugation. The development of corrugation on rails in the Belfast to Steelpoort railway line may possibly be influenced by rail wear from this irregularity.

The irregularity is not found in the wheel-rail system with steel sleepers. However, displacements around the wheel-rail contact point are minimal, since they are less than a millimeter, which may pose a lower risk for wheel-rail material wear. Nonetheless, placing the rail upright on its rail foot along the vertical axis should be taken as an additional measure in reducing the damage mechanisms for rail corrugation.

**Appendix B.** Additional views of results for wheel-rail contact point analysis, for FEM with steel sleepers.

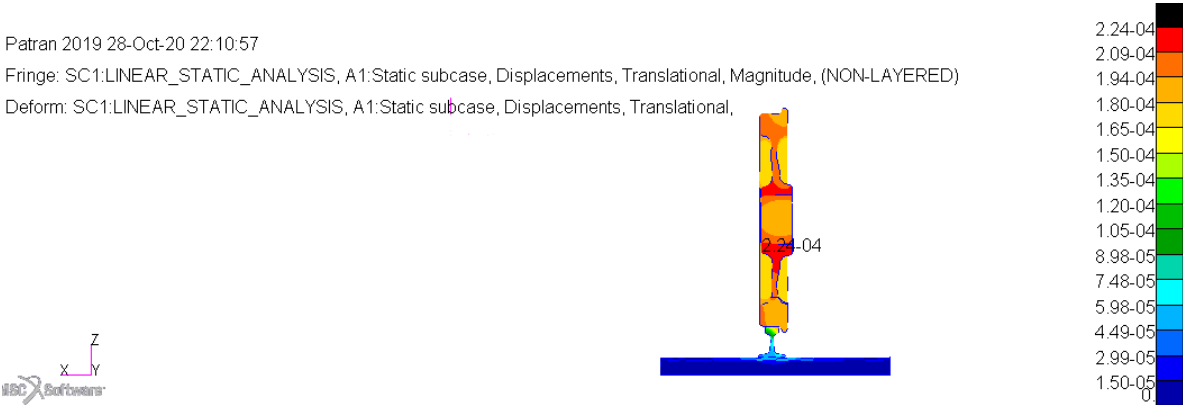


**Figure B1** – Front view of the wheel-rail model with steel sleepers

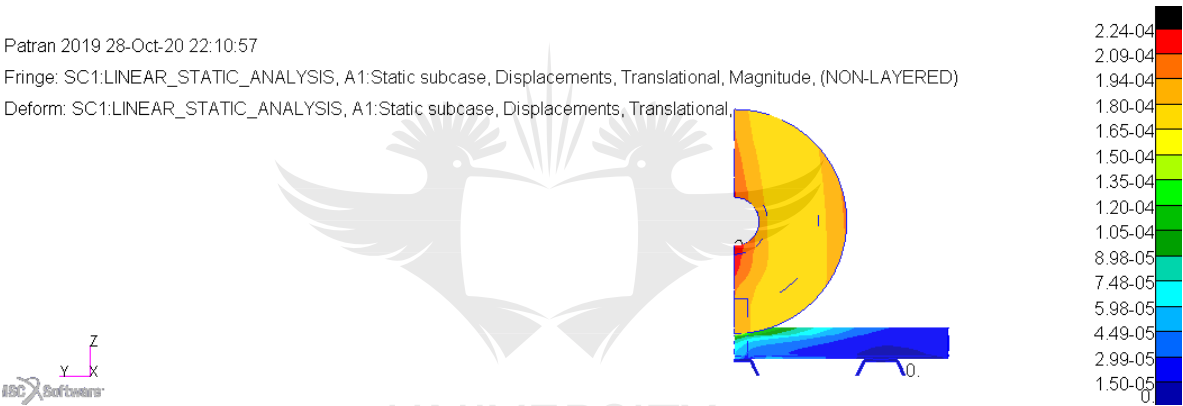


**Figure B2** – Left view of the wheel-rail model with steel sleepers

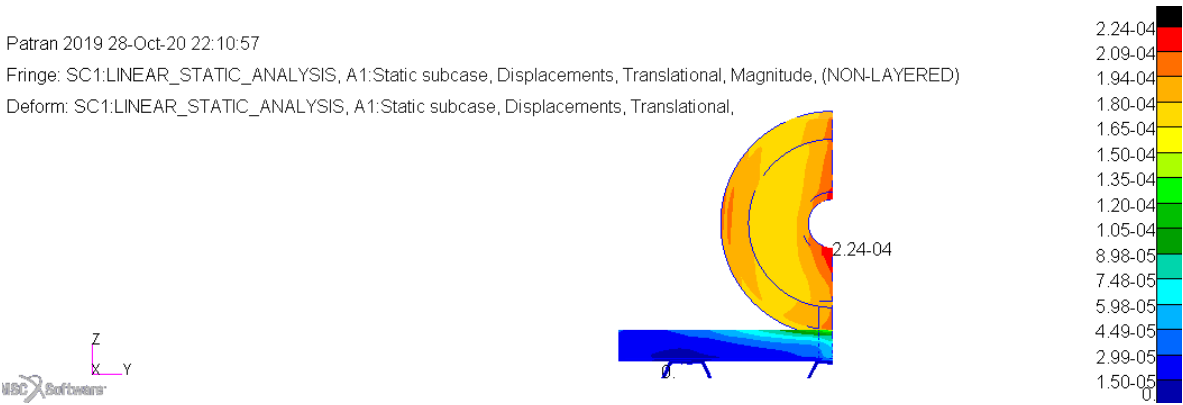


**Figure B3** – Right view of the wheel-rail model with steel sleepers

Patran 2019 28-Oct-20 22:10:57

Fringe: SC1:LINEAR\_STATIC\_ANALYSIS, A1:Static subcase, Displacements, Translational, Magnitude, (NON-LAYERED)

Deform: SC1:LINEAR\_STATIC\_ANALYSIS, A1:Static subcase, Displacements, Translational,

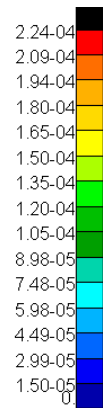
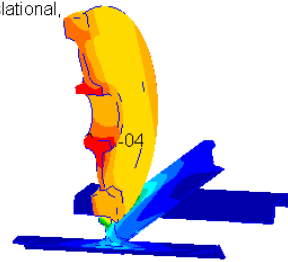
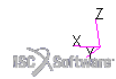


**Figure B4** – Isometric view of the wheel-rail model with steel sleepers



**Appendix C.** Additional views of results for wheel-rail contact point analysis, for FEM with FY-type concrete sleepers.

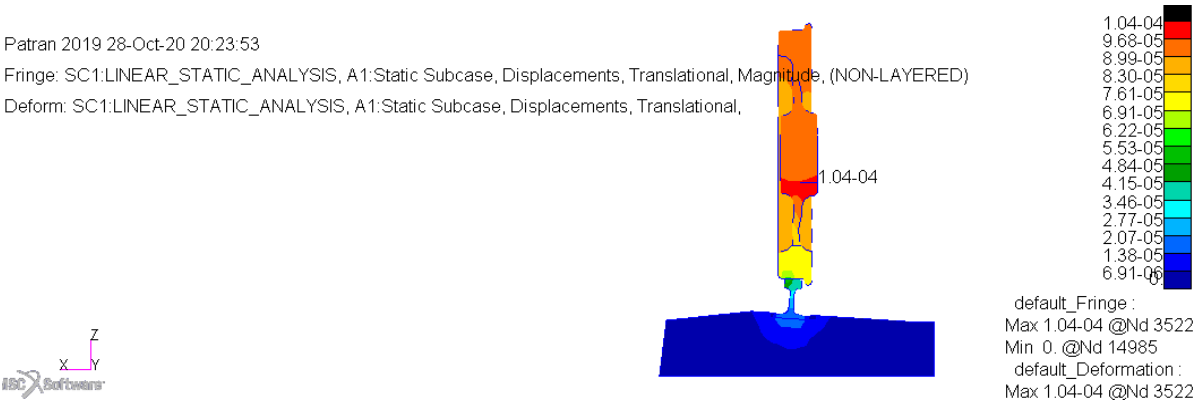


**Figure C1** – Front view of the wheel-rail model with concrete sleepers

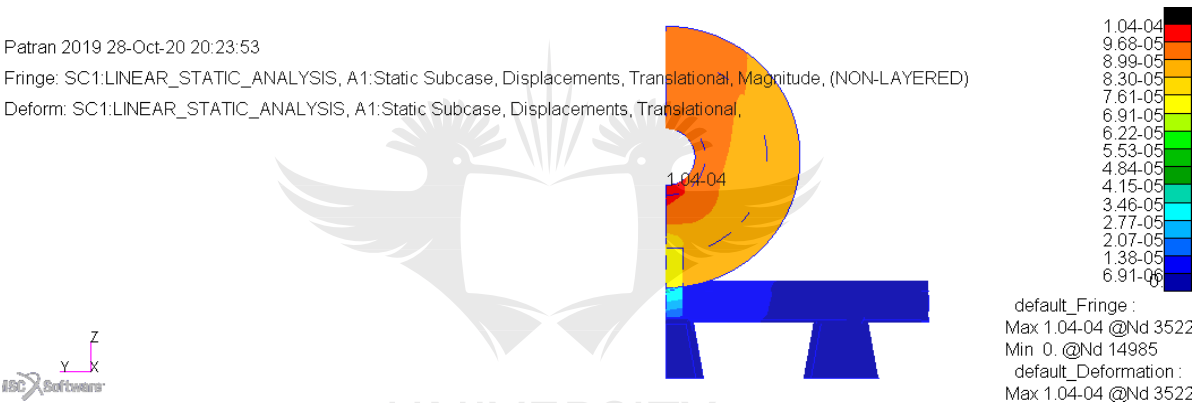


**Figure C2** – Left view of the wheel-rail model with concrete sleepers

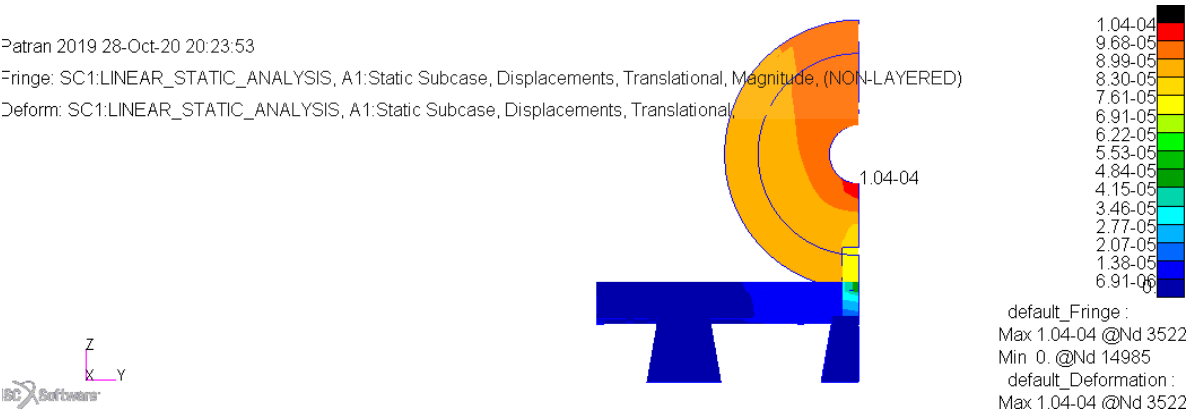
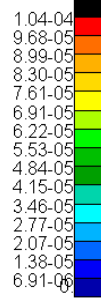
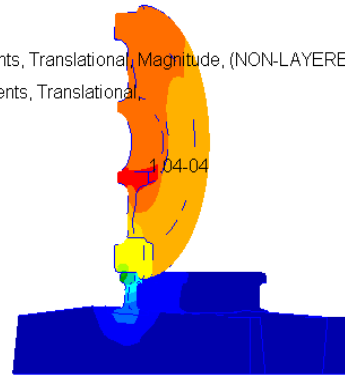
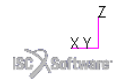


**Figure C3** – Right view of the wheel-rail model with concrete sleepers

Patran 2019 28-Oct-20 20:23:53

Fringe: SC1:LINEAR\_STATIC\_ANALYSIS, A1:Static Subcase, Displacements, Translational, Magnitude, (NON-LAYERED)

Deform: SC1:LINEAR\_STATIC\_ANALYSIS, A1:Static Subcase, Displacements, Translational,



default\_Fringe :  
Max 1.04-04 @Nd 3522  
Min 0. @Nd 14985  
default\_Deformation :  
Max 1.04-04 @Nd 3522

**Figure C4** – Isometric view of the wheel-rail model with concrete sleepers



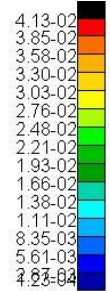
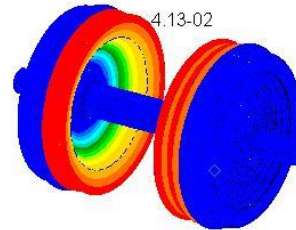


**Appendix D.** Additional views of modal analysis results for the D39 200 wheelset model.

Patran 2019 17-Sep-20 22:41:27

Fringe: SC1:NORMAL\_MODES, A1:Mode 12 : Freq. = 232.2, Eigenvectors, Translational, Magnitude, (NON-LAYERED)

Deform: SC1:NORMAL\_MODES, A1:Mode 12 : Freq. = 232.2, Eigenvectors, Translational,



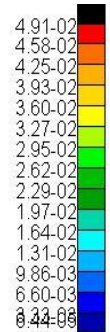
default\_Fringe :  
Max 4.13-02 @Nd 980414  
Min 1.23-04 @Nd 5431  
default\_Deformation :  
Max 4.13-02 @Nd 980414

**Figure D1** – Traction wheelset – axial bending of the wheels

Patran 2019 17-Sep-20 22:42:31

Fringe: SC1:NORMAL\_MODES, A1:Mode 13 : Freq. = 337.43, Eigenvectors, Translational, Magnitude, (NON-LAYERED)

Deform: SC1:NORMAL\_MODES, A1:Mode 13 : Freq. = 337.43, Eigenvectors, Translational,



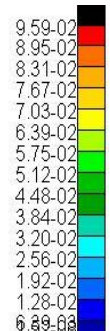
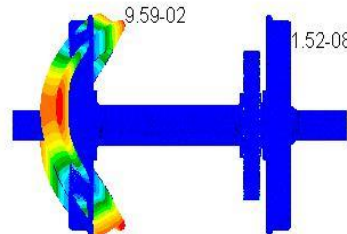
default\_Fringe :  
Max 4.91-02 @Nd 378168  
Min 6.44-05 @Nd 913126  
default\_Deformation :  
Max 4.91-02 @Nd 378168

**Figure D2** – Traction wheelset – axial bending of the wheels and bull gear

Patran 2019 17-Sep-20 22:43:34

Fringe: SC1:NORMAL\_MODES, A1:Mode 19 : Freq. = 374.49, Eigenvectors, Translational, Magnitude, (NON-LAYERED)

Deform: SC1:NORMAL\_MODES, A1:Mode 19 : Freq. = 374.49, Eigenvectors, Translational,



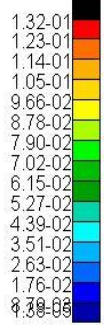
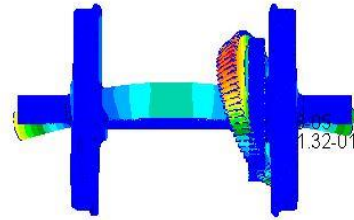
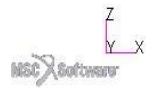
default\_Fringe :  
Max 9.59-02 @Nd 980463  
Min 1.52-08 @Nd 705363  
default\_Deformation :  
Max 9.59-02 @Nd 980463

**Figure D3** – Traction wheelset – axial bending of the wheel

Patran 2019 17-Sep-20 22:44:10

Fringe: SC1:NORMAL\_MODES, A1:Mode 21 : Freq. = 497.57, Eigenvectors, Translational, Magnitude, (NON-LAYERED)

Deform: SC1:NORMAL\_MODES, A1:Mode 21 : Freq. = 497.57, Eigenvectors, Translational,



default\_Fringe :  
Max 1.32-01 @Nd 373110  
Min 1.38-05 @Nd 578572  
default\_Deformation :  
Max 1.32-01 @Nd 373110

**Figure D4 – Traction wheelset – axial bending of the axle and bull gear**



**Appendix E.** Additional views of results for the complex eigenvalue analysis, for FEM with steel sleepers.

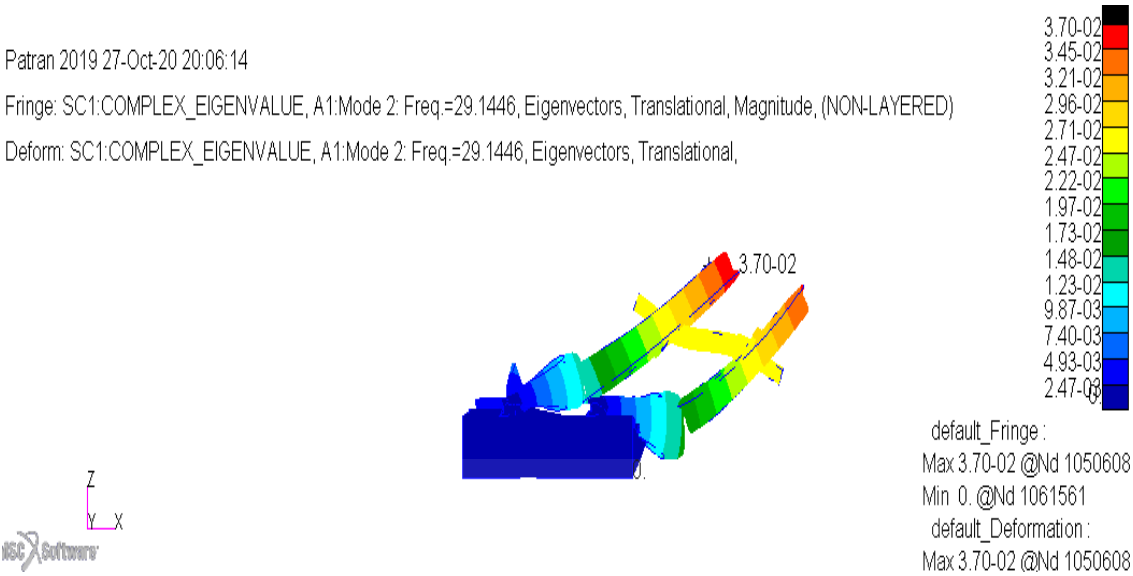


**Figure E1** – Mode shape at 29.1446Hz from complex eigenvalue analysis for wheelset-track FEM with steel sleepers

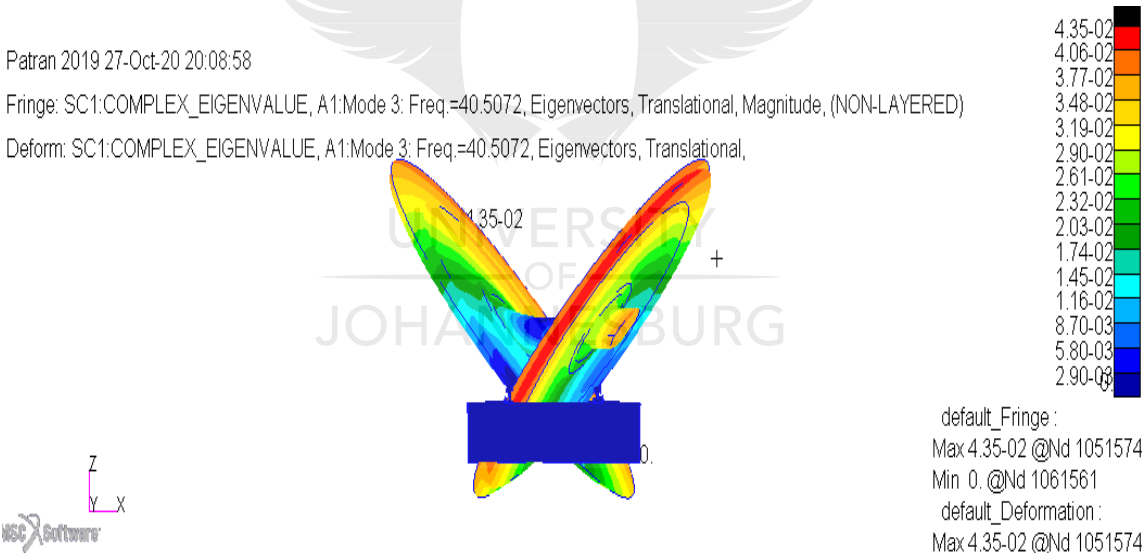


**Figure E2** – Mode shape at 40.5072Hz from complex eigenvalue analysis for wheelset-track FEM with steel sleepers

Patran 2019 27-Oct-20 20:12:44

Fringe: SC1:COMPLEX\_EIGENVALUE, A1:Mode 4: Freq.=82.3875, Eigenvectors, Translational, Magnitude, (NON-LAYERED)

Deform: SC1:COMPLEX\_EIGENVALUE, A1:Mode 4: Freq.=82.3875, Eigenvectors, Translational, Magnitude, (NON-LAYERED)

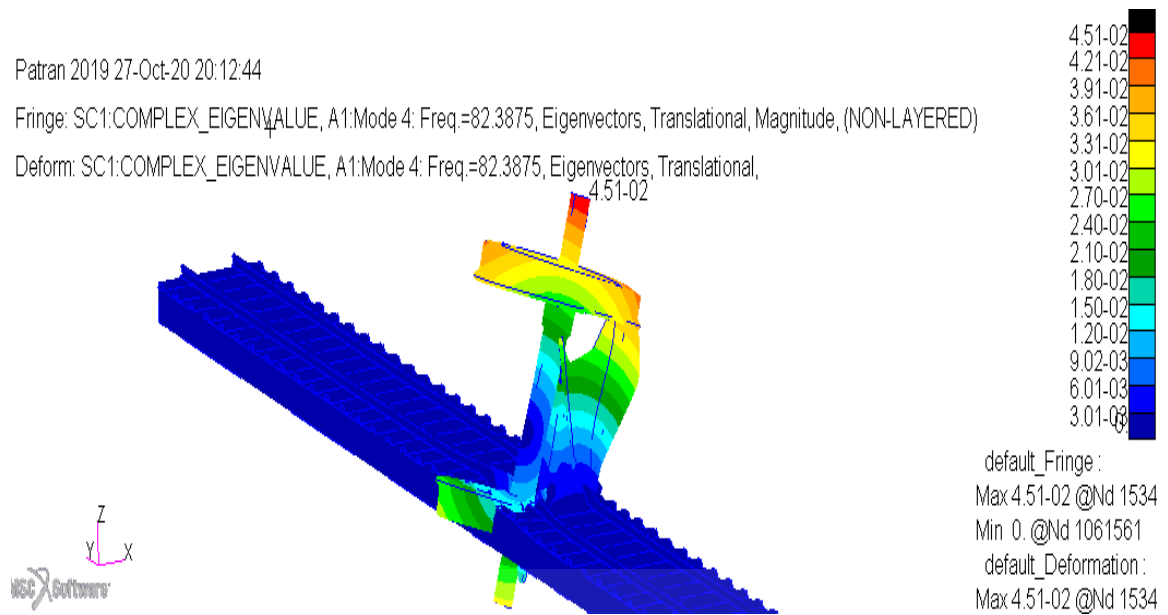


**Figure E3** – Mode shape at 82.3875Hz from complex eigenvalue analysis for wheelset-track FEM with steel sleepers

Patran 2019 27-Oct-20 20:16:07

Fringe: SC1:COMPLEX\_EIGENVALUE, A1:Mode 5: Freq.=88.2272, Eigenvectors, Translational, Magnitude, (NON-LAYERED)

Deform: SC1:COMPLEX\_EIGENVALUE, A1:Mode 5: Freq.=88.2272, Eigenvectors, Translational, Magnitude, (NON-LAYERED)



**Figure E4** – Mode shape at 88.2272Hz from complex eigenvalue analysis for wheelset-track FEM with steel sleepers

**Appendix F.** Additional views of results for the complex eigenvalue analysis, for FEM with concrete sleepers.

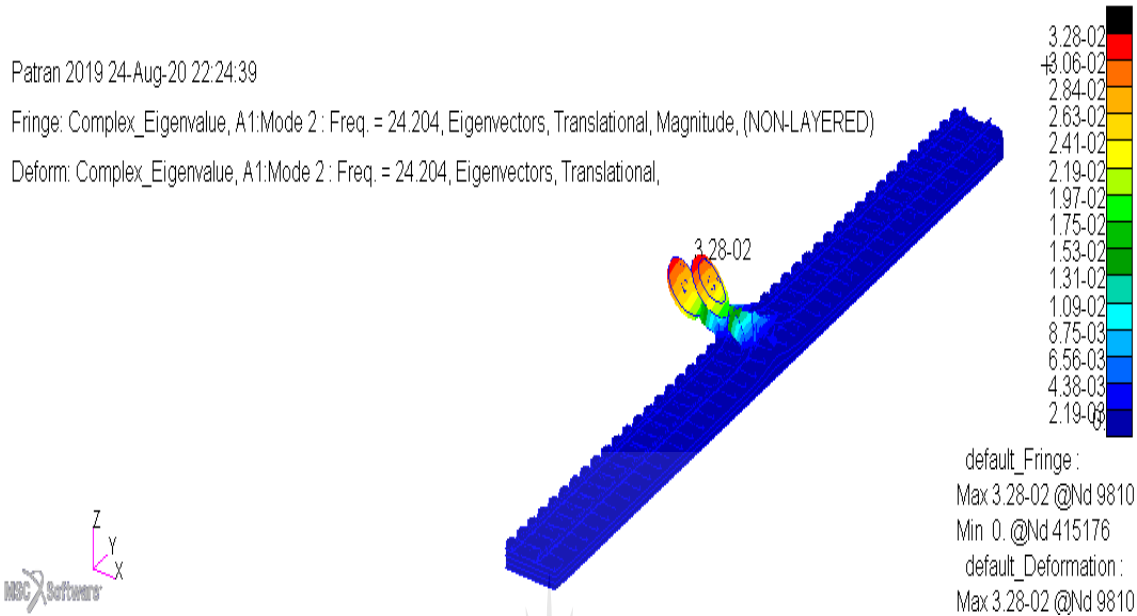


**Figure F1** – Mode shape at 24.204Hz from complex eigenvalue analysis for wheelset-track FEM with concrete sleepers

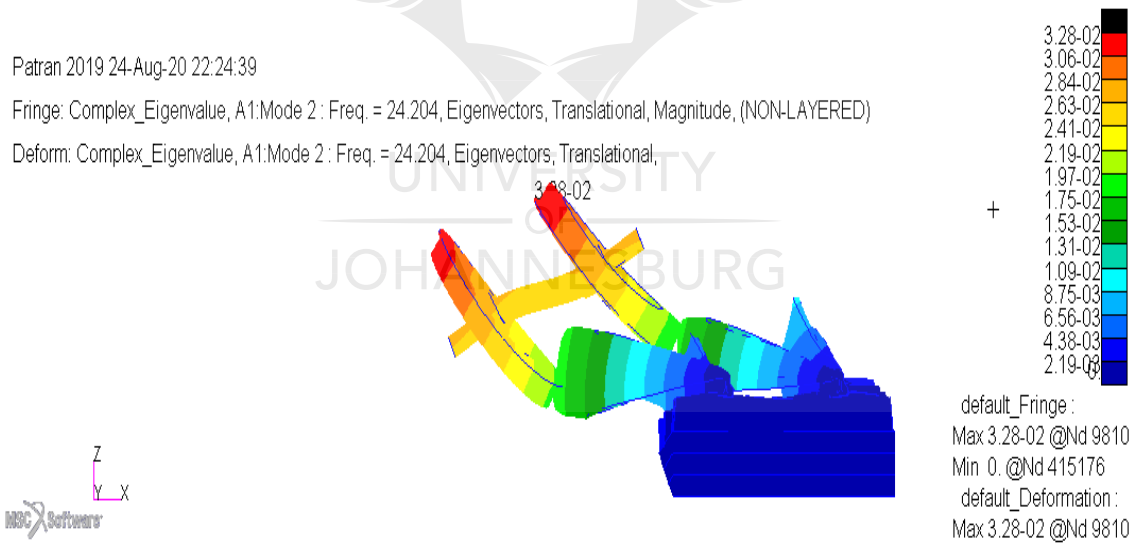
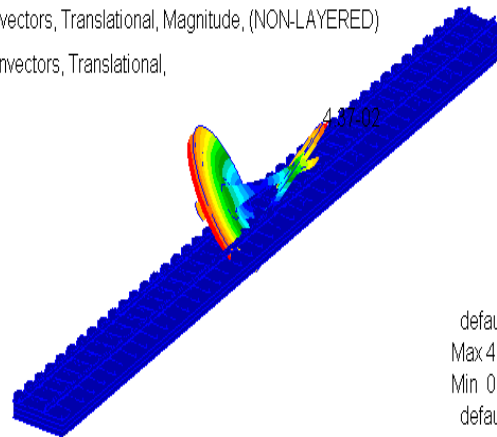
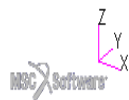


**Figure F2** – Mode shape at 24.204Hz from complex eigenvalue analysis for wheelset-track FEM with concrete sleepers

Patran 2019 24-Aug-20 22:26:42

Fringe: Complex\_Eigenvalue, A1:Mode 3 : Freq. = 42.242, Eigenvectors, Translational, Magnitude, (NON-LAYERED)

Deform: Complex\_Eigenvalue, A1:Mode 3 : Freq. = 42.242, Eigenvectors, Translational,



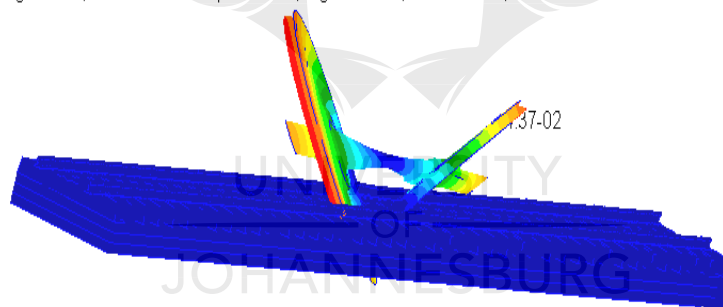
default\_Fringe :  
Max 4.37-02 @Nd 10853  
Min 0. @Nd 415176  
default\_Deformation :  
Max 4.37-02 @Nd 10853

**Figure F3** – Mode shape at 42.242Hz from complex eigenvalue analysis for wheelset-track FEM with concrete sleepers

Patran 2019 24-Aug-20 22:26:42

Fringe: Complex\_Eigenvalue, A1:Mode 3 : Freq. = 42.242, Eigenvectors, Translational, Magnitude, (NON-LAYERED)

Deform: Complex\_Eigenvalue, A1:Mode 3 : Freq. = 42.242, Eigenvectors, Translational,



+  
default\_Fringe :  
Max 4.37-02 @Nd 10853  
Min 0. @Nd 415176  
default\_Deformation :  
Max 4.37-02 @Nd 10853

**Figure F4** – Mode shape at 42.242Hz from complex eigenvalue analysis for wheelset-track FEM with concrete sleepers

Patran 2019 24-Aug-20 22:26:42

Fringe: Complex\_Eigenvalue, A1:Mode 3 : Freq. = 42.242, Eigenvectors, Translational, Magnitude, (NON-LAYERED)

Deform: Complex\_Eigenvalue, A1:Mode 3 : Freq. = 42.242, Eigenvectors, Translational,

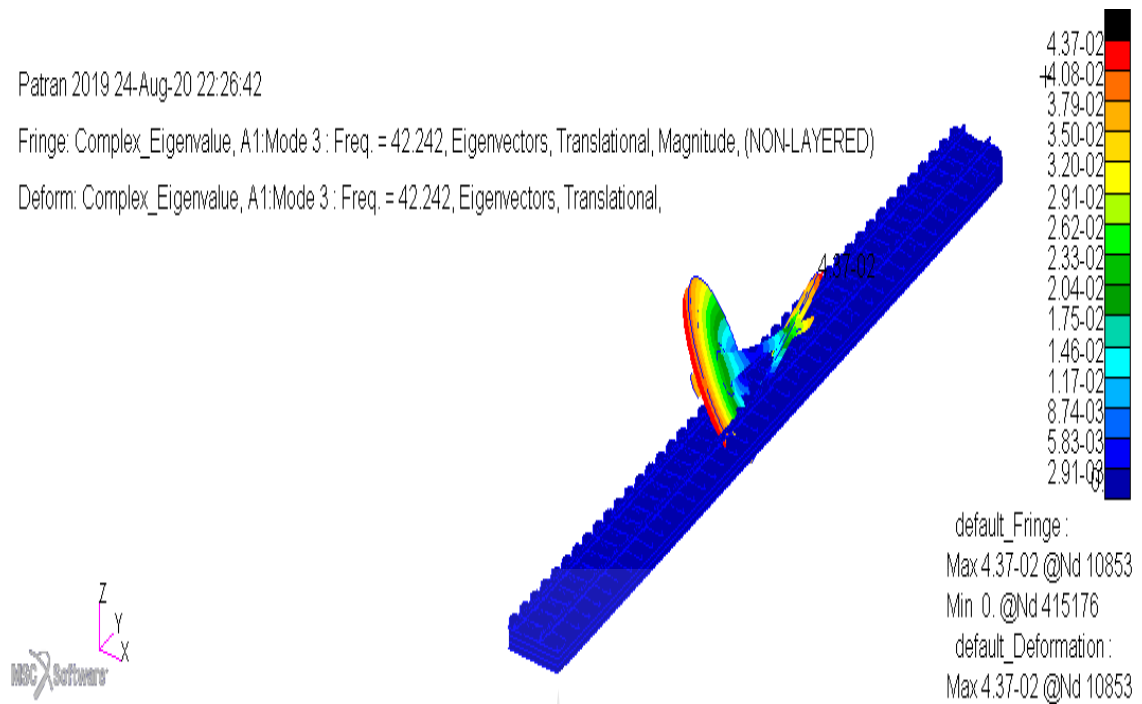


**Figure F5** – Mode shape at 42.242Hz from complex eigenvalue analysis for wheelset-track FEM with concrete sleepers

Patran 2019 24-Aug-20 22:08:56

Fringe: Complex\_Eigenvalue, A1:Mode 27 : Freq. = 108.71, Eigenvectors, Translational, Magnitude, (NON-LAYERED)

Deform: Complex\_Eigenvalue, A1:Mode 27 : Freq. = 108.71, Eigenvectors, Translational,

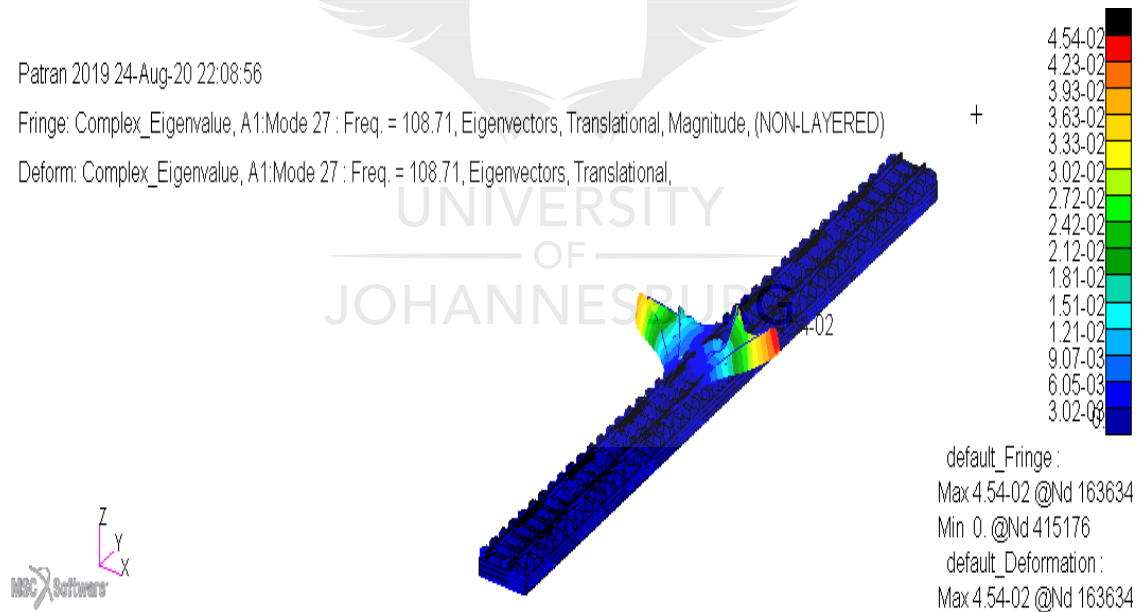


**Figure F6** – Mode shape at 108.71Hz from complex eigenvalue analysis for wheelset-track FEM with concrete sleepers

Patran 2019 24-Aug-20 22:19:26

Fringe: Complex\_Eigenvalue, A1:Mode 27 : Freq. = 108.71, Eigenvectors, Translational, Magnitude, (NON-LAYERED)

Deform: Complex\_Eigenvalue, A1:Mode 27 : Freq. = 108.71, Eigenvectors, Translational,

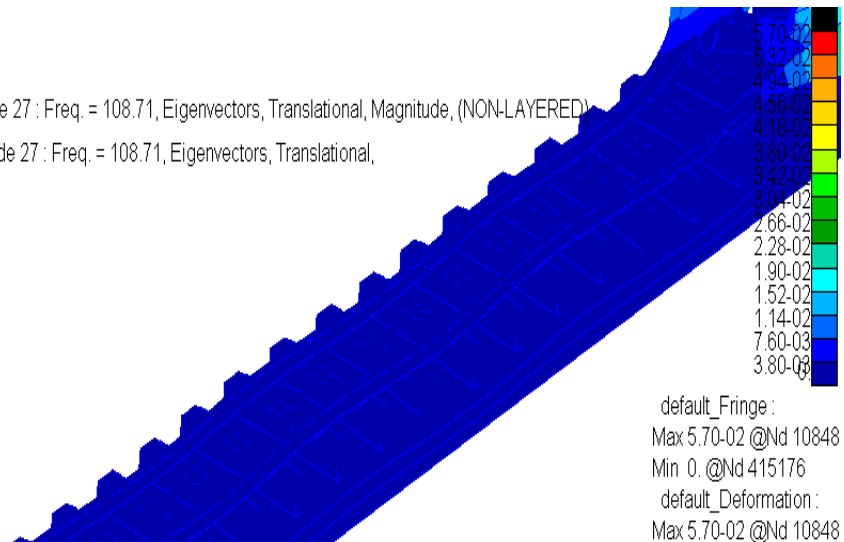
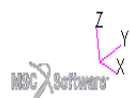


**Figure F7** – Mode shape at 108.71Hz from complex eigenvalue analysis for wheelset-track FEM with concrete sleepers

Patran 2019 24-Aug-20 22:11:05

Fringe: Complex\_Eigenvalue, A1:Mode 27 : Freq. = 108.71, Eigenvectors, Translational, Magnitude, (NON-LAYERED)

Deform: Complex\_Eigenvalue, A1:Mode 27 : Freq. = 108.71, Eigenvectors, Translational,

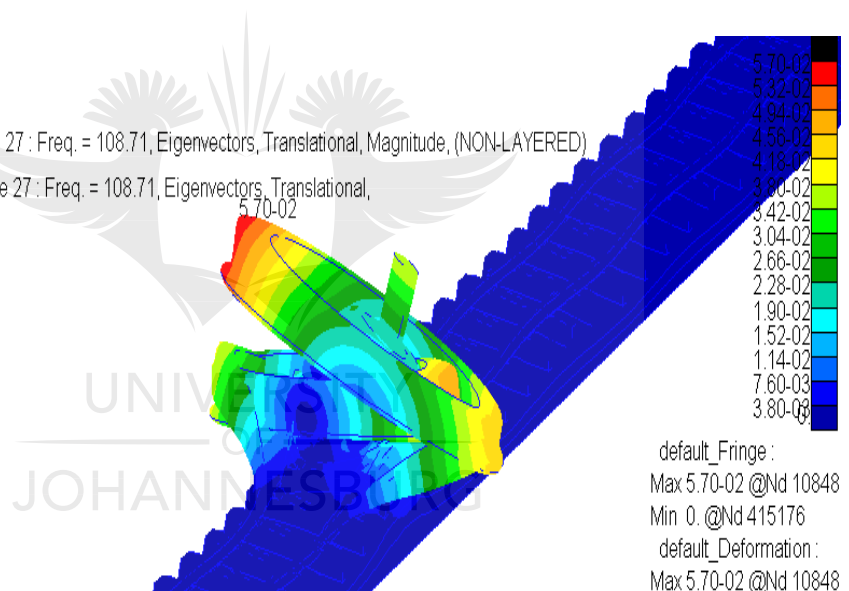


**Figure F8** – Mode shape at 108.71Hz from complex eigenvalue analysis for wheelset-track FEM with concrete sleepers



**Appendix G.** Images for symptoms of excessive corrugation-born vibration.



**Figure G1** – (a) Rail pad damage (b) effect of rail pad damage due to excessive vibration

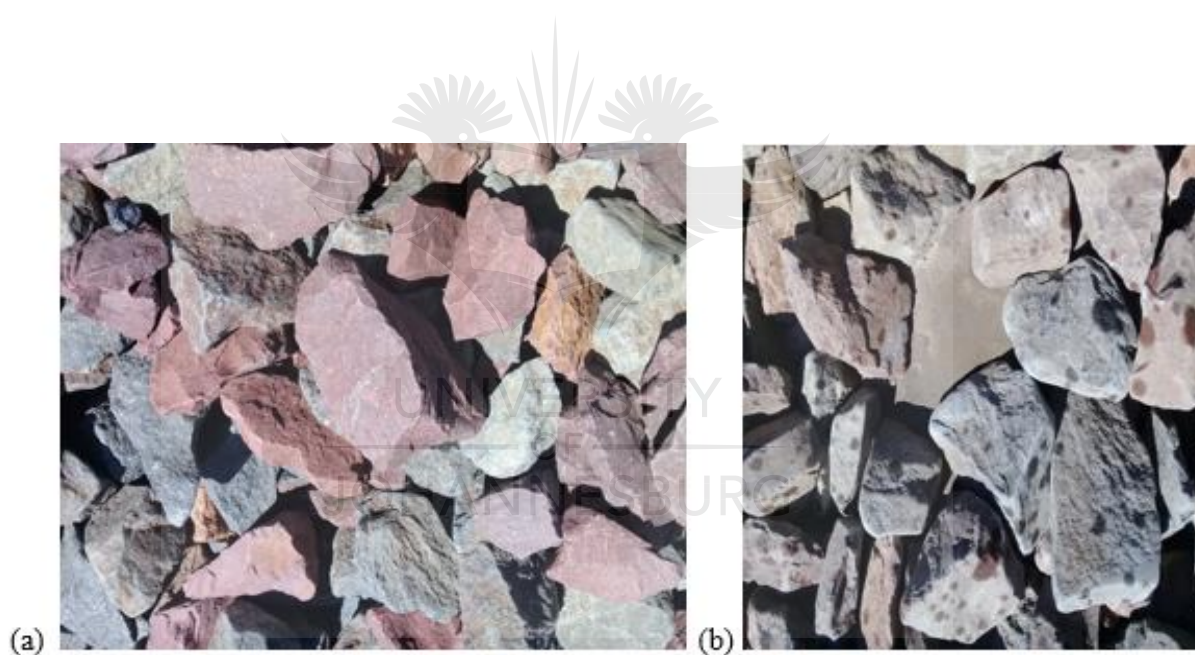


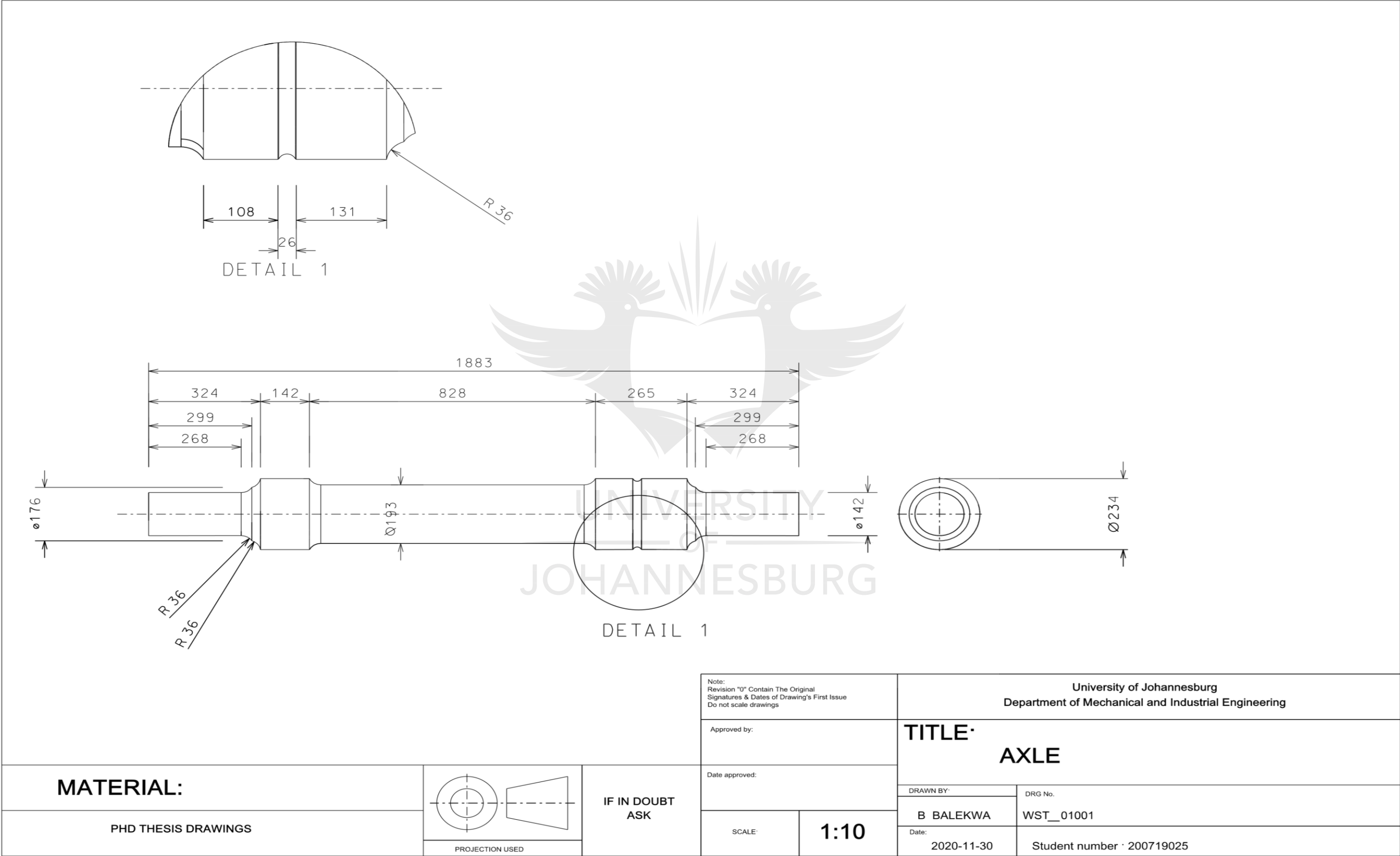
**Figure G2** – (a) Fair condition ballast, with desired quality (b) bad condition ballast due to excessive shaking from corrugation-born vibrations, undesirable quality

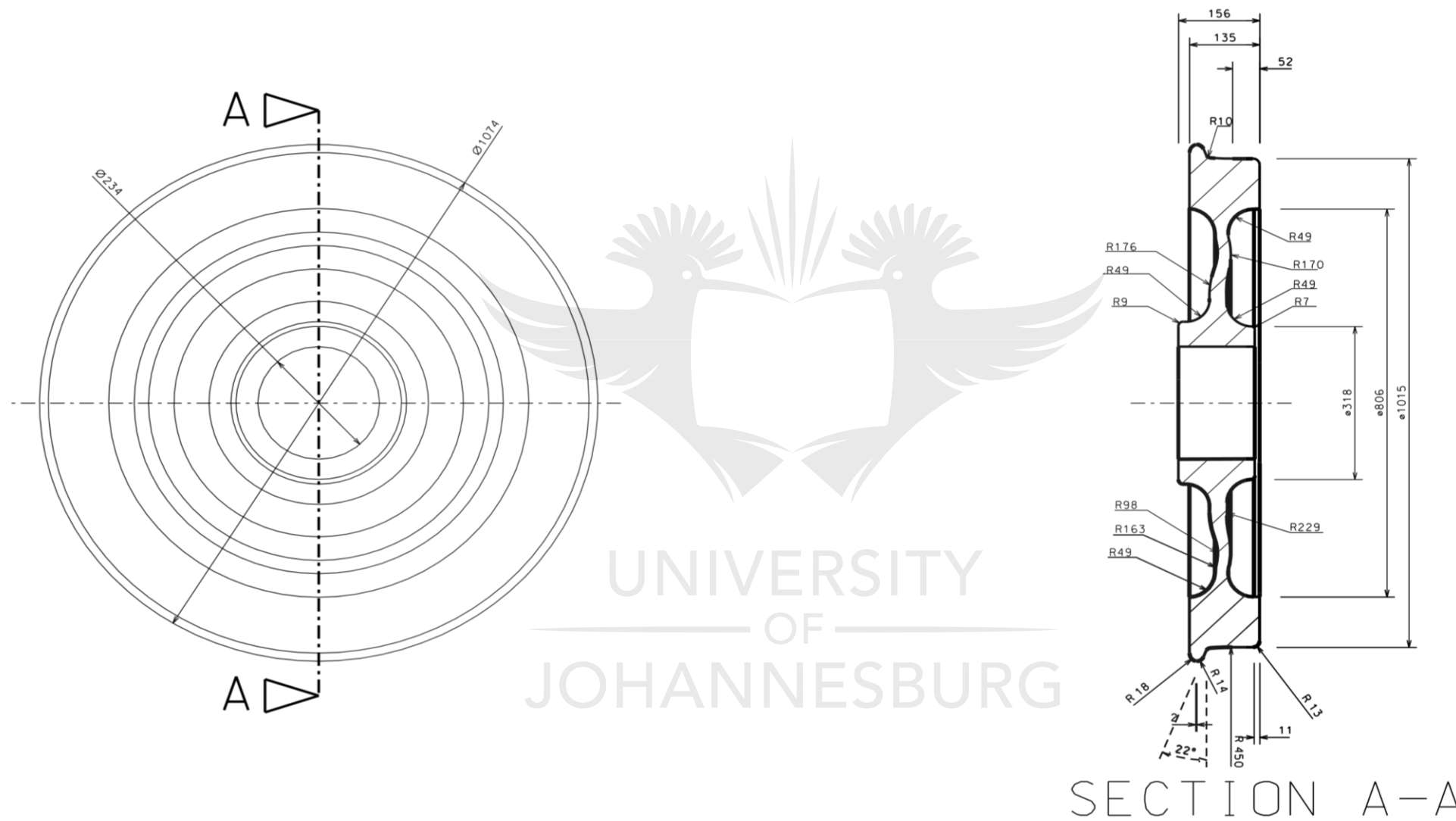


**Figure G3** – Whitish colour of ballast around concrete sleepers due to excessive corrugation-borne vibration



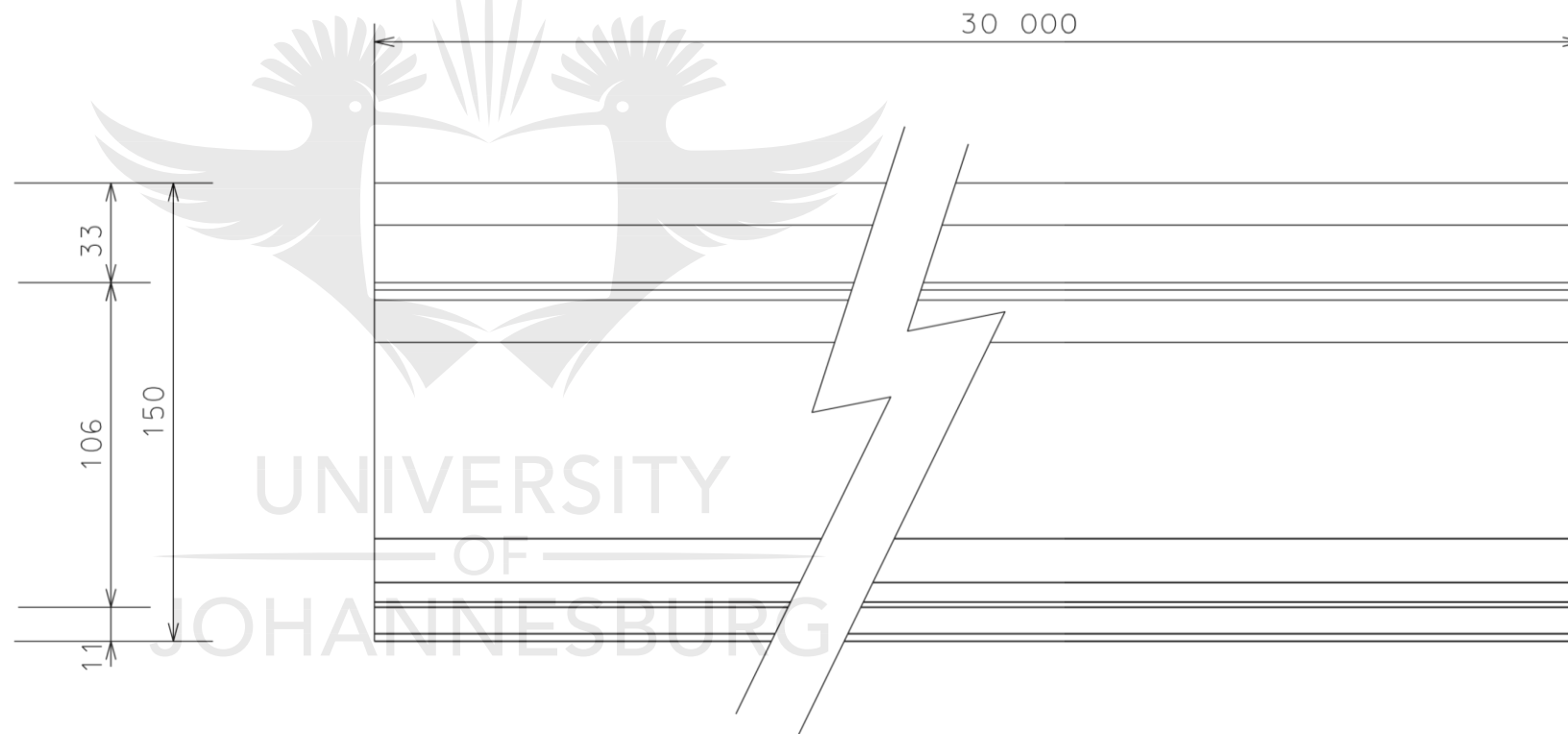
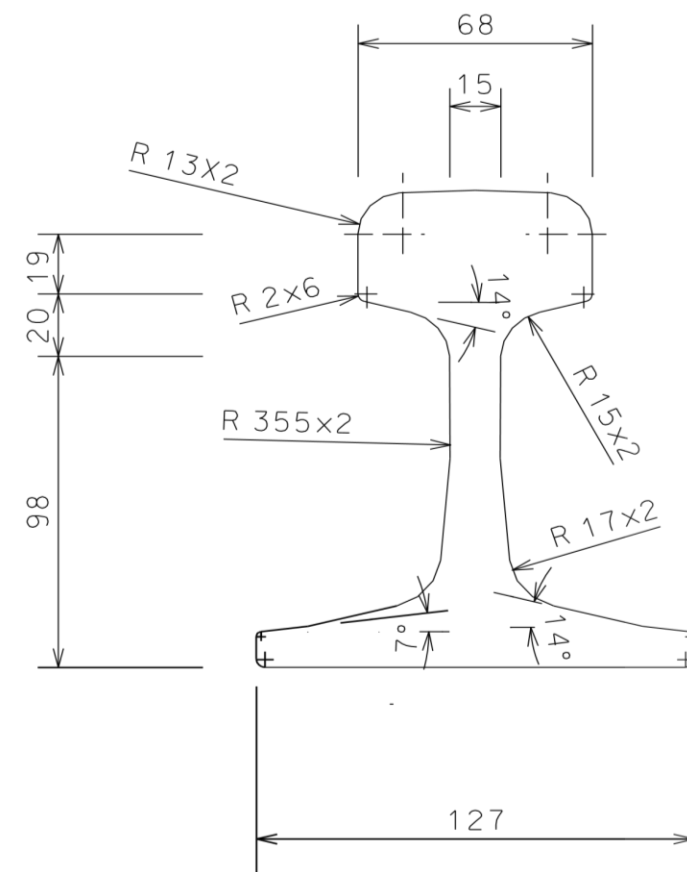
1 **Appendix H.** Detailed design drawings of CAD models for wheelset and rail track components.



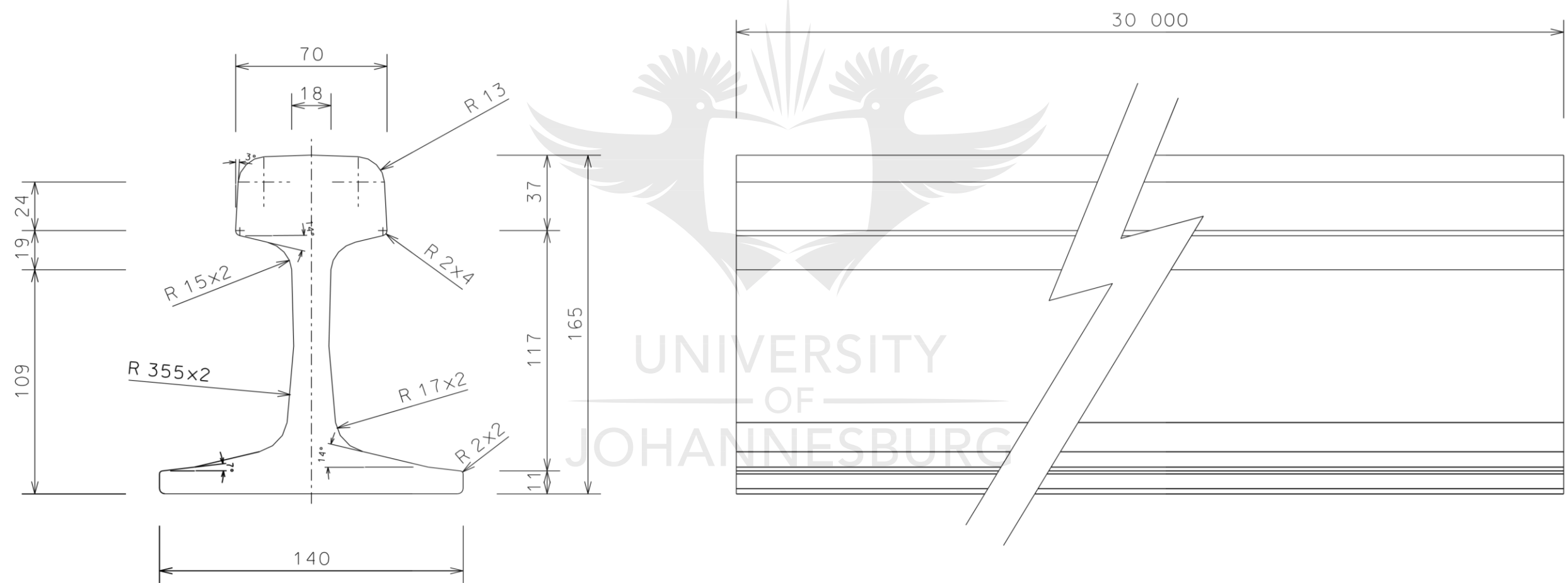


SECTION A-A

<b>MATERIAL:</b>  PHD THESIS DRAWINGS		 PROJECTION USED	IF IN DOUBT ASK	Note: Revision "0" Contain The Original Signatures & Dates of Drawing's First Issue Do not scale drawings		University of Johannesburg Department of Mechanical and Industrial Engineering	
				Approved by:		<b>TITLE:</b> <b>WHEEL</b>	
Date approved:		DRAWN BY:		DRG No.			
SCALE:		1:10		B BALEKWA		WST__01002	
				Date:		Student number · 200719025	
				2020-11-30			

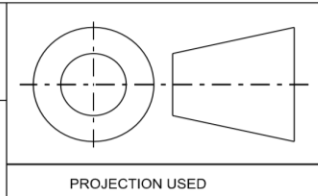


MATERIAL:		 PROJECTION USED	IF IN DOUBT ASK	Note: Revision "0" Contain The Original Signatures & Dates of Drawing's First Issue Do not scale drawings		University of Johannesburg Department of Mechanical and Industrial Engineering	
				Approved by:		TITLE: <b>RAIL 48</b>	
PHD THESIS DRAWINGS		 PROJECTION USED	IF IN DOUBT ASK	Date approved:			
				SCALE:	1:2	DRG No. RL_48	
				Date:		Student number : 200719025	



MATERIAL:

PHD THESIS DRAWINGS

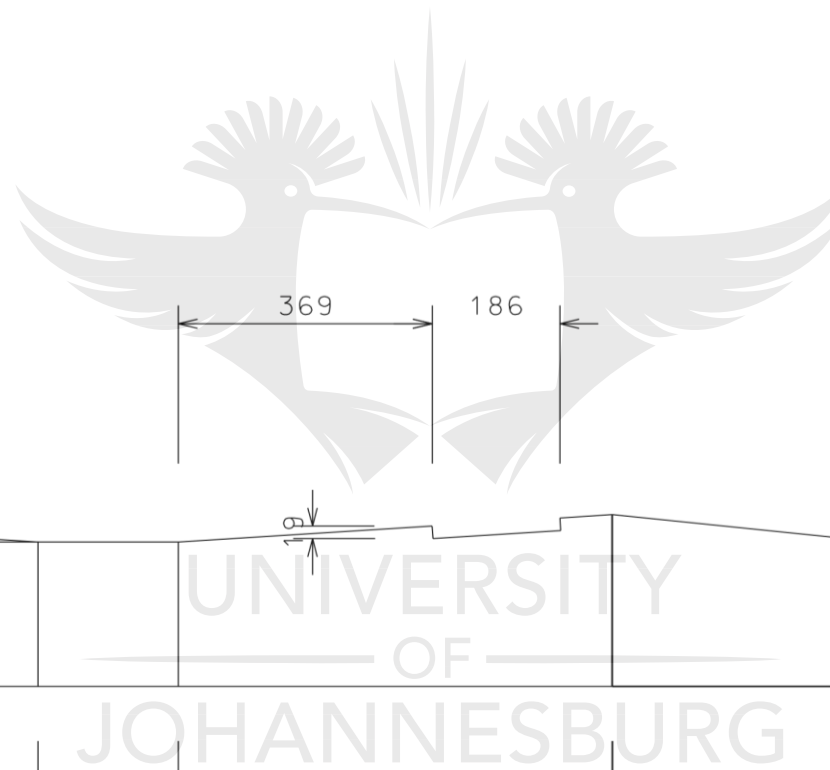
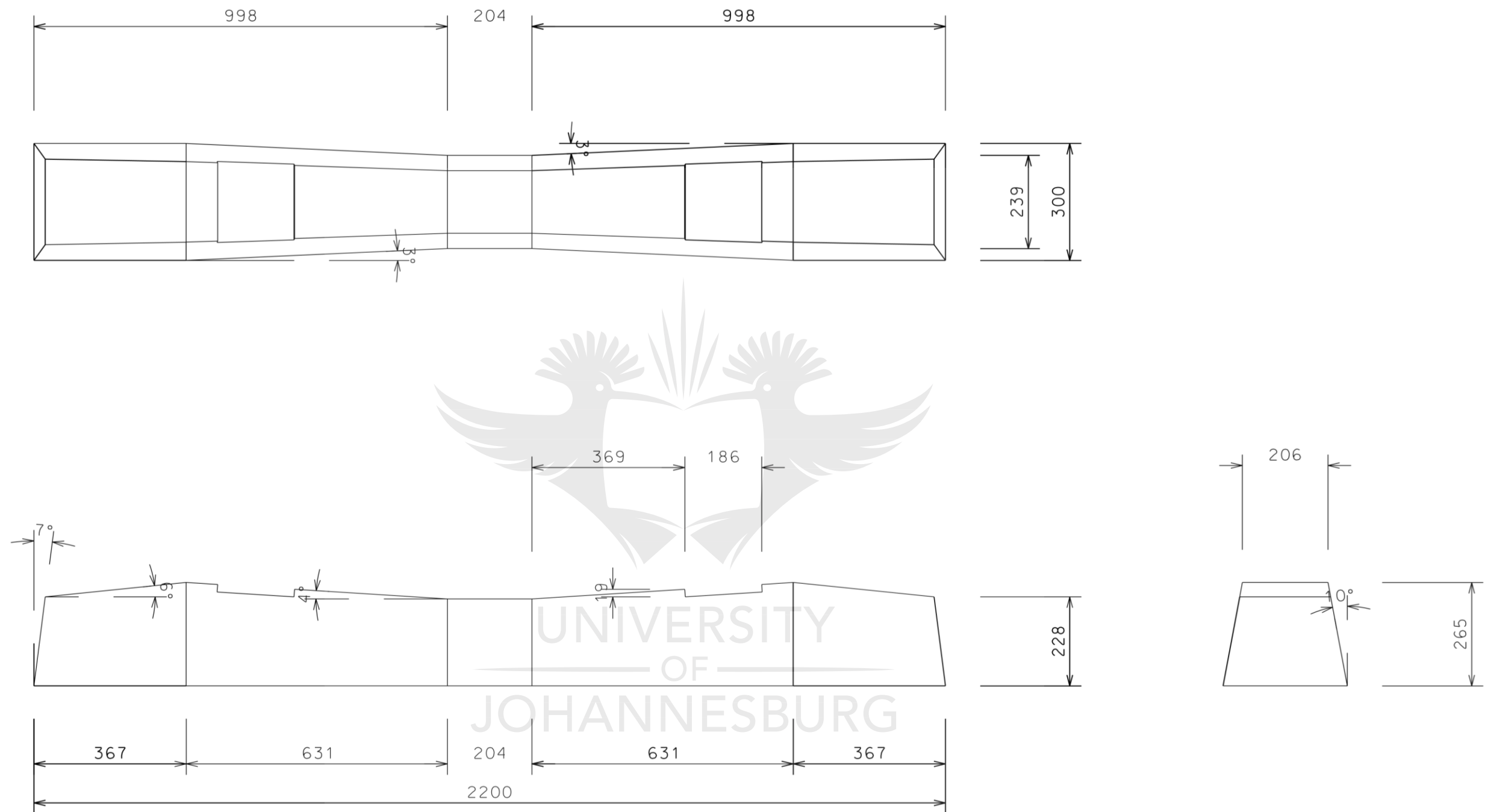


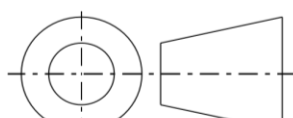
PROJECTION USED

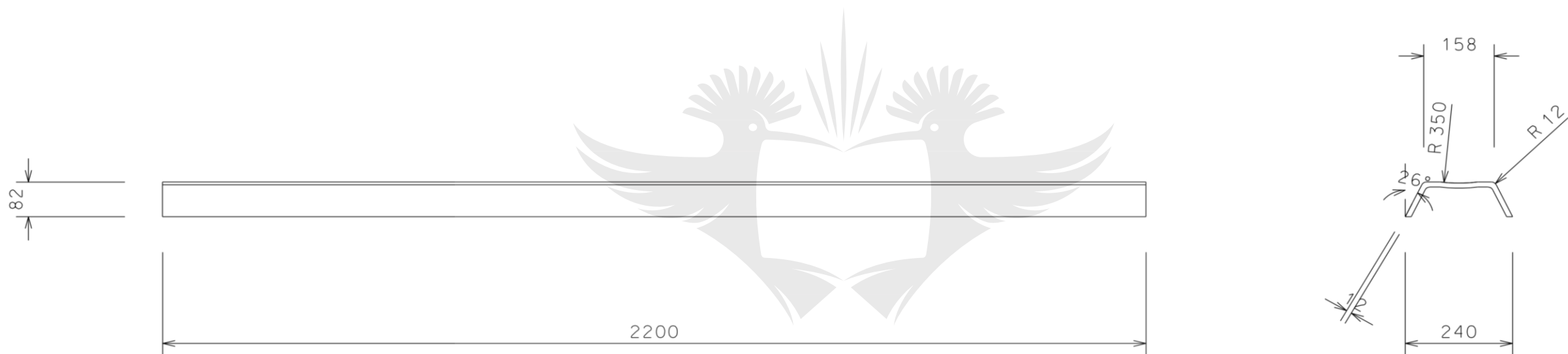
IF IN DOUBT  
ASK

Note: Revision "0" Contain The Original Signatures & Dates of Drawing's First Issue Do not scale drawings		University of Johannesburg Department of Mechanical and Industrial Engineering	
Approved by:		TITLE  RAIL 57	
Date approved:			
SCALE	1:2	DRAWN BY	DRG No.
		B BALEKWA	RL_57
		Date: 2020-11-30	Student number : 200719025

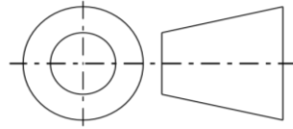




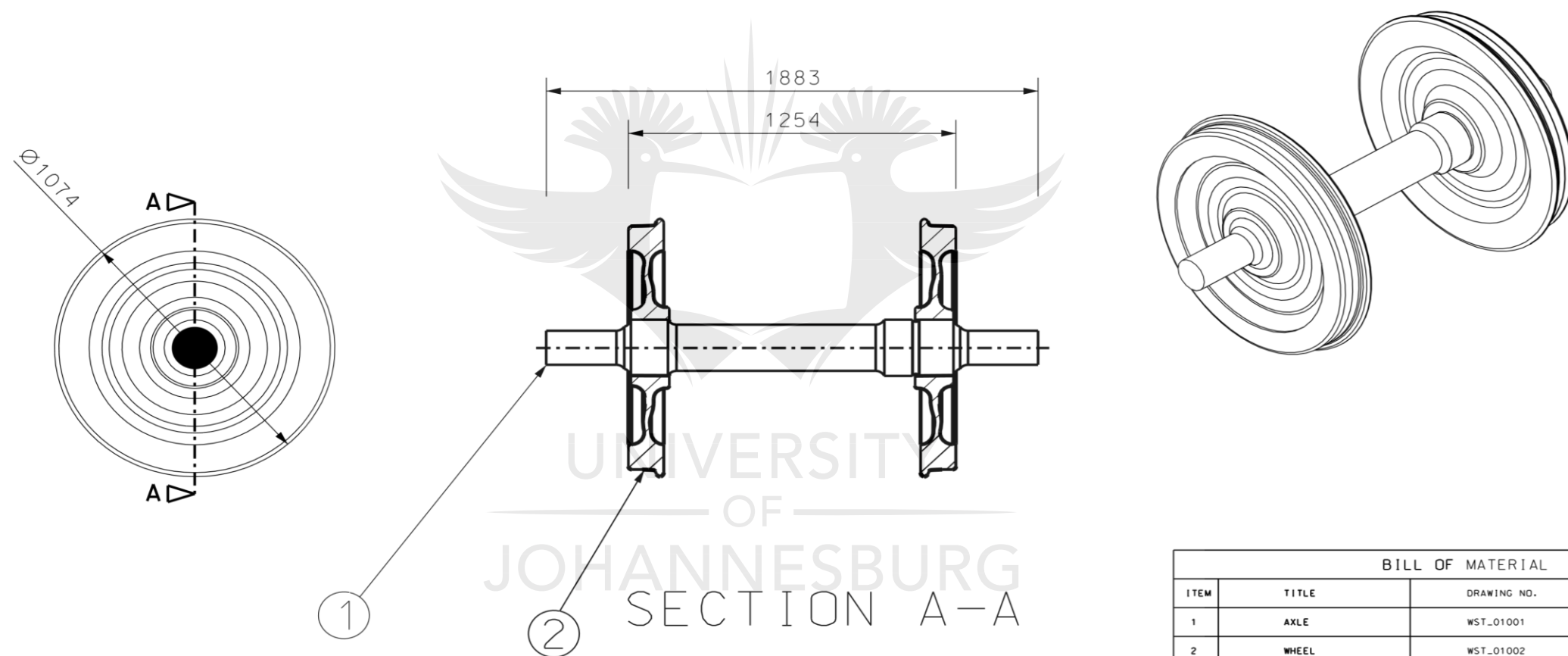
				Note: Revision "0" Contain The Original Signatures & Dates of Drawing's First Issue Do not scale drawings		University of Johannesburg Department of Mechanical and Industrial Engineering					
				Approved by:		TITLE CONCRETE SLIPPER					
MATERIAL:			IF IN DOUBT ASK	Date approved:				DRAWN BY		DRG No.	
				PHD THESIS DRAWINGS		SCALE		1:10		B BALEKWA	
								Date: 2020-11-30		Student number · 200719025	
				PROJECTION USED							



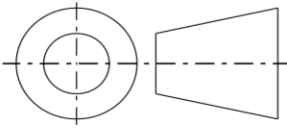
UNIVERSITY  
OF  
JOHANNESBURG

<b>MATERIAL:</b>  PHD THESIS DRAWINGS		 PROJECTION USED	IF IN DOUBT ASK	Note: Revision "0" Contain The Original Signatures & Dates of Drawing's First Issue Do not scale drawings		University of Johannesburg Department of Mechanical and Industrial Engineering	
				Approved by:		<b>TITLE:</b>  <b>STEEL SLIPPER</b>	
				Date approved:			
				SCALE:	1:10	DRAWN BY:	DRG No.
		B BALEKWA	SLS__01				
		Date:	Student number :				
		2020-11-30	200719025				

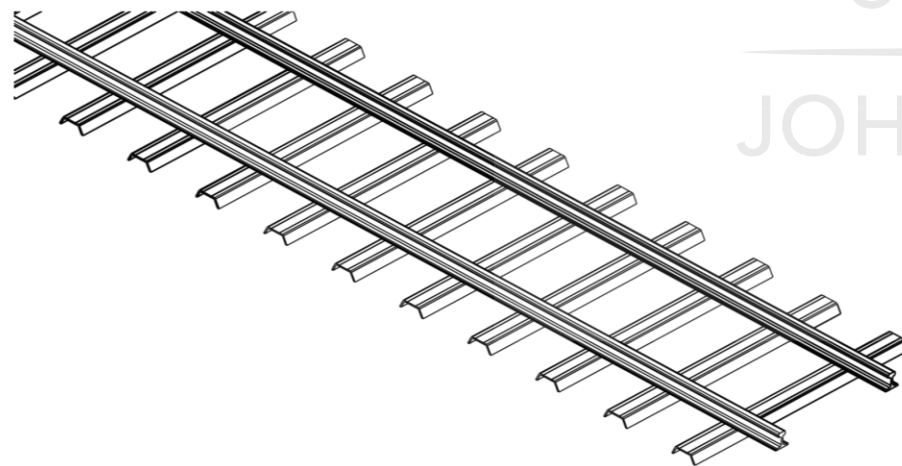
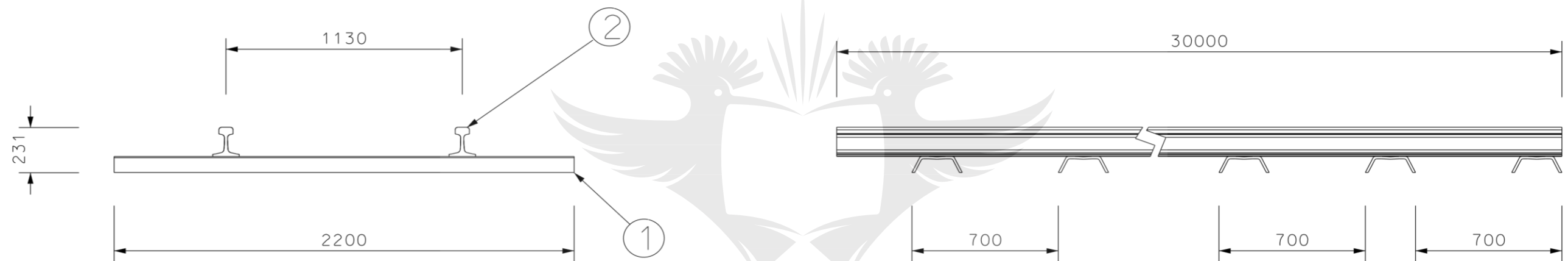




BILL OF MATERIAL			
ITEM	TITLE	DRAWING NO.	QUANTITY
1	AXLE	WST_01001	2
2	WHEEL	WST_01002	1

<b>MATERIAL:</b>  PHD THESIS DRAWINGS		 PROJECTION USED	IF IN DOUBT ASK	Note: Revision "0" Contain The Original Signatures & Dates of Drawing's First Issue Do not scale drawings	University of Johannesburg Department of Mechanical and Industrial Engineering	
				Approved by:  Date approved:	<b>TITLE:</b> <b>AXLE AND WHEEL ASSEMBLY</b>	
				SCALE: <b>1:20</b>	DRAWN BY: B BALEKWA	DRG No. WST__01
					Date: 2020-11-30	Student number : 200719025

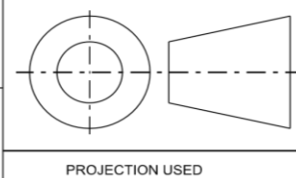




BILL OF MATERIAL			
ITEM	TITLE	DRAWING NO.	QUANTITY
1	STEEL SLEEPER	SLS_01	42
2	RAIL 48	RL_48	2

**MATERIAL:**

PHD THESIS DRAWINGS



PROJECTION USED

IF IN DOUBT  
ASK

Note:  
Revision "0" Contain The Original  
Signatures & Dates of Drawing's First Issue  
Do not scale drawings

Approved by:

Date approved:

SCALE:

**1:20**

University of Johannesburg  
Department of Mechanical and Industrial Engineering

**TITLE:**  
**RAIL STEEL SLEEPER ASSEMBLY**

DRAWN BY:

B BALEKWA

Date:

2020-11-30

DRG No.

RSS\_01

Student number · 200719025